POLITECNICO DI TORINO
Dipartimento Scienza Applicata e Tecnologia DISAT

XXIII PhD course in Chemical Engineering

ECOSUSTAINABLE BIOMETHANE AND FERTILIZER PRODUCTION THROUGH ANAEROBIC CO-DIGESTION OF ANIMAL MANURE AND ENERGY CROPS

Enrico Brizio

Supervisor: Prof. Ing. Giuseppe Genon
External reviewer: Prof. Dott. Pierluigi Navarotto

PhD coordinator: Prof. Ing. Vito Specchia

February 2012

Abstract

In Italy and many European countries energy production from biomass is encouraged by strong economic subsidies so that renewable energy plants, anaerobic digestion plant producing biogas in particular, are getting large diffusion. Nevertheless, it is necessary to define the environmental compatibility as well as technological and economic issues dealing with the emerging renewable energy scenario. This evaluation should take into account global parameters as well as environmental impacts at regional and local scale coming from new polluting emissions. The environmental balances regarding new energy plants are of primary importance within very polluted areas such as Northern Italy where air quality limits are systematically exceeded, in particular for PM_{10}, NO_2 and ozone.

The most important environmental shortcomings that should be solved or at least minimized as far as biogas production and utilisation are concerned are:
1. macro-pollutants emissions from biogas engine at the local scale and low fuel utilization index (biogas plants generally don't recover all thermal energy at disposal);
2. indirect GHG emissions, mainly involving post-methanation emissions from the digestate storage;
3. ammonia emissions from the storage and land spreading of digested materials, low fertilising efficiency of manure and digestate, nitrate contamination of groundwater.

The described emissions and energy inefficiency could involve negative environmental balances at the local scale, conflicting with the possible benefits arising from biomass energy production.

An alternative technological choice for biogas valorisation could be biomethane production (also called green gas) through biogas purification and upgrading processes in order to remove CO_2 and trace components. Biomethane production and its injection into natural gas grid (or its use as a transport vehicle fuel) could bring about strong energy and environmental benefits such as higher energy efficiencies and lower specific emissions (district heating CHP units, combined cycle gas turbines, methane powered vehicles).

The present study mainly aims at analysing biogas upgrading techniques under the aspects of energy consumptions and environmental sustainability, with a specific focus on minimizing methane losses from the process by means of suitable design and operative choices (temperature, pressures, sorbents, recirculation strategies, etc.) that are fully described and simulated. The considered upgrading techniques are based on the principles of physical and chemical absorption and pressure/vacuum swing adsorption (PSA).

The analysis highlights that there are strong differences among the examined upgrading techniques, as far as specific sorbent flows, absorbing tower dimensions, methane losses, power required, recoverable heat and environmental impacts (use of resources, gaseous releases of odorous and polluting molecules, GHG balances) are concerned.

In particular, all the analysed upgrading techniques could be designed in order to achieve very low methane slip, below 0.1%, except PSA for which methane losses are hardly reducible below 2%, even at very high energy consumptions. The actual range of methane slip for the considered technologies is 0.1÷5% whereas the energy consumption to upgrade biogas lies in the range 0.05÷0.54 kWh_e/m^3 of raw biogas.

The following analysis reports also some economic evaluations including electric energy costs, thermal energy requirements, biomethane sale incomes and external costs due to environmental impacts of biogas production+upgrading techniques. Within the described cost-benefit approach, the best overall balances seems to be assured by absorption with DEPG and chemical absorption with MEA.

Finally, the last part of the present work shows a technical analysis of a specific digestate treatment process that could help reaching both the reduction of GHG and ammonia emissions and, at the same time, the production of fertilizers.

The present analysis therefore confirms that biogas/biomethane technology is absolutely ready and suitable to reach very high levels of productivity, efficiency and environmental performances at sustainable costs and the right technological approach could solve many environmental problems regarding nitrate contamination of groundwater, ammonia emissions and global warming issues.

Keyword: biomethane, upgrading techniques, methane losses, energy consumptions, ammonia, externalities

CONTENTS

1 Introduction

Renewable energy plants (mainly based on biogas produced by anaerobic digestion of manure and energy crops, vegetable oil burned by diesel engines, wood and solid biomass combustion and so on) are getting large diffusion in Northern Italy because of the benefits deriving from the production of energy on one's own, the claimed reduction of odour nuisance from manure and the increase of its biological stability and, most of all, the economic return (pay-back times can be as short as 3-5 years in Italy) based on electricity production. The new energy scenario has to be considered within the environmental background of the area where it is introduced, involving air quality limits compliance, the use of best available techniques, energetic efficiency (also thermal), emissive balances, global warming issues, biomass origins, aspects dealing with the use of water and fertilizers for energy crops, nitrates leaching towards groundwater. These aspects are the focus of the many studies.

Air quality of Northern Italy is one of the most polluted of the world, maybe the worst in Europe, due to the strong human activities and the orography of its territory. PM_{10}, NO_2 and ozone concentrations measured at the ground level diffusely and permanently go beyond the quality standards. In particular, PM_{10} concentration is only partly due to particulate primary emissions because the chemical analysis of PM measured in Northern Italy confirm that secondary particles (deriving from NO_x, SO_x, NH_3 and VOC) account for 60-70 % of total PM concentration (see Giugliano and Lonati (2005) and CNEIA (2006)). Moreover, some European studies report (De Leeuw, 2002) the following aerosol formation factors, to be considered by weight, starting from gaseous pollutants: NO_x 0.88; SO_x 0.54; NH_3 0.64. As it is clear from the reported figures, in order to control and improve air quality in Northern Italy, the emissions of gaseous compounds such as NO_x and ammonia (mostly emitted by agriculture) should be mainly reduced. Another strong environmental critical issue of Northern Italy is nitrate contamination of surface and ground-water resources mainly due to the use of fertilizers and the land-spreading of animal manures. As far as specific emissions towards atmosphere are concerned, Table 1.1 (Brizio et al., 2011) reports the comparison between the most frequent renewable energy technologies (biomass combustion, biogas plants and vegetable oil combustion) and fossil fuel energy plants (average Italian power plants and industrial boilers).

Table 1.1: comparison of energy and emissive performances between fossil and renewable energy plants

	italian power plants (*)	industrial boilers (**)	biomass direct combustion	veg oil engine	anaerobic digestion→ biogas
electrical efficiency	38%	0%	18%	42%	40%
thermal efficiency	-	90%	60% (1)	40% (1)	40% (1)
CO_2 (g/kWh$_e$)	746	258	virtually 0	up to 1500 (4)	250-600 (7)
NO_x (g/kWh$_e$)	0.498	0.2	1.24 (2)	0.56 (5)	1.826 (8)
SO_x (g/kWh$_e$)	0.525	0.201	~0	0.14	~0.183 (9)
PM (g/kWh$_e$)	0.024	0.0104	0.124 (3)	0.056 (6)	~0

(*) ENEL report 2009
(**) natural gas-gasoil 50/50
(1) almost never applied
(2) SNCR+recirculation: <100 mg/Nm^3 O$_2$ @ 11%
(3) MC+ESP or FF: < 10 mg/Nm^3 O$_2$ @ 11%
(4) depending on growing area

(5) SCR: < 200 mg/Nm^3 O$_2$ @ 5%
(6) catox + SCR: < 20 mg/Nm^3 O$_2$ @5%
(7) due to indirect GHG emissions
(8) < 500 mg/Nm^3 O$_2$ @ 5%
(9) < 50 mg/Nm^3 O$_2$ @ 5%

As one can easily observe, renewable energy plants, unless they are equipped with efficient abatement devices (fabric filters for particulate, Selective Catalytic and Non Catalytic Reduction for NOx and so on), generally cause higher NO_x emissions, twice, three times larger than traditional energy plants burning natural gas, the most common fuel for new settlements in Italy. Similar remarks could be done for PM emissions

from solid biomass combustion and VOC due to biogas or vegetable oil burned by engines. In spite of their impacting potential, renewable energy plants in Italy undergo very fast authorizing procedures (they are defined as public utility, not post-ponable and urgent); moreover, technical and emissive limits imposed by Italian law are not suitable to limit the possible environmental impacts; as a matter of facts, it's very difficult to impose abatement systems (catalytic/thermal oxidation, SCR, SNCR, air/fuel staging, etc,,) that could mitigate the impacts.

Moreover, it's important to remember that emissions from renewable energy plants could be counterbalanced by the so-called avoided emissions relating to displaced existing releases; within this context, the recovery of thermal energy plays a crucial role (the potential thermal recovery for an engine is around 40%, for a wood combustor even larger than 60%). Unfortunately, cogeneration is often disregarded or not adequately applied because the aspect that does really matter in economic terms is electricity and so large quantities of thermal energy is dispersed and the emissive balance could become strongly negative at the local scale. These circumstances are mainly due to the structure of renewable energy national subsidies that, up to now, are strongly based on electricity production and not on energy efficiency or environmental balance requirements.

1.1 Environmental compatibility for anaerobic digestion plants

The main environmental concerns referring to animal manure management are odours due to uncontrolled fermentation, ammonia emissions from the storage and the land-spreading and greenhouse gases (GHG) release (CH_4 and N_2O). Anaerobic digestion (AD) can be an answer to odour nuisance but it is totally ineffective on nitrogen content of digested materials; moreover, as we will see later on, also CH_4 and N_2O could be enhanced with respect to the *ante operam* conditions.

Due to obvious economic drivers, manure is rarely digested alone; on the contrary, energy crops such as maize, triticale and sorghum and, sometimes, agro-residues are fed to digesters in order to increase the volatile solid (VS) content and then biogas production (higher methane yields). AD plants formally proposed in Northern Italy in the last months are several and they are all characterised by high crop/manure ratios within the mixture to be digested, (crops sometimes represent much more than 50% of the feedstock).

As previously mentioned, within anaerobic digesters, nitrogen contained in the primary mixture is not removed and almost the same amount can be found in the digested material, under different forms: as a matter of fact, a large part of nitrogen contained in proteins is hydrolyzed to ammonium ion (NH_4^+) and dissolved ammonia (NH_3) that can be volatilized; an increase in pH, NH_3 concentration and temperature, 3 conditions that do occur after anaerobic digestion, enhance ammonia emissions during storage and after field application. Moreover, nitrogen content of the mixture to be digested is strongly increased by the use of energy crops (for example, maize silage contain ~4 kg N/ton of fresh matter)

This way, the nitrogen amount to be managed along with digested materials can be strongly larger than that in primary manure and it is surely more suitable for volatilization.

Based on reliable emission factors and international studies (CORINAIR, IPCC and IPPC BAT reference documents, Italian experimental results and so on) it is possible to assess that 34 ±11% of nitrogen contained in the storage is emitted as NH_3-N from the storage and land-spreading (19 % from the storage and almost 15% from the land-spreading) of fresh animal manure. The reported ammonia emission factor referring to traditional manure management (no Best Available Techniques are applied) could be confirmed by theoretical studies simulating all the phenomena involved in ammonia releases from a lagoon (acidic dissociation, ammonia diffusion in manure, Henry's constant defined by different models, mass transfer coefficients, both empirical and theoretical ones), according to the two-film theory. This kind of approach gives back calculated yearly total ammonia release from the storage of fresh manure as large as 20% of the nitrogen initial content under the climatic conditions of Northern Italy.

As already described, this amount of emitted ammonia can be enhanced by anaerobic digestion: Clemens (2006) describes that, during the summer, ammonia emissions from the storage of digested cattle slurry are twice the releases from untreated manure (222,5 g NH_3/m^3 slurry vs. 110,5 g NH_3/m^3 slurry). Balsari (2009)

reports an increase of 12,5% due to anaerobic digestion of manure whereas Immovilli et al. (2007) describe that the increase can be up to 73%.

Figure 1.1 reports the emission of ammonia and NOx from the storage and land-spreading of digested manure and energy crop (maize) on the basis of the described average emission factors, without considering the chemical-physical conditions induced by digestion (that could still enhance the emissions, as previously explained); as a matter of fact, according to different crop/manure ratios, ammonia emissions can be much larger than those from fresh manure (scenario 0), up to three times when manure represents just one third of the mixture to be digested.

As obvious, the reported figures refer to plants without any ammonia abatement devices, that are not generally planned for new installations. The large amount of ammonia release could be strongly reduced by employing stripping-absorbing towers for digested materials (H_2SO_4 solutions are usually applied as absorbents in order to obtain a fertilising by-product that could be sold); alternatively, the storage tank could be covered (a solid cover should be implemented because straw covers or natural crusts could be less effective in reducing NH_3 emissions and have the potential to increase GHG emissions, as reported by Amon et al. (2006) and Best Available Techniques to the land spreading of digestates (immediate incorporation, use of deep injectors) should be applied. On the other hand, NOx emissions could be largely reduced by Selective Catalytic Reduction (up to 90%), but the technical feasibility of this solution depends on the poisoning potential of waste gas and the purification possibilities. Finally, a different use of biogas could be thought: this is the case of biogas upgrading in order to produce biomethane to inject into the natural gas grid or to be used as car fuel. The described technical configuration could avoid the use of a biogas engine with large emissions at the local scale; the present study is mostly focused on the feasibility aspects of biogas upgrading techniques, as better explained in the following chapters.
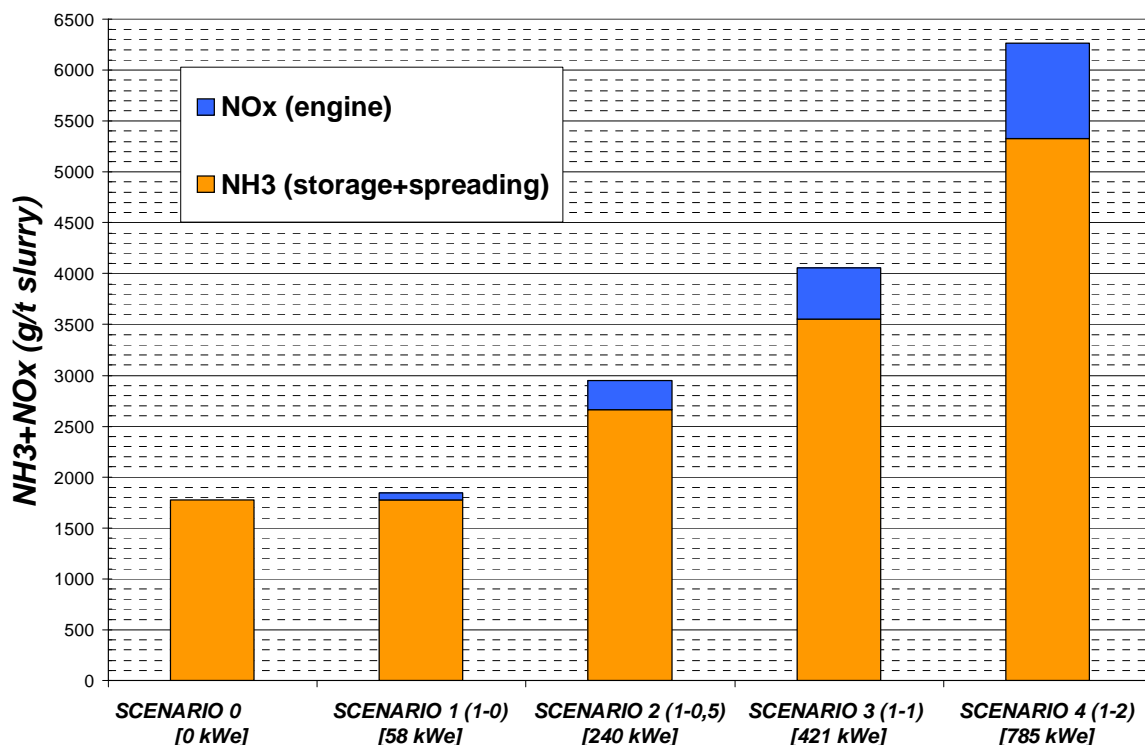

Figure 1.1: Ammonia and NO$_x$ emissions due to anaerobic digestion; in brackets t manure/h – t maize/h fed to digesters

As far as greenhouse gases balances are concerned, 0.0032±0.0012 kg N_2O-N/kg excreted N are expected to be emitted from the storage of fresh manure on the basis of the same literature international studies reported in the previous chapters for ammonia; moreover, an indirect N_2O should be considered, dealing with volatilised nitrogen: the IPCC proposed emission factor is 0.01 kg N_2O-N/(kg NH_3-N + NOx-N volatilised). We do not have experimental information about the effect of increased nitrogen content due to co-digestion of manure and energy crops but, according to the approach followed by international emission factors (N_2O releases are likely to be proportional to nitrogen content), a further emissive increase for N_2O could be expected in this case.

Another environmental aspect that should be analysed when dealing with anaerobic digestion is the post-methanation potential, that is the uncontrolled emission of methane from the storage of digested materials. As a matter of fact, the post-methanation somehow depends on the volatile solid content of the slurry and it is well known that the VS removal efficiency of AD is never 100%; on the contrary VS conversion to biogas is for the most part a function of the biodegradability of the primary mixture to be digested and the dimension of the digester through the hydraulic retention time (HRT). Based on several experimental data, the VS removal efficiency is often lower than 50%, rarely larger than 70%.

This way, taking into account the VS content in the digested material that sometimes can be remarkable (more than 50% of the original quantity) on the one hand, given the temperature of digested materials, the presence of specialized anaerobic biomass coming from the digesters and the long time at disposal for the storage (even more than 100 days) on the other hand, the post-methanation could represent a considerable emission.

Some authors (Weiland, 2003) report that "typically 5-15% of the total biogas produced can be obtained from post-methanation of residues" while the CROPGEN project inform that up to 12-31% of total methane production can be recovered from post-methanation of digestates. The post-methanation potentials measured within the CROPGEN project for digestates incubated for 100 days at 5, 20 and 35°C were 1-9, 73-120, 133-197 l CH_4/kg VS respectively. As far as the mentioned project is concerned, the post-methanation potential doesn't change during feeding regimes with 30-40% of crops in the feedstock. Other studies (Kaparaju, 2010) report post-methanation potentials of 160-210 at 35-55°C, 53-87 at 15-20 °C and 26 l CH_4/kg VS at 10°C for a storage of 250 days.

In order to develop proper GHG balances around the technical choice of anaerobically digesting manure and crops, a post-methanation potential of 50 l CH_4/kg VS and a VS removal efficiency of 50% can be used to calculate the indirect GHG emissions from the storage of digested materials. As far as GHG emissions from untreated manure are concerned, the emission factors proposed by IPCC can be considered a good reference: for a mixture of swine and dairy cattle manure and a climate between cool and temperate, an emission around 4 kg CH_4/t of manure can be expected.

As pointed out by Figure 1.2 (Genon et al., 2011), co-digestion of manure and energy crops (when energy crops represent from 30 to 70% of feedstock), causes indirect GHG emissions that nullify the "energy bonus" due to CO_2 avoided emissions (Brizio et al., 2010): based on our assumption the indirect emissions of GHG could be quantified as 400 ± 67 g CO_{2eq}/kWh$_{el}$, mainly due to CH_4 releases from the storage of digestate, that is comparable to the Italian average CO_2 emission factor for energy production (496 g CO_2/kWh$_{el}$, ENEL, 2009): the reported figure represent the average value for three different post-methanation models. Furthermore, it should be said that the proposed balances neglect the emissions of CH_4 and N_2O from the biogas engine, as well as CO_{2eq} emissions relating to cultivation and transport of energy crops; these contributions would even worsen the reported GHG balances. This way, in the case energy bonus, that is strongly economically propelled, is cancelled by uncontrolled GHG released, the renewable energy mission of AD would be betrayed.

The negative impacts of indirect emissions from co-digestion of manure and energy crop are confirmed by some recent studies (Balsari, 2010, Gronauer); the first presentation points out a range from 150 to 700 g CO_{2eq}/kWh$_{el}$ for AD (the higher value corresponds to co-digestion of manure and energy crops and it is mainly due to production and transport of biomass), while the second author reports (personal communication) that "in extreme cases (open storage of digestate and low HRT) the CO_{2eq} balance can reach levels of 600–700 g CO_{2eq}/kWh$_{el}$, that means: biogas production causes the same GHG emissions as German conventional electricity production". A very similar range of indirect GHG emissions (200-700 g CO_{2eq}/kWh$_{el}$) is reported by Blengini et al. (2011).

As one can easily observe from the mentioned data, energy production from AD could have a negative meaning as far as sustainability aspects are concerned. As obvious, the solution can be both technological and operational: higher HRT, thermophilic digestion regimes, gas-tight storage of digestates (and recovery of released methane in a biogas engine or an upgrading plant), thermal oxidation of waste gas from the engine, reduction of valuable energy crop fraction within feedstock can strongly reduce GHG indirect emissions. Moreover, cogeneration of thermal energy can save up to 300 g CO_{2eq}/kWh$_{th}$, as showed by Figure 1.2, improving GHG overall balance. So far, the strong economic subsidies mainly based on electricity production represent a demotivating factor for this kind of technical devices.
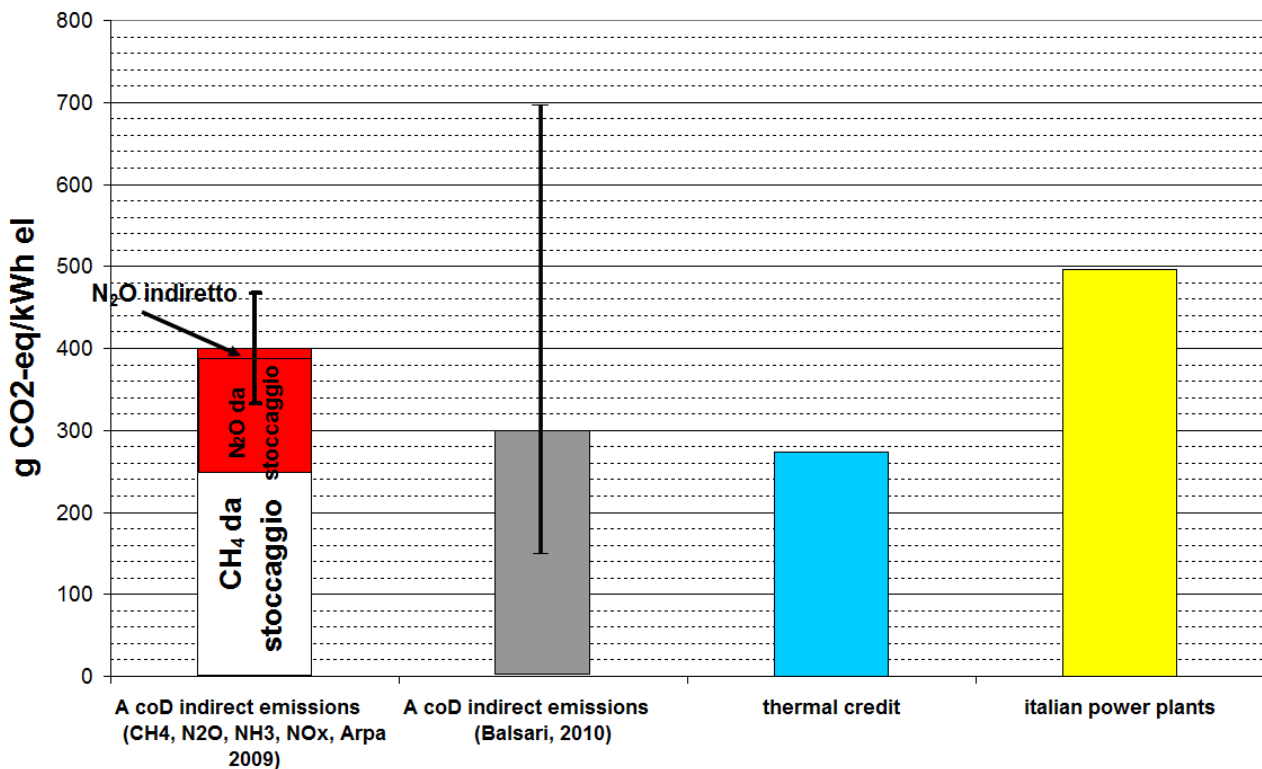
Figure 1.2: indirect GHG emissions for Anaerobic coDigestion

1.2 Technological answers to environmental compatibility shortcomings

As widely described in the previous chapters, three are the main environmental drawbacks that should be solved or at least minimized as far as biogas is concerned:

1. macro-pollutants emissions from biogas engine at the local scale and low fuel utilization index;
2. indirect GHG emissions, mainly involving post-methanation emissions from the digestate storage;
3. ammonia emissions from the storage and land spreading of digested materials, low fertilising efficiency of manure and digestate, nitrate contamination of groundwater.

The present study mainly aims at analysing biogas upgrading techniques under the aspects of energy consumptions and environmental sustainability, with a specific focus on minimizing methane losses from the process.

The advantages brought about by biomethane production are many. First of all, contrary to fossil fuel derived methane which is available only in limited amounts, biomethane is a renewable source of energy. It is produced from organic waste (dead animal and plant material), sewage, manure, slurry, etc. which will never run out as long as there will be life on this planet. In addition to providing a renewable source of energy, biomethane can be produced just about everywhere in the world. The access to natural gas and other fossil fuels, on the other hand, is available only in a few parts of the world because the deposits are distributed very unevenly. In addition, they can be located in hard to reach areas such as deep beneath the ocean floor making extraction very expensive and dangerous for both the environment and people. Biomethane, on the other hand, requires only collection of organic matter which is easily available throughout the world. It provides a stable and efficient source of energy to regions which do not have the ability to generate power from solar energy, wind power, etc.

Usability is another great advantage of biomethane besides availability. Since it is identical to fossil fuel derived methane, it can be used for space heating, water heating, cooking, etc. but it can also be used for electricity generation. The use of biomethane to produce electricity brings about better energy performances than those achievable by small biogas burning engines (natural gas turbine for example can have efficiencies larger than 55% for modern and larger power plants).

Biomethane, if adequately compressed, could be used as fuel for vehicles as well. In transport applications, biomethane burns cleaner (and also more quietly) than liquid biofuels, helping to improve air quality. Using biomethane as a vehicle fuel can therefore help to meet both greenhouse gas and air quality strategy objectives.

Finally, biomethane production, as already mentioned, could avoid strong atmospheric emissions of NOx and VOC from the direct biogas combustion at the local scale.

As far as the second and the third points are concerned, the possible solutions could be many, but the most effective ones involve the recovery of residual biogas from the storage and the treatment of digested materials in order to produce a fertilizer through the salification of ammonia.

The last part of the present work shows a technical analysis of a specific digestate treatment process that could help reaching both the described requirements, the reduction of GHG and ammonia emissions and, at the same time, the production of fertilizers, as already applied in some biogas facilities in the southern part of Piedmont.

2 Biogas treatment techniques

Biogas produced by anaerobic digestion of manure and energy crops is composed mainly by methane (40÷75%) and carbon dioxide (15÷60%). Trace amount of other components such as water (5÷10%), hydrogen sulphide (H_2S, 0.005÷2%), ammonia (NH_3, < 1%), carbon monoxide (CO, < 0.6%) and Nitrogen (N_2, < 2%) can be present and should be removed.

Biogas treatment processes are divided into:

- biogas cleaning to remove trace components harmful to the natural gas grid through chemical, physical and biological processes (condensation, filtration, adsorption, absorption, biological removal, cryogenic separation and so on);
- biogas upgrading, where CO_2 is removed to meet the purity and calorific value required for natural gas use.

After transformation, the produced gas is called biomethane.

According to its intended use (injection into natural gas pipeline or vehicle fuel), biomethane should consist of maximum 3% of CO_2 that will be the process target for the following calculations. The biomethane compression requirements are very different: 250 bar when biomethane is used as vehicle fuel whereas local natural gas pipelines generally allow maximum 5 bars.

In the present paper, the latter option has been assumed in order to calculate the energy requirements for upgrading processes (the previous cleaning methodologies are excluded from the technical analysis), but the reported results could be easily used to obtain the extra consumptions due to compression up to vehicle injection needs.

Biogas upgrading techniques could be:

- physical absorption with pressurized water;
- physical absorption with pressurized organic solvent (glycol ethers are the most used);
- chemical absorption with aqueous alkanolamine solutions (MEA, DEA, etc.);
- Pressure and Vacuum Swing Adsorption (PSA/VSA);
- Membrane separation;
- Cryogenic separation.

The most applied techniques in Europe are absorption with pressurized water and PSA.

Upgrading techniques can be strongly different as far as process pressure, temperature, purity performances, methane losses and energy consumptions are concerned. Literature reports many "state of the art" analyses, with advantages and disadvantages of each technology, as reported by Figure 2.1, taken from Ryckebosch et al. (2011). Sometimes precise technical details are present: the most relevant data are collected by Table 2.1.

Table 2.1: technical data for biogas upgrading techniques

	process pressure	process temperature	sorbent flow	final CO_2	CH_4 loss	Operative costs
	atm	°C	m^3/100 Nm^3 biogas	v/v	v/v	-
absorption with water	6 - 12	10 – 35	10 - 20	<3%	up to 4%	< 0.25 kWh_e/m^3
absorption with glycol ethers	7 - 12	20 - 35	3 - 6	<3%	2-4%	0.24÷0.33 kWh_e/m^3
chemical absorption with amines	atmospheric	40	?	<1%	< 0.1%	< 0.5 kWh_{th}/m^3
pressure and vacuum swing adsorption	4 - 10	30-60	-	<3%	"significant"	?
membrane separation	low membrane selectivity: CH_4 losses up to 25%, high pressure (25÷40 atm), compromise between purity of CH_4 and amount of biomethane					
cryogenic separation	expensive investment and operation, pressure at 80 atm, mainly pilot plants					

Method	Advantages	Disadvantages
Absorption with water	High efficiency (>97% CH_4) Simultaneous removal of H_2S When $H_2S < 300 \text{ cm}^3 \text{ m}^{-3}$ Easy in operation Capacity is adjustable by changing pressure or temperature Regeneration possible Low CH_4 losses (<2%) Tolerant for impurities	Expensive investment Expensive operation Clogging due to bacterial growth Foaming possible Low flexibility toward variation of input gas
Absorption with polyethylene glycol	High efficiency (>97% CH_4) Simultaneous removal of organic S components, H_2S, NH_3, HCN and H_2O Energetic more favorable than water Regenerative Low CH_4 losses	Expensive investment Expensive operation Difficult in operation Incomplete regeneration when stripping/vacuum (boiling required) Reduced operation when dilution of glycol with water
Chemical absorption with amines	High efficiency (>99% CH_4) Cheap operation Regenerative More CO_2 dissolved per unit of volume (compared to water) Very low CH_4 losses (<0.1%)	Expensive investment Heat required for regeneration Corrosion Decomposition and poisoning of the amines by O_2 or other chemicals Precipitation of salts Foaming possible

PSA/VSA
  Carbon molecular sieves
  Molecular sieves (zeolites)
  Alumina silicates
	Highly efficient (95−98% CH_4)
	H_2S is removed
	Low energy use: high pressure, but regenerative
	Compact technique
	Also for small capacities
	Tolerant to impurities
		Expensive investment
		Expensive operation
		Extensive process control needed
		CH_4 losses when malfunctioning of valves

Membrane technology
  Gas/gas
  Gas/liquid
	H_2S and H_2O are removed
	Simple construction
	Simple operation
	High reliability
	Small gas flows treated without proportional
	increase of costs
	Gas/gas
	  Removal efficiency:
	  <92% CH_4 (1 step) or > 96% CH_4
	  H_2O is removed
	Gas/liquid
	  Removal efficiency: > 96% CH_4
	  Cheap investment and operation
	  Pure CO_2 can be obtained
		Low membrane selectivity: compromise between
		purity of CH_4 and amount of upgraded biogas
		Multiple steps required (modular system) to reach
		high purity
		CH_4 losses
		Little operational experience

Cryogenic separation	90−98% CH_4 can be reached CO_2 and CH_4 in high purity Low extra energy cost to reach liquid biomethane (LBM)	Expensive investment and operation CO_2 can remain in the CH_4
Biological removal	Removal of H_2S and CO_2 Enrichment of CH_4 No unwanted end products	Addition of H_2 Experimental − not at large scale

Figure 2.1: advantages and disadvantages for biogas upgrading techniques

What is really missing in literature reports is a sensitivity analysis of the influence of process parameters on removal performance, methane loss and energy consumptions. For instance, how much would it cost to reduce methane loss of water scrubbing below 1%? Is it possible and how?

It should be remembered that methane losses should be minimized both for economic and environmental reasons since its global warming potential is 25 times larger than CO_2 and GHG indirect emissions from biogas production aren't negligible, as described by the introduction chapter. It is worth remembering that

each 1% of methane slip means around 50 g CO_{2eq}/kWh$_{el}$ (in the case biomethane is burned by a gas engine with an electrical efficiency of 40%).

The following chapters will try to develop a calculation approach in order to assess all relevant data regarding in particular methane loss reduction and energy consumptions, provided that the purity target of upgrading is at least 97% of methane. The upgrading techniques that will be analysed are physical and chemical absorptions and pressure/vacuum swing adsorption. Membrane and cryogenic technologies seems to be still too high in methane slip and energy consumption and too little proven in real scale plants to be considered for the present assessment. However, a specific section (chapter 4) will deepen the most recent developments regarding membrane and cryogenic technologies.

Nevertheless, in order to develop a sensible assessment of upgrading technical performances, it should be remembered that biogas cleaning processes could strongly influence the feasibility of many upgrading techniques, in particular as far as hydrogen sulphide removal is concerned. As a matter of fact, H_2S must be almost totally removed when the upgrading technique is Pressure Swing Adsorption (in fact, hydrogen sulphide would be adsorbed irreversibly); the removal of hydrogen sulphide is also strongly advisable for chemical absorption with aqueous alkanolamine solutions and physical absorption with organic solvents in order to reduce costs (the selectivity for hydrogen sulphide is very high compared to carbon dioxide and regeneration of both solvents from H_2S would require increased energy input).
On the contrary, when CO_2 is removed by means of pressurized water, hydrogen sulphide abatement is not strictly necessary, in particular when concentrations are not large. Nonetheless, if water regeneration is carried out through air stripping, elemental sulphur is formed which can cause operational problems (deposits/clogging); moreover, hydrogen sulphide has an extremely low odour threshold (in the order of ppb), then any odour nuisance should be avoided.
Based on the reported reasoning, even though the cleaning requirements are not the same for all the considered upgrading techniques, it could be concluded that an efficient H_2S removal before any upgrading process is performed is strongly advisable. The next chapter will report some general information about H_2S removal.

2.1 Removal of hydrogen sulphide

Hydrogen sulphide contained by biogas produced by the anaerobic digestion of cattle slurry and energy crops could show concentrations up to 2000 ppm. Pre-treatment process that could be considered suitable for the most delicate upgrading techniques should reduce the concentration to a few ppm, typically less than 10 ppm.
Hydrogen sulphide can be removed at a very early stage inside the digester through the biological aerobic oxidation of H_2S to elemental sulphur by a group of specialized microorganisms. Most of those sulphide oxidizing micro-organisms (Thiobacillus) are autotrophic and use CO_2 from the biogas to cover their carbon need. They grow on the surface of the digestate or on the framework of the digester and do not require inoculation. A small amount (2-6%) of O_2 needed for the reaction to occur is introduced in the biogas system by an air pump. The removal efficiency is quite good but the remaining concentration is still too high for our purposes (100-300 ppm); moreover, the presence of oxygen could imply difficult upgrading (in particular when oxygen decomposes reagents such as alkanolamines). A second possibility is the introduction of iron chloride directly into the digester or through the influent mixing tank. It reacts with the H_2S present in the biogas to form F_eS that is almost insoluble and precipitates; also in this case, the final H_2S concentration is not as low as the required one, being around 100-150 ppm. As a consequence, hydrogen sulphide removal inside the digester could be considered as pre-treatment stages for a more efficient abatement device when the starting H_2S concentrations are very large.
As far as H_2S removal after digestion is concerned, the first principle that should be described is adsorption on activated carbon. Hydrogen sulphide is adsorbed on the inner surfaces of engineered activated carbon with defined pore sizes. Addition of oxygen (in the presence of water) oxidizes H_2S to plane sulphur that binds to the surface. In order to increase the speed of the reaction and the total load, the activated carbon is

either impregnated or doped (by addition of a reactive species before formation of the activated carbon) with permanganate or potassium iodide (KI), potassium carbonate (K_2CO_3) or zinc oxide (ZnO) as catalysers. H_2S removal is extremely efficient with resulting concentrations of less than 3 ppm. Best efficiency is obtained at pressures of 7-8 atm and temperatures of 50-70 °C. In spite of the very good removal efficiencies, adsorption involves expensive investment and operative costs (due in particular to biogas compression requirements), the presence of oxygen that is negative for the following upgrading and, most of all, large methane losses. Since the reduction of methane losses and energy costs is one of the main target of the present study, H_2S removal by means of adsorption on activated carbon doesn't seem to be particularly suitable.

The third option to eliminate H_2S is physical absorption with pressurized water as hydrogen sulphide is much more soluble than CO_2 and CH_4 (respectively 2.6 and 74 times more soluble); in this case, very low H_2S concentration would be reached by means of quite large pressures (around 10 atm), causing high operative costs and, again, very important methane losses. Moreover, the H_2S desorbed after contacting can result in fugitive emissions and odour problems.

One of the oldest methods for H_2S removal involves sodium hydroxide (NaOH) chemical absorbing. A solution of sodium hydroxide and water enhances scrubbing capabilities (for both H_2S and CO_2 removal) because the physical absorption capacity of the water is increased by the chemical reaction of the NaOH and the H_2S. The enhanced absorption capacity results in lower volumes of process water and reduced pumping demands. Because of the high technical requirement to deal with the caustic solution, its application is hardly applied anymore except when very large gas volumes are treated or high concentrations of H_2S are present, that is not the case of biogas plants. Moreover, NaOH would react also with CO_2 contained into biogas, that has a much larger partial pressure and then would consume a considerable part of reactant. A selective scrubbing for H_2s with CO_2 present should be based on different absorption rates through a short-contact-time reactor and the control of Temperature and pH. However, this kind of design would be quite complicated in order to achieve the desired H_2S removal while minimizing caustic consumption and CO_2 absorption; moreover, the reaction results in the formation of sodium sulphide and sodium hydrogen sulphide, which are insoluble and non-regenerative, involving prohibitive costs.

Another possible method to remove H_2S is the use of a semi-permeable membrane. H_2S (and CO_2) can pass the membrane whereas CH_4 cannot. Nevertheless, the use of membranes to remove hydrogen sulphide involves complex and expensive operation and maintenance; moreover, separated H_2S should be correctly managed.

As one can easily observe, the so far described treatment techniques wouldn't comply with the requirements of low energy-reactant-disposal costs and minimized methane losses that we are putting as a target. The author individuates the following removal processes as the most interesting in this sense:

- Biological filtration on a trickling filter;
- Chemical absorption with a solution of ferric chloride;
- Reaction beds made up of metal oxides and hydroxides.

The first method is similar to the technique where air/O_2 was added to the digestion tank. It is based on the use of specific bacteria that are able to oxidize H_2S. Before entering the filter bed, filled with plastic carriers, 4-6% air is added to the biogas. The H_2S is absorbed in the liquid phase, made up from gas condensate and liquid from effluent slurry separation. After absorption, H_2S is oxidized by the bacteria, growing on the filter bed. A temperature of approximately 35 °C promotes the process in which the H_2S is biologically converted to sulphur. The utilization of this method is increasing because it is cheaper than chemical cleaning. The method is also able to remove ammonia from the biogas. In this case, final H_2S concentration can be lower than 10 ppm, low operative costs and methane losses, but the presence of oxygen implies some additional upgrading step.

Chemical absorption with a solution of ferric chlorides aims at the formation of an insoluble sulphide, involves low pressures and consequently low methane losses, but it is not regenerative, precipitates need to be disposed of.

Finally, the most suitable technique seems to be the use of metal oxide processed to granules/pellets to be used in a reaction bed (the example of the registered trademark Sulfa Treat is often reported).

The solid phase is packed in a circular reactor vessel. Biogas is fed into the reactor from the top. The reason for this is that the reaction is exothermic and water is used to cool the solid bed. With a downstream gas flow the water is better distributed in the bed. The gas flow is saturated with water and excess water is added to the reaction bed. Reaction temperature is dependent on the hydrogen sulphide content in the biogas. The

reaction bed is not heated. If it is important to keep the H_2S content in the cleaned gas to virtually zero (the removal efficiency is very high), gas sampling can be done in the bed at some distance from the gas outlet. When the H_2S content increases in the sample, the bed material is removed and the reactor is recharged with fresh material. For completely continuous running, two reactors can be installed and switched when the H_2S content starts to increase. Adsorption using iron boxes is a simple, cheap and easy to operate and maintain method in which high removal efficiencies can be obtained. The Swedish Gas Center (SGC, 2001) reports an operative cost of 6000 €/y for a contaminant load of 0.5 m^3 H_2S/h, that is a very low cost.

On the basis of the reported technological analysis, it can be concluded that hydrogen sulphide removal is a fundamental step of the overall biogas treatment; in the case operative costs, methane losses and environmental impacts due to this phase are minimized, as we tried to do in the present chapter, the pre-treatment stage wouldn't have heavy influences on the results of the following upgrading process analysis as far as environmental and energy performances are concerned. Otherwise, hydrogen sulphide removal could involve industrial costs and environmental drawbacks that could strongly address the choice of the subsequent upgrading technique.

3   Upgrading process optimization

Before the development of assessments regarding the upgrading processes, it is important to define biogas flow rates and biogas features to be treated in order to produce biomethane.

The present study assumes that biogas is produced through the anaerobic digestion of animal manure and energy crops according to the most frequent observed technical configuration in Northern Italy.

Anaerobic digestion is a series of processes in which microorganisms break down biodegradable material in the absence of oxygen. It is generally used for industrial or domestic purposes to manage waste and/or to release energy.

The digestion process begins with bacterial hydrolysis of the input materials to break down insoluble organic polymers, such as carbohydrates, and make them available for other bacteria. Acidogenic bacteria then convert the sugars and amino acids into carbon dioxide, hydrogen, ammonia, and organic acids. Acetogenic bacteria then convert these resulting organic acids into acetic acid, along with additional ammonia, hydrogen, and carbon dioxide. Finally, methanogens convert these products to methane and carbon dioxide.

In Italy the feedstock for anaerobic digestion plants is usually formed by cattle slurry and energy crops (maize in most of the cases) with a proportion usually very close to 50/50; in the present paper we took into account a mesophilic (42 °C) digestion plant fed by 41 t/d of cattle slurry and 40 t/d of maize (109 m^3/d of fresh matter), with a hydraulic retention time around 60 days, producing 11845 Nm^3/d of biogas (53% formed by methane) according to the most reliable biogas producibility data.

The produced biogas amount, corresponding to 2.5 MW of thermal energy at disposal, is generally burned by a Otto engine, generating around 1 MWe (the engine electric efficiency is around 40%) and more or less the same amount as far as the thermal power is concerned. Table 3.1 reports all the described data.

Table 3.1: biogas production data

	t/d	m^3/d	DM	VS on DM	VS (kg/d)	biogas producibility (Nm^3/t SV)	expected biogas (Nm^3/d)	expected CH_4 (Nm^3/d)	power IN (MW_{th})	power OUT (MW_e)
cattle slurry	41	58.57	0.22	0.75	6765	400	2706	1434	0.57	0.27
maize silage	40	50.00	0.34	0.96	13056	700	9139	4844	1.93	0.73
total	81	108.57	0.28	-	19821	-	11845.20	6277.96	**2.51**	**1.00**

The next analyses will take into account the upgrading treatment of the expected biogas flow rate that would produce 1 MW_e if burned in an ordinary biogas engine, that is:

Expected biogas production: 11 845.2 Nm^3/d / 24= 493.55 Nm^3/h.
Methane content v/v: 53%.
CO_2 initial molal fraction: $y_b = 0.47$.
Biogas molal flow: V_b = 493.55 Nm^3/h / 22.414 Nl/mol · 1000= 22 019.7 mol/h.
or, in customary USA units: V_b = 493.55 Nm^3/h · 35.315 ft^3/m^3 / 379.48 ft^3/lb-mol = 48.55 lb-mol/h.
CO_2 percentage accepted for biomethane (to be injected into NG grid): 3%.
Biomethane molal flow: V_a= V_b*0.53/0.97 = 12 031 mol/h (or 26.53 lb-mol).
CO_2 final molal fraction: $y_a = 0.03$.

3.1 Physical absorption with water

This technique is based on the principle of using water to absorb carbon dioxide at high pressures, while methane mainly remains in gaseous phase. Biogas is generally introduced from the bottom of a tall vertical tower and water is fed at the top of the column to achieve an intimate gas-liquid contact in counter flow. Physical absorption or scrubbing is based on the solubility of CO_2 into water, that is the physical equilibrium ruled by Henry's law.
In physics, Henry's law is states that:
at a constant temperature, the amount of a given gas that dissolves in a given type and volume of liquid is directly proportional to the partial pressure of that gas in equilibrium with that liquid.
An equivalent way of stating the law is that the solubility of a gas in a liquid at a particular temperature is proportional to the pressure of that gas above the liquid. Henry's law has since been shown to apply for a wide range of dilute solutions, not merely those of gases.

Henry's law constant (generally called H) for CO_2-water system (after Carroll et al, 1991, for dilute solutions) can be calculated as:

$$\ln(H/MPa) = -6.8346 + 1.2817 \cdot 10^4 /T - 3.7668 \cdot 10^6 /T^2 + 2.997 \cdot 10^8 /T^3$$

Table 3.2 reports the calculated CO_2 solubility for different temperatures.

Table 3.2: solubility of carbon dioxide in water

T (K)	H (MPa/mol frac)	H (atm*l/moli)
283	1.04E+02	1.85E+01
288	1.22E+02	2.16E+01
293	1.41E+02	2.50E+01
298	1.61E+02	2.87E+01
303	1.83E+02	3.25E+01
308	2.06E+02	3.66E+01
313	2.30E+02	4.09E+01

Figure 3.1 shows the same correlations reported by Table 3.2.
In order to define the border conditions, the initial CO_2 water concentration x_a is defined by the equilibrium with the partial pressure of CO_2 in air (388 ppm): so, both in the case we use always new water and we regenerate absorbing water by means of air stripping at 1 atm, equilibrium molar fraction of CO_2 in water at 283 K before a new absorption is:

$x_a \sim 388 * 10^{-6} /104/10 = 3.7\ 10^{-7}$ as CO_2 atmospheric concentration is around 388 ppm

The overall material balance on the terminal streams of an absorbing tower (showed by Figure 3.2), based on component A (in this case CO_2), can be expressed as:

$$L_a x_a + V_b y_b = L_b x_b + V_a y_a$$

$$x_b = \frac{L_a x_a + V_b y_b - V_a y_a}{L_b}$$

where L and V are molal flow rate for liquid and gas phase, x and y are CO_2 mole fraction.

Moreover, the material balance for the portion of the column above an arbitrary section (see Figure 3.2) and the operating-line equation for a differential-contact plant can be written down as follows:

$$L_a x_a + V y = L x + V_a y_a$$

$$y = \frac{L}{V} x + \frac{V_a y_a - L_a x_a}{V}$$

Figure 3.1: Henry's law constant for carbon dioxide in water

17
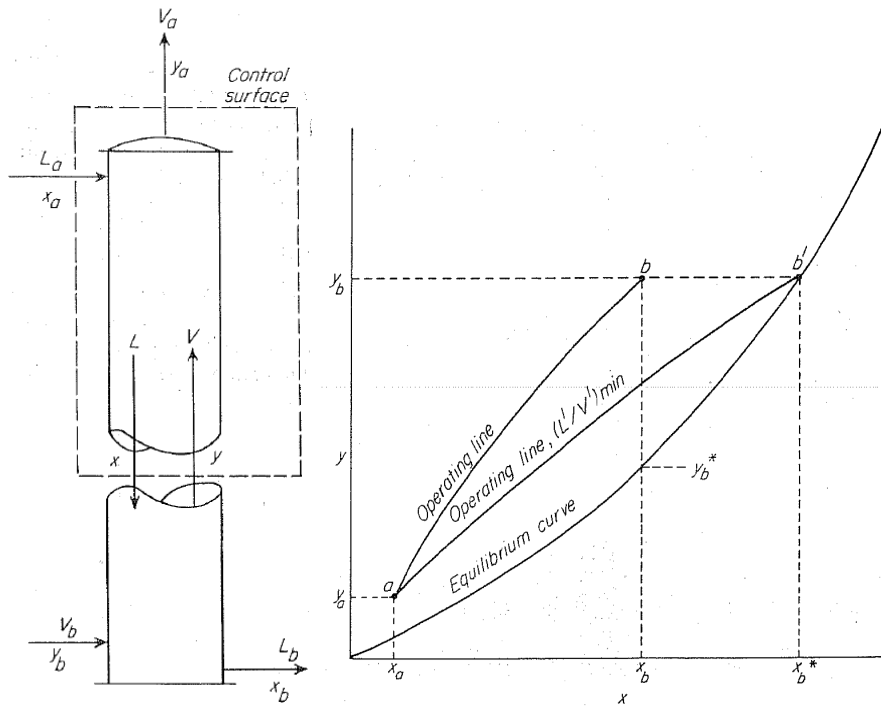
Figure 3.2: material-balance diagram for a packed column

As far as pressure drop inside the column is concerned, for absorption packed towers the design values should be between 0.25 and 0.5 inch H_2O per foot of packing in order to avoid flooding. Obviously, the lower the gas velocity, the lower the cost of power and the larger the tower; the higher the gas velocity, the larger the power cost and the smaller the tower. Figure 3.3 gives correlations for estimating flooding velocities and pressure drops in packed towers. It consists of a logarithmic plot of

$$\frac{G_y^2 F_p \mu_x^{0.1}}{g_c(\rho_x - \rho_y)\rho_y} \quad vs \quad \frac{G_x}{G_y}\sqrt{\frac{\rho_x}{\rho_x - \rho_y}}$$

Where G_x = mass velocity of liquid, lb/ft^2-s

G_y = mass velocity of gas, lb/ft^2-s

F_p = packing factor, ft^{-1}

ρ_x = density of liquid, lb/ft^3

ρ_y = density of gas, lb/ft^3

μ_x = viscosity of liquid, cP

g_c = Newton's law proportionality factor, 32.174 ft-lb/lb-s^2

For the studied case, if we assume:
tower surface of 1 m^2,
V_b= 22 020 mol/h,
G_y = 22 020 mol/h * (0.53*16 + 0.47 * 44) g/mol /1 m^2 =642.1 kg/h/m^2 = 131.6 lb/ft^2/h,
Liquid flow rate = 50 m^3/h, G_x = 10 248 lb/ft^2/h,
Tower packings made up of pall rings, steel, 1 inch, porosity at 94%, Fp = 48,

we would obtain that pressure drop is below 0.1 inch H_2O per foot of packing, that is far enough from the flooding. Table 3.3 reports some simulations regarding the pressure drops deriving from different water flow rates and tower surfaces: the bold font highlights the feasibility conditions (that is pressure drops lower than 0.5 inch H_2O/foot).

Table 3.3: pressure drop in packed towers

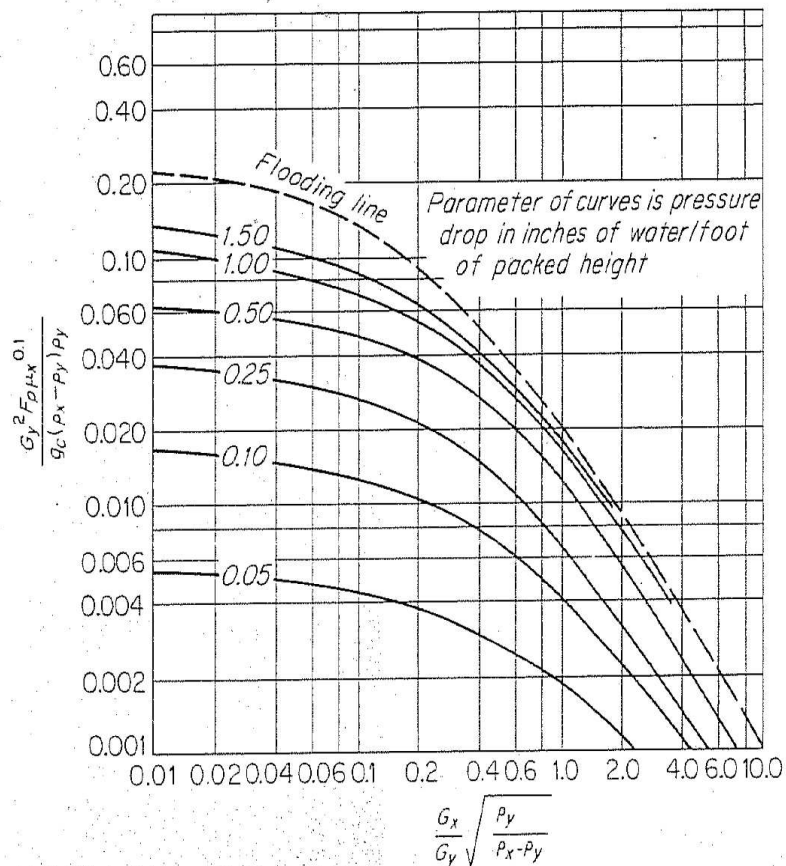| tower surface S (cm^2)	L (m^3/h)	G_x (lb/ft^2/h)	pressure drop (inch H_2O/foot)
1 962 ($\Phi = 0.5$ m)	50	52 229	> flooding line
3 847 ($\Phi = 0.7$ m)	50	26 648	**<0.5**
7 850 ($\Phi = 1$ m)	50	13 057	**<0.1**
7 850 ($\Phi = 1$ m)	50	13 057	**<0.1**
3 847 ($\Phi = 0.7$ m)	75	39 971	0.5-1
5 672 ($\Phi = 0.85$ m)	75	27 109	**0.1-0.25**
7 850 ($\Phi = 1$ m)	75	19 586	**<0.1**
3 847 ($\Phi = 0.7$ m)	100	53 295	> flooding line
7 850 ($\Phi = 1$ m)	100	26 115	**<0.25**
7 850 ($\Phi = 1$ m)	120	31 338	**<0.5**
7 850 ($\Phi = 1$ m)	175	45 701	**~0.5**

Figure 3.3: generalized correlation for flooding and pressure drop in packed towers

Provided that the operating curve can be defined on the base of the reported correlations, it's important to observe the behaviour of the parameters L and V along the column. L is likely to be very large if compared to the CO_2 amount to be absorbed. For example, 50 m³/h = 50 * 10^6 g/h / 18 g/mol =2.7 x 10^6 mol/h of water; CO_2: 22 020 · 0.47 – 12 031 · 0.03 = 9 988 mol/h = 439.5 kg/h, that is the molal variation between L_a and L_b is around 0.36%. As a consequence, the variation could be considered negligible and L could be assumed to be constant along the absorbing tower. Anyway, in order to produce a strictly analytical approach, L is determined on the base of a simple mass balance:

$$L = L_a \cdot \frac{1 - x_a}{1 - x}$$

As far as V is concerned, the variation along the column is very large, from 22 020 to 12 031 mol/h, so that the operating line is not straight but it is strongly curved.

$$V = V_b - (L_b \cdot x_b - L \cdot x)$$

Figure 3.4 reports the curves at 15 atm and 283 K, the one at the top refers to a water flow rate of 50 m³/h whereas at the bottom the limiting gas-liquid ratio condition is reported (26,5 m³/h of water flow), that correspond to the minimum liquid flow rate that is ideally required for a tower of infinite height.

It is important to observe that, when a rich gas is fed to an absorption tower, that is our case, the solution temperature can raise according to CO_2 heat of absorption (around 19 kJ/mol at 288 K) and this configuration would change the equilibrium curve. In our case it could be calculated that when L correspond to 50 m³/h, the temperature increase of water is:
ΔT = 9 988 mol CO_2/h · 19 kJ/mol / 4.186 kJ/kcal / 50 / 10^3 kg/h / 1 kcal/kg/K = 0.91 K
That is we can neglect the temperature variation between the top and the bottom of the packed tower.

The general discussion about mass transfer dealing with absorption can be resumed as:

$$r\left[\frac{kmol}{m^3 \cdot h}\right] = k_y \cdot a \cdot (y - y_i) = k_x \cdot a \cdot (x_i - x)$$

$$r\left[\frac{kmol}{m^3 \cdot h}\right] = K_y \cdot a \cdot (y - y^*) = K_x \cdot a \cdot (x^* - x)$$

$$\frac{1}{K_y} = \frac{1}{k_y} + \frac{H}{k_x}$$

$$\frac{1}{K_x} = \frac{1}{k_x} + \frac{1}{H \cdot k_y}$$

where r is the rate of absorption per unit volume of packed column, k_x and k_y are individual mass transfer coefficients for liquid and gas phase, a is the area of interface per unit packed volume, y_i and x_i are interface concentration or mole fraction of solute (CO_2), y* and x* are concentration or mole fractions at the equilibrium (according to Henry's law), H is Henry's constant, K_x and K_y are overall mass transfer coefficients (see also Figure 3.5).
Within the present analyses, chemical reactions that occur for the mixture CO_2-water, that is equilibrium CO_2(aq)-carbonic acid-bicarbonate-carbonate, won't be taken into account since mass transfer and chemical reaction could be very difficult to treat together; however, the present analysis, just physical, is going to produce more conservative results as chemical reactions would increase the driving force at disposal for absorption, helping CO_2 removal from biogas.
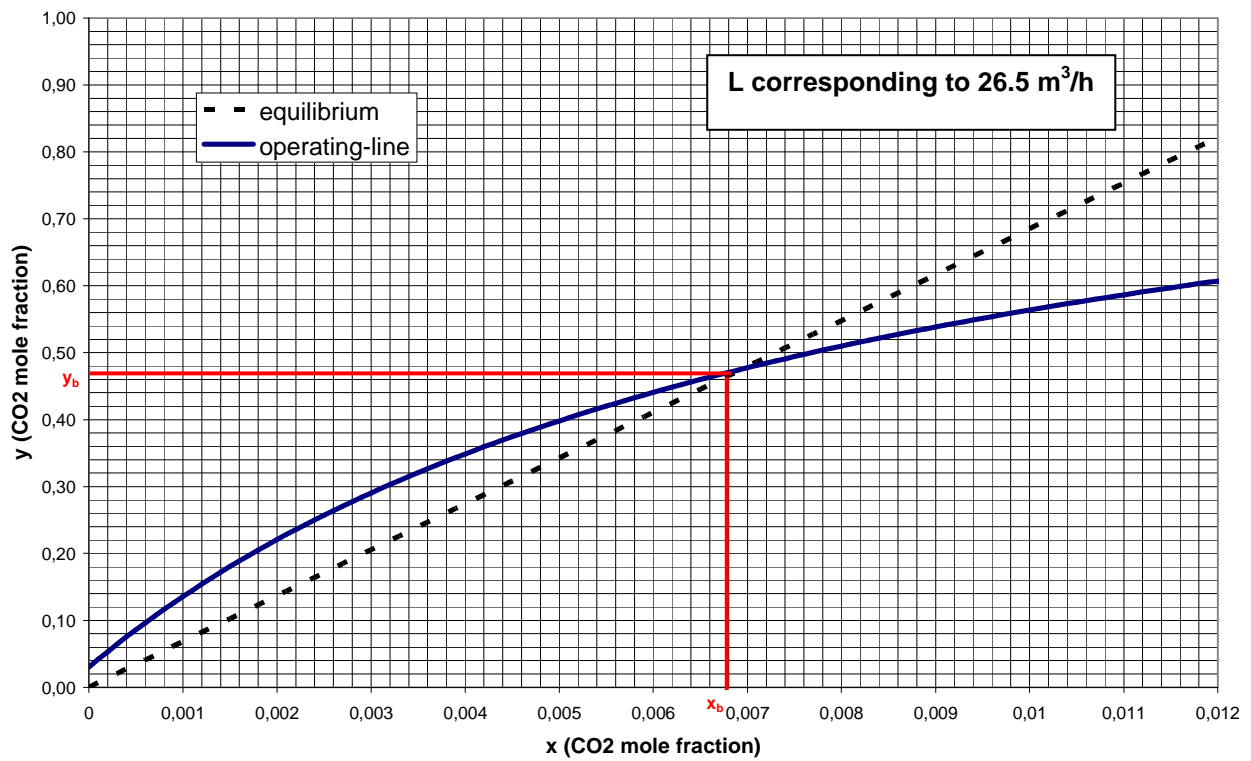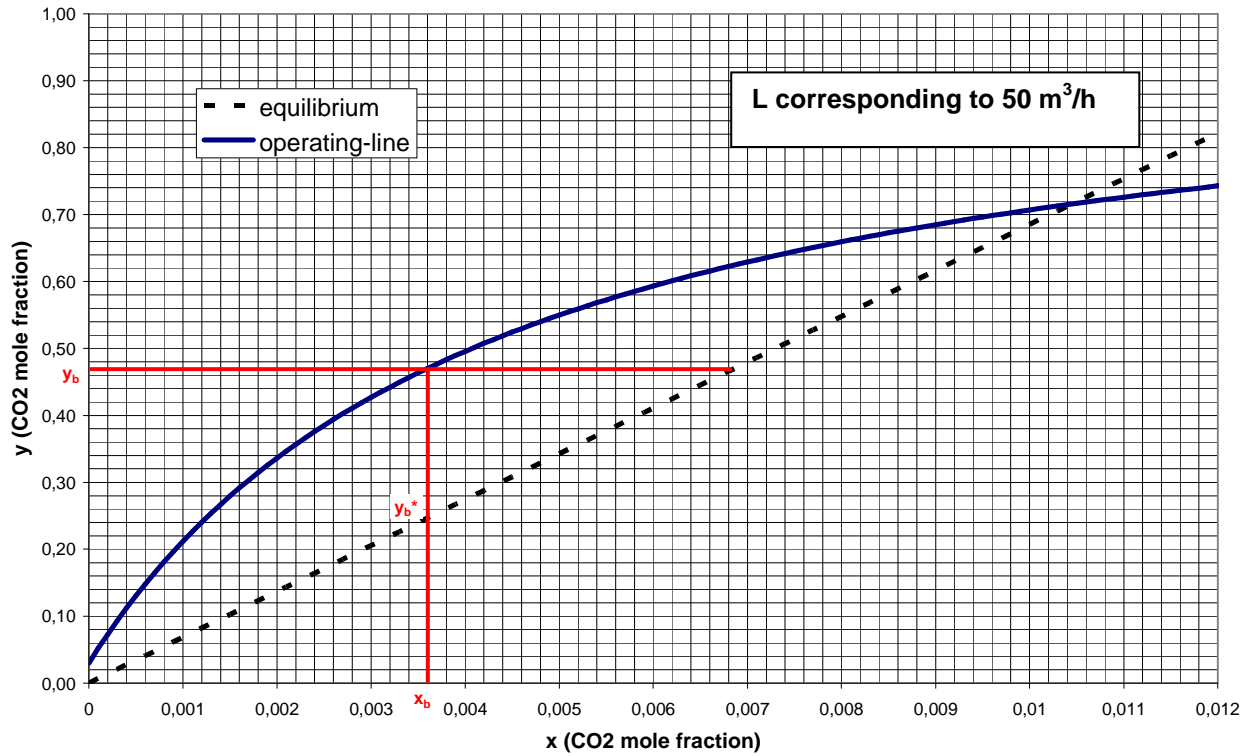
Figure 3.4: equilibrium line (dashed) and operating curve (continuous)
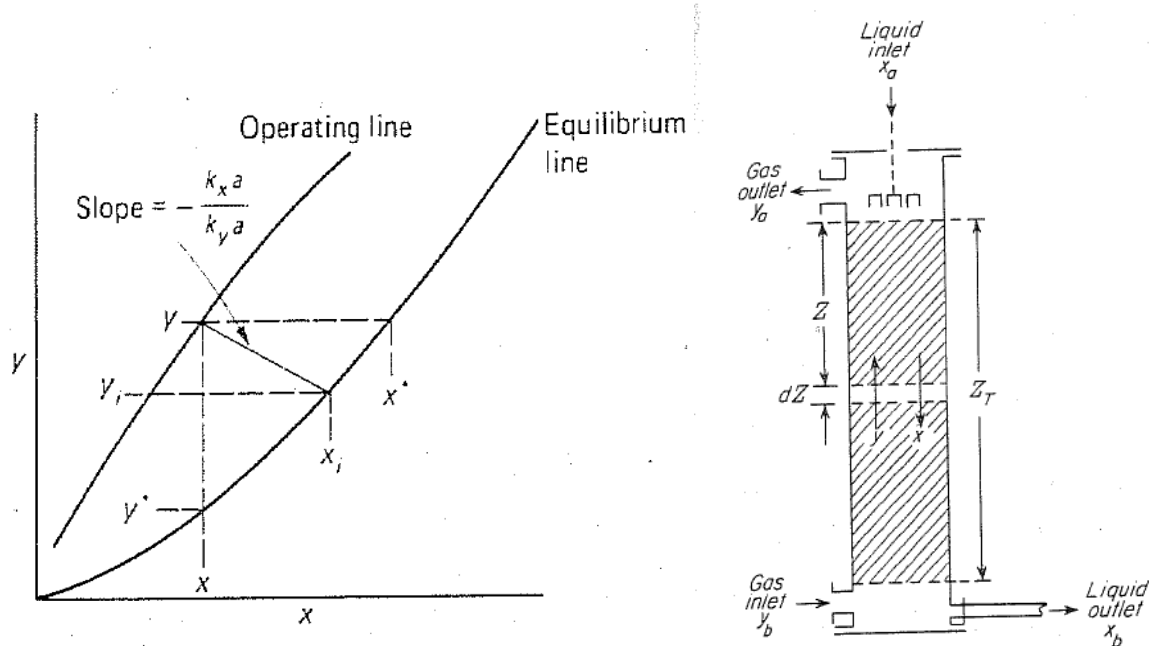
Figure 3.5: location of interface composition

The amount of solute dN_{CO2} absorbed in a differential height dZ (see also Figure 3.5) is $d(Vy)$, since both V and y decrease as the gas rises through the column (absorption from rich gases).

$$dN_{CO2} = d(Vy) = Vdy + ydV$$

If only CO_2 is transferred from gas to liquid phase, dN_{CO2} equals dV, so:

$$dN_{CO2} = Vdy + ydN_{CO2}$$

$$dN_{CO2} = \frac{V \cdot dy}{1-y} = K_y a \cdot S \cdot dZ \cdot (y - y^*)$$

In this case, the effect of one way diffusion in the gas film, that should increase the mass transfer rate of the gas film is neglected in order to realize an easier and more conservative examination.

$$Z_T = \frac{1}{S} \int_a^b \frac{Vdy}{(1-y) \cdot (y - y^*) \cdot K_y a}$$

As far as the definition of mass transfer coefficients is concerned, experimental data are generally based on system where one resistance (the liquid or the gas film) is controlling, since it is very difficult to separate the two resistances accurately when they are of comparable magnitude.

In the case of CO_2 absorption in pure water or aqueous solutions, the liquid film resistance is normally dominant and the mass transfer coefficients are quite variable, according to the liquid flow rate and the tower surface (that is to say G_x, mass velocity of liquid). Figure 3.6 reports the mass transfer coefficients for the absorption and reaction of CO_2 in 4 percent NaOH solution, taken from McCabe Handbook; it is important to underline that in this case the mass transfer coefficients units refers to USA ones, that is lb-mol/ft^3/atm/h.

The K_ga values (or K_ya, that is the same after the multiplication by the total pressure) are claimed to be 20 to 40 times the normal values for CO_2 absorption in water, because the chemical reaction between CO_2 and NaOH takes place very close to the interface, making the concentration gradient (or driving force) for CO_2 much steeper. The typical values of mass transfer coefficients for CO_2 and water are 0.05-0.2 lb-mol/ft³/atm/h. Assuming tower surfaces and liquid flow rates suitable to acceptable pressure drops (that is the bold font cases reported by Table 3.3), G_x ranges from 13,000 to 26,000 lb/ft²/h, that is K_ga for pall rings − 1 inch is around 4 lb-mol/ft³/atm/h for CO_2-NaOH systems, that is at least 0.1 lb-mol/ft³/atm/h for CO_2 absorbed in pure water. Very similar mass transfer coefficients are confirmed by Kohl (1997), as pointed out by Figure 3.7 (K_ga = 0.07 lb-mol/ft³/atm/h). Based on the reported reasoning, the overall mass transfer coefficient K_ga (referring hence to CO_2 partial pressures) is assumed equal to 0.1 lb-mol/ft³/atm/h, that is to say around 1589 mol/m³/atm/h (45 mol/ft³/atm/h).
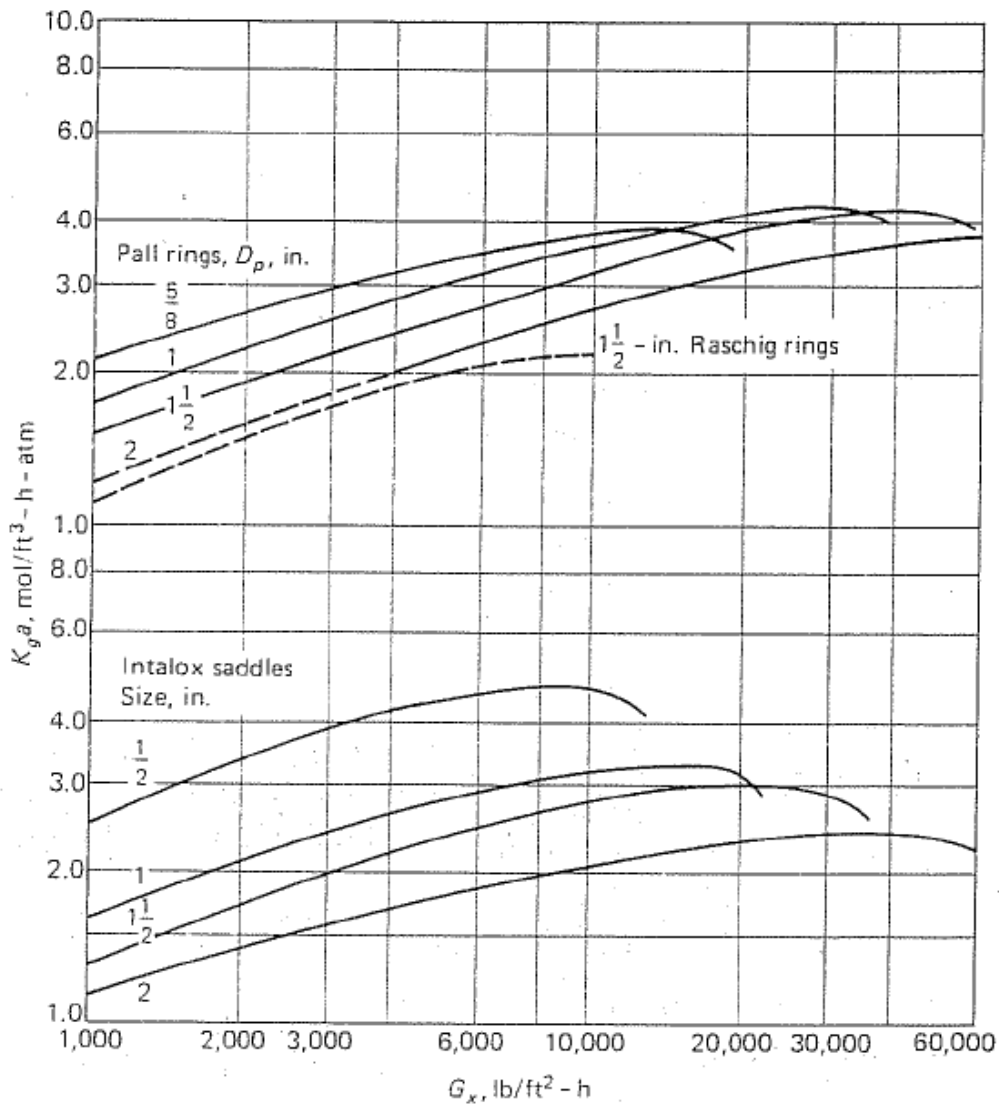
Figure 3.6: mass transfer coefficients for the absorption and reaction of CO_2 in 4 percent NaOH solution

Table 1-5 Typical K_Ga Values for Various Absorbate/Absorbent Systems						
	KGa, lb moles/(hr) (ft3) (atm)					
	Absorbent					
	Water			Aqueous Solutions		
Absorbate	A	B	C	Solution	A	B
CO_2			0.07	4% NaOH	2.0	1.5
H_2S			0.4	4% NaOH	5.92	4.4
SO_2	2.96	2.2	0.32	11% Na_2CO_3	11.83	8.93
HCN	5.92	4.4				
HCHO	5.92	4.4				
Cl_2	4.55	3.4	0.14	8% NaOH	14.33	10.8
Br_2				5% NaOH	5.01	3.7
ClO_2	4.4	4.4				
HCl	18.66	14.0	16.0			
HBr	5.92					
HF	7.96	6.0				
NH_3	17.30		13.0	Dilute acid	13.0	13.0
O_2			0.007			

Notes:

A = data for #2 plastic Super Intalox packing, gas velocity 3.5 ft/s, liquid rate 10 gpm/sq ft. (ASHRAE Handbook, 1988)

B = data for #2 plastic Super Intalox packing, gas velocity 3.5 ft/s, liquid rate 4 gpm/sq ft. (Strigle, 1994)

C = data for 1.5 in Intalox Saddles, conditions not stated. (Eckert et al., 1967)

Figure 3.7: mass transfer coefficients for various absorbate/absorbent systems

If we assume that mass transfer coefficient doesn't changes along the column provided that L is quite constant and K_ga depends on liquid velocities, then the tower height can be obtained numerically by means of the reported integral equation. The calculation step of the numerical approach has been set at $\Delta x=1.0\ E^{-5}$ that is suitable to the analysis' purpose. Table 3.4 reports the results according to different operative parameters: liquid flow rates and tower diameters are all within the feasibility conditions given by acceptable pressure drops (see Table 3.3), operative pressures lie in the range 6-12 atm and temperatures are 283-303 K (10-30 °C), that is ordinary ambient conditions.

As one can easily observe, the absorption of CO_2 with pure water is surely possible, but it requires high pressures (higher than 6 atm) and high L/V rates (12÷24 m^3 of liquid for every 100 Nm^3 of processed biogas), in particular when temperatures approaches 30°C (one of the main assumptions is that refrigeration of liquid flows is not scheduled). Under these conditions, the height of the packed tower that can reduce the CO_2 mole fraction contained in ~500 Nm^3/h of biogas to 3% lies in the range of 10÷20 m when the tower diameter is 1 m.

Table 3.4: absorbing tower dimensions

L (m³/h)	P (atm)	T (K)	tower diam (m)	L/V (m³ of liquid for every 100 Nm³ of processed biogas)	tower height (m)
50	6	283	1	10.1	not possible
100	6	283	1	20.3	10.92
100	6	298	1	20.3	pinch point
120	6	298	1	24.3	14.93
120	6	303	1	24.3	22.25
50	8	283	1	10.1	19.69
50	8	298	1	10.1	not possible
100	8	298	1	20.3	9.54
100	8	303	1	20.3	11.72
40	10	283	1	8.1	15.58
75	10	298	1	15.2	8.37
75	10	303	1	15.2	11.17
35	12	283	1	7.1	9.74
55	12	298	1	11.1	9.27
60	12	303	1	12.2	11.04

Nevertheless, it is important to report that the application of pure water scrubbing to upgrade biogas is attested by several technical articles; in particular, the Swedish Gas Center (SGC, 2001) claimed that some water scrubbers were running in 2001 in Sweden, as reported by Figure 3.8.

As one can easily observe from the reported data, pressures, temperatures and specific water flows (12-20 m³ for every 100 m³/h of biogas) are very close to those assumed or obtained by the present analysis but figures regarding the specific tower volumes (m³ of tower / m³/h of processed gas) are totally missing.

Parameter	Unit	Process	Plant examples			
			Plant 1	Plant 2	Plant 3	Plant 4
Location/name			Trollhättan	Uppsala	Linköping	Kalmar
Capacity range	m³ biogas/h	10 - 1000	140	200	660	60 - 70
Input						
· methane	%	45 - 75	60 - 70	63 - 70	68 - 69	64 - 67
· carbon dioxide	%	25 - 55	29 - 39	29 - 36	30 - 32	33 - 36
· nitrogen	%	< 1	no data	no data	0 - 0.1	0
· hydrogen sulphide	ppm	< 200[7]	no data	no data	70	100 - 450
Output						
· methane	%	> 98	96 - 97	93 - 97	96 - 98	94 - 96
· carbon dioxide	%	< 2	1.5 - 2	2 - 4	2.3	4 - 6
· air	%	< 1.5	1	1 - 2.5	0-1	0 - 1
· dewpoint	°C	20 - 35	-100	-80	< -80	< -30
Process conditions						
· adsorption pressure	Bar	6 - 12	6 - 7	7.5	8 - 8.5	8
· adsorption temperature	°C	20 - 35	no data	no data	no data	no data
· pressure in flash tank	bar	2 - 5	no data	no data	no data	no data
· desorption pressure	bar	atmospheric	atmospheric	atmospheric	atmospheric	atmospheric
· water flow[8]	m³/h	12 - 20	no data	no data	no data	no data
Supplier			FEAB	FEAB	FEAB	FEAB
Investment	M€		no data	0.86	2.5	no data
Operational costs	K€/year		no data	no data	no data	no data

Table 13: Removal of carbon dioxide using water wash with regeneration

[7] High pressure system included

[8] Depending on the absorption pressure and degree of regeneration, for every 100 m³/h processed biogas

Figure 3.8: biogas upgrading plants is Sweden (SGC, 2001)

Besides the already described direct carbon dioxide absorption design, it should be remembered that CO_2 is not the only molecule to be absorbed by water: methane can be absorbed as well, though CH_4 is much less soluble than CO_2 in water, making overall design calculation not so straightforward.
Henry's law constant for methane in water is given by Lide and Frederikse (1995):

$$H\left[\frac{mol/l}{atm}\right] = 1.4 \cdot 10^{-3} \cdot \exp\left[1600 * \left(\frac{1}{T} - \frac{1}{298.15}\right)\right]$$

As one can easily observe from Table 3.5, methane is about 25 times less soluble in water than CO_2; nonetheless, some methane is absorbed in water when upgrading biogas and we should avoid the release of methane towards the atmosphere during water regeneration or disposal (when water is note recycled) because of environmental and economic reasons. As a consequence we should calculate the simultaneous absorbing of methane and CO_2 into water, and, first of all, we need to know mass transfer coefficients of methane in water, that are not frequently discussed by literature.

Table 3.5: Henry's law constant for methane in water

T (K)	H (mol/l/atm)	H (atm/mol frac)
283	0.0019	29773.8
293	0.0015	36110.6
298	0.0014	39575.5
303	0.0013	43241.9

The definition of overall mass transfer coefficients can be carried out through the application of empirical correlations, such as the ones suggested by Sherwood and Holloway (1940) for random packings towers, that are usually based on the Schmidt number ($\mu_L/\rho_L D_L$) for the liquid phase, where D_L represents the parameter diffusivity of CH_4 in water.
The diffusivity in liquids are defined by Wilke and Chang (1955) as:

$$D_{AB} = \frac{7.4 \cdot 10^{-8} (\phi_B M_B)^{0.5} \cdot T}{\mu_B V_A^{0.6}}$$

where:
A is the solute (CH_4), B is the solvent (water);
Φ_B is the association factor (=2.26 for water);
M_B is molecular weight of solvent;
T is temperature in K;
μ_B is viscosity of solvent (centipoise): for water at ambient temperature μ_B=1 cP;
V_A is molecular volume of methane, defined as 29.6 cm^3/mol by La-Scalea et al (2005).

Based on this approach, diffusivity of methane in water is around 1.81 x 10^{-5} cm^2/s at 20°C (the diffusivity of CO_2 in water at 20°C is around 1.78 x 10^{-5} cm^2/s), whereas diffusivity of methane in air is around 1.58 x 10^{-5} m^2/s (Kirk and Othmer, 1998).

Sherwood and Holloway correlations state that:

$$H_L = a_L \left(\frac{L}{\mu_L} \right)^n \cdot \left(\frac{\mu_L}{\rho_L D_L} \right)^{0.5}$$

$$H_L = \frac{L_M}{k_L a}$$

$$H_G = \frac{a_G G^b Sc_v^{0.5}}{L^c}$$

$$H_G = \frac{G_M}{k_G a}$$

Where L and G are expressed as $lb/ft^2/h$, L_M and G_M in $lb\text{-}mol/ft^2/h$, Sc_v is the Schmidt number for the gas phase ($\mu_G/\rho_G/D_G$, where μ_G for gaseous methane is 0.01027 cP), n, a_L, a_G are defined by the following Figure 3.9 (taken from Perry's Chemical Engineer Handbook). If one consider 1 inch Berl saddles as packing material, the overall mass transfer coefficient $K_g a$ for methane in an absorbing tower ranges from 0.012 and 0.023 $lb\text{-}mol/ft^3/atm/h$ for the assumed operative conditions (tower diameter 1 m and L between 50 and 120 m^3/h), as reported by Table 3.6. Based on the reported reasoning, the overall mass transfer coefficient $K_g a$ (referring hence to CH_4 partial pressures) is assumed equal to 0.015 $lb\text{-}mol/ft^3/atm/h$, that is to say around 247 $mol/m^3/atm/h$ (7 $mol/ft^3/atm/h$).

Packing	a_G	b	c	G	L	a_L	n
				Raschig rings			
3/8 inch	2.32	0.45	0.47	200–500	500–1500	0.00182	0.46
1	7.00	0.39	0.58	200–800	400–500	0.010	0.22
1	6.41	0.32	0.51	200–600	500–4500	—	—
2	3.82	0.41	0.45	200–800	500–4500	0.0125	0.22
				Berl saddles			
1/2 inch	32.4	0.30	0.74	200–700	500–1500	0.0067	0.28
1/2	0.811	0.30	0.24	200–800	400–4500	—	—
1	1.97	0.36	0.40	200–800	400–4500	0.0059	0.28
1.5	5.05	0.32	0.45	200–1000	400–4500	0.0062	0.28

Figure 3.9: parameters suggested by Sherwood and Holloway for random packing towers

The overall mass transfer coefficient for methane is much lower than for CO_2, in spite of a very similar diffusivity of the molecules in water. This is due to the very low solubility of methane if compared to CO_2 (more than 20 times lower), since:

$$\frac{1}{K_G a} = \frac{1}{k_G a} + \frac{H}{k_L a}$$

Table 3.6: calculation of overall mass transfer coefficients for methane in water at 20°C

tower diam (m)	1	1	1.5	1.5	2	2
tower surface (cm2)	7850	7850	17662.5	17662.5	31400	31400
tower surface (ft2)	8.45	8.45	19.00	19.00	33.79	33.79
ρl (g/l)	1000.0	1000.0	1000.0	1000.0	1000.0	1000.0
ρl (lb/ft3)	64.0	64.0	64.0	64.0	64.0	64.0
ρg (lb/ft3)	0.0812	0.0812	0.0812	0.0812	0.0812	0.0812

L (m3/h)	50	120	50	120	50	120
L (moli/h)	2.78E+06	6.67E+06	2.78E+06	6.67E+06	2.78E+06	6.67E+06
Vb (moli/h)	22019.7	22019.7	22019.7	22019.7	22019.7	22019.7
L (lb/ft2/s)	3.627	8.705	1.612	3.869	0.907	2.176
G (lb/ft2/s)	0.047	0.047	0.021	0.021	0.012	0.012
μl (cP)	1	1	1	1	1	1
μl (lb/h/ft)	2.419	2.419	2.419	2.419	2.419	2.419
μg (cP)	0.01027	0.01027	0.01027	0.01027	0.01027	0.01027
μg (lb/h/ft)	0.025	0.025	0.025	0.025	0.025	0.025
Dl (ft2/h)	7.01E-05	7.01E-05	7.01E-05	7.01E-05	7.01E-05	7.01E-05
Dg (ft2/h)	0.61	0.61	0.61	0.61	0.61	0.61
H_L (ft)	1.52	1.94	1.21	1.55	1.03	1.32
kl a (lb-mol/h/ft3)	477.48	896.83	266.31	500.19	175.98	330.54
H_G (ft)	0.20	0.14	0.21	0.14	0.21	0.15
kg a (lb-mol/h/ft3)	29.19	41.43	12.56	17.83	6.90	9.80
Kg a (lb-moli/h/atm/ft3)	**0.012**	**0.023**	**0.007**	**0.013**	**0.005**	**0.008**

Based on the data calculated as described in the previous chapter, now the problem is to calculate the simultaneous absorption of the molecules CO_2 and CH_4. This is a very difficult matter that should be solved numerically. In order to try an analytical solution, even though approximated, one can write down the following 5 equations (and 5 unknown quantities: x_b, x'_b, L_b, Z and V_a):

$$CO_2) \quad L_b \cdot x_b = K_y a \cdot S \cdot Z \cdot \overline{\Delta y_L}$$

$$CH_4) \quad L_b \cdot x'_b = K'_y a \cdot S \cdot Z \cdot \overline{\Delta y'_L}$$

$$V_b \cdot y_b - V_a \cdot y_a = L_b \cdot x_b$$

$$V_a = V_b \cdot y_b - L_b \cdot x_b + V_b \cdot y'_b - L_b \cdot x'_b$$

$$L_b = L_a \cdot \frac{1}{1 - x_b - x'_b}$$

where Z is the tower height, quantities with the superscript refer to methane (for example x_b', y_b'), otherwise to CO_2, $K_y a$ and $K'_y a$ are overall mass transfer coefficients respectively for CO_2 and CH_4, Δy_L is the logarithmic mean of $y_b - y_b^*$ and y_a and y_a^*. The mass balances reported are all rigorous equations, the only approximation is the use of the described logarithmic mean values that would be applicable only when operating and equilibrium lines are straight.
The solution of the equations' system has been carried out for 4 specific conditions, the most conservative of those reported in Table 3.4 (that is when temperature is 303 K, pressures 6, 8, 10 and 12 atm). Table 3.7 points out that CO_2 liquid mole fractions at the bottom of the tower x_b are just slightly higher than those calculated with the mono-absorption approach, whereas methane final concentration in absorbing water is around one twentieth of CO_2 concentration; that is to say that more than 4% of methane contained by biogas is absorbed into water, not a small quantity. The calculated tower heights don't change substantially, in spite of the introduced approximations.

Table 3.7: calculation of simultaneous absorption of CO_2 and CH_4

L (m3/h)	P (atm)	T (K)	tower diam (m)	x_b *	x_b (recalculated)**	x'_b	CH_4 absorbed (%)	tower height (m)
120	6	303	1	1.496E-03	1.501E-03	7.35E-05	4.20%	22.25
100	8	303	1	1.795E-03	1.801E-03	9.81E-05	4.67%	11.72
75	10	303	1	2.392E-03	2.401E-03	1.23E-04	4.38%	11.17
60	12	303	1	2.988E-03	3.001E-03	1.47E-04	4.20%	11.04

* calculated by mono absorption approach (only CO_2 is absorbed)
** calculated by multi-absorption approach (CO_2 and CH_4 are absorbed into water)

To minimise the losses of methane, the water is usually depressurised in a flash tank (2÷5 atm) after leaving the absorption column, whether the water is regenerated or not.
Figure 3.10 and 3.11 report the layout of the two water wash configurations.
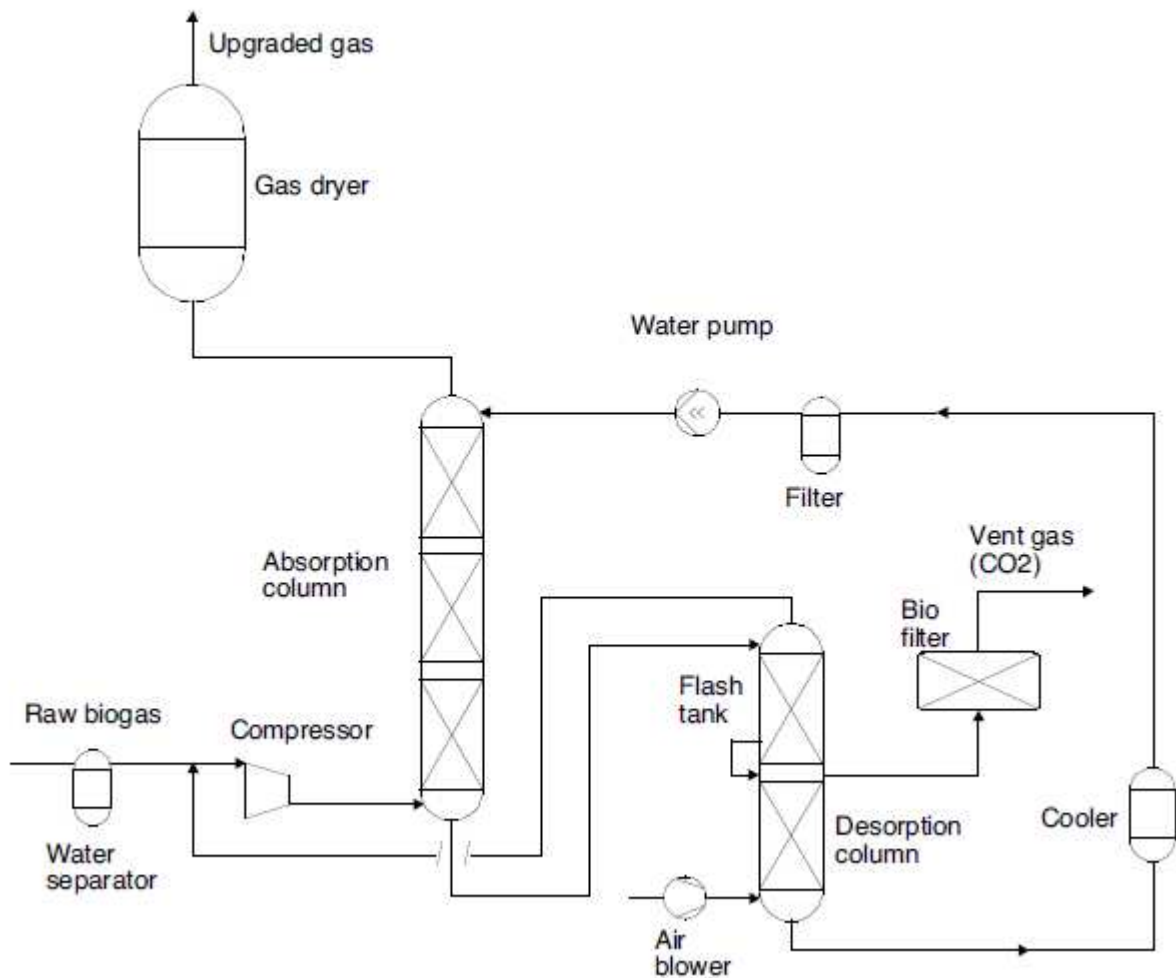
Figure 3.10: water wash upgrading technique including the regeneration of the water
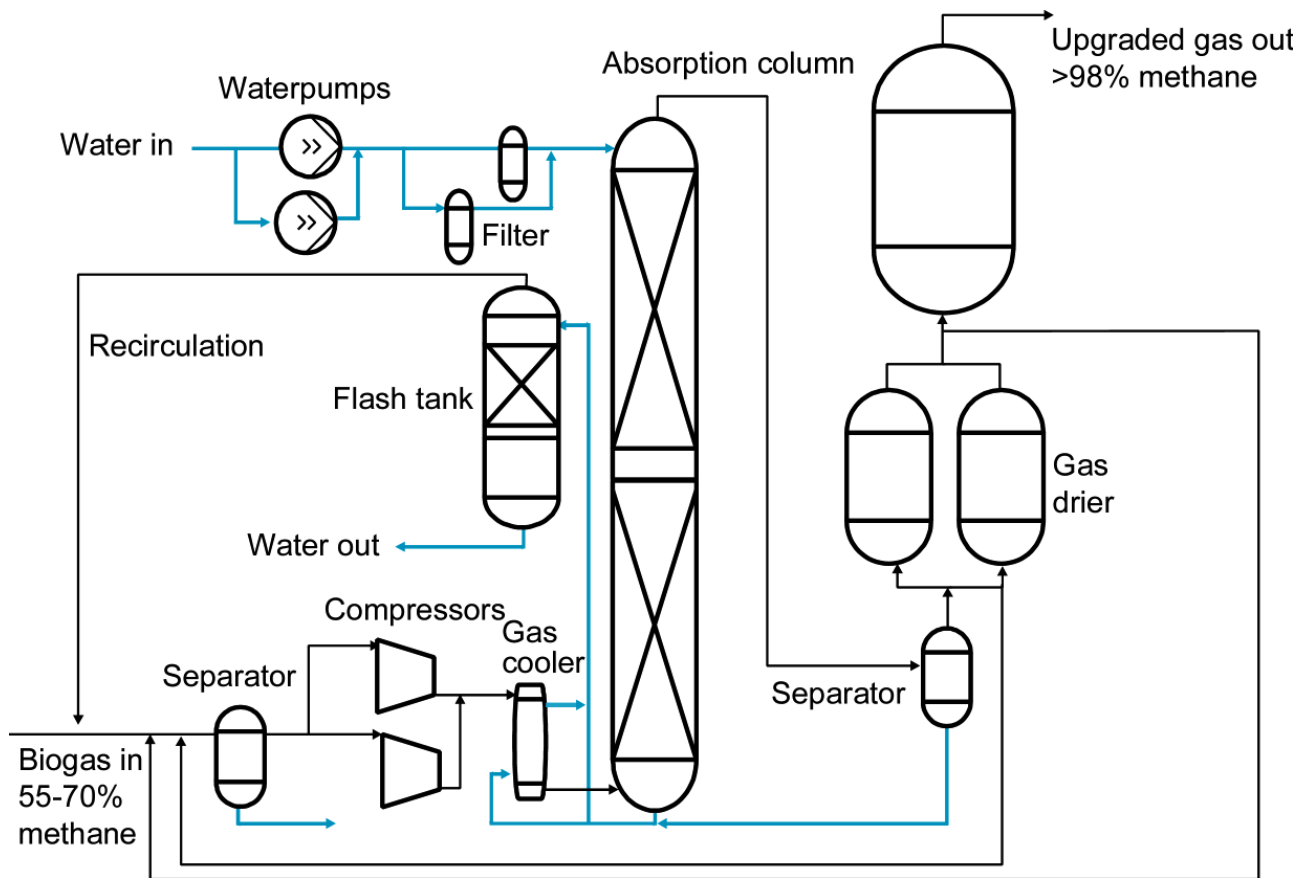
Figure 3.11: water wash upgrading technique without the regeneration of the water

The gas mixture released from the flash tank is rich in methane and is re-circulated to the raw biogas input, before the compressor. We need to know the flow rate that comes from the flash tank in order to recalculate the tower height with the new features (V_b and y_b surely change). It is quite obvious that, when the flashed gas is recirculated, the methane recovery depends on the flash tank pressure as well as the recirculated gas flow rate and consequently, the tower design (height and required water flow rates). The design process turns out to be iterative, including the simultaneous absorption in the tower and the mass balance at the flash tank. The latter calculation can be written as:

$$P = H \cdot x_{FT} = y_{FT} \cdot P^{FT}$$
$$P' = H' \cdot x'_{FT} = y'_{FT} \cdot P^{FT}$$
$$L \cdot (x_b - x_{FT}) = F \cdot y_{FT}$$
$$L \cdot (x'_b - x'_{FT}) = F \cdot y'_{FT}$$
$$F = L \cdot (x_b - x_{FT} + x'_b - x'_{FT})$$

where F is the recirculated molal flow rate (the flashed gas from the flash tank), quantities with the superscript refer to methane, otherwise to CO_2, P and P' are partial pressure of CO_2 and CH_4 in the flash

tank, P^{FT} is the total pressure at the flash tank (2÷5 atm), H and H' are Henry's law constant for CO_2 and CH_4, x_{FT} and x'_{FT} are respectively CO_2 and CH_4 concentration in the liquid flow leaving the flash tank, y_{FT} and y'_{FT} are respectively CO_2 and CH_4 concentration in the gas flow leaving the flash tank; the variations of L along the treatment are negligible in the case of water scrubbing, as already demonstrated. For a better interpretation of symbols, Figure 3.12 reports the layout of the process with the described quantities.
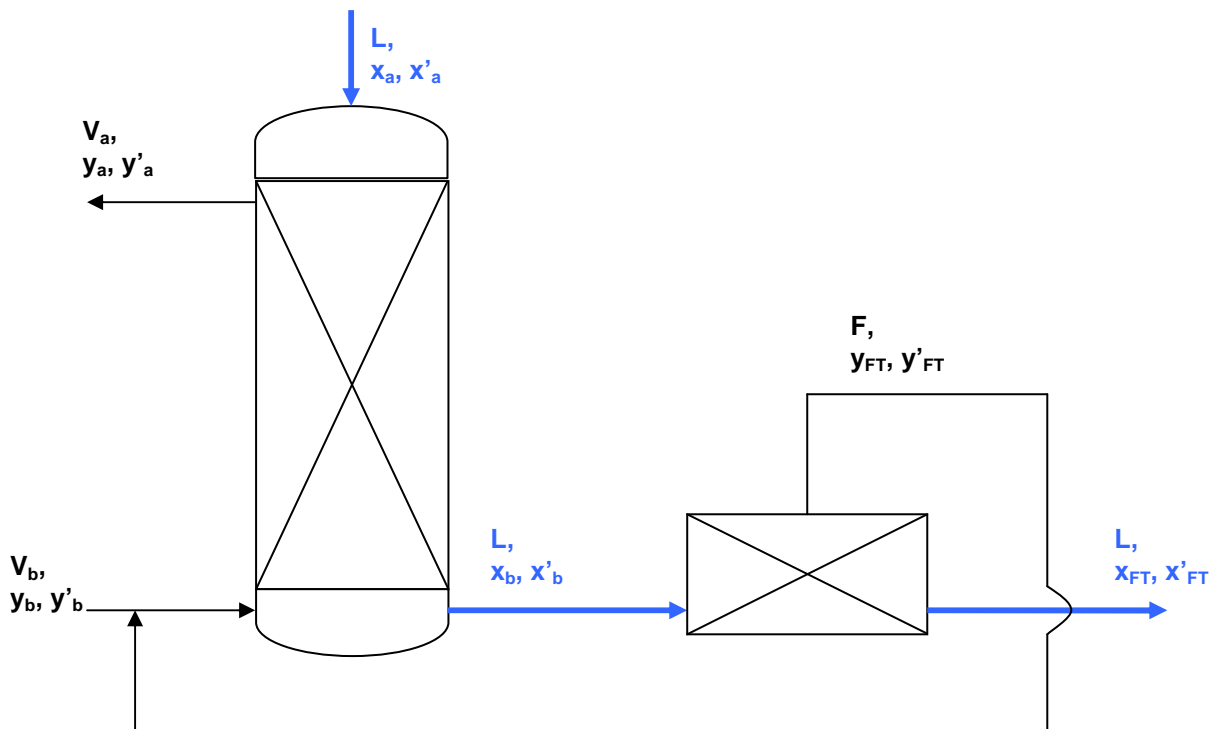
Figure 3.12: absorbing tower and flash tank layout (L is considered constant) for water scrubbing

The mentioned iterative assessment is quite complex but it is very useful in order to predict methane losses according to different flash tank pressures. Based on the reported results (see Table 3.8 and 3.9), one can observe that when flash tank pressure is around 5 atm, the recirculated gas flow rates are not so large, always less than 10% of the raw biogas input (22 000 mol/h), and they are quite rich in methane (20÷50%). Moreover, the water flow rates that are needed to reach the methane purity target (> 97%) after absorbing are increased by 10 to 30% whereas the tower height could be slightly reduced (due to the effect of an larger L/V ratio). On the other hand, the methane losses are still quite considerable, from 0.8 to 3.8% of biogas methane input).

On the contrary, when depressurising down to 2 atm, the recirculation flow rates increase substantially, up to an overall V_b around 55 000 mol/h (+145% if compared to the raw biogas input) and also the tower height could be doubled. At the same time one can observe a strong reduction of the methane losses, down to 0.1%, the same technical performance that can be observed for the chemical absorption with amines that will be commented in the next chapter 3.3.

Table 3.8: water wash upgrading design through simultaneous absorption of carbon dioxide and methane and flash tank calculation (the tower diameter is assumed 1 m, the temperature is 303 K)

	L (m³/h)	P (atm)*	y_b	x_b	x'_b	x_{FT}	x'_{FT}	y_{FT}	y'_{FT}	F (mol/h)	tower height (m)
flash tank @ 5 atm	135	6	0.47	1.3E-03	7.4E-05	1.3E-03	6.0E-05	0.48	0.52	197.6	15.67
flash tank @ 2 atm	175	6	0.60	1.8E-03	5.6E-05	1.0E-03	2.9E-06	0.94	0.06	8201.9	22.22
flash tank @ 5 atm	120	8	0.47	1.6E-03	9.8E-05	1.5E-03	5.3E-05	0.54	0.46	652.8	9.48
flash tank @ 2 atm	160	8	0.69	2.9E-03	5.8E-05	1.1E-03	1.4E-06	0.97	0.03	17136.4	23.84
flash tank @ 5 atm	90	10	0.49	2.2E-03	1.2E-04	2.0E-03	3.2E-05	0.72	0.28	1560.1	9.07
flash tank @ 2 atm	160	10	0.72	3.5E-03	6.5E-05	1.1E-03	1.2E-06	0.97	0.03	21965.5	14.47
flash tank @ 5 atm	80	12	0.50	2.7E-03	1.3E-04	2.2E-03	2.2E-05	0.81	0.19	2492.1	7.46
flash tank @ 2 atm	150	12	0.77	4.9E-03	6.3E-05	1.1E-03	7.4E-07	0.98	0.02	32589.1	18.30

* absorbing tower pressure

Table 3.9: comparison between configurations with and without the recirculation of flashed gas (the tower diameter is assumed 1 m, the temperature is 303 K)

	L (m³/h)	F (mol/h)	Z (m)	CH_4 losses
6 atm (*), 303 K				
without recirc	120	-	22.25	4.20%
with recirc (5 atm)	135	197.6	15.67	3.85%
with recirc (2 atm)	175	8201.9	22.22	0.24%
8 atm (*), 303 K				
without recirc	100	-	11.72	4.67%
with recirc (5 atm)	120	652.8	9.48	3.02%
with recirc (2 atm)	160	17136.4	23.84	0.10%
10 atm (*), 303 K				
without recirc	75	-	11.17	4.38%
with recirc (5 atm)	90	1560.1	9.07	1.38%
with recirc (2 atm)	160	21965.5	14.47	0.09%
12 atm (*), 303 K				
without recirc	60	-	11.40	4.20%
with recirc (5 atm)	80	2492.1	7.46	0.85%
with recirc (2 atm)	150	32589.1	18.30	0.05%

* absorbing tower pressure

The present chapter dedicated to pressurized water scrubbing won't provide the reader with any specific assessment of regeneration step, that is normally carried out by air stripping in a packed tower. The regeneration phase could occur or not as water sometimes is released without treatment after the flash tank. The stripping process will be carefully designed in chapter 3.2 where solvent must be regenerated and reused in a cyclic process.

Apart from the economically and environmental importance of minimizing methane losses from the system, it should be carefully analysed energy consumptions of different plant configurations, depending in particular on absorption pressure design.

Compression of input raw biogas is usually carried out by compressors made up of stainless steel and equipped with specific safety devices. As a matter of fact, methane is an inflammable gas. A common gas compressor poses fire hazards, since the auto-ignition temperature of biogas is 537 °C. Leakage and excessive temperature rise can be fatal. Hermetically sealed reciprocating compressors can be used, but they need extensive cooling systems. Otherwise, due care during operation must be done so as not to allow the temperature to rise above safe limits.

The energy required for gas compression represents a major operating cost of a biogas system. Accordingly, estimating the energy requirement becomes an important component of the system design effort. Estimates are usually based on adiabatic compression process (compression without cooling) since such a calculation estimates the maximum energy required for compression in a frictionless compressor (and it is quite realistic assumption since compression takes place rapidly, with little time allowed for heat transfer).

Mathematically, the relationship between the system pressure, the compressor capacity, and the energy required for compression in a frictionless, adiabatic compressor can be stated as (Kidnay et al., 2006):

$$w \ [Btu/lb] = \frac{\gamma \cdot R \cdot T_1}{M \cdot (\gamma - 1)} \left[1 - \left(\frac{P_2}{P_1} \right)^{(\gamma - 1)/\gamma} \right]$$

$$\gamma = \frac{C_p}{C_v}$$

where T_1 is the inlet temperature (expressed in °R), R is the gas constant (1.986 Btu/lb-mol/°R), M is the molecular weight (in the case methane is 53% of input biogas, M = 29.2 g/mol = 29.2 lb/lb-mol), P_2 and P_1 are discharge and inlet pressures (expressed in psi absolute), γ is the ratio of molar heat capacities (in the base case, when methane is 53% of biogas, $\gamma = 1.31$).

The outlet temperature T_2 for a reversible adiabatic compression of an ideal gas can be calculated by:

$$T_2 \ [°R] = T_1 \cdot \left(\frac{P_2}{P_1} \right)^{(\gamma - 1)/\gamma}$$

The reported calculations should take into account that compressors are never 100% efficient because of friction and heat transfer that occur during the compression process; and, therefore, the actual energy required will be greater than that computed using the preceding equation. Figure 3.13 reports isentropic efficiencies and usual working ranges for different types of compressors (Kidnay et al., 2006): it should be remembered that biogas plants usually apply reciprocating (piston) compressors, single or multiple stages according to the pressure requirements. A conservative efficiency of 75% has been applied to the present assessment.

In order to calculate energy consumptions for raw biogas compressions, it is important to underline that the pressure drop to be won within the tower is always less than 0.5 inch H_2O/foot to avoid flooding and the designed towers are mainly smaller than 20 m (65 feet). Therefore, the maximum pressure drop within the tower is less than 0.1 atm, negligible for our purposes (the process pressure lies in the range 6÷12 atm). Moreover, the inlet pressure is slightly higher than atmospheric one, as ordinary over-pressures within anaerobic digesters are around 400 mm H_2O (~1.04 atm absolute). Finally, it's important to underline that the recirculating biogas fraction (called F), coming from the flash tank, is already pressurized at 5 or 2 atm, so the specific compressor work (w) and the final temperature T_2 will be somewhat lower: the weighted calculations are based on the molar heat capacities of biogas and recirculated gas from the flash tank.

Table 3.10 reports the electricity consumptions due to raw biogas compression according to all pressure/recirculation conditions described in the previous chapters. As one can easily observe, the energy consumption are very large, in particular for elevated pressure scrubbing and low pressure flash evaporation: the specific consumption for compression ranges from 0.09 to 0.27 kWh$_e$/m^3 of raw biogas.

It should be highlighted the strong increase in the outlet biogas temperature, ranging from 175 to 250 °C. The resulting thermal power (from 30 to more than 80 thermal kW) have no consequences on process temperatures since the maximum temperature increase of the liquid flow rate would be around 0.5 °C in the case biogas entering the scrubbing tower isn't cooled down; nevertheless, the corresponding energy could be recovered to obtain the anaerobic digestion heat requirements and other possible technological uses.

TABLE 4.2
Typical Cost Effective Ranges of Compressors Used in Gas Processing

	Inlet Flow Rate[a] acfm (m³/h)	Maximum Pressure psig (barg)		Isentropic Efficiency, %
		Inlet	Discharge	
Reciprocating				
Single stage	1 – 300 (2 – 500)	No limit	< 3,000 (200)	75 – 85
Multistage	1 – 7,000 (2 – 12,000)	No limit	< 60,000 (4,000)	
Centrifugal				
Single stage	50 – 3,000 (80 – 5,000)	No limit	1,500 (100)	70 – 75
Multistage	500 – 200,000 (800 – 350,000)	No limit	10,000 (700)	
Oil-free rotary screw	<40,000 (70,000)	<150 (10)	<350 (25)	70 – 85
Oil-injected rotary screw	< 10,000 (20,000)	< 400 (30)	< 800 (60)	70 – 85

[a] Compressor-gas volumes are based upon actual gas volumes at suction temperature and pressure.

Figure 3.13: Compressors used in gas processing

As far as the energy consumption due to water compression is concerned, a general equation could be:

$$w \ [kW] = \frac{\Delta P \cdot L}{\eta_{overall}}$$

$$\eta_{overall} = \eta_{pump} \cdot \eta_{em}$$

where ΔP is the pressurization requirements (process + hydraulic circuit) in Pa, L is water flow rate (m³/s), η_{pump} is pump efficiency (assumed 0.75÷0.85), η_{em} is electric motor efficiency (0.85÷0.92). Therefore, overall efficiency of a pumping plant rarely exceeds 70%, here it has been assumed equal to 65%. It should be remembered that desorption/regeneration tower usually operates at atmospheric pressure in order to regenerate water (see Figure 3.8), so flash tank pressure is not influent on total solvent compression requirements even when water regeneration through air stripping is carried out. Anyway, the hydraulic head to be given in order to push the liquid flow above the tower of height Z is a considerable contribution to the overall consumption (see $\Delta P = f(Z)$), as pointed out by Table 3.11.

Table 3.10: biogas compression energy consumptions for pressurized water scrubbing

	P = 6 atm (*), T = 303 K			P = 8 atm (*), T = 303 K			P = 10 atm (*), T = 303 K			P = 12 atm (*), T = 303 K		
L (m^3/h)	120	135	175	100	120	160	75	90	160	60	80	150
flash tank P (atm)	-	5	2	-	5	2	-	5	2	-	5	2
Raw biogas (mol/h)	22019.7	22019.7	22019.7	22019.7	22019.7	22019.7	22019.7	22019.7	22019.7	22019.7	22019.7	22019.7
F (mol/h)	0	197.6	8201.9	0	652.8	17136.4	0	1560.1	21965.5	0	2492.1	32589.1
y_b (raw biogas)	0.47	0.47	0.47	0.47	0.47	0.47	0.47	0.47	0.47	0.47	0.47	0.47
y_{FT} (rec F)	-	0.48	0.94	-	0.54	0.97	-	0.72	0.97	-	0.81	0.98
V_b (mol/h)	22019.7	22217.4	30221.6	22019.7	22672.5	39156.1	22019.7	23579.8	43985.2	22019.7	24511.8	54608.8
y_b	0.47	0.47	0.60	0.47	0.47	0.69	0.47	0.49	0.72	0.47	0.50	0.77
V_b (lb/h)	1415.6	1428.4	2179.5	1415.6	1460.5	3046.7	1415.6	1540.2	3511.3	1415.6	1627.7	4521.9
γ	1.311	1.311	1.312	1.311	1.311	1.312	1.311	1.311	1.312	1.311	1.311	1.312
MW (raw biogas) (lb/lb-mol)	29.2	29.2	29.2	29.2	29.2	29.2	29.2	29.2	29.2	29.2	29.2	29.2
MW (F) (lb/lb-mol)	0.0	29.5	42.2	0.0	31.2	43.2	0.0	36.2	43.3	0.0	38.6	43.6
MW (V_b) (lb/lb-mol)	29.2	29.2	32.7	29.2	29.2	35.3	29.2	29.6	36.2	29.2	30.1	37.6
T1 (°C)	20	20	20	20	20	20	20	20	20	20	20	20
T1 (°F)	68	68	68	68	68	68	68	68	68	68	68	68
T2 raw biogas (°F)	340.4	340.4	340.5	396.9	396.9	397.2	443.6	443.6	444.0	483.5	483.6	484.1
T2 rec F (°F)	-	91.3	225.4	-	130.3	273.9	-	162.4	313.9	-	190.0	348.2
T2 V_b (°F)	340.4	338.2	301.3	396.9	389.2	330.2	443.6	424.3	363.7	483.5	451.9	384.7
T2 V_b (°C)	171.3	170.1	149.6	202.7	198.5	165.7	228.6	218.0	184.3	250.8	233.3	195.9
P1 (atm abs)	1.04	1.04	1.04	1.04	1.04	1.04	1.04	1.04	1.04	1.04	1.04	1.04
P2 (atm abs)	6	6	6	8	8	8	10	10	10	12	12	12
P1 (psia)	15.3	15.3	15.3	15.3	15.3	15.3	15.3	15.3	15.3	15.3	15.3	15.3
P2 (psia)	88.2	88.2	88.2	117.6	117.6	117.6	147.1	147.1	147.1	176.5	176.5	176.5
w (Btu/lb) isentrop	78.1	77.6	61.7	94.3	92.1	65.3	107.7	100.9	71.9	119.2	107.2	74.6
Power required (kW$_e$, η=0.75)	43.2	43.3	52.5	52.1	52.5	77.6	59.5	60.7	98.5	65.9	68.1	131.7
specific consumption (kWh$_e$/m^3 raw biogas)	0.09	0.09	0.11	0.11	0.11	0.16	0.12	0.12	0.20	0.13	0.14	0.27
thermal recovery (kW)	29.0	29.0	34.1	35.0	35.2	49.7	40.0	40.6	62.9	44.2	45.5	83.6

* absorbing tower pressure

Table 3.11: water compression energy consumptions for pressurized water scrubbing

	P = 6 atm (*), T = 303 K			P = 8 atm (*), T = 303 K			P = 10 atm (*), T = 303 K			P = 12 atm (*), T = 303 K		
L (m^3/h)	120	135	175	100	120	160	75	90	160	60	80	150
flash tank P (atm)	-	5	2	-	5	2	-	5	2	-	5	2
absorbing tower height Z (m)	22.25	15.67	22.22	11.72	9.48	23.84	11.17	9.07	14.47	11.4	7.46	18.3
P1 (atm abs)	1	1	1	1	1	1	1	1	1	1	1	1
$\Delta P = f$ (Z) atm	2.2	1.5	2.2	1.1	0.9	2.3	1.1	0.9	1.4	1.1	0.7	1.8
P2 (atm abs)	6	6	6	8	8	8	10	10	10	12	12	12
Power required (kW$_e$, η=0.65)	**37.2**	**38.1**	**54.2**	**35.2**	**41.1**	**64.5**	**32.7**	**38.5**	**72.1**	**31.4**	**40.6**	**83.0**
specific consumption (kWh$_e$/m^3 raw biogas)	**0.08**	**0.08**	**0.11**	**0.07**	**0.08**	**0.13**	**0.07**	**0.08**	**0.15**	**0.06**	**0.08**	**0.17**

* absorbing tower pressure

Table 3.12: total energy consumptions for water wash biogas upgrading

	P = 6 atm (*), T = 303 K			P = 8 atm (*), T = 303 K			P = 10 atm (*), T = 303 K			P = 12 atm (*), T = 303 K		
L (m^3/h)	120	135	175	100	120	160	75	90	160	60	80	150
flash tank P (atm)	-	5	2	-	5	2	-	5	2	-	5	2
tower height (m)	22.25	15.67	22.22	11.72	9.48	23.84	11.17	9.07	14.47	11.4	7.46	18.3
Power required for biogas compression (kW$_e$, η=0.75)	43.2	43.3	52.5	52.1	52.5	77.6	59.5	60.7	98.5	65.9	68.1	131.7
Power required for solvent compression (kW$_e$, η=0.65)	37.2	38.1	54.2	35.2	41.1	64.5	32.7	38.5	72.1	31.4	40.6	83.0
total power (kW$_e$)	**80.3**	**81.4**	**106.7**	**87.4**	**93.6**	**142.1**	**92.3**	**99.2**	**170.6**	**97.3**	**108.7**	**214.7**
specific consumption for biogas compression (kWh$_e$/m^3 raw biogas)	0.09	0.09	0.11	0.11	0.11	0.16	0.12	0.12	0.20	0.13	0.14	0.27
specific consumption for solvent compression (kWh$_e$/m^3 raw biogas)	0.08	0.08	0.11	0.07	0.08	0.13	0.07	0.08	0.15	0.06	0.08	0.17
total consumptions (kWh$_e$/m^3 raw biogas)	**0.16**	**0.16**	**0.22**	**0.18**	**0.19**	**0.29**	**0.19**	**0.20**	**0.35**	**0.20**	**0.22**	**0.43**

* absorbing tower pressure

The overall power consumption, biogas and water compression, lies in the range 0.16÷0.43 kWh$_e$/m^3 of raw biogas, that is, in our case study, from 80 to 215 kWh$_e$, mainly due to biogas compression (see also Table 3.12).

It is important to observe that, up to now, the pressure drops of water through pipes have been neglected. In order to check the validity of this assumption we can calculate pressure drops along plant lines for the worst case:
L = 150 m^3/h;
Pipe diameter D = 200 mm;
Mean water velocity V = 1.33 m/s;
Water dynamic viscosity = 0.001 Pa·s;
Roughness of commercial steel pipes: 0.046 mm;
Reynolds number = 266 000;
Relative roughness = 0.00023;
Friction factor ξ = 0.018 (from the Moody Diagram reported in Figure 3.14);
Circuit length l = 100 m (hypothesis);

$$\Delta P \, [Pa] = \zeta \cdot \frac{l}{D} \cdot \frac{V^2}{2} \cdot \rho \cong 8000 \ \ Pa$$
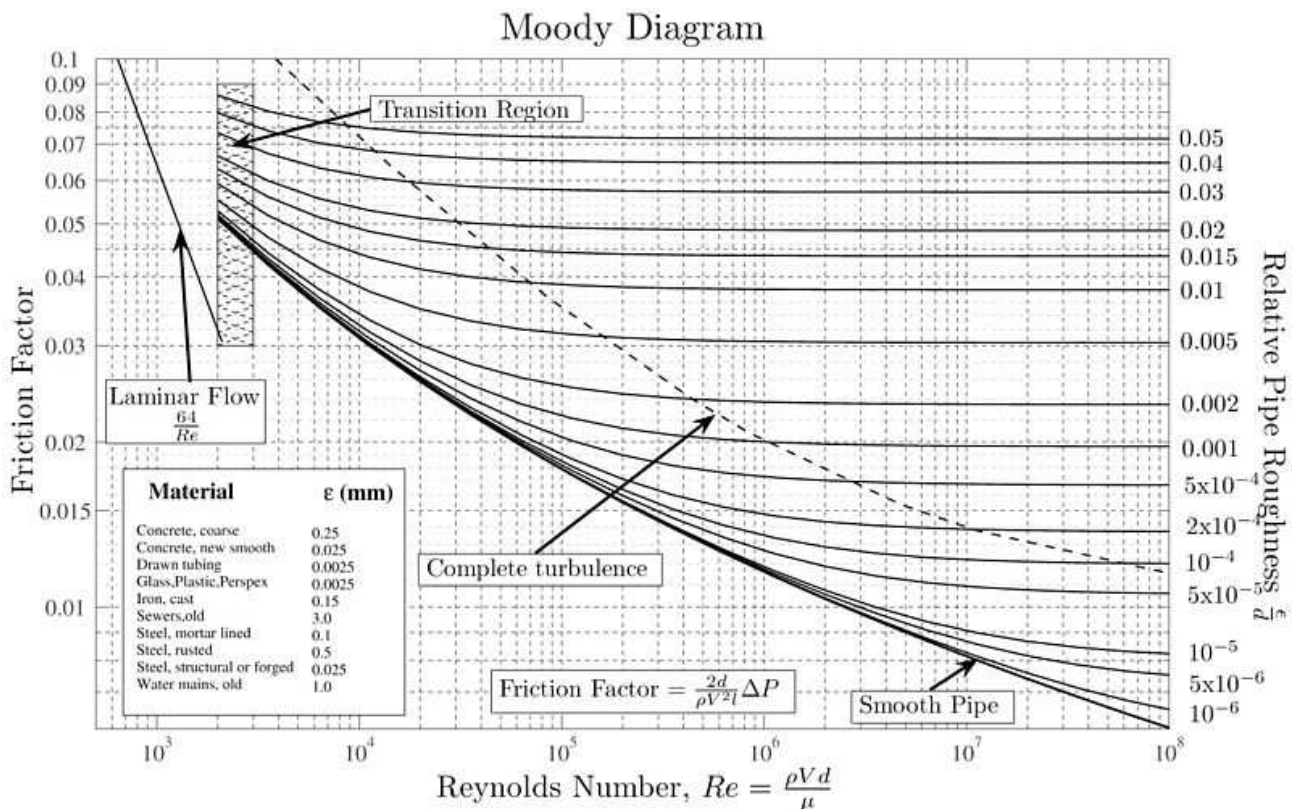
Figure 3.14: friction-factor chart

Therefore, in the worst situation (very large water flow rate and quite small pipe diameter), the pressure drops for a 100 m circuit is less than 0.1 atm, that is reasonably negligible if compared to the total pressurization requirements (8-14 atm, comprehensive of hydraulic head to be overcome). The discussed assumption should be verified for different solvents, in the case they are very viscous (polyethylene glycol,

for example). Anyway, pipelines pressure drops regarding the gaseous phase are surely not influent in our analysis. At the same time, compression requirements for water regeneration process, substantially coincident with hydraulic head of the stripping tower, are expected to be very low compared to other energy consumptions: less than 6 kW_e (~ 0.01 kWh_e/m^3 of raw biogas). Consequently they have been disregarded. Finally, biomethane exiting the absorbing tower is at least at 6 atm, well above the maximum allowed pressure for local natural gas grid injection (5 bar); this means that no further compressions are required for biomethane.

In conclusion, based on the results described in the present chapter and literature suggestions, biogas upgrading through the use of pressurized water is surely feasible, indeed the most frequently applied solution. On the other hand, methane losses could be very important for the usual plant configurations, up to 4 % of biogas content, that is the environmental compatibility in terms of CO_2 balance could be questionable or at least largely compromised. In order to improve sustainability by reducing methane losses, energy consumptions tends to strongly increase up to 0.5 kWh_e/m^3 of raw biogas, that is double the figures reported by literature (Regione Piemonte, 2009) for the analysed technique (<0.25 kWh_e/m^3 of raw biogas).

Therefore, it is convenient to consider also other technological possibilities, such as, first of all, the use of solvents different from water and the employment of specific water solutions that could absorb and make CO_2 react. In the latter case, mass transfer coefficients could increase by orders of magnitude and, consequently, the tower dimensions and general energy costs could be reduced.

3.2 Physical absorption with Glycol Ethers

Knowledge of the solubility of carbon dioxide in polar solvent is important both industrially and environmentally. Contrary to chemical solvents, physical solvents are not limited in their absorption capacity by the stoichiometry of a reaction. As already discussed, this capacity is proportional to the partial pressure of the acid gas in the stream. Much lower energy consumption is expected for regeneration compared to chemical solvents. Methyl and dimethyl ethers of polyethylene glycols, also known as methoxypolyethylene glycol and polyglymes, have been used for over 30 years as physical absorbents for acid gas or mercaptans removal from natural or synthetic gases. Polyethylene glycol ethers are high molecular weight solvents. Polyethylene glycol ethers are characterized by low vapour pressure (high boiling point), miscibility with water and, in some cases (unfortunately), high viscosities. Selexol is a trade name of a specific mixture of polyethylene glycol dimethyl ethers (DEPG), properly studied to absorb acid gases. The Selexol process can operate selectively to recover hydrogen sulfide and carbon dioxide as separate streams. Henni et al. (2005) report the Henry's law constants described by Figure 3.15, expressed as MPa (i.e. MPa/liquid mole fraction) at different temperatures.

Table 1. Henry's law constant of CO_2 in glycol ethers and other promising solvents			
Solvents (Acronym, Average boiling points, °C)	H (MPa)		
	25 °C	40°C	60°C
Ethylene glycol monomethyl ether (EGMME, 123)	10.3	10.8	13.9
Diethylene glycol monomethyl ether (DEGMME, 192)	6.4	8.4	10.1
Triethylene glycol monomethyl ether (TEGMME, 122)	6.8	7.7	8.2
Ethylene glycol dimethyl ether (EGDME, 83)	5.5	5.9	7.1
Diethylene glycol dimethyl ether (DEGDME, 162)	4.8	8.2	11.9
Triethylene glycol dimethyl ether (TEGDME, 216)	4.4	6.0	8.9
Tetraethylene glycol dimethyl ether (TTEGDME, 275)	3.0	4.3	6.5
Diethylene glycol monoethyl ether (DEGMEE, 202)	7.7	9.2	10.7
Diethylene glycol diethyl ether (DEGDEE, 185)	4.3	5.4	7.2
Ethylene glycol monobutyl ether (EGMBE, 170)	12.1	13.5	15.7
Diethylene glycol monobutyl ether (DEGMBE, 226)	9.8	11.2	12.8
Triethylene glycol monobutyl ether (TEGMBE, 307)	5.3	6.8	8.2
Polyethelene glycol dimethyl ether (PEGDME250, 250)	3.2	4.3	6.6
N-formyl morpholine (NFM, 240)	9.5	10.8	13.3
Sulfolane[a] (285)	8.7	11.1	15.8
Selexol[b,c]	3.6	4.7	6.5

[a] Jou et al. (1990)
[b] Xu et al. (1990)
[c] Schmidt (1997) vapor pressure of 0.00011 kPa at 25 °C

Figure 3.15: solubility of CO_2 in glycol ethers

The mean Henry's law constant for the 16 glycol ethers reported in Figure 3.15 is 6.59 MPa at 25°C and 8 MPa at 40 °C, that is more or less 7 MPa at 30°C, assuming a linear behaviour of H with temperature. In the present chapter this average value (7 MPa/mol frac), is used in order to carry out the absorbing tower design when using a generic polyethylene glycol ether; the design will be also performed with together with specific data for Selexol, that is clearly more favourable than other glycol ethers as far as thermodynamics of absorption is concerned.

Figure 3.16 reports some physical properties of Selexol, such as:
Density @ 25°C = 8.57 lb/gal = 64.1 lb/ft^3 = 1027 kg/m^3;
Dynamic viscosity @ 25°C = 5.8 cp = 0.0058 Pa·s (6 times more viscous than water);
Vapor Pressure @ 25 °C = 0.0007 mmHg = 0.09 Pa (water is 24 mmHg).

3.0 SOLVENT CHARACTERISTICS

o   Physical and Chemical Properties (Source: Ref. 1 & 2)

Freeze Point	-8 to -20°F
Flash Point	304°F
Vapor Pressure @ 77°F	.0007 mmHg
Specific Heat @ 77°F	.49 BTU/lb°F
Density @ 77°F	8.57 lb/gal
Viscosity @ 77°F	5.8 cp
Thermal Conductivity @ 77°F	.11
Surface tension @ 77°F	34.3 dynes/cm
Heat of solution @ 77°F	
CO_2	160 Btu/lb solute
H_2S	190 Btu/lb solute
CH_4	75 Btu/lb solute
Typical Molecular Weight	280

o   Typical Composition (Source: Ref. 2)

Compound	Wt%
Triethylene glycol-dimethylether	12
Tetraethylene glycol - dimethylether	24
Pentaethylene glycol - dimethylether	25
Hexaethylene glycol-dimethylether	19
Heptethylene glycol - dimethylether	11
Octaethylene glycol - dimethylether	6
Nenaethylene glycol - dimethylether	3

Figure 3.16: physical properties of Selexol

As already explained for water scrubbing, one of the first aspect to define in order to design an absorbing packed tower is the pressure drop within the column. Based on the assumption of a packing made up of pall rings, steel, 1 inch, porosity 94%, Packing Factor Fp = 48, Table 3.13 reports some simulations regarding the pressure drops deriving from different polyethylene glycol flow rates and tower surfaces: the bold font highlights the feasibility conditions (that is pressure drops lower than 0.5 inch H_2O/foot). The proposed liquid flow rates (15÷30 m^3/h) come from some literature indication reporting a range of 3÷6 m^3 for every 100 m^3/h of biogas to be treated; anyway, these assumptions are going to be completely checked in the following chapter.

Table 3.13: pressure drop in packed towers for glycol ether solvent

tower surface S (cm^2)	L (m^3/h)	Gx (lb/ft^2/h)	pressure drop (inch H_2O/foot)
7850 (Φ = 1 m)	15	4 023	**< 0.05**
3846 5 (Φ = 0.7 m)	15	8 210	**< 0.1**
1962 5 (Φ = 0.5 m)	15	16 092	**0.25-0.50**
7850 (Φ = 1 m)	30	8 046	**< 0.05**
3846 5 (Φ = 0.7 m)	30	16 420	**0.25**
1962 5 (Φ = 0.5 m)	30	32 184	> flooding line

Anyway, assuming a tower diameter of 1 m, the pressure drop along the tower is still less than 0.1 inch H_2O/foot up to a sorbent flow rate of 70 m^3/h.

Since overall mass transfer coefficients for CO_2-glycol ether absorbing tower are not easily found in literature, the same theoretical approach as methane absorption in water has been applied.

Therefore we employed the empirical correlations suggested by Sherwood and Holloway (1940) for random packings towers, that are based on the Schmidt number ($\mu_L/\rho_L D_L$) for the liquid phase, where D_L represents the parameter diffusivity of CO_2 in polyethylene glycol.

The diffusivity in liquids are defined by Wilke and Chang (1955) as:

$$D_{AB} = \frac{7.4 \cdot 10^{-8} (\phi_B M_B)^{0.5} \cdot T}{\mu_B V_A^{0.6}}$$

where:
A is the solute (CO_2), B is the solvent (for example, Selexol);
Φ_B is the association factor (=1 for solvents different from water);
M_B is molecular weight of solvent (280);
T is temperature in K;
μ_B is viscosity of solvent (centipoise): for Selexol at ambient temperature μ_B=5.8 cP;
V_A is molecular volume of carbon dioxide, defined as 34 cm^3/mol by Wilke and Chang (1955)

Based on this approach, diffusivity of CO_2 in Selexol is around 7.5 x 10^{-6} cm^2/s at 20°C (the diffusivity of CO_2 in water at 20°C is around 1.78 x 10^{-5} cm^2/s), whereas diffusivity of CO_2 in air is around 1.19 x 10^{-5} m^2/s (Kirk and Othmer, 1998). The diffusivity data obtained for Selexol are considered valid also for other glycol ethers.

Sherwood and Holloway and general correlations state that:

$$H_L = a_L \left(\frac{L}{\mu_L} \right)^n \cdot \left(\frac{\mu_L}{\rho_L D_L} \right)^{0.5}$$

$$H_L = \frac{L_M}{k_L a}$$

$$H_G = \frac{a_G G^b Sc_v^{0.5}}{L^c}$$

$$H_G = \frac{G_M}{k_G a}$$

$$\frac{1}{K_G a} = \frac{1}{k_G a} + \frac{H}{k_L a}$$

Where L and G are expressed as lb/ft^2/h, L_M and G_M in lb-mol/ft^2/h, Sc_v is the Schmidt number for the gas phase ($\mu_G/\rho_G/D_G$, where μ_G for gaseous CO_2 is 0.01372 cP), n, a_L, a_G are defined by Figure 3.9 of the chapter 3.1. If one consider 1 inch Berl saddles as packing material, the overall mass transfer coefficient $K_g a$ for CO_2 in an absorbing tower using an unspecific glycol ether with a Henry's law constant around 7 MPa at 303 K ranges from 0.08 and 0.37 lb-mol/ft^3/atm/h for the assumed operative conditions (tower diameter 0.5÷1 m and L between 15 and 30 m^3/h), as reported by Table 3.14. Based on the reported reasoning, assuming a tower diameter of 1 m to be conservative and to make tower height comparable to previous

upgrading solutions, the overall mass transfer coefficient K_ga (referring hence to CO_2 partial pressures) is assumed equal to 0.11 lb-mol/ft^3/atm/h, that is to say around 1766 mol/m^3/atm/h (50 mol/ft^3/atm/h).

The overall mass transfer coefficient for CO_2 in the unspecific glycol ether is quite the same value as that for pure water, in spite of a lower diffusivity of CO_2 in polyethylene glycol and much lower sorbent flow rates. This is due to the very good solubility of CO_2 in organic solvents.

In the case Selexol is used (Henry's law constant = 3.6 MPa at 298 K), the overall mass transfer coefficient K_ga turns out to be around 3355 mol/m^3/atm/h (95 mol/ft^3/atm/h) due to the higher solubility.

Table 3.14: calculation of overall mass transfer coefficients for CO_2 in glycol ethers at 20°C

tower diam (m)	1	1	0.7	0.7	0.5	0.5
tower surface (cm2)	7850	7850	3846.5	3846.5	1962.5	1962.5
tower surface (ft2)	8.45	8.45	4.14	4.14	2.11	2.11
ρl (g/l)	1027.0	1027.0	1027.0	1027.0	1027.0	1027.0
ρl (lb/ft3)	64.1	64.1	64.1	64.1	64.1	64.1
ρg (lb/ft3)	0.0812	0.0812	0.0812	0.0812	0.0812	0.0812
L (m3/h)	15	30	15	30	15	30
L (moli/h)	5.50E+04	1.10E+05	5.50E+04	1.10E+05	5.50E+04	1.10E+05
Vb (moli/h)	22019.7	22019.7	22019.7	22019.7	22019.7	22019.7
L (lb/ft2/s)	1.117	2.235	2.281	4.561	4.470	8.940
G (lb/ft2/s)	0.047	0.047	0.095	0.095	0.186	0.186
μl (cP)	5.8	5.8	5.8	5.8	5.8	5.8
μl (lb/h/ft)	14.0302	14.0302	14.0302	14.0302	14.0302	14.0302
μg (cP)	0.01372	0.01372	0.01372	0.01372	0.01372	0.01372
μg (lb/h/ft)	0.033	0.033	0.033	0.033	0.033	0.033
Dl (ft2/h)	2.98E-05	2.98E-05	2.98E-05	2.98E-05	2.98E-05	2.98E-05
Dg (ft2/h)	0.46	0.46	0.46	0.46	0.46	0.46
HL (ft)	2.46	2.99	3.01	3.65	3.63	4.41
kl a (lb-mol/h/ft3)	5.83	9.60	9.74	16.05	15.82	26.06
HG (ft)	0.42	0.32	0.41	0.31	0.40	0.30
kg a (lb-mol/h/ft3)	13.56	17.90	28.48	37.58	57.35	75.67
Kg a (lb-moli/h/atm/ft3)	**0.083**	**0.136**	**0.139**	**0.228**	**0.225**	**0.370**

Table 3.15 reports the tower dimensions according to different L/V ratios when the mono-absorption of CO_2 in glycol ethers is considered. As one can easily observe, the resulting tower height can considerably change in the case of Selexol at 25°C (H = 3.6 MPa, K_ga ~3355 mol/ft^3/atm/h) and the unspecific glycol ether considered in our analysis (H = 7 MPa at 30°C, K_ga ~1766 mol/m^3/atm/h). The reported results confirm that the requested sorbent flow rates lies in the range 3÷6 m^3 for every 100 m^3/h of biogas when Selexol is employed at a pressure between 6 and 12 atm and 25°C. On the other hand, when a less performing glycol ether is used, at the same pressure one need around twice the sorbent flow rate than for Selexol, and the tower height is more or less two times larger as well. The fact is pointed out by Figure 3.17, reporting the operating and equilibrium curves for both the configurations: in the case of unspecific glycol ether, the equilibrium line is much more steep, making the minimum required L/V ratio larger, and the average driving force (y-y*) is pretty smaller than in the case of Selexol.
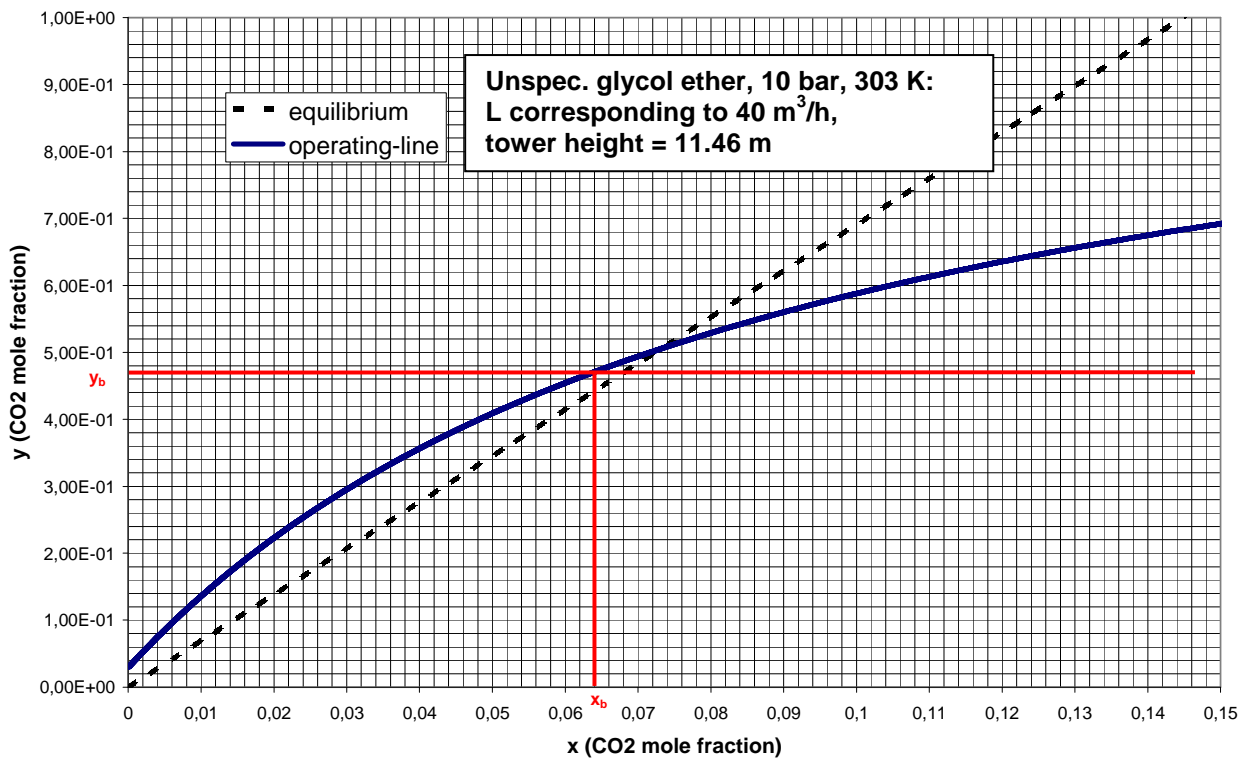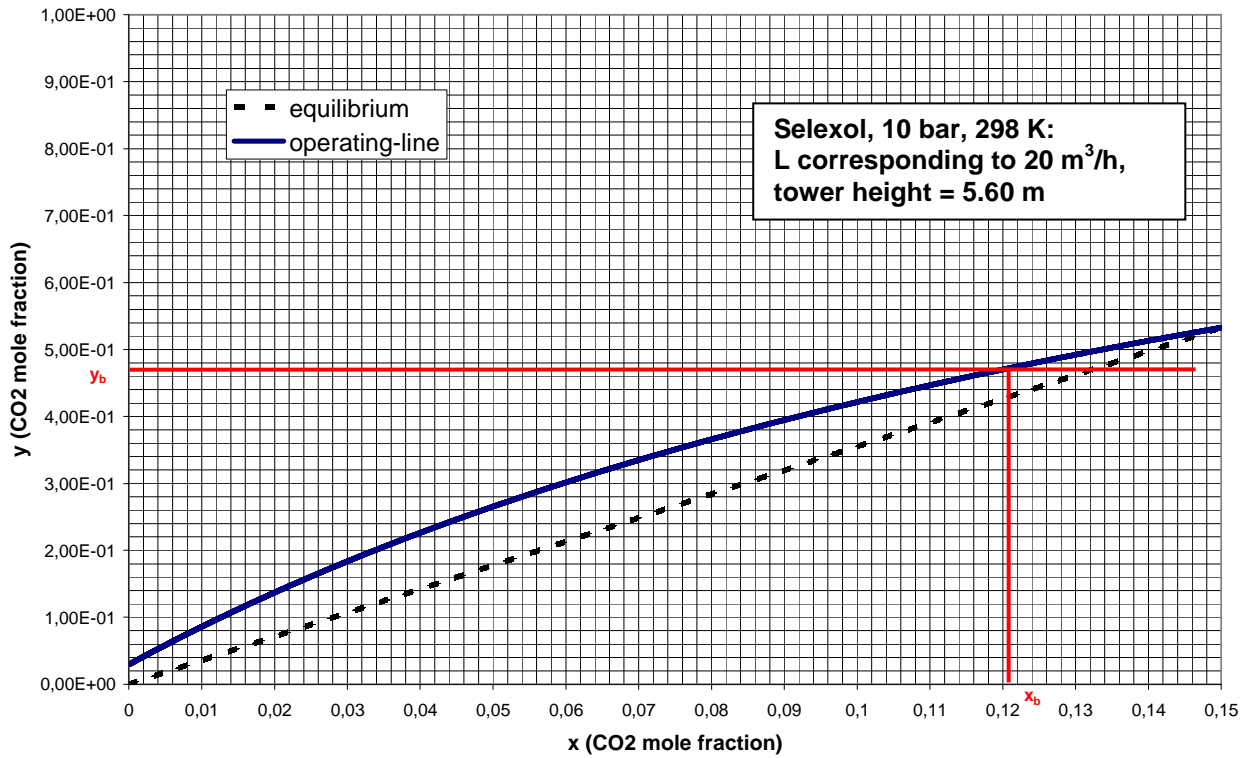
Figure 3.17: equilibrium and operating lines for CO_2-Selexol/glycol ether absorbing tower

Table 3.15: packed tower dimensions for CO_2 absorbed in Selexol/unspecific glycol ether

	L (m³/h)	P (atm)	T (K)	tower diam (m)	L/V *	x_b	tower height (m)
Selexol, H = 3.6 Mpa, 298 K	35	6	298	1	7.1	0.072	9.06
Selexol, H = 3.6 Mpa, 298 K	25	8	298	1	5.1	0.098	7.50
Selexol, H = 3.6 Mpa, 298 K	20	10	298	1	4.1	0.120	5.60
Selexol, H = 3.6 Mpa, 298 K	15	12	298	1	3.0	0.154	6.42
generic glycol ether, H = 7 Mpa, 303 K	70	6	303	1	14.2	0.037	17.20
generic glycol ether, H = 7 Mpa, 303 K	50	8	303	1	10.1	0.052	15.05
generic glycol ether, H = 7 Mpa, 303 K	40	10	303	1	8.1	0.064	11.46
generic glycol ether, H = 7 Mpa, 303 K	35	12	303	1	7.1	0.072	7.92
generic glycol ether, H = 7 Mpa, 303 K	45	12	303	1	9.1	0.057	5.41

*solvent m^3 for every 100 m^3/h of biogas

Again, as previously explained dealing with pressurized water absorption, CO_2 is not the only gas to be absorbed into glycol ethers, methane enters the liquid phase according to its specific solubility that is larger than that for water. Henry's law constant for methane and glycol ether is not so easy to find in literature. Some data can be obtained from Henni et al. (2006), as reported by Figure 3.18, dealing with methane solubility in DEGDME (Diethylene glycol dimethyl ether), TEGDME (Triethylene glycol dimethyl ether), TTEGDME (Tetraethylene glycol dimethyl ether), TEGMBE (Triethylene glycol monobutyl ether), PEGDME 250 (a commercial mixture of poly(ethylene glycol) dimethyl ethers). Based on the reported data, it is important to highlight that methane is around 100 times more soluble in Selexol that in water (the Henry's law constant al 25°C is around 40 MPa vs 4000 MPa for water). Moreover, Kohl and Nielsen (1997) report that the relative solubility of CO_2 referred to methane in Selexol is 15.2, confirming that the Henry's law constant for methane in Selexol could be 3.6 x 15.2 = 55 MPa at 298 K (see Figure 3.19).

solvents	(H/MPa) at 25 °C	(H/MPa) at 40 °C	(H/MPa) at 60 °C
DEGDME	40.5	41.4	43.1
TEGDME	37.3	38.2	39.4
TTEGDME	38.1	39.7	41.2
TEGMBE	38.7	41.3	45.1
PEGDME 250	36.4	38.7	40.4

Figure 3.18: solubility of methane in glycol ethers

As a consequence, because of the hydrocarbon absorption in polyethylene glycol dimethyl ethers (DEPG), in the past it was not used for natural gas treating until later and even then was not used with rich gas streams (Raney, 1976). Selexol has been typically used for high pressure (>500 psia, that is > 24.5 atm) applications. At higher pressures, the solubilities of H_2S, CO_2, and other contaminants is higher, and the feed gas is at a sufficiently high pressure for subsequent solvent pressure let-down in a series of flashes involved in regeneration. Air stripping, vacuum flashing, and occasionally reboiling or steam stripping are also used if a very lean solvent is required to meet the sweet gas specifications.

As a matter of facts, when Selexol or other glycol ethers are used to upgrade biogas, the spent solvent solution should be depressurised in a flash tank after leaving the absorption column. The released gas mixture is rich in methane and is recirculated to the compressor inlet in the same way as in the case of pressurized water. Then, the glycol ether solution from the flash tank is depressurised to atmospheric pressure and fed into the top of a desorption column. Air is blown from the bottom of the desorption column to remove dissolved carbon dioxide from the sorbent. The regenerated liquid is pressurized, cooled in a heat exchanger to maintain the absorption temperature and then recycled to the absorption column. The vent gas is either released to the atmosphere or treated in some kind of gas filter to remove odours.

Table 14-9
Relative Solubilities of Various Gases in SELEXOL Solvent

Component	$R = \dfrac{K'\ \text{Methane}}{K'\ \text{Component}}$	Component	$R = \dfrac{K'\ \text{Methane}}{K'\ \text{Component}}$
H_2	0.20	NH_3	73
N_2	0.30	nC_5	83
CO	0.43	H_2S	134
C_1	1.0	C_6	167
C_2	6.5	CH_3SH	340
C_2H_4	7.2	C_7	360
CO_2	15.2	CS_2	360
C_3	15.4	SO_2	1,400
iC_4	28	C_6H_6	3,800
COS	35	CH_2Cl_3	5,000
nC_4	36	C_4H_4S	8,200
iC_5	68	H_2O	11,000
C_2H_2	68	HCN	19,000

$K' = y/x'$ where y is the mole fraction of the component in the vapor phase and x' is the mole fraction of the component in the liquid phase considering only the solvent and the component.
Sources: Shah and McFarland (1988); Epps (1992B)

Figure 3.19: solubilities of various gases in Selexol

Hydrogen sulphide is potentially absorbed together with carbon dioxide in the absorption column. The solubility for H_2S in Selexol is very high and H_2S cannot be removed in the desorption column unless heating is provided. It is therefore desirable that H_2S is removed before the absorption, during biogas cleaning treatments, to minimise energy costs.

The product gas has a very low water content since Selexol absorbs water. Further drying is normally not needed. Figure 3.20 shows a typical plant layout.

The Swedish Gas Center (2001) reports the process parameters for one Selexol plant operating in Sweden, as pointed out by Figure 3.21. In these figures one can notice the specific solvent flows (10÷15 m^3 for every 100 m^3/h of raw biogas) that is much larger than the predicted one (3÷6 m^3 for every 100 m^3/h of biogas). This is probably due to the use of a solution of Selexol and water instead of pure Selexol (this solution strongly reduces the volatilization of lower boiling points Selexol components). Moreover, as previously demonstrated, the large solvent flow rates could be explained by the high recirculation requirements from the flash tank, aiming at minimising methane losses. The latter reason seems to be confirmed by the very low pressure in the flash tank (1.5-2 bar).

As a consequence, in the next paragraphs, an attempt to quantify methane losses according to different plant configurations will be carried out.
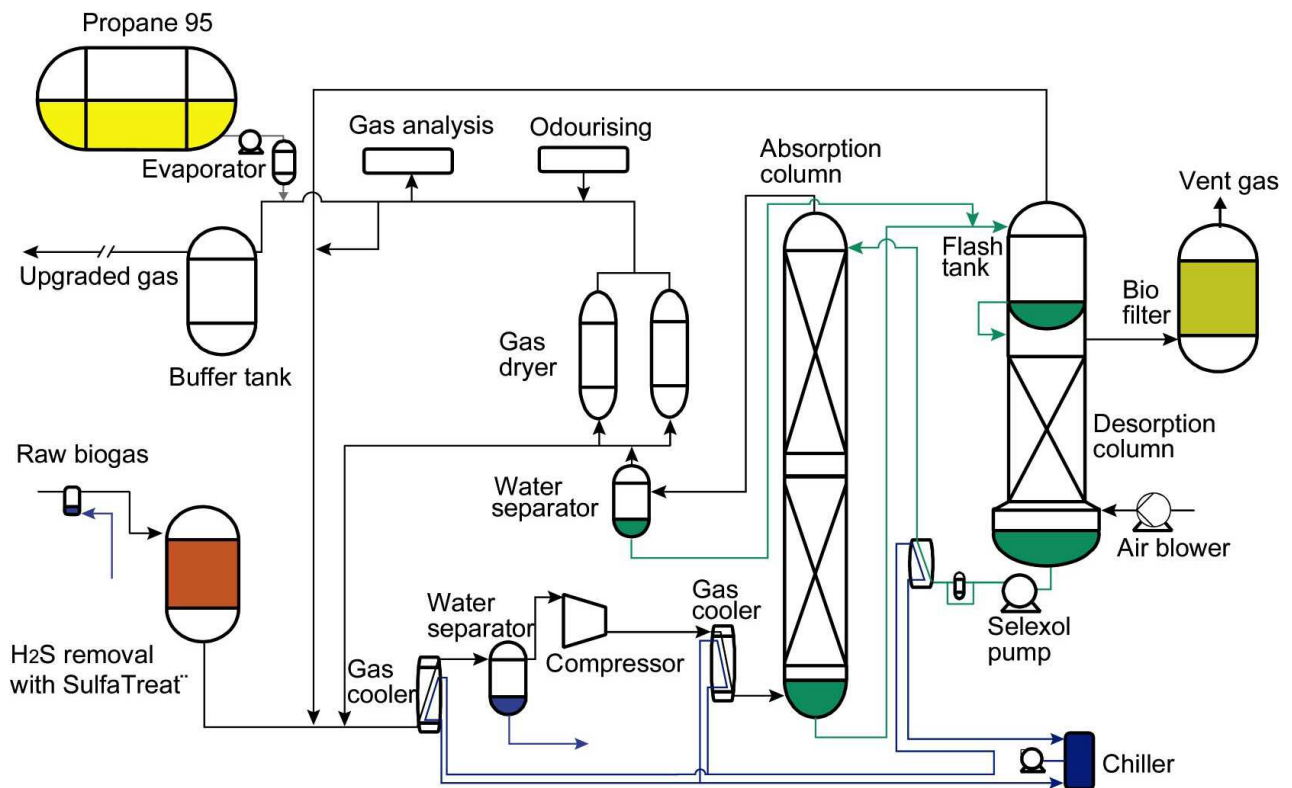
Figure 3.20: typical plant layout for biogas cleaning and upgrading with Selexol (from SGC, 2001)

Parameter	Unit	Process	Plant example
Location/name			Laholm
Capacity range	M^3 biogas/h	100 to > 10,000	250
Input			
· methane	%	45 - 75	69 - 72
· carbon dioxide	%	25 - 55	28 - 31
· nitrogen	%	< 1	0 - 0.2
· hydrogen sulphide	ppm	< 10^{10}	0 - 15
Output			
· methane	%	> 98	95 - 98
· carbon dioxide	%	< 2	2 - 5
· air	%	< 1.5	0 - 0.5
· dewpoint	°C	< -20	< -60
· hydrogen sulphide	ppm	0	0
Process conditions			
Absorption pressure	Bar	10 - 12	7 - 9
Absorption temperature	°C	20 - 35	7
Pressure in flash tank	bar	2 - 5	1.5 - 2
Desorption pressure	mbar (abs)	atmospheric to 200	950
Selexol flow	m^3/h	3 - 6[11]	10 - 15

[10] Excess H_2S (> 10 ppm) removed separately to reduce energy costs
[11] Depending on the absorption pressure, for every 100 m^3/h processed biogas

Figure 3.21: biogas upgrading plant in Sweden using Selexol (from SGC, 2001)

As already explained in details, the first calculation to carry out for the simultaneous absorption of carbon dioxide and methane is the definition of mass transfer coefficients for methane and glycol ethers. The following assessments deal specifically with Selexol: the solubility of CO_2 in Selexol is 3.6 MPa/mol frac whereas methane's one is 55 MPa/mol frac at 25°C. Based on the physical properties of Selexol and methane (Diffusivity of methane in Selexol turn out to be around 8.3×10^{-6} cm^2/s at 25 °C, according to Wilke and Chang's approach), Table 3.16 reports the mass transfer coefficients for methane and Selexol depending on different solvent flow rates. According to these results, supposing that Selexol flow rate would increase because of recirculation up to 50-60 m^3/h and the tower diameter is still 1 m, the overall mass transfer coefficient for methane in Selexol has been assumed equal to 0.026 lb-mol/ft^3/atm/h, that is to say around 424 mol/m^3/atm/h (12 mol/ft^3/atm/h).

Table 3.16: calculation of overall mass transfer coefficients for methane in Selexol at 25°C

tower diam (m)	1	1	1	0,7	0,7	0,5	0,5
tower surface (cm2)	7850	7850	7850	3846.5	3846.5	1962.5	1962.5
tower surface (ft2)	8.45	8.45	8.45	4.14	4.14	2.11	2.11
ρl (g/l)	1027.0	1027.0	1027.0	1027.0	1027.0	1027.0	1027.0
ρl (lb/ft3)	64.1	64.1	64.1	64.1	64.1	64.1	64.1
ρg (lb/ft3)	0.0812	0.0812	0.0812	0.0812	0.0812	0.0812	0.0812
L (m3/h)	15	30	50	15	30	15	30
L (moli/h)	5.50E+04	1.10E+05	1.83E+05	5.50E+04	1.10E+05	5.50E+04	1.10E+05
Vb (moli/h)	22019.7	22019.7	22019.7	22019.7	22019.7	22019.7	22019.7
L (lb/ft2/s)	1.117	2.235	3.725	2.281	4.561	4.470	8.940
G (lb/ft2/s)	0.047	0.047	0.047	0.095	0.095	0.186	0.186
μl (cP)	5.8	5.8	5.8	5.8	5.8	5.8	5.8
μl (lb/h/ft)	14.0302	14.0302	14.0302	14.0302	14.0302	14.0302	14.0302
μg (cP)	0.01027	0.01027	0.01027	0.01027	0.01027	0.01027	0.01027
μg (lb/h/ft)	0.025	0.025	0.025	0.025	0.025	0.025	0.025
Dl (ft2/h)	3.22E-05	3.22E-05	3.22E-05	3.22E-05	3.22E-05	3.22E-05	3.22E-05
Dg (ft2/h)	0.61	0.61	0.61	0.61	0.61	0.61	0.61
HL (ft)	2.37	2.88	3.33	2.90	3.52	3.50	4.25
kl a (lb-mol/h/ft3)	6.05	9.97	14.40	10.12	16.66	16.42	27.05
HG (ft)	0.32	0.24	0.20	0.31	0.23	0.30	0.23
kg a (lb-mol/h/ft3)	18.06	23.84	29.24	37.93	50.05	76.38	100.78
Kg a (lb-moli/h/atm/ft3)	**0.011**	**0.018**	**0.026**	**0.018**	**0.030**	**0.030**	**0.049**

Based on the calculated data, the simultaneous absorption of the molecules CO_2 and CH_4 in Selexol is carried out by means of the same 5 equations (and 5 unknown quantities: x_b, x'_b, L_b, Z and V_a) already showed in the previous chapter for pressurized water scrubbing. It should be remembered that quantities with the superscript refer to methane (for example x_b', y_b'), otherwise to CO_2,

The solution of the equations' system has been carried out for the same 4 specific conditions presented by Table 3.15 (four lines at the top, referring to the use of Selexol); the results are pointed out by Table 3.17. As one can easily observe, CO_2 liquid mole fractions at the bottom of the tower x_b are very similar to those calculated with the mono-absorption approach, whereas methane final concentration in absorbing Selexol is 13 times smaller than CO_2 concentration; that is to say that almost 7% of methane contained by biogas is

absorbed into water and would be dispersed, unless a flash tank recirculation system is adopted to recover it. The calculated tower height doesn't change substantially from the mono-absorption case, so the same already calculated values are maintained.

Table 3.17: calculation of simultaneous absorption of CO_2 and CH_4 in Selexol without flash tank recirculation

L (m3/h)	P (atm)	T (K)	tower diam (m)	x_b *	x_b (recalculated)**	x'_b	CH_4 absorbed (%)	tower height (m)
35	6	298	1	0.072	0.072	0.006	6.90%	9.06
25	8	298	1	0.098	0.098	0.008	6.77%	7.50
20	10	298	1	0.120	0.119	0.010	6.95%	5.60
15	12	298	1	0.154	0.152	0.012	6.52%	6.42

* calculated by mono absorption approach (only CO_2 is absorbed)
** calculated by multi-absorption approach (CO_2 and CH_4 are absorbed into Selexol)

The calculated methane losses are absolutely inacceptable under many aspects, economic and environmental in particular.
As a matter of fact, a recovery through a flash tank operating at low pressure is strictly required. In the present study, the author considered a depressurization down to 2 bar, the lower value in the range assumed by the Swedish Gas Centre and reported in Figure 3.21.

As already explained, the definition of the recirculated flow rates, depending on the flash tank pressure, influences the tower washing performances, making larger dimensions or larger solvent flow rates necessary. The design process is clearly iterative, including the simultaneous absorption in the tower and the mass balance at the flash tank.
Figure 3.22 reports the layout relating to the packed tower and the flash tank, with a precise indications of the involved quantities. It should be noted that, because of the very large molecular weight of Selexol (280 g/mol), the solvent flow rate changes significantly along the treatment, therefore one cannot use just L as done for water scrubbing. This way, we used the subscript L_a, L_b and L_{FT} in order to take into account the variability of the solvent flow rate along the treatment. Consequently, the mass balance reported in the previous chapter dealing with water depressurization at the flash tank should be changed by introducing L variability:

$$P = H \cdot x_{FT} = y_{FT} \cdot P^{FT}$$
$$P^{'} = H^{'} \cdot x^{'}_{FT} = y^{'}_{FT} \cdot P^{FT}$$
$$L_b x_b - L_{FT} x_{FT} = F \cdot y_{FT}$$
$$L_b x^{'}_b - L_{FT} x^{'}_{FT} = F \cdot y^{'}_{FT}$$
$$F = L_b x_b - L_{FT} x_{FT} + L_b x^{'}_b - L_{FT} x^{'}_{FT}$$
$$L_{FT} = L_b - F$$

Remembering that F is the recirculated molal flow rate (the flashed gas from the flash tank), quantities with the superscript refer to methane, otherwise to CO_2, x_{FT} and x'_{FT} are respectively CO_2 and CH_4 concentration in the liquid flow leaving the flash tank, y_{FT} and y'_{FT} are respectively CO_2 and CH_4 concentration in the gas flow leaving the flash tank, Table 3.18 reports the calculation results.
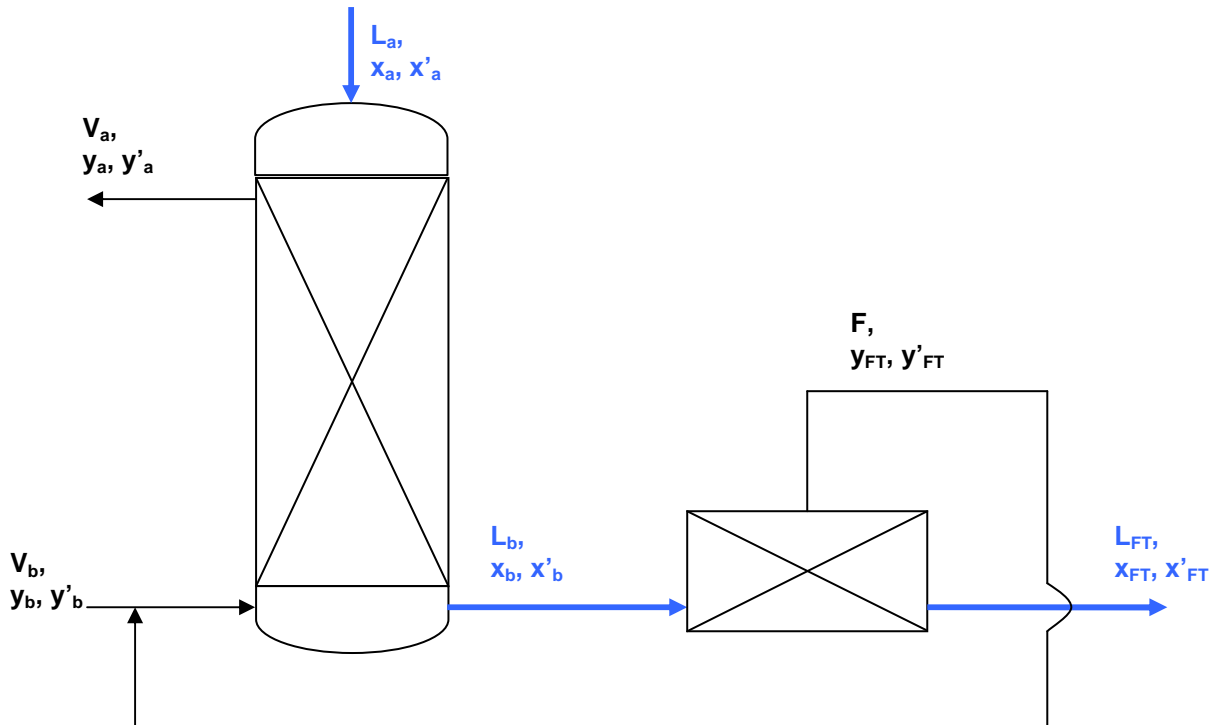
Figure 3.22: absorbing tower and flash tank layout for Selexol scrubbing

Table 3.18: Selexol scrubbing design through simultaneous absorption of carbon dioxide and methane and flash tank simulation (the tower diameter is 1 m, the temperature is 298 K, the flash tank pressure is 2 atm)

L_a (m³/h)	L_a (mol/h)	L_b (mol/h)	P (atm)*	y_b	x_b	x'_b	x_{FT}	x'_{FT}	y_{FT}	y'_{FT}	F (mol/h)	tower height (m)
55	2.02E+05	2.18E+05	6	0.55	0.069	0.0049	4.7E-02	5.8E-04	0.84	0.16	6013.1	7.39
50	1.83E+05	2.03E+05	6	0.61	0.094	0.0043	5.1E-02	2.9E-04	0.92	0.08	10081.2	11.84
50	1.83E+05	2.06E+05	8	0.64	0.106	0.0053	5.1E-02	2.9E-04	0.92	0.08	12962.8	6.41
45	1.65E+05	1.97E+05	8	0.72	0.158	0.0041	5.4E-02	1.3E-04	0.97	0.04	22580.1	20.24
50	1.83E+05	2.26E+05	10	0.77	0.183	0.0042	5.4E-02	1.1E-04	0.97	0.03	31705.2	8.24
45	1.65E+05	2.09E+05	10	0.78	0.206	0.0041	5.4E-02	8.8E-05	0.98	0.02	34476.5	11.69
50	1.83E+05	2.35E+05	12	0.80	0.214	0.0044	5.4E-02	9.0E-05	0.98	0.02	40599.4	6.81
40	1.47E+05	2.01E+05	12	0.81	0.265	0.0041	5.5E-02	6.5E-05	0.98	0.02	45645.2	13.50

* absorbing tower pressure

Based on the reported results, one can calculate methane losses for any of the simulated configurations when the flash tank operates at 2 atm, as pointed out by Table 3.19. The reported figures are not immediately comprehensible, due to the complexity of the involved phenomena. Nonetheless, it is important to observe that, at the same absorbing pressure, the larger the solvent flow rate (L_a) the smaller the CO_2 concentration in the liquid phase after the tower (x_b), the larger methane concentration in the same liquid

phase (x'_b), the richer in methane the recirculated gas after the flash tank (y'_{FT}) and then the lower CO_2 concentration in the gas flow rate (y_b). As a consequence, relatively smaller y_b would justify a better absorption of methane in the solvent (larger x'_b), that is consistent with the previous correlations; moreover, larger solvent flow rates (L_a) and then larger x'_b involves increased x'_{FT} and then the methane losses would be more consistent.

Under the described conditions, the calculated gas flow rates to be re-circulated are very important, up to 200% of the raw biogas input (22 000 mol/h) when scrubbing occurs at 12 atm, the Selexol flow rates that are needed to reach the methane purity target (> 97%) are increased by 40 to more than 200% whereas the tower height could be either slightly reduced (due to the effect of a larger L/V ratio), or even double, according to a smaller solvent flow rate. In spite of the low pressure at the flash tank, the methane losses are not negligible, from 0.1 to 1.1% of biogas methane input). Consequently, pressure at the flash tank could be further decreased in order to minimize methane losses, increasing at the same time plant investment and operating costs.

Table 3.19: comparison between configurations with and without recirculation of flashed gas (the tower diameter is assumed 1 m, the temperature is 298 K) for Selexol scrubbing

	L (m^3/h)	L/V **	F (mol/h)	Z (m)	CH_4 losses
6 atm (*), 298 K					
without recirc	35	7.1	-	9.06	6.90%
with recirc (2 atm)	50	10.1	10081.2	11.84	0.48%
with recirc (2 atm)	55	11.1	6013.1	7.39	1.07%
8 atm (*), 298 K					
without recirc	25	5.1	-	7.50	6.77%
with recirc (2 atm)	45	9.1	22580.1	20.24	0.19%
with recirc (2 atm)	50	10.1	12962.8	6.41	0.48%
10 atm (*), 298 K					
without recirc	20	4.1	-	5.60	6.95%
with recirc (2 atm)	45	9.1	34476.5	11.69	0.13%
with recirc (2 atm)	50	10.1	31705.2	8.24	0.18%
12 atm (*), 298 K					
without recirc	15	3.0	-	6.42	6.52%
with recirc (2 atm)	40	8.1	45645.2	13.50	0.09%
with recirc (2 atm)	50	10.1	40599.4	6.81	0.15%

* absorbing tower pressure
** m^3 for every 100 m^3/h of biogas

The Selexol absorbing plant design includes the desorption tower, generally based on air stripping of the solvent, that is important to regenerate the solvent before a new absorbing cycle. The stripping should be carried out at high temperature and low pressure, in order to make conditions more favourable for CO_2 desorption. In the present case, desorption pressure is fixed at atmospheric pressure (as suggested by Figure 3.21) and temperature at 25°C (the same temperature assumed for absorption process that has been considered conservative for scrubbing design). Figure 3.23 represents the quantities involved in the stripping process, taking into account that:
$L_A = L_{FT}$, that is the solvent flow to treat is the same leaving the flash tank at 2 atm;
$x_A = x_{FT}$, that is carbon dioxide mole fraction in the solvent to be desorbed;
V_B is the air flow rate at the bottom of the tower;

x_B is CO_2 concentration in the regenerated solvent, that is the purity target of the process (x_B will become x_a for the scrubbing process; at the same time L_B will become again L_a).
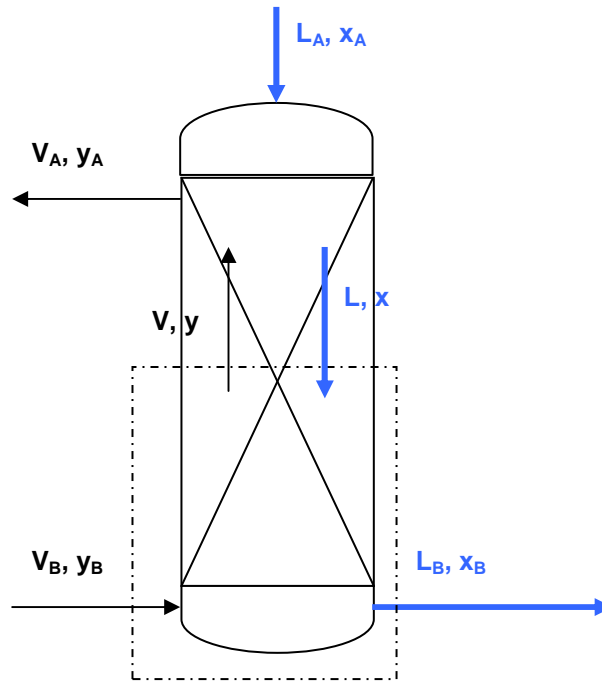
Figure 3.23: material-balance diagram for stripping column

The overall material balance on the terminal streams of the stripping column can be written as:

$$L_A x_A + V_B y_B = L_B x_B + V_A y_A$$

$$L = L_A \cdot \frac{1 - x_A}{1 - x}$$

$$V = V_B + L \cdot x - L_B \cdot x_B$$

$$y_A = \frac{L_A x_A + V_B y_B - L_B x_B}{V_A}$$

where L and V are molal flow rate for liquid and gas phase, x and y are CO_2 mole fraction.

Moreover, the material balance for the portion of the column above an arbitrary section (see Figure 3.23) and the operating-line equation for a differential-contact stripping plant can be written down as follows:

$$L_A x_A + Vy = Lx + V_A y_A$$

$$y = \frac{L}{V} x + \frac{V_A y_A - L_A x_A}{V}$$

The absorption process has been designed by assuming a CO_2 mole fraction in clean solvent x_B (that is x_a, at the top of the absorbing tower, before absorption) corresponding to saturation at atmospheric pressure and 25°C, that is:

$x_a \sim 388 * 10^{-6}$ x 1 atm /(3.6 MPa x 10^6/101 325 atm/MPa) $=1.08 \cdot 10^{-5}$ as CO_2 atmospheric concentration is around 388 ppm and the Henry's law constant for CO_2 in Selexol is 3.6 MPa.

The assumed purity condition is an ideal equilibrium configuration between stripper air and Selexol, that cannot be reached in a stripping tower; however, if one assumes that CO_2 concentration is 10 times larger than the assumed one in clean solvent at the top of the absorbing tower (that is $x_a = 1.08 \cdot 10^{-4}$), the calculated absorbing tower height would change by few centimetres, as reported by Table 3.20. The parameter x_a, within the considered range, is not so influent on the tower absorbing performances.

Table 3.20: influence of x_a (CO_2 concentration at the top of the washing tower) on the absorbing tower height

L_a (m^3/h)	L_a (mol/h)	L_b (mol/h)	L_{FT} (mol/h)	P (atm)*	y_b	x_b	x_a	tower height (m)
55	2.02E+05	2.18E+05	2,12E+05	6	0.55	0.069	1.08E-05 → 1.08E-04	7.39 → 7.44
50	1.83E+05	2.06E+05	1,93E+05	8	0.64	0.106	1.08E-05 → 1.08E-04	6.41 → 6.43
50	1.83E+05	2.26E+05	1,94E+05	10	0.77	0.183	1.08E-05 → 1.08E-04	8.24 → 8.26
50	1.83E+05	2.35E+05	1,94E+05	12	0.80	0.214	1.08E-05 → 1.08E-04	6.81 → 6.82

* absorbing tower pressure

As a consequence, the stripping tower could be designed aiming at obtaining a final CO_2 mole fraction x_B equal to $1.08 \cdot 10^{-4}$.

Before defining the stripping tower height in details, we need to set the tower diameter in order to obtain acceptable pressure drops along the packed column. In this case the worst conditions are represented by the highest gas and liquid flow rates, that is around 212 000 mol/h of solvent to be regenerated (the case deriving from an absorption process carried out at 6 atm), and something like 100 000 mol/h of stripping air (this value corresponds to a confirmed hypothesis). Under this conditions, pressure drops is still lower than 0.5 inch H_2O/foot for a tower diameter of 1 m, that is thoroughly suitable, as pointed out by Figure 3.24.

Another aspect to solve is the overall mass transfer coefficient assessment. As a matter of fact, the following equation, already described for water and glycol ether scrubbing, is still valid:

$$Z_T = \frac{1}{S} \int_B^A \frac{V dy}{(1-y) \cdot (y*-y) \cdot K_y a}$$

As far as the definition of mass transfer coefficients is concerned, the most conservative conditions are represented by the lowest solvent flow rate (L_{FT}), provided that the liquid film resistance is controlling: in this case, the lowest liquid flow rate to be stripped is represented by the condition reported in the last raw by Table 3.18: absorbing pressure 12 atm, $L_a = 40$ m^3/h, $L_b = 2.01$E+05 mol/h, F = 45 645.2 mol/h, $L_{FT} \sim 155$ 000 mol/h of Selexol.

Under these conditions, when stripping air flow rate is just 10 000 mol/h, the mass transfer coefficient for CO_2 and Selexol is 0.332 lb-mol/ft^3/atm/h, that is to say around 5318 mol/m^3/atm/h (150.6 mol/ft^3/atm/h).

Based on the reported figures, it is possible to calculate the stripping tower height according to the solvent conditions (L_{FT} and x_{FT}) reported in Table 3.21. As one can easily observe, 30 000 mol/h of stripping air are enough, in any case, to desorb CO_2 contained in exhausted Selexol within a tower high around 10 m, with a diameter of 1 m, operating at 25°C and atmospheric pressure.

tower diam (m)	1
tower surface (cm2)	7850
L (m3/h)	57,8
L_A (moli/h)	212.000
V_B (moli/h)	100.000
Gx (lb/ft2/s)	4,306
Gy (lb/ft2/s)	0,209
ρx (lb/ft3)	64,085
ρy (lb/ft3)	0,080
Fp	48
μx (cP)	5,8
x-axis	0,729
y-axis	0,01513
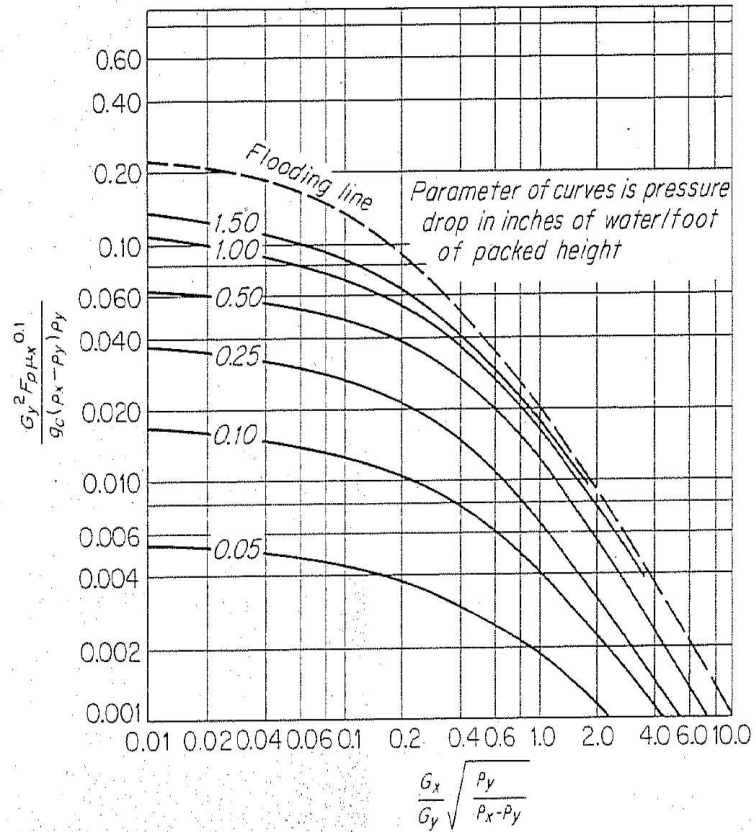
Figure 3.24: pressure drop evaluation for a Selexol stripping tower

Table 3.21: Stripping tower height and involved quantities for Selexol regeneration (the tower diameter is 1 m, T is 298 K, pressure 1 atm)

P (atm) *	L_A (mol/h)	x_A	x_B	V_B (mol/h)	L_B (mol/h)	V_A (mol/h)	y_A	Tower height (m)
6	211 757.8	4.68E-02	1.08E-04	30 000.0	201 875.3	39 882.5	0.248	10.03
6	193 328.0	5.11E-02	1.08E-04	20 000.0	183 469.1	29 858.9	0.330	9.88
8	193 330.5	5.11E-02	1.08E-04	20 000.0	183 469.8	29 860.7	0.330	9.88
8	174 426.7	5.36E-02	1.08E-04	15 000.0	165 093.2	24 333.5	0.384	9.42
10	193 867.3	5.39E-02	1.08E-04	18 000.0	183 433.6	28 433.7	0.367	10.25
10	174 531.4	5.42E-02	1.08E-04	12 000.0	165 087.9	21 443.5	0.441	10.22
12	193 915.6	5.42E-02	1.08E-04	17 000.0	183 430.2	27 485.4	0.382	10.43
12	155 190.0	5.46E-02	1.08E-04	10 000.0	146 738.2	18 451.8	0.458	9.35

* absorbing tower pressure

As far as solvent losses are concerned, sometimes solvent licensor recommends water washing of both the treated gas (biomethane) and the rejected acid gases for solvent recovery; in the analysed case, glycol ethers in general and, more specifically, Selexol (polyethylene glycol dimethyl ethers, DEPG), have very low vapour pressures if compared to other solvents such as Propylene Carbonate (PC), methanol (MeOH), N-Methyl-2-Pyrrolidone (NMP), often used for gas treating, as pointed out by Figure 3.25 (Bryan Research & Engineering).

Solvent	DEPG	PC	NMP	MeOH
Process Name	Selexol or Coastal AGR	Fluor Solvent	Purisol	Rectisol
Viscosity at 25°C (cP)	5.8	3.0	1.65	0.6
Specific Gravity at 25°C (kg/m^3)	1030	1195	1027	785
Molecular Weight	280	102	99	32
Vapor Pressure at 25°C (mmHg)	0.00073	0.085	0.40	125
Freezing Point (°C)	-28	-48	-24	-92
Boiling Point at 760 mm Hg (°C)	275	240	202	65
Thermal Conductivity (Btu/hr*ft*°F)	0.11	0.12	0.095	0.122
Maximum Operating Temperature (°C)	175	65	-	-
Specific Heat 25°C	0.49	0.339	0.40	0.566
CO_2 Solubility (ft^3/U.S. gal) at 25°C	0.485	0.455	0.477	0.425

Figure 3.25: comparison of solvents' physical properties

Based on the reported Selexol vapour pressure, corresponding to 1×10^{-4} kPa, under the worst conditions for solvent volatilization during the washing process (lower absorbing pressure, that is 6 atm) and considering that treated biogas is saturated in Selexol when leaving the absorbing tower, the maximum solvent loss is:

Selexol vapor pressure / total pressure x V_a = $y_{Selexol}$ x V_a = 1×10^{-4} x 1000 / 101,325 atm / 6 atm x 11,850 mol/h x 8000 h/y x 280 g/mol ~ 5 kg Selexol lost in 1 year, that is a very small amount of the circulating solvent.

As far as solvent loss in the stripped acid gas is concerned, the worst conditions are represented by a rejected gas flow rate (V_A) around 40 000 mol/h, saturated in Selexol when leaving the stripping tower, that is:

Selexol vapor pressure / total pressure x V_A = $y_{Selexol}$ x V_A = 1×10^{-4} x 1000 / 101 325 atm / 1 atm x 40 000 mol/h x 8000 h/y x 280 g/mol ~ 100 kg Selexol lost in 1 year, corresponding to a Selexol concentration in stripped air around 13 mg/Nm^3. The calculated solvent loss is still not so large, around 0.17% of the circulating solvent.

As already pointed out, apart from the economically and environmental importance of reducing methane losses from the system, it should be carefully analysed energy consumptions of different plant configuration, depending in particular on pressure design.

In order to calculate energy requirements to compress biogas and recirculated gas flow rates as well as solvent, the same approach followed in the previous chapter 3.1 dealing with water scrubbing has been applied for Selexol wash upgrading process; the same efficiencies for pump and compressors have been considered (respectively 65 and 75%).

Moreover, the absorbing tower has been designed to give pressure drop smaller than 0.5 inch H_2O/foot and the calculated towers are mainly smaller than 10 m (33 feet). Therefore, the maximum pressure drop within

the absorbing tower is less than 0.05 atm, negligible for our purposes (the process pressure lies in the range 6÷12 atm). The same consideration could be done for the stripping tower.

Table 3.22, 3.23 and 3.24 report the electricity consumptions due to biogas and solvent compression according to all pressure/recirculation conditions described in the previous paragraphs.

As one can easily observe, the energy consumptions for biogas compression are very large, in particular for elevated pressure scrubbing: the specific consumption for biogas compression ranges from 0.09 to 0.30 kWh_e/m^3 of raw biogas.

It should be highlighted the strong increase of the biogas temperature after compression, ranging from 170 to 250 °C. The resulting thermal power, (from 30 to more than 100 thermal kW), could be recovered in order to increase solvent temperature in order to facilitate the regeneration process or used for other industrial purposes.

On the other hand, the power need to pump Selexol is lower than in the case of water scrubbing as solvent flow rates are considerably lower. In the present case, the energy requirements regarding the stripping tower have been considered (the stripping tower height being always around 10 m), but they turned out to be quite small, less than 2 kW_e (< 0.005 kWh_e/m^3 of raw biogas).

The overall power consumption, biogas and water compression, lies in the range 0.11÷0.37 kWh_e/m^3 of raw biogas, that is, in our case study, from 54 to 181 kWh_e, mainly due to biogas compression.

Table 3.22: biogas compression energy consumptions for Selexol scrubbing process

	P = 6 atm (*), T = 298 K			P = 8 atm (*), T = 298 K			P = 10 atm (*), T = 298 K			P = 12 atm (*), T = 298 K		
L (m³/h)	35	50	55	25	45	50	20	45	50	15	40	50
flash tank P (atm)	-	2	2	-	2	2	-	2	2	-	2	2
Raw biogas (mol/h)	22019.7	22019.7	22019.7	22019.7	22019.7	22019.7	22019.7	22019.7	22019.7	22019.7	22019.7	22019.7
F (mol/h)	0	10081.2	6013.1	0	22580.1	12962.8	0	34476.5	31705.2	0	45645.2	40599.4
y_b (raw biogas)	0.47	0.47	0.47	0.47	0.47	0.47	0.47	0.47	0.47	0.47	0.47	0.47
y_{FT} (rec F)	-	0.92	0.84	-	0.97	0.92	-	0.98	0.97	-	0.98	0.98
V_b (mol/h)	22019.7	32101.0	28032.9	22019.7	44599.9	34982.5	22019.7	56496.2	53724.9	22019.7	67665.0	62619.2
y_b	0.47	0.61	0.55	0.47	0.72	0.64	0.47	0.78	0.77	0.47	0.81	0.80
V_b (lb/h)	1415.6	2343.6	1940.2	1415.6	3557.2	2608.9	1415.6	4708.4	4433.5	1415.6	5774.4	5291.6
γ	1.311	1.312	1.312	1.311	1.312	1.312	1.311	1.312	1.312	1.311	1.312	1.312
MW (raw biogas) (lb/lb-mol)	29.2	29.2	29.2	29.2	29.2	29.2	29.2	29.2	29.2	29.2	29.2	29.2
MW (F) (lb/lb-mol)	0.0	41.8	39.6	0.0	43.0	41.8	0.0	43.3	43.2	0.0	43.5	43.3
MW (V_b) (lb/lb-mol)	29.2	33.1	31.4	29.2	36.2	33.8	29.2	37.8	37.4	29.2	38.7	38.3
T1 (°C)	20	20	20	20	20	20	20	20	20	20	20	20
T1 (°F)	68	68	68	68	68	68	68	68	68	68	68	68
T2 raw biogas (°F)	340.4	340.5	340.4	396.9	397.3	397.1	443.6	444.1	444.1	483.5	484.2	484.2
T2 rec F (°F)	-	225.4	225.3	-	273.9	273.8	-	314.0	313.9	-	348.3	348.3
T2 V_b (°F)	340.4	296.5	311.3	396.9	322.2	341.2	443.6	350.4	353.0	483.5	376.4	380.8
T2 V_b (°C)	171.3	147.0	155.2	202.7	161.2	171.8	228.6	176.9	178.3	250.8	191.3	193.8
P1 (atm abs)	1.04	1.04	1.04	1.04	1.04	1.04	1.04	1.04	1.04	1.04	1.04	1.04
P2 (atm abs)	6	6	6	8	8	8	10	10	10	12	12	12
P1 (psia)	15.3	15.3	15.3	15.3	15.3	15.3	15.3	15.3	15.3	15.3	15.3	15.3
P2 (psia)	88.2	88.2	88.2	117.6	117.6	117.6	147.1	147.1	147.1	176.5	176.5	176.5
w (Btu/lb) isentrop	78.1	59.7	66.1	94.3	61.7	70.1	107.7	65.6	66.9	119.2	70.1	71.6
Power required (kW$_e$, η=0.75)	43.2	54.7	50.0	52.1	85.7	71.4	59.5	120.7	115.8	65.9	158.0	147.9
specific consumption (kWh$_e$/m³ raw biogas)	0.09	0.11	0.10	0.11	0.17	0.14	0.12	0.24	0.23	0.13	0.32	0.30
thermal recovery (kW)	29.0	35.5	33.0	35.0	54.8	46.2	40.0	77.2	74.0	44.2	100.9	94.7

* absorbing tower pressure

Table 3.23: Selexol compression energy consumptions

	P = 6 atm (*), T = 298 K			P = 8 atm (*), T = 298 K			P = 10 atm (*), T = 298 K			P = 12 atm (*), T = 298 K		
L (m^3/h)	35	50	55	25	45	50	20	45	50	15	40	50
flash tank P (atm)	-	2	2	-	2	2	-	2	2	-	2	2
absorbing tower height Z_a (m)	9.06	11.84	7.39	7.50	20.24	6.41	5.60	11.69	8.24	6.42	13.50	6.81
stripping tower height Z_s (m)	~10	~10	~10	~10	~10	~10	~10	~10	~10	~10	~10	~10
P1 (atm abs)	1	1	1	1	1	1	1	1	1	1	1	P1
$\Delta P = f(Z_a+Z_s)$ atm	1.9	2.2	1.7	1.7	3.0	1.6	1.6	2.2	1.8	1.6	2.3	1.7
P2 (atm abs)	6	6	6	8	8	8	10	10	10	12	12	12
Power required (kW$_e$, η=0.65)	**10.4**	**15.5**	**16.0**	**9.5**	**19.5**	**18.7**	**9.1**	**21.7**	**23.4**	**8.2**	**23.1**	**27.4**
specific consumption (kWh$_e$/m^3 raw biogas)	**0.02**	**0.03**	**0.03**	**0.02**	**0.04**	**0.04**	**0.02**	**0.04**	**0.05**	**0.02**	**0.05**	**0.06**

* absorbing tower pressure

Table 3.24: total energy consumptions for Selexol wash biogas upgrading process

	P = 6 atm (*), T = 298 K			P = 8 atm (*), T = 298 K			P = 10 atm (*), T = 298 K			P = 12 atm (*), T = 298 K		
L (m^3/h)	35	50	55	25	45	50	20	45	50	15	40	50
flash tank P (atm)	-	2	2	-	2	2	-	2	2	-	2	2
tower height (m)	9.06	11.84	7.39	7.50	20.24	6.41	5.60	11.69	8.24	6.42	13.50	6.81
Power required for biogas compression (kW$_e$, η=0.75)	43.2	54.7	50.0	52.1	85.7	71.4	59.5	120.7	115.8	65.9	158.0	147.9
Power required for solvent compression (kW$_e$, η=0.65)	10.4	15.5	16.0	9.5	19.5	18.7	9.1	21.7	23.4	8.2	23.1	27.4
total power (kW$_e$)	**53.6**	**70.2**	**66.1**	**61.6**	**105.2**	**90.1**	**68.7**	**142.4**	**139.2**	**74.1**	**181.1**	**175.3**
specific consumption for biogas compression (kWh$_e$/m^3 raw biogas)	0.09	0.11	0.10	0.11	0.17	0.14	0.12	0.24	0.23	0.13	0.32	0.30
specific consumption for solvent compression (kWh$_e$/m^3 raw biogas)	0.02	0.03	0.03	0.02	0.04	0.04	0.02	0.04	0.05	0.02	0.05	0.06
total consumptions (kWh$_e$/m^3 raw biogas)	**0.11**	**0.14**	**0.13**	**0.12**	**0.21**	**0.18**	**0.14**	**0.29**	**0.28**	**0.15**	**0.37**	**0.36**

* absorbing tower pressure

The pressure drops of Selexol through pipes have been calculated for the worst conditions as follows:
L = 55 m^3/h;
Pipe diameter D = 100 mm;
Mean water velocity V = 1.94 m/s;
Selexol dynamic viscosity = 0.0058 Pa·s;
Roughness of commercial steel pipes: 0.046 mm;
Reynolds number = 34 351;
Relative roughness = 0.00046;
Friction factor ξ = 0.023 (from the Moody Diagram reported in Figure 3.14 of chapter 3.1);
Circuit length l = 100 m (hypothesis);

$$\Delta P \, [Pa] = \zeta \cdot \frac{l}{D} \cdot \frac{V^2}{2} \cdot \rho \cong 44{,}500 \ Pa$$

Therefore the pressure drops for a 100 m circuit of circulating Selexol could be as large as 0.44 atm, that is pretty small, but not negligible, if compared to the total solvent pressurization requirements (8-14 atm, comprehensive of hydraulic heads). Finally, pipeline pressure drops regarding the gaseous phase are surely not influent in our analysis and no further compression is required to inject biomethane into natural gas grid.

Based on the described calculations, the analysis could be concluded by saying that the use of an organic solvent for carbon dioxide strongly reduces the absorbing tower dimension (by 30% on the average of the simulated conditions) and the required solvent flow rates, that are more than halved. As a consequence, the power requirements to compress solvent are reduced on the average to one third of those for water scrubbing.
On the other hand, methane solubility in glycol ethers is quite large and consequently losses could be very important for the usual plant configurations, up to 7 % of the raw input.
In order to improve sustainability by reducing methane losses, it is strongly suggested that the designer apply a low pressure flash tank evaporation and operate a large flashed gas recirculation; the described configuration increases the energy consumptions for gas phase compression, so that the overall power consumption could be as large as 0.37 kWh$_e$/m^3 of raw biogas (the figures are confirmed by literature that reports a range of 0.24÷0.33 kWh$_e$/m^3 of raw biogas, Regione Piemonte, 2009).
Solvent losses aren't really significant.

3.3 Chemical absorption by aqueous alkanolamine solutions

Biogas can be upgraded by chemical absorption with alkanolamines. CO_2 is absorbed in the liquid and reacts at quasi atmospheric pressure with the chemical substance in the absorption column. Afterward, the chemical is regenerated with steam or heat and CO_2 can possibly be recovered. H_2S should be removed in advance to prevent poisoning of the chemical. Chemical scrubbing with amines uses monoethanol amine (MEA CAS# 141-43-5), diethanol amine (DEA CAS# 111-42-2) or diglycol amine (DGA CAS# 929-06-6) as absorbents for CO_2 at atmospheric pressure. Chemical absorption with amines is claimed to have very high efficiencies (>99% CH_4), very low methane losses (< 0.1%), lower energy costs and smaller equipments, more cost competitive for larger plants than for smaller. Chemo-absorption with MEA, one of the most frequently used chemical absorbers, has the advantages of lower solution costs if compared to DEA; on the other hand, it is a colourless, viscous, poisonous and aggressive liquid, that is strategies to reduce corrosion and foaming are required. Moreover, alkanolamines in general can be decomposed by oxygen, then the maximum attention should be paid to limit the introduction of air into digesters.

Based on literature data at disposal, that are more frequent for MEA than for other reactants, provided that many upgrading plants are running with MEA in the world, MEA has been chosen for the following design calculation. MEA chemical and physical properties are reported by Figure 3.26 (from Wikipedia).

Properties		Hazards	
Molecular formula	C_2H_7NO	MSDS	JT Baker
		R-phrases	R20, R34, R36/37/38
Molar mass	61.08 g mol^{-1}	S-phrases	S26, S27, S36/37, S39, S45
Appearance	Viscous colourless liquid with ammonia odour	NFPA 704	
Density	1.012 g/cm^3		
Melting point	10.3 °C, 283 K, 51 °F		
Boiling point	170 °C, 443 K, 338 °F	Flash point	85 °C (closed cup)
Solubility in water	Miscible	Autoignition temperature	410 °C
Vapor pressure	64 Pa (20 °C)[1]	Explosive limits	5.5 - 17%
Acidity (pK_a)	9.50[2]	U.S. Permissible exposure limit (PEL)	3 ppm
Refractive index (n_D)	1.4539 (20 °C)[3]		

Figure 3.26: MEA properties

When CO_2 is absorbed and reacts with aqueous MEA solutions, if the carbonation ratio r_c (or CO_2 loading) is less than 0.5 mole of CO_2 per mole of MEA, the following three reactions take place:

$$CO_{2,g} \rightarrow CO_{2,l} + H_{absorption}$$

$$CO_{2,l} + 2BNH_2 \xrightarrow{k_2} BNHCOO^- + BNH_3^+ + H_{reaction}$$

$$CO_{2,l} + BNHCOO^- + 2H_2O \rightarrow BNH_3^+ + 2HCO_3^-$$
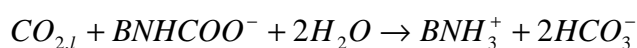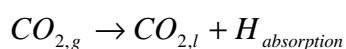
where letter B represents the group $HOCH_2CH_2^-$ and the first step is the physical absorption of CO_2 in MEA solution. At very short times of the liquid-gas contact realised in industrial absorbers, the third reaction (conversion of carbamate to bicarbonate) can be neglected and only the second reaction (carbamate formation) affects the absorption rate of CO_2 (Astarita, 1967), according to the following kinetic:

$$reaction\ rate\ Rc = k_2 [CO_2][MEA]$$

$$\log K_2 = 10.99 - 2152/T$$

The reaction heat of the considered reaction is 1920 kJ/kg CO_2.

Therefore, the absorption of CO_2 in MEA solutions can be considered as gas absorption accompanied by an irreversible and virtually instantaneous second-order reaction with a stoichiometric coefficient of 2, that is to say each CO_2 mole requires 2 moles of MEA to react and then disappear from the liquid phase bulk. As a matter of fact, carbon dioxide will be present in liquid phase just in a very narrow volume close to the interface, being the liquid bulk concentration of CO_2 equal to zero due to the described reaction.

Nevertheless, it is important to know CO_2 solubility in aqueous MEA solution in order to calculate mass transfer coefficients. The following approach is suggested by Liu et al (2006):

$$X_{i,CO_2} = H_{CO_2,l} \cdot P \cdot y$$

$$H_{CO_2,l} = H_{N_2O,l} \cdot \frac{H_{CO_2,w}}{H_{N_2O,w}}$$

$$H_{CO_2,w} = (2.82 \cdot 10^6 \exp(-2044/T))^{-1}$$

$$H_{N_2O,w} = (8.5522 \cdot 10^6 \exp(-2284/T))^{-1}$$

$$\ln H_{N_2O,l} = v_{MEA} \cdot \ln H_{N_2O,MEA} + v_{H_2O} \cdot \ln H_{N_2O,w} + \chi_{MEA,H_2O}$$

$$\chi_{MEA,H_2O} = -v_{MEA}v_{H_2O}(4.793 - 7.466 \cdot 10^{-3}T - 2.201v_{H_2O})$$

$$H_{N_2O,MEA} = (1.2072 \cdot 10^5 \exp(-1136.5/T))^{-1}$$

where $X_{i,CO2}$ is molar concentration of CO_2 at the interface (kmol/m^3), y is molar fraction of CO_2 in the gas phase, $H_{CO2,l}$ is Henry's law constant of CO_2 in MEA aqueous solution, obtained by using N_2O analogy, v_{MEA} and v_{H2O} are the volume fractions of MEA and water in aqueous solution respectively, P is total pressure, T is temperature in K.

Table 3.25 reports Henry's law constant calculated by the described approach according to different temperatures and MEA concentrations.

In our case, in order to be conservative, the solubility of CO_2 in MEA solutions have been calculated at the top of the chemo-absorbing tower, where MEA concentration is at the maximum (MEA is consumed while going down through the absorbing tower), and then solubility is the lowest of the entire column. The effect of temperature on solubility will be analysed later on.

The viscosity μ_l of aqueous MEA solutions strongly depends on temperature, MEA concentration (expressed as average mass fraction C) and carbonation ratio r_c Liu et al (2006):

$$\mu_l / \mu_{H2O} = \exp\left(\frac{100C(2373 + 2118.6C)[r_c(-2.2589 + 0.0093T + 1.015C) + 1]}{T^2}\right)$$

Table 3.25: CO$_2$ solubility in MEA aqueous solutions

H$_{CO2,l}$ (kmol/m^3/kPa)	molar concentration of MEA in liquid phase (kmol/m^3)					pure water
T (K)	10	7	5	3	1	
283	0.000356	0.000375	0.000406	0.000442	0.000475	0.000486
288	0.000331	0.000344	0.000369	0.000397	0.000422	0.000429
298	0.000288	0.000292	0.000307	0.000324	0.000336	0.000338
303	0.000269	0.000271	0.000282	0.000295	0.000302	0.000302
H$_{CO2,l}$ (atm*l/mol)	molar concentration of MEA in liquid phase (kmol/m^3)					pure water
T (K)	10	7	5	3	1	
283	2.77E+01	2.63E+01	2.43E+01	2.23E+01	2.08E+01	2.03E+01
288	2.98E+01	2.87E+01	2.68E+01	2.48E+01	2.34E+01	2.30E+01
298	3.43E+01	3.38E+01	3.21E+01	3.04E+01	2.93E+01	2.92E+01
303	3.66E+01	3.65E+01	3.50E+01	3.35E+01	3.27E+01	3.27E+01

In order to take into account the variability of the carbonation ratio and MEA concentration along the tower, the mass fraction C and the carbonation ratio can be calculated as logarithmic mean values, that seems to be a very good approximation of the parameters' behaviour in the space. Table 3.26 reports the viscosity of different MEA solutions.

Table 3.26: MEA aqueous solutions viscosity μ$_l$ (kg/m/s) at 25°C

μ$_l$ (kg/m/s)	molar concentration of MEA in liquid phase (kmol/m^3)					pure water
T (K)	10	7	5	3	1	
298	0.009825	0.004044	0.002434	0.001569	0.001299	0.001

Similarly to the definition of Henry's law constant, molecular diffusivity of CO$_2$ in MEA solution D$_{CO2,l}$ can be determined by N$_2$O analogy:

$$D_{CO_2,l} = D_{N_2O,l} \cdot \frac{D_{CO_2,w}}{D_{N_2O,w}}$$

$$D_{CO_2,w} = 2.35 \cdot 10^{-6} \exp(-2119/T)$$

$$D_{N_2O,w} = 5.075 \cdot 10^{-6} \exp(-2371/T)$$

$$D_{N_2O,l} = \left(5.07 + 0.865 X_{MEA} + 0.278 X_{MEA}^2\right) \cdot \exp\left(\frac{-2371.0 - 93.4 X_{MEA}}{T}\right) \cdot 10^{-6}$$

$$D_{MEA,l} = \exp(-13.275 - 2198.3/T - 0.078142 X_{MEA})$$

where X$_{MEA}$ is molar concentration of MEA in liquid phase (kmol/m^3). Table 3.27 reports the calculated molecular diffusivity.

Table 3.27: molecular diffusivity of CO_2 in MEA aqueous solutions

$D_{CO2,l}$ (m^2/s)	molar concentration of MEA in liquid phase (kmol/m^3)					pure water
T (K)	10	7	5	3	1	
T = 298 K	6.84E-10	1.04E-09	1.29E-09	1.5E-09	1.6E-09	1.92E-09
T = 313 K	1.12E-09	1.63E-09	1.96E-09	2.21E-09	2.32E-09	2.70E-09

Again, the molecular diffusivity of CO_2 in MEA solutions has been calculated at the top of the chemo-absorbing tower, where MEA concentration is at the maximum and then diffusivity is the lowest of the entire column: this way the mass transfer calculations turn out to be conservative.

Absorption followed by reaction in the liquid phase is often used to get more complete removal of a solute from a gas mixture as reaction in the liquid phase reduces the equilibrium partial pressure of the solute (CO_2) over the solution, which greatly increases the driving force for mass transfer. As we will comment later on, if the reaction can be considered essentially irreversible at absorption conditions, the equilibrium CO_2 partial pressure is zero. A further advantage of chemo-absorption is the increase of mass transfer coefficient; some of this increase comes from a greater effective interfacial area, since absorption can now take place in the nearly stagnant regions as well as in the dynamic liquid holdup. When the liquid film resistance is dominant, as in the case of CO_2 absorption in aqueous solutions, a rapid chemical reaction in the liquid can lead to a strong increase in the overall mass-transfer coefficient. The rapid reaction consumes much of carbon dioxide very close to the gas-liquid interface, which makes the gradient for CO_2 steeper and enhances the mass transfer process in the liquid. The ratio of the mass transfer coefficient for the absorption with chemical reaction $k_{R,l}$ to the mass transfer coefficient k_l for the physical absorption is defined as enhancement factor E and varies along the column height. As a matter of fact, the overall mass transfer coefficient referred to the gas phase K_g can be determined as:

$$\frac{1}{K_g} = \frac{1}{k_g} + \frac{1}{k_l \cdot E \cdot H_{CO_2,l}}$$

Where $H_{CO2,l}$ is expressed as kmol/m^3/kPa, k_l in m/s, k_g and K_g in kmol/m^2/s/kPa.
The single mass transfer coefficients for the liquid and the gas phases are determined from the correlations by Onda et al. (1968), that give results pretty similar to those calculated by the already applied Sherwood and Holloway's approach.

$$k_l = 0.0051 \cdot \left(\frac{\mu_l g}{\rho_l}\right)^{\backslash 1/3} \left(\frac{L_m}{a_w \mu_l}\right)^{2/3} \left(\frac{\mu_l}{\rho_l D_{CO_2,l}}\right)^{-0.5} (a \cdot dp)^{0.4}$$

$$k_g = 5.23 \cdot \left(\frac{G_m}{a\mu_g}\right)^{0.7} \left(\frac{\mu_g}{\rho_g D_g}\right)^{1/3} (a \cdot dp)^{-2} \left(\frac{RT}{aD_g}\right)^{-1}$$

where ρ_l is the liquid density (changing along the tower; in the case CO_2 loading is fairly lower than 0.5, it doesn't change significantly), L_m is the liquid flow rate per unit cross-section area (kg/m^2/s), G_m is the gas phase flow rate per unit cross-section area (kg/m^2/s), μ_g is the gas viscosity (μ_{CH4} = 0.01027 cP, μ_{CO2} is 0.01372 cP, that is μg changes along the tower, reaching the minimum at the top where methane is 97%), ρ_g is gas density (strongly changing from the bottom to the top, from 1.3 to 0.75 g/l), D_g is CO_2 molecular diffusivity in the gas phase (around 1.19 x 10^{-5} m^2/s), a is surface area per unit volume of packed bed in m^{-1} (for example, for 1 inch Berl saddles a is 76 ft^2/ft^3), dp is the nominal diameter of the packed particle in m (1 inch Berl saddles = 0.0254 m), R is gas universal constant (8.314 kJ/kmol/K), a_w is wetted surface area (m^{-1}).

According to Onda's research, a_w is considered to be equal to a_{eff}, that is the effective area for mass transfer between gas and liquid phase. a_w can be obtained by the following correlations by Weiland et al. (1998).

$$\frac{a_w}{a} = \frac{a_{eff}}{a} = 1 - \exp\left[-1.45\left(\frac{\sigma_{ct}}{\sigma_l}\right)^{0.75}\left(\frac{L_m}{a\mu_l}\right)^{0.1}\left(\frac{L_m^2 a}{\rho_l^2 g}\right)^{-0.05}\left(\frac{L_m^2}{\rho_l a \sigma_l}\right)^{0.2}\right]$$

where σ_{ct} is the critical surface tension of the packing material (0.061 N/m for ceramic materials), σ_l is the surface tension of MEA aqueous solution in N/m that can be obtained as follows:

$$\sigma_l = \sigma_{H_2O} - \left(\sigma_{H_2O} - \sigma_{MEA}\right)\cdot\left(1 + \frac{(0.63036 - 1.3\cdot 10^{-5}(T - 273.15))\cdot x_{H_2O}}{1 - (0.947 - 2\cdot 10^{-5}(T - 273.15))\cdot x_{H_2O}}\right)x_{MEA}$$

$$\sigma_{H_2O} = 76.0852 - 0.1609\cdot (T - 273.15)$$

$$\sigma_{MEA} = 53.082 - 0.1648\cdot (T - 273.15)$$

where x_{H2O} and x_{MEA} are the molar fraction of water and MEA in the aqueous solution.

The enhancement factor E for the irreversible second-order reaction such as CO_2-MEA reaction can be determined by the following explicit correlation based on the Hatta number (Ha), obtained by Wellek et al. (1978) with deviation less than 3%:

$$Ha = \frac{D_{CO_2,l}\cdot k_2\cdot X_{MEA}}{k_l^2}$$

$$E_1 = \frac{\sqrt{Ha}}{\tanh\sqrt{Ha}}$$

$$E_i = 1 + \frac{D_{MEA,l} X_{MEA}}{2D_{CO_2,l} X_{i,CO_2}}$$

$$E = 1 + \left((E_i - 1)^{-1.35} + (E_1 - 1)^{-1.35}\right)^{-1/1.35}$$

As one can easily observe, many of the involved parameters changes along the tower, determining a variable enhancement factor (E is maximum at the top of the chemo-absorbing column) and, consequently, a variable overall mass transfer coefficient. In our calculations, we assumed the most conservative conditions for CO_2 solubility (the minimum one), CO_2 diffusivity in the MEA solution (the minimum one) and the wetted area (the minimum one, at the top of the column), MEA solution density is considered constant, liquid viscosity is calculated by means of logarithmic mean values, gas phase density, gas phase viscosity, liquid and gas phase flow rates are variable through the chemo-absorption process.

In the studied case, it is important to observe that, for very large enhancement factor values, the gas film may become the controlling resistance, that is precisely what happens here.

Table 3.28 reports some simulated overall mass transfer coefficients, obtained for the following conditions:
- Chemo-absorption carried out at pressure similar to atmospheric,
- Temperature from 25 to 40°C;

- MEA concentration in aqueous solution: 3÷5 kmol/m^3 (as suggested by the experience of many plants);
- CO_2 loading < 0.5 mol of CO_2 per mol of MEA;
- Liquid flow rate L_a: 8.5÷20 m^3/h of MEA solution;
- Tower diameter of 0.5 m.

In the case of chemo-absorption, the minimum liquid flow rate is not decided on the base of the equilibrium curve (solubility) as occurring for physical absorption; when the absorption is followed by a reaction, the minimum La is fixed by reaction stoichiometry, that corresponds to CO_2 loading < 0.5 mol of CO_2 per mol of MEA. This condition must be verified at any tower level, being the bottom stage of the column the most important section (there, CO_2 loading shows the maximum values). If one considers that at the bottom 0.47 x 22020 mol/h = 10 349 mol CO_2/h enters the chemo-absorbing tower and 9 988 mol CO_2/h should be absorbed and react in order to comply with the biomethane purity target at the top of the column (3% of CO_2), the minimal condition for the solvent flow rate and MEA concentration could be expressed as:

$$L_a \cdot X_{MEA}(top) \cdot 1000 - 2 \cdot 9988 \left[\frac{mol\ MEA}{h} \right] \geq 2 \cdot 10349 \left[\frac{mol\ CO_2}{h} \right]$$

that is to say that L_a [m^3/h] x X_{MEA} [kmol/m^3] ≥ 40 674 mol MEA/h.

As pointed out by Table 3.28, considering the assigned conditions (L_a and X_{MEA}), the enhancement factor at the bottom of the tower are in the range 17÷37 at 298 K and 23÷48 at 313 K; at the top of the column it lies in the range 31÷81 at 298 K and 44÷116 at 313 K; the calculated values are confirmed by many studies, both computational and experimental, as pointed out by Figure 3.27 (Liu et al, 2006).

Table 3.28: enhancement factor and mass transfer coefficients calculation for MEA aqueous solutions

tower diam (m)	0,5	0,5	0,5	0,5	0,5	0,5	0,5	0,5	0,5	0,5	0,5	0,5
tower surface (cm2)	1962,5	1962,5	1962,5	1962,5	1962,5	1962,5	1962,5	1962,5	1962,5	1962,5	1962,5	1962,5
tower surface (ft2)	2,11	2,11	2,11	2,11	2,11	2,11	2,11	2,11	2,11	2,11	2,11	2,11
P (atm)	1	1	1	1	1	1	1	1	1	1	1	1
T (K)	298	298	298	298	298	298	313	313	313	313	313	313
Vb (moli/h)	22019,7	22019,7	22019,7	22019,7	22019,7	22019,7	22019,7	22019,7	22019,7	22019,7	22019,7	22019,7
Vb (kg/m2/s)	0,909	0,909	0,909	0,909	0,909	0,909	0,909	0,909	0,909	0,909	0,909	0,909
Va (moli/h)	12031,4	12031,4	12031,4	12031,4	12031,4	12031,4	12031,4	12031,4	12031,4	12031,4	12031,4	12031,4
Va (kg/m2/s)	0,287	0,287	0,287	0,287	0,287	0,287	0,287	0,287	0,287	0,287	0,287	0,287
La (m3/h)	20	15	15	10	14	8,5	20	15	15	10	14	8,5
La (mol/h)	970189	657181	727642	438120	679132	372402	970189	657181	727642	438120	679132	372402
La (kg/m2/s)	28,37	21,31	21,28	14,21	19,86	12,07	28,37	21,31	21,28	14,21	19,86	12,07
CO2 at the bottom (mol/h)	9988,3	9988,3	9988,3	9988,3	9988,3	9988,3	9988,3	9988,3	9988,3	9988,3	9988,3	9988,3
CO2 at the top (mol/h)	360,9	360,9	360,9	360,9	360,9	360,9	360,9	360,9	360,9	360,9	360,9	360,9
X MEA top (kmol/m3)	3	5	3	5	3	5	3	5	3	5	3	5
MEA (g in 1 m3 solution)	183000	305000	183000	305000	183000	305000	183000	305000	183000	305000	183000	305000
H2O (g in 1 m3 solution)	819170	698617	819170	698617	819170	698617	819170	698617	819170	698617	819170	698617
X MEA top (% by w)	0,18	0,30	0,18	0,30	0,18	0,30	0,18	0,30	0,18	0,30	0,18	0,30
vMEA (volume fraction)	0,181	0,301	0,181	0,301	0,181	0,301	0,181	0,301	0,181	0,301	0,181	0,301
vH2O (volume fraction)	0,819	0,699	0,819	0,699	0,819	0,699	0,819	0,699	0,819	0,699	0,819	0,699
xMEA top (molar fraction)	0,062	0,114	0,062	0,114	0,062	0,114	0,062	0,114	0,062	0,114	0,062	0,114
xH20 top (molar fraction)	0,938	0,886	0,938	0,886	0,938	0,886	0,938	0,886	0,938	0,886	0,938	0,886
ρl top (g/l)	1002,2	1003,6	1002,2	1003,6	1002,2	1003,6	1002,2	1003,6	1002,2	1003,6	1002,2	1003,6
ρl (lb/ft3)	62,6	62,6	62,6	62,6	62,6	62,6	62,6	62,6	62,6	62,6	62,6	62,6
MWl (g/mol)	20,7	22,9	20,7	22,9	20,7	22,9	20,7	22,9	20,7	22,9	20,7	22,9
CO2 loading top (mol CO2/mol MEA)	0,0060	0,0048	0,0080	0,0072	0,0086	0,0085	0,0060	0,0048	0,0080	0,0072	0,0086	0,0085
CO2 loading bottom (mol CO2/mol MEA)	0,2586	0,1881	0,4136	0,3447	0,4699	0,4595	0,2586	0,1881	0,4136	0,3447	0,4699	0,4595
CO2 loading log-mean(mol CO2/mol MEA)	0,0672	0,0500	0,1029	0,0873	0,1153	0,1130	0,0672	0,0500	0,1029	0,0873	0,1153	0,1130
Lb (moli/h)	970189	657181	727642	438120	679132	372402	970189	657181	727642	438120	679132	372402
Lb (kg/m2/s)	28,99	21,93	21,90	14,83	20,48	12,70	28,99	21,93	21,90	14,83	20,48	12,70
MEA final mass fraction (% by w)	0,12	0,22	0,10	0,17	0,09	0,15	0,12	0,22	0,10	0,17	0,09	0,15
X MEA bottom (kmol/m3)	1,958	3,564	1,621	2,876	1,525	2,520	1,958	3,564	1,621	2,876	1,525	2,520
xMEA bottom (molar fraction)	0,041	0,084	0,034	0,069	0,032	0,060	0,041	0,084	0,034	0,069	0,032	0,060
DN2O,l (m2/s)	1,39E-09	1,20E-09	1,39E-09	1,20E-09	1,39E-09	1,20E-09	2,13E-09	1,89E-09	2,13E-09	1,89E-09	2,13E-09	1,89E-09
DCO2,w (m2/s)	1,92E-09	1,92E-09	1,92E-09	1,92E-09	1,92E-09	1,92E-09	2,70E-09	2,70E-09	2,70E-09	2,70E-09	2,70E-09	2,70E-09
DNO2,w (m2/s)	1,78E-09	1,78E-09	1,78E-09	1,78E-09	1,78E-09	1,78E-09	2,60E-09	2,60E-09	2,60E-09	2,60E-09	2,60E-09	2,60E-09
DCO2,l (m2/s)	1,50E-09	1,29E-09	1,50E-09	1,29E-09	1,50E-09	1,29E-09	2,21E-09	1,96E-09	2,21E-09	1,96E-09	2,21E-09	1,96E-09
DMEA,l (m2/s)	8,50E-10	7,27E-10	8,50E-10	7,27E-10	8,50E-10	7,27E-10	1,21E-09	1,03E-09	1,21E-09	1,03E-09	1,21E-09	1,03E-09
k2 (m3/kmol/s)	5868,45	5868,45	5868,45	5868,45	5868,45	5868,45	13019,69	13019,69	13019,69	13019,69	13019,69	13019,69
HCO2,w (kmol/m3/kPa)	3,38E-04	3,38E-04	3,38E-04	3,38E-04	3,38E-04	3,38E-04	2,43E-04	2,43E-04	2,43E-04	2,43E-04	2,43E-04	2,43E-04
HN2O,w (kmol/m3/kPa)	2,49E-04	2,49E-04	2,49E-04	2,49E-04	2,49E-04	2,49E-04	1,73E-04	1,73E-04	1,73E-04	1,73E-04	1,73E-04	1,73E-04
HN2O,MEA (kmol/m3/kPa)	3,75E-04	3,75E-04	3,75E-04	3,75E-04	3,75E-04	3,75E-04	3,13E-04	3,13E-04	3,13E-04	3,13E-04	3,13E-04	3,13E-04
ξ MEA,H2O	-0,11	-0,22	-0,11	-0,22	-0,11	-0,22	-0,10	-0,19	-0,10	-0,19	-0,10	-0,19
HN2O,l (kmol/m3/kPa)	2,39E-04	2,27E-04	2,39E-04	2,27E-04	2,39E-04	2,27E-04	1,74E-04	1,70E-04	1,74E-04	1,70E-04	1,74E-04	1,70E-04
HCO2,l (kmol/m3/kPa)	3,24E-04	3,07E-04	3,24E-04	3,07E-04	3,24E-04	3,07E-04	2,46E-04	2,39E-04	2,46E-04	2,39E-04	2,46E-04	2,39E-04
μl (kg/m/s)	0,00161	0,00244	0,00157	0,00229	0,00156	0,00222	0,00155	0,00225	0,00151	0,00214	0,00151	0,00208
ρg (lb/ft3)	0,0812	0,0812	0,0812	0,0812	0,0812	0,0812	0,0812	0,0812	0,0812	0,0812	0,0812	0,0812
ρg bottom (g/l)	1,3010	1,3010	1,3010	1,3010	1,3010	1,3010	1,3010	1,3010	1,3010	1,3010	1,3010	1,3010
ρg top (g/l)	0,7513	0,7513	0,7513	0,7513	0,7513	0,7513	0,7513	0,7513	0,7513	0,7513	0,7513	0,7513
L (lb/ft2/s)	5,816	4,368	4,362	2,912	4,071	2,475	5,816	4,368	4,362	2,912	4,071	2,475
G (lb/ft2/s)	0,186	0,186	0,186	0,186	0,186	0,186	0,186	0,186	0,186	0,186	0,186	0,186
μl (cP)	1,61	2,44	1,57	2,29	1,56	2,22	1,55	2,25	1,51	2,14	1,51	2,08
μl (lb/h/ft)	3,90	5,89	3,80	5,53	3,77	5,37	3,75	5,45	3,66	5,17	3,64	5,04
μg bottom (cP)	0,0118915	0,0118915	0,0118915	0,0118915	0,0118915	0,0118915	0,0118915	0,0118915	0,0118915	0,0118915	0,0118915	0,0118915
μg bottom (lb/h/ft)	0,029	0,029	0,029	0,029	0,029	0,029	0,029	0,029	0,029	0,029	0,029	0,029
μg bottom (kg/m/s)	0,0000119	0,0000119	0,0000119	0,0000119	0,0000119	0,0000119	0,0000119	0,0000119	0,0000119	0,0000119	0,0000119	0,0000119
μg top (cP)	0,0103735	0,0103735	0,0103735	0,0103735	0,0103735	0,0103735	0,0103735	0,0103735	0,0103735	0,0103735	0,0103735	0,0103735
μg top (lb/h/ft)	0,025	0,025	0,025	0,025	0,025	0,025	0,025	0,025	0,025	0,025	0,025	0,025
μg top (kg/m/s)	0,0000104	0,0000104	0,0000104	0,0000104	0,0000104	0,0000104	0,0000104	0,0000104	0,0000104	0,0000104	0,0000104	0,0000104
Dl (ft2/h)	5,82E-05	5,00E-05	5,82E-05	5,00E-05	5,82E-05	5,00E-05	8,56E-05	7,58E-05	8,56E-05	7,58E-05	8,56E-05	7,58E-05
Dg (ft2/h)	0,46	0,46	0,46	0,46	0,46	0,46	0,46	0,46	0,46	0,46	0,46	0,46
Dg (m2/s)	0,0000119	0,0000119	0,0000119	0,0000119	0,0000119	0,0000119	0,0000119	0,0000119	0,0000119	0,0000119	0,0000119	0,0000119
σH2O (dynes/cm)	72,09	72,09	72,09	72,09	72,09	72,09	69,67	69,67	69,67	69,67	69,67	69,67
σMEA (dynes/cm)	48,99	48,99	48,99	48,99	48,99	48,99	46,51	46,51	46,51	46,51	46,51	46,51
σL (dynes/cm)	63,12	60,34	63,12	60,34	63,12	60,34	60,71	57,92	60,71	57,92	60,71	57,92
a (m2/m3)	249,28	249,28	249,28	249,28	249,28	249,28	249,28	249,28	249,28	249,28	249,28	249,28
aeff/a	0,7653	0,7260	0,7262	0,6697	0,7166	0,6469	0,7792	0,7424	0,7406	0,6864	0,7311	0,6636
kl top (m/s)	1,67E-04	9,39E-05	1,46E-04	7,97E-05	1,41E-04	7,51E-05	2,07E-04	1,22E-04	1,80E-04	1,02E-04	1,74E-04	9,58E-05
kl bottom (m/s)	1,69E-04	9,57E-05	1,49E-04	8,20E-05	1,44E-04	7,76E-05	2,10E-04	1,24E-04	1,84E-04	1,05E-04	1,78E-04	9,91E-05
kg top (kmol/m/s/kPa)	4,49E-06	4,49E-06	4,49E-06	4,49E-06	4,49E-06	4,49E-06	4,28E-06	4,28E-06	4,28E-06	4,28E-06	4,28E-06	4,28E-06
kg bottom (kmol/m/s/kPa)	7,98E-06	7,98E-06	7,98E-06	7,98E-06	7,98E-06	7,98E-06	7,59E-06	7,59E-06	7,59E-06	7,59E-06	7,59E-06	7,59E-06
Ha top	949,33	4292,62	1242,88	5960,29	1322,93	6720,37	2015,27	8618,25	2662,27	12184,38	2840,74	13861,84
E1 top	30,81	65,52	35,25	77,20	36,37	81,98	44,89	92,83	51,60	110,38	53,30	117,74
Ei top	861,05	1508,47	861,05	1508,47	861,05	1508,47	1101,46	1818,86	1101,46	1818,86	1101,46	1818,86
Enhancement factor top	30,58	64,85	34,93	76,21	36,02	80,84	44,48	91,64	51,02	108,59	52,67	115,66
Kg top (kmol/m2/s/kPa)	1,21E-06	1,32E-06	1,21E-06	1,32E-06	1,21E-06	1,32E-06	1,48E-06	1,64E-06	1,48E-06	1,64E-06	1,48E-06	1,64E-06
Kg aeff top (moli/h/atm/ft3)	2386,17	2471,07	2261,59	2275,24	2231,11	2196,29	2968,69	3142,16	2817,91	2898,86	2780,84	2799,97
Ha bottom	602,01	2944,75	646,19	3238,37	645,53	3167,61	1277,96	5912,14	1384,15	6620,06	1386,15	6533,71
E1 bottom	24,54	54,27	25,42	56,91	25,41	56,28	35,75	76,89	37,20	81,36	37,23	80,83
Ei bottom	36,83	69,59	30,66	56,35	28,91	49,50	46,85	83,71	38,95	67,75	36,71	59,48
Enhancement factor bottom	17,88	36,79	17,00	34,29	16,57	31,90	24,58	48,35	23,17	44,58	22,53	41,23
Kg bottom (kmol/m2/s/kPa)	8,75E-07	9,53E-07	7,44E-07	7,80E-07	7,07E-07	6,94E-07	1,09E-06	1,21E-06	9,18E-07	9,78E-07	8,71E-07	8,67E-07
Kg aeff bottom (moli/h/atm/ft3)	1724,66	1782,38	1392,14	1345,28	1306,15	1157,61	2180,43	2307,91	1752,02	1729,66	1641,17	1481,75

The overall mass transfer coefficients $K_g a_{eff}$ are very large, ranging between 1000 and 3000 mol/h/atm/ft^3, 20-40 times larger than in the case of pure water absorption, confirming many literature indications. Higher temperatures, in spite of the decreased CO_2 solubility, involve a quite strong increase in mass transfer coefficients: this means that the effect of a larger reaction rate (k_2), summed up to a smaller liquid viscosity and a higher molecular diffusivity in the solution, is stronger than a reduction in Henry's law constant.

Before any calculation of tower height is performed, it is important to predict the effect of absorption and chemical reaction on temperature: as already seen, the CO_2 heat of absorption ($H_{absorption}$) in water is 19 kJ/mol CO_2 at 288 K, whereas the reaction is exothermic and $H_{reaction}$ = 84.5 kJ/mol CO_2 (1920 kJ/kg CO2). When L_a is 20 m^3/h, the MEA solution temperature increase from the top to the bottom is 12 °C, 16.5 °C when L_a is 15 m^3/h, 25 °C when L_a is 10 m^3/h and 29°C when L_a is 8.5 m^3/h. The calculated values are consistent with other simulations reported by literature (Figure 3.27). The temperature increase doesn't represent a problem since it involves a pretty large growth in overall mass transfer coefficients. As a consequence, in order to be very conservative, the following absorbing tower design process will take into account the lower mass transfer coefficient for all the considered conditions, that is to say the bottom value, and a temperature equal to that at the top (the minimum value) along all the column (isothermal conditions).

Differently to what applied for physical scrubbing, the mass transfer coefficient in the case of chemo-absorption has been calculated case by case, because it strongly depends on both solvent flow rate and reactant concentration, consequently showing a great variability that must be considered.
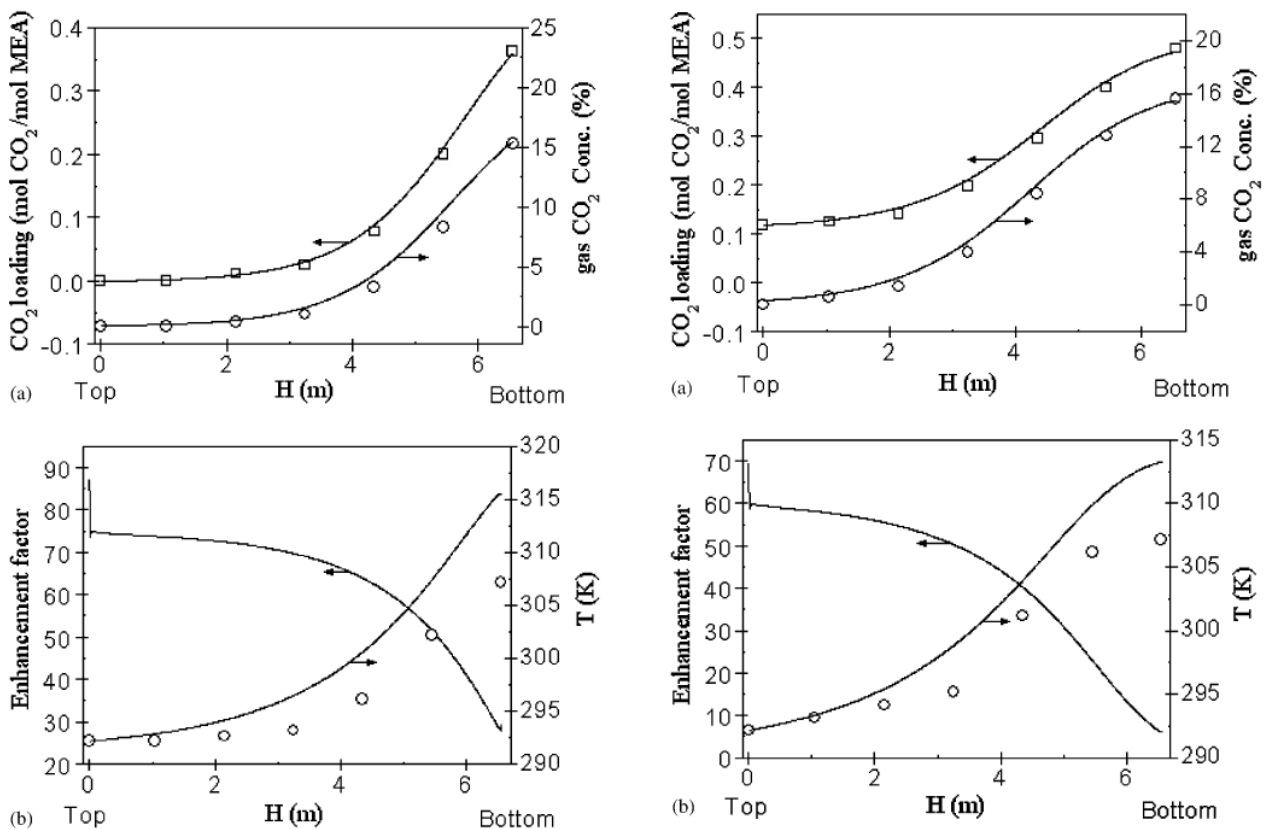
Figure 3.27: predicted and experimental results for CO_2 gas concentration, CO_2 loading, enhancement factor and temperature along a chemo-absorbing tower (Liu et al, 2006)

Finally, Figure 3.28, taken from Dey and Aroonwilas (2009), proposes an overview of parametric effects on mass transfer coefficients that confirms our results, even though under different conditions of CO_2 partial

pressure in the treated gas (here y_b is within the range 5÷15 %). In order to better understand the reported plots, the author underlines that lines of interest refer to "MEA only" and 1 $kmol/m^3/h/kPa$ corresponds to 2800 $mol/ft^3/h/atm$.
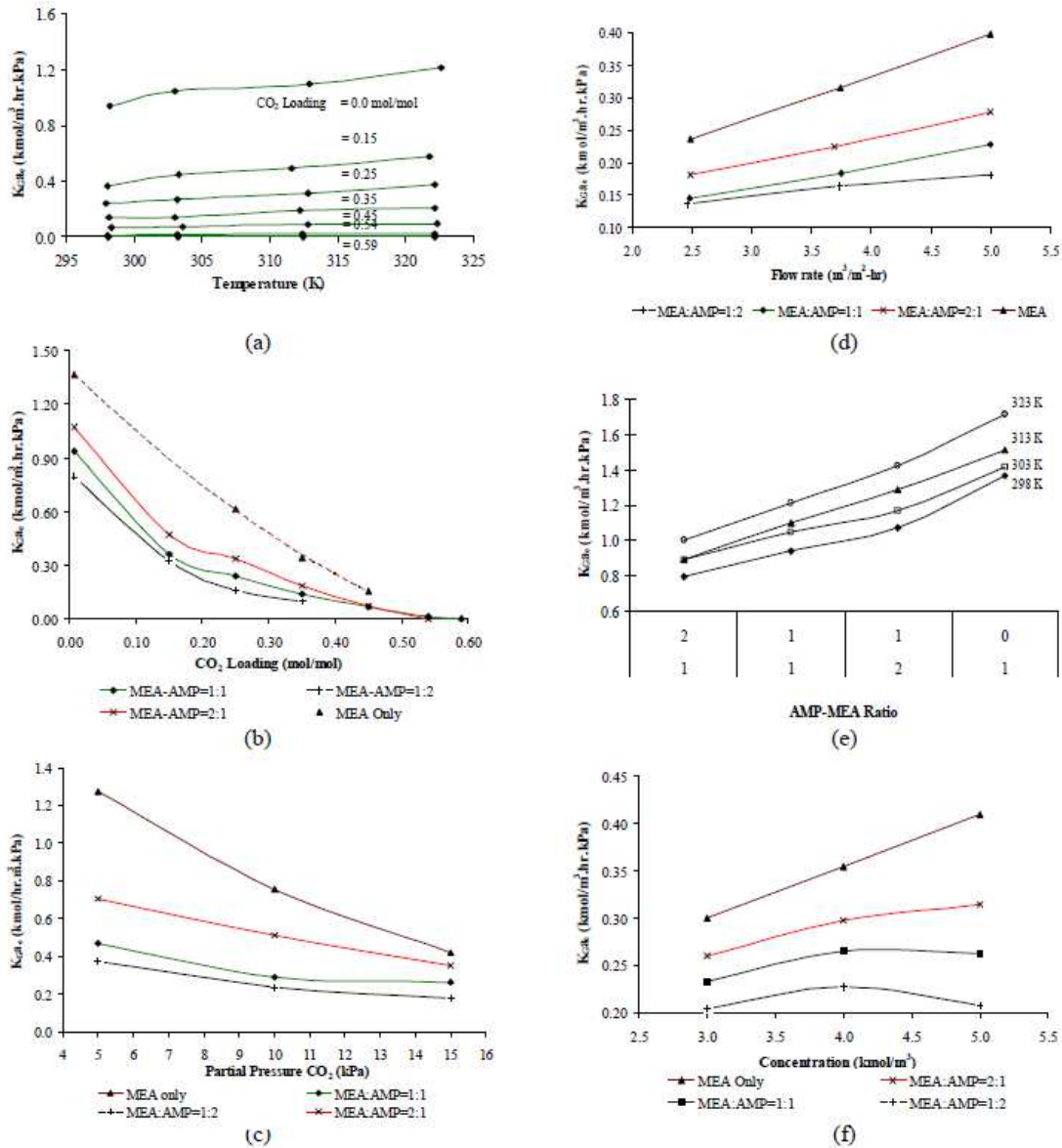
Parametric effects on mass-transfer coefficient (a) Effect of temperature (molar ratio of MEA/AMP is 1:1), (b) Effect of CO_2 loading on K_{Ga_e} at 298K, (c) Effect of CO_2 partial pressure at 0.35 mol/mol CO_2 loading, (d) Effect of liquid flow rate at 0.35 mol/mol CO_2 loading, (e) Effect of MEA-AMP ratio at 0.00 mol/mol CO_2 loading, and (f) Effect of amine concentration on K_{Ga_e} at 0.35 mol/mol CO_2 loading.

Figure 3.28: parametric effects on mass transfer coefficients for a MEA-CO_2 chemo-absorption process (Dey and Aroonwilas, 2009)

As one can easily observe from the reported figures:
- the higher the temperatures, the higher the mass transfer coefficients;
- the higher MEA concentration (X_{MEA}), the higher the mass transfer coefficient;

- the higher the liquid flow rate, the higher the mass transfer coefficient;
- the lower the CO_2 loading, the higher the mass transfer coefficient;
- the lower the CO_2 partial pressure (y), the higher the mass transfer coefficient.
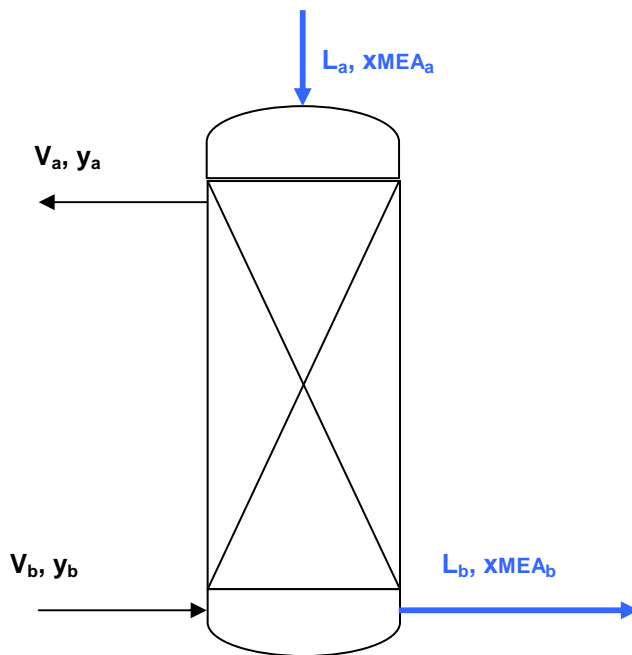
Figure 3.29: chemo-absorbing tower layout

As far as the tower design (Figure 3.29 reports a general layout of chemo-absorption) is concerned, similarly to what reported for physical absorption, the overall material balance on the terminal streams, based on component CO_2 can be expressed as:

$$L_a x_a + V_b y_b = L_b x_b + V_a y_a + \phi_{reaction}$$

where L and V are molal flow rate for liquid and gas phase, x and y are CO_2 mole fraction for liquid and gas phase. In the specific case of chemical absorption, x_a and x_b are equal to zero, as any CO_2 molecule reacts with MEA contained in the aqueous solution (assuming that MEA concentration is not limiting the reaction, that is CO_2 loading < 0.5 at any section of the column). The term $\phi_{reaction}$ accounts for the CO_2 disappearance, in this case 9 988.3 mol CO_2/h are transformed into reaction products.

The general material balance can be written as:

$$L_a + V_b = L_b + V_a + \phi_{reaction}$$

Where $L_a = L_b$ due to the stoichiometry of the MEA-CO_2 reaction (1 mole of CO_2 is absorbed and react together with 2 moles of MEA, producing 2 moles of products, that is the chemical absorption is equimolal).

As a matter of fact, provided that x = 0 everywhere, the operating-line equation for the column cannot be expressed as a function of x. On the contrary, the quantities y and V will depend on MEA mole fraction in the liquid phase xMEA:

$$2 \cdot (V \cdot y - V_a \cdot y_a) = L \cdot x_{MEA\,a} - L \cdot x_{MEA}$$

$$V = V_a + L \cdot \left(\frac{x_{MEA\,a} - x_{MEA}}{2} \right)$$

that is:

$$y = \frac{2 \cdot V_a y_a + L \cdot x_{MEA\,a} - L \cdot x_{MEA}}{2 \cdot V}$$

The parameter xMEA is in close relation with X_{MEA}, that is expressed as $kmol/m^3$. Figure 3.30 reports the operating line for the case L_a = 15 m^3/h and X_{MEA} = 3 $kmol/m^3$. As already observed for the absorption cases, the operating line is actually a curve due to the variation of the gas flow rate V.
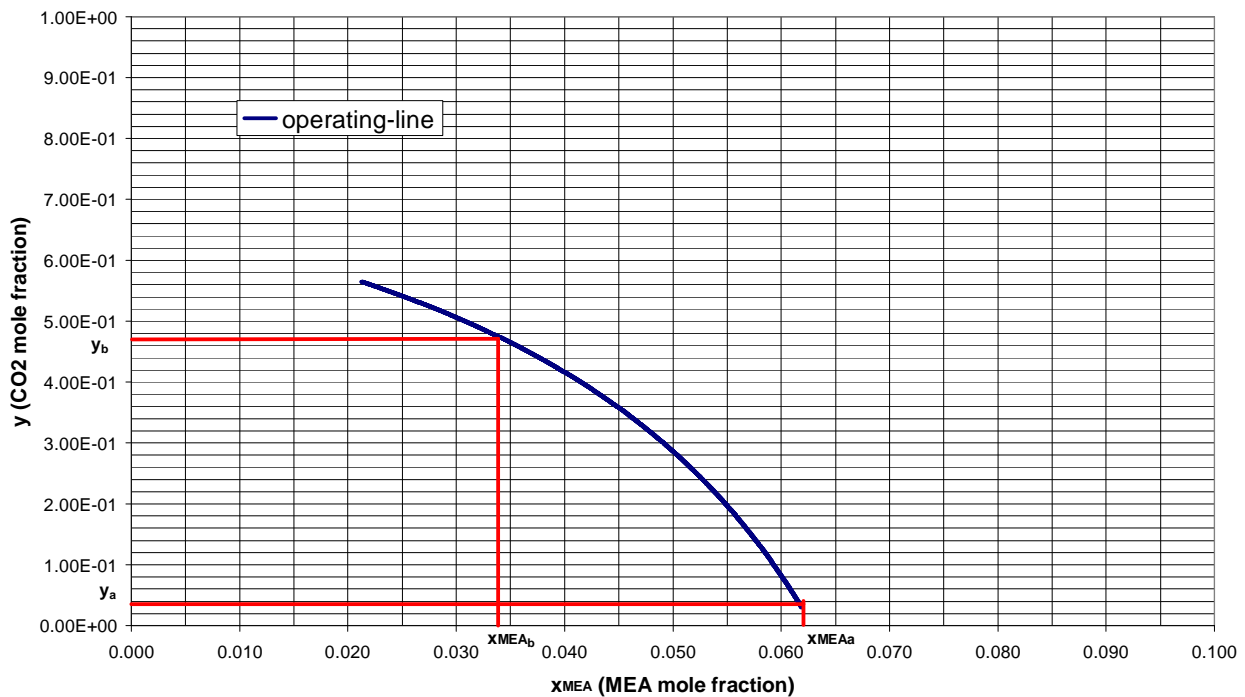
Figure 3.30: operating line in the case of MEA-CO$_2$ chemical absorption (L_a = 15 m^3/h, X_{MEA} = 3 $kmol/m^3$)

Similarly to the approach followed in the case of physical absorption from rich gases, the amount of solute dN$_{CO2}$ absorbed in a differential height dZ is d(Vy), since both V and y decrease as the gas rises through the column.

$$dN_{CO2} = d(Vy) = Vdy + ydV$$

If only (or mainly) CO_2 is transferred from gas to liquid phase, dN_{CO2} equals dV, so:

$$dN_{CO2} = V dy + y dN_{CO2}$$

$$dN_{CO2} = \frac{V \cdot dy}{1 - y} = K_y a \cdot S \cdot dZ \cdot (y - y^*)$$

If the reaction is substantially irreversible at absorption conditions, the equilibrium partial pressure is zero, that is $y^* = 0$. The chemo-absorbing column height Z can be obtained by the following integration, where $K_y a_{eff}$ can be obtained by multiplying $K_g a_{eff}$ by total pressure.

$$Z = \frac{1}{S} \int_a^b \frac{V dy}{(1 - y) \cdot y \cdot K_y a_{eff}}$$

Based on the described equations, the tower height can be obtained numerically by applying a calculation step set at $\Delta xMEA = 1.0\,E^{-5}$; the results are reported in the following Table 3.29.

Table 3.29: chemo-absorbing tower dimensions for MEA aqueous solutions

tower diameter (m)	0.5	0.5	0.5	0.5	0.5	0.5
P (atm)	1	1	1	1	1	1
T (K)	313	313	313	313	313	313
V_b (moli/h)	22019.7	22019.7	22019.7	22019.7	22019.7	22019.7
V_a (moli/h)	12031.4	12031.4	12031.4	12031.4	12031.4	12031.4
L_a (m³/h)	20	15	15	10	14	8.5
L_a (mol/h)	970189	657181	727642	438120	679132	372402
X_{MEA} top (kmol/m³)	3	5	3	5	3	5
$K_g a_{eff}$ bottom (mol/h/atm/ft³)	2180.4	2307.9	1752	1729.7	1641.2	1481.8
tower height (m)	**3.25**	**3.07**	**4.05**	**3.87**	**4.32**	**4.22**

As one can easily observe, the tower heights are quite small even when a tower diameter of 0.5 m is chosen and pressure is kept near atmospheric values. The effect of an increase of total pressure is a remarkable decrease of tower height required, even though overall mass transfer coefficients $k_g a_{eff}$ are lowered; this is due to the consequent enhancement of the driving forces between gas and liquid phase. Since the tower heights are not so big even at atmospheric pressures, there is no need to complicate the process design with a pressure increase.

As far as pressure drop within the chemo-absorbing tower is concerned, the same approach followed for physical absorbing tower has been applied. Table 3.30 reports the simulated pressure drops for the considered conditions of liquid flow rate (8.5÷20 m³/h), MEA concentration (3÷5 kmol/m³), tower diameter (0.5 m) and temperature (313 K). In all conditions, the feasibility has been verified (pressure drops always lower than 0.5 inch H_2O/foot).

Table 3.30: pressure drops for the CO_2-MEA absorption process under the simulated conditions

tower surface (cm²)	L (m³/h)	G_x (lb/ft²/h)	pressure drop (inch H_2O/foot)
1 962 (Φ = 0.5 m)	20	20 937	**<0.5**
1 962 (Φ = 0.5 m)	15	15 727	**<0.5**
1 962 (Φ = 0.5 m)	10	10 487	**0.1-0.25**
1 962 (Φ = 0.5 m)	8.5	8 908	**0.1-0.25**

As already calculated for the previous case studies relating to physical absorption, also chemical absorption can involve the simultaneous absorption of methane in MEA aqueous solution. In this case, methane is not interested by chemical reaction with MEA, its absorption depends on its solubility in MEA solution, its diffusivity in the liquid phase, viscosity and temperature. The liquid viscosity μ_l of aqueous MEA solutions has been already calculated for the simulated 6 conditions according to temperature and MEA concentration, whereas the Henry's law constant $H_{CH4,l}$ and methane diffusivity in the liquid phase $D_{CH4,l}$ should be calculated by using the already described N_2O analogy. It should be remembered that the methane diffusivity in water, calculated by Wilke and Chang approach, is around 1.935×10^{-5} cm^2/s at 313 K, whereas diffusivity of methane in gas phase is around 1.58×10^{-5} m^2/s. $D_{CH4,l}$ goes down to $1.4 \div 1.6 \times 10^{-5}$ cm^2/s at 313 K, respectively for MEA concentration of 5 and 3 $kmol/m^3$. Also methane solubility is decreased by the presence of MEA from 51200 atm/mol frac to $41000 \div 44000$ atm/mol frac when MEA concentration is 5 and 3 $kmol/m^3$.

In order to calculate mass transfer coefficients for methane absorption in MEA solution we applied again the already described Sherwood and Holloway correlations, obtaining the values reported by Table 3.31.

If one consider 1 inch Berl saddles as packing material, the overall mass transfer coefficient K_ga for methane in the simulated chemo-absorbing conditions (tower diameter 0.5 m and L between 8.5 and 20 m^3/h, T = 313 K) ranges from 0.005 and 0.011 lb-mol/ft^3/atm/h for, as reported by Table 3.31. Based on the reported reasoning, in order to be conservative, the overall mass transfer coefficient K_ga (referring hence to CH_4 partial pressures) is assumed equal to 0.010 lb-mol/ft^3/atm/h, that is to say around 177 mol/m^3/atm/h (5 mol/ft^3/atm/h), whereas the calculated value for methane absorbing in pure water at 20°C was 0.015 lb-mol/ft^3/atm/h.

Table 3.31: calculation of overall mass transfer coefficients for methane in MEA aqueous solution at 40°C

tower diam (m)	0.5	0.5	0.5	0.5	0.5	0.5
P (atm)	1	1	1	1	1	1
T (K)	313	313	313	313	313	313
L_a (m3/h)	20	15	15	10	14	8.5
X_{MEA} top (kmol/m3)	3	5	3	5	3	5
ρl (g/l)	1002.2	1003.6	1002.2	1003.6	1002.2	1003.6
ρl (lb/ft3)	62.6	62.6	62.6	62.6	62.6	62.6
ρg (lb/ft3)	0.0812	0.0812	0.0812	0.0812	0.0812	0.0812
La (mol/h)	970189	657181	727642	438120	679132	372402
Vb (moli/h)	22019.7	22019.7	22019.7	22019.7	22019.7	22019.7
La (kg/m2/s)	28.36999	21.30821	21.27749	14.20547	19.85899	12.075
La (lb/ft2/s)	5.815848	4.368183	4.361886	2.912122	4.071094	2.475304
G (lb/ft2/s)	0.186	0.186	0.186	0.186	0.186	0.186
MWI (g/mol)	20.659	22.907	20.659	22.907	20.659	22.907
μl (cP)	1.55	2.25	1.51	2.14	1.51	2.08
μl (lb/h/ft)	3.75	5.45	3.66	5.17	3.64	5.04
μg (cP)	0.0119	0.0119	0.0119	0.0119	0.0119	0.0119
μg (lb/h/ft)	0.029	0.029	0.029	0.029	0.029	0.029
DN2O,l (m2/s)	2.13E-09	1.89E-09	2.13E-09	1.89E-09	2.13E-09	1.89E-09
DCH4,w (m2/s)	1.94E-09	1.94E-09	1.94E-09	1.94E-09	1.94E-09	1.94E-09
DNO2,w (m2/s)	2.60E-09	2.60E-09	2.60E-09	2.60E-09	2.60E-09	2.60E-09
$D_{CH4,l}$ (m^2/s)	1.59E-09	1.40E-09	1.59E-09	1.40E-09	1.59E-09	1.40E-09
DI (ft2/h)	6.14E-05	5.44E-05	6.14E-05	5.44E-05	6.14E-05	5.44E-05
Dg (ft2/h)	0.61	0.61	0.61	0.61	0.61	0.61
HCH4,w (kmol/m3/kPa)	1.07E-05	1.07E-05	1.07E-05	1.07E-05	1.07E-05	1.07E-05
HN2O,w (kmol/m3/kPa)	1.73E-04	1.73E-04	1.73E-04	1.73E-04	1.73E-04	1.73E-04
HN2O,MEA (kmol/m3/kPa)	3.13E-04	3.13E-04	3.13E-04	3.13E-04	3.13E-04	3.13E-04

ξ MEA,H2O	-0.10	-0.19	-0.10	-0.19	-0.10	-0.19
HN2O,l (kmol/m3/kPa)	1.74E-04	1.70E-04	1.74E-04	1.70E-04	1.74E-04	1.70E-04
$H_{CH4,l}$ (kmol/m³/kPa)	1.08E-05	1.05E-05	1.08E-05	1.05E-05	1.08E-05	1.05E-05
$H_{CH4,l}$ (atm/mol frac)	4.43E+04	4.10E+04	4.43E+04	4.10E+04	4.43E+04	4.10E+04
HL (ft)	2.06	2.20	1.89	1.94	1.86	1.84
kl a (lb-mol/h/ft3)	491.17	312.48	401.25	236.15	382.31	211.25
HG (ft)	0.29	0.33	0.33	0.38	0.34	0.41
kg a (lb-mol/h/ft3)	78.86	70.33	70.29	59.80	68.37	56.04
Kg a (lb-moli/h/atm/ft3)	**0.011**	**0.008**	**0.009**	**0.006**	**0.009**	**0.005**

In order to calculate the simultaneous absorption of CO_2 (reacting with MEA) and methane, we rearranged the analytical approach reported for the case of pressurized water absorption and 4 equations in 4 unknown quantities (x'_b, L_b, Z and V_a) can be written as:

$$CO_2) \quad \phi_{reacvtion} = \Delta_{CO2} = V_b \cdot y_b - V_a \cdot y_a = K_y a \cdot S \cdot Z \cdot \overline{\Delta y_L} = K_y a \cdot S \cdot Z \cdot \frac{y_b - y_b^* - y_a + y_a^*}{\ln\left(\frac{y_b - y_b^*}{y_a - y_a^*}\right)}$$

$$CH_4) \quad L_b \cdot x'_b = K'_y a \cdot S \cdot Z \cdot \overline{\Delta y'_L} = K'_y a \cdot S \cdot Z \cdot \frac{y'_b - H' x'_b - y'_a + H' x'_a}{\ln\left(\frac{y'_b - H' x'_b}{y'_a - H' x'_a}\right)}$$

$$V_a = V_a \cdot y_a + V_b \cdot y'_b - L_b \cdot x'_b$$

$$L_b = L_a \cdot \frac{1}{1 - x_b - x'_b} = L_a \cdot \frac{1}{1 - x'_b}$$

where Z is the tower height, quantities with the superscript refer to methane (for example x_b', y_b'), otherwise to CO_2, $K_y a$ and $K'_y a$ are overall mass transfer coefficients respectively for CO_2 and CH_4, Δy_L is the logarithmic mean of $y_b - y_b^*$ and y_a and y_a^*. Due to the presence of an irreversible reaction between MEA and CO_2, $x_b=0$ and also $y_b^*=y_a^*=0$.

The mass balances reported are all rigorous equations, the only approximation is the use of the described logarithmic mean values that would be applicable only when operating and equilibrium lines are straight. In spite of the approximation, the calculated tower height doesn't change substantially, as already demonstrated for the absorbing processes seen before.

The solution of the equations' system has been carried out for the 6 simulated tower conditions at a temperature of 313 K and the results are reported in Table 3.32. Based on the described approach, it's easy to observe that methane absorbed into MEA aqueous solution (that is methane loss) is less than 0.1%, that is the best results up to now. This is mainly due to the low pressure at which the process occurs (1 atm), but also to the low solubility of methane into MEA solution.

Table 3.32: calculation of simultaneous absorption of CO_2 and CH_4 into MEA aqueous solution

L_a (m³/h)	X_{MEA} (kmol/m³)	P (atm)	T (K)	tower diam (m)	L_b (mol/h)	x'_b	CH_4 absorbed (%)	tower height (m)
20	3	1	313	0.5	970197.9	9.36E-06	0.08%	3.25
15	5	1	313	0.5	657187.6	1.09E-05	0.06%	3.07
15	3	1	313	0.5	727649.4	1.06E-05	0.07%	4.05
10	5	1	313	0.5	438125.7	1.22E-05	0.05%	3.87
14	3	1	313	0.5	679139.6	1.09E-05	0.06%	4.32
8.5	5	1	313	0.5	372407.0	1.25E-05	0.04%	4.22

As far as MEA scrubbing is concerned, apart from the several and significant challenges dealing with the removal of residual oxygen, H_2S, and other species that cause chemical degradation of the MEA, the energy costs associated with the amine regeneration step is particularly high and therefore much research has been directed at reducing these costs.

MEA is rather weak base and will re-release CO_2 when the scrubbing solution is heated (reversal chemical reaction). Then, CO_2 in the solution can be stripped and MEA solution regenerated.

Existing MEA scrubbing plants generally use a boiler-stripper system, with the boiler placed at the bottom of the stripper, evaporating some water-MEA that would became the stripping gas phase, passing through the column counter-current with the rich MEA aqueous solution (rich in CO_2) coming down (see Figure 3.31) the stripper.
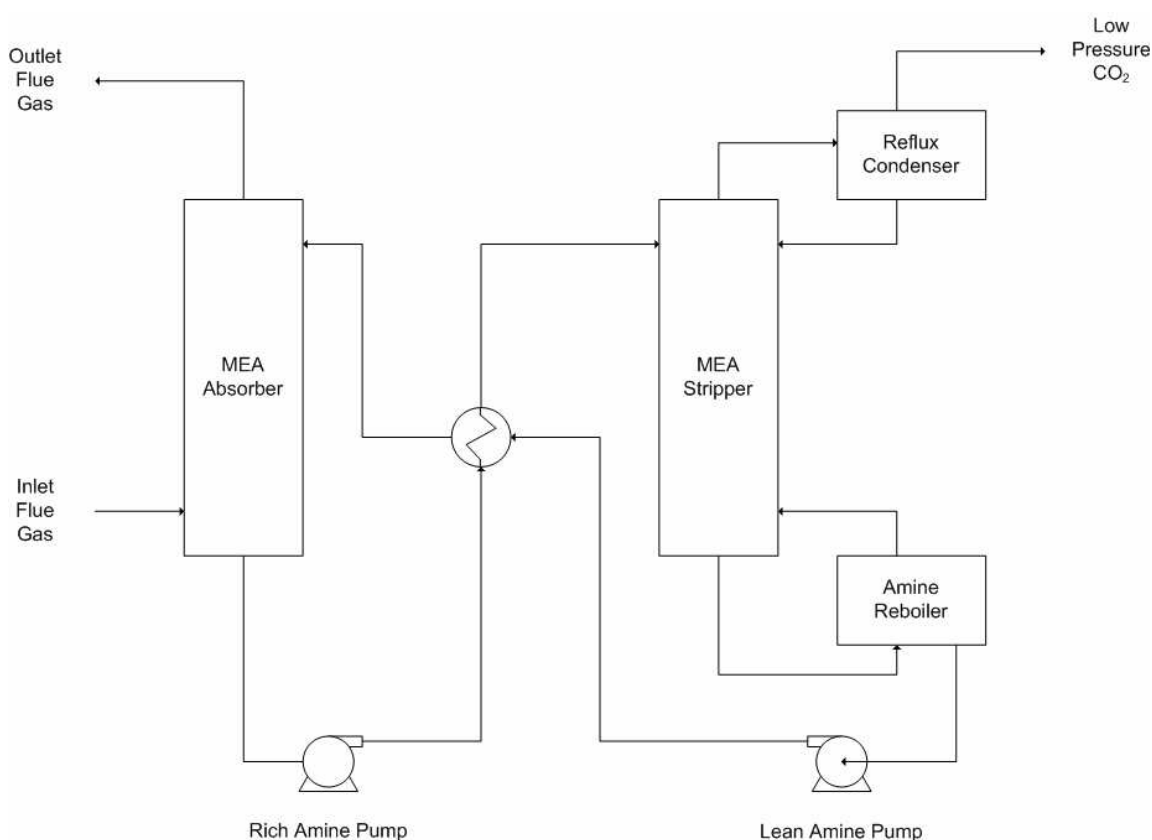
Figure 3.31: traditional MEA unit with regeneration (from Fisher, 2005)

As a matter of fact, the sensible heat of regenerated MEA solution (called lean amine) is recovered by the rich solution coming from the bottom of the chemo-absorbing tower whit a thermal efficiency that can be considered close to 90%. Then the rich MEA solution, heated at the boiling temperature, contains no more carbamate but all reacted CO_2 is now free in solution; then the solution is stripped by a vapour phase that is originated from the bottom part of the stripper and CO_2 is totally desorbed. So, the boiler must provide the system with the thermal energy that is required to evaporate a stripping flow that is enough to strip CO_2. The required stripping flow could be easily calculated according to temperature, stripper dimensions, CO_2 solubility in MEA solution, MEA solution flow rate, by means of the same calculation process described for the Selexol stripping process. It should be remembered that at the bottom of the tower free CO_2 in solution would be close to zero, that is one would observe a water-MEA solution with the same composition in terms of MEA concentration than at the top of the absorbing tower (again 3÷5 kmol/m³, i.e. 18÷30% by weight or 0.062÷0.114 by mole fraction).

The boiling point of the solution is not just one but it is represented by a range of temperatures between 100°C (boiling point for pure water) and 170°C (boiling point for pure MEA), as showed by Figure 3.32. The quantities and the composition of the liquid and gas phase that can be observed during evaporation (that is when we are between the bubble point and the dew point curves) can be calculated from the specific vapour-liquid equilibria diagram for MEA aqueous solution reported by Figure 3.33 (DOW Chemical Company).
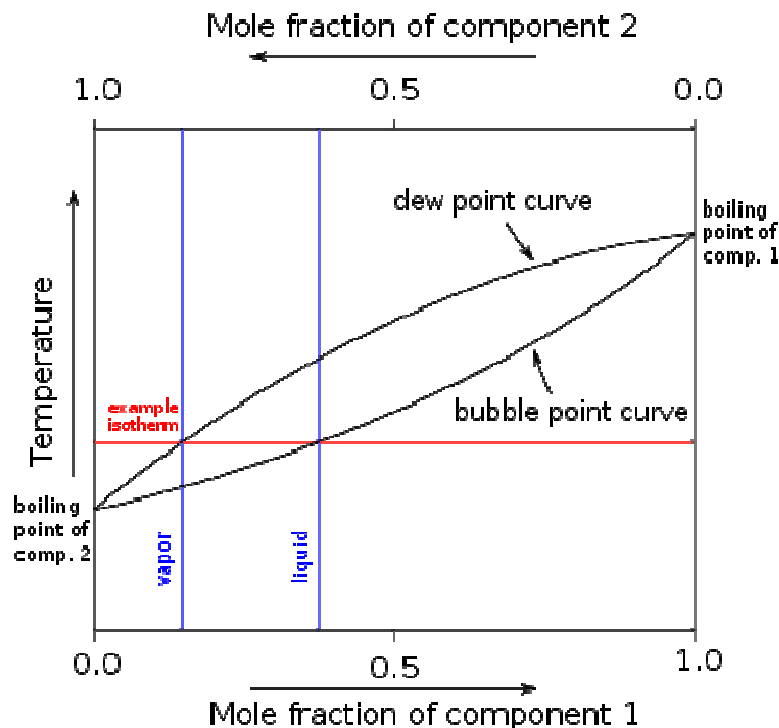
Figure 3.32: binary boiling point for a solution

Literature reports that the reboiler generally operates at 150°C, that means that, at the concentration conditions that we have at the bottom of the stripper (18-30% of MEA by weight), we obtain a vapour phase with the same composition of the original liquid phase. This phase will be the stripper in the column and gas flow rate will grow along the tower because of the desorbed CO_2 flows (9988 mol/h). On the other hand, the stripper works at temperature very close to boiling ones, but lower than those (105-110°C, according to MEA concentration). Then, at the top of the stripper, a mix of water vapour, MEA vapour and CO_2 is obtained; after that a condensation phase occur to recirculate water-MEA solution to the tower. Condensation generally takes place at 40°C.
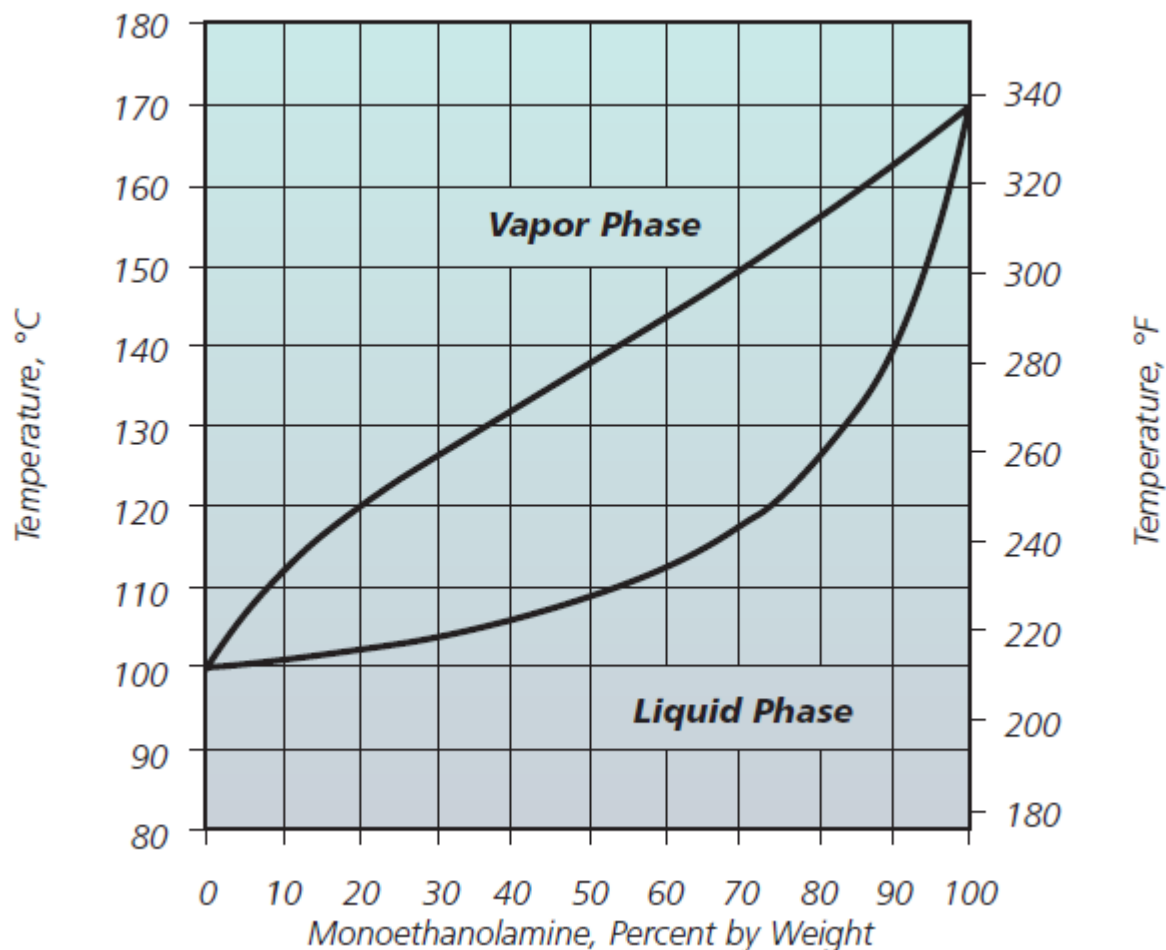
Figure 3.33: vapour-liquid equilibria for MEA water-solution

In order to predict the thermal expenses to regenerate MEA we need to know the stripper flow rate. According to the already described approach, overall mass transfer coefficients for the stripping in the worst conditions (at lowest L, that is 8.5 m^3/h) have been calculated, as reported by the next Figure 3.34 (the left plot). As obvious, the calculation considers the diffusivity of CO_2 in MEA solution at 110°C (1 x 10^{-8} m^2/s), the change in MEA solution viscosity (1.34 cP) and the solubility of CO_2 at 110°C (5900 atm/mol frac). The overall mass transfer coefficient turns out to be more or less 1765 mol/m^3/atm/h (50 mol/atm/h/ft^3) assuming a stripper diameter of 0.5 m. For the calculated conditions, a vapour flow rate of 5000 mol/h is enough to desorb all CO_2 from the largest exhausted MEA solution flow rate (20 m^3/h, that is 970 000 mol/h) in a stripper 3.76 m high (diameter 0.5 m) (see Figure 3.34, the right plot). The minimum vapour flow rate that doesn't show flooding in this kind of conditions (L_A = 20 m^3/h, ϕ=0.5 m) is 2500 m^3/h.

As a consequence, it should be enough to evaporate 5000 mol/h of the liquid flow rate taken from the bottom of the stripper to produce the required vapour flow rate. The heat of evaporation are 600 kcal/kg for water and 235.2 kcal/kg for MEA at 150°C (see also Figure 3.35). Assuming that MEA represent 30% by weight of the liquid phase to be evaporated (0.114 as mole fraction), the heat consumption would be 65 kW, that is 0.13 kWh$_{th}$/m^3 of raw biogas. As far as the heat requirements to compensate the heat loss of the system, a heat exchanger efficiency of 90% has been considered. Since specific heat of water and MEA are respectively 1 and 0.7 kcal/kg/°C and the temperature variation is between 40 and 110°C, the heat loss when the maximum MEA solution flow rate is considered (20 m^3/h) could be around 143 kW$_{th}$, that is 0.29

kWh$_{th}$/m^3 of raw biogas. The total thermal energy consumption is around 0.42 kWh$_{th}$/m^3 of raw biogas confirming some literature indications reporting specific consumptions lower than 0.5 kWh$_{th}$/m^3 of raw biogas.

tower diam (m)	0,5
tower surface (cm2)	1962,5
tower surface (ft2)	2,11
ρl (g/l)	1002,2
ρl (lb/ft3)	64,1
ρg (lb/ft3)	0,080178
L (m3/h)	8,5
L (moli/h)	3,72E+05
Vb (moli/h)	2000,0
L (lb/ft2/s)	2,472
G (lb/ft2/s)	0,015
μl (cP)	1,337028
μl (lb/h/ft)	3,234271
μg (cP)	0,01372
μg (lb/h/ft)	0,033
Dl (ft2/h)	4,08E-04
Dg (ft2/h)	0,46

HL (ft)	0,60
kl a (lb-mol/h/ft3)	644,41

HG (ft)	0,21
kg a (lb-mol/h/ft3)	9,13

Kg a (lb-moli/h/atm/ft3)	**0,109**
Kg a (moli/h/atm/ft3)	49,28994

Ztot (m)	**3,76**

La (m3/h)	
L$_A$ (moli/h)	980.176,8
V$_B$ (moli/h)	5000
y$_B$	0
x$_B$	0,00E+00
V$_A$ (moli/h)	14988,0
y$_A$	0,666399786
x$_A$	1,02E-02
L$_B$ (moli/h)	970.188,8

Kg a (mol/ft3/h/atm)	49,32346867
P (atm)	1
T (K)	393
H (MPa/mol frac)	5,93E+02
tower diam (m)	0,5
tower surface (cm2)	1962,50
tower surface (ft2)	2,11

Figure 3.34: mass transfer coefficient and stripping tower design for MEA regeneration in the most conservative conditions

As far as biomethane and waste gas flow rates are concerned, literature remembers that MEA is pretty volatile and consequently its loss (towards the final use of biomethane or atmosphere) must be reintegrated. A part from the costs of the reactant, MEA losses could also have environmental impact that should be assessed.

Within the described context, condensation of the stripper (summed up to the desorbed CO_2) occur at 35-40°C. If we assume the same stripper flow rate considered for energy calculations, that is 5000 mol/h at 30% by weight of MEA (0.114 mol fraction), provided that the vapour pressure of pure MEA is around 1 mm Hg at 40°C (see Figure 3.36), MEA molar fraction after the condensation step, in equilibrium with condensate, will be: y_{MEA} = MEA vapour pressure · x_{MEA} / total pressure = 1/760·0.114/1 = 1.5 x 10^{-4}. MEA molar fraction should be multiplied by waste gas flow rate, more or less 9988 mol/h of CO_2, that is a MEA loss equal to 91 g/h (at concentration around 400 mg MEA /Nm^3 of waste gas), more than 700 kg/y that represent from 16 to 29% of MEA circulating quantity. If the same assessment is carried out for biomethane flow rate (V_a = 12031 mol/h), assuming again that the gas flux exiting the chemo-absorbing tower is saturated by MEA at the maximum liquid concentration (X_{MEA} = 5 kmol/m^3, that is 30 % by weight), other 900 kg of MEA are lost with biomethane. On the whole, reactant loss when monoethanol amine is employed could range between 35 and 62% every year, and so, remarkable and frequent MEA refills are required.
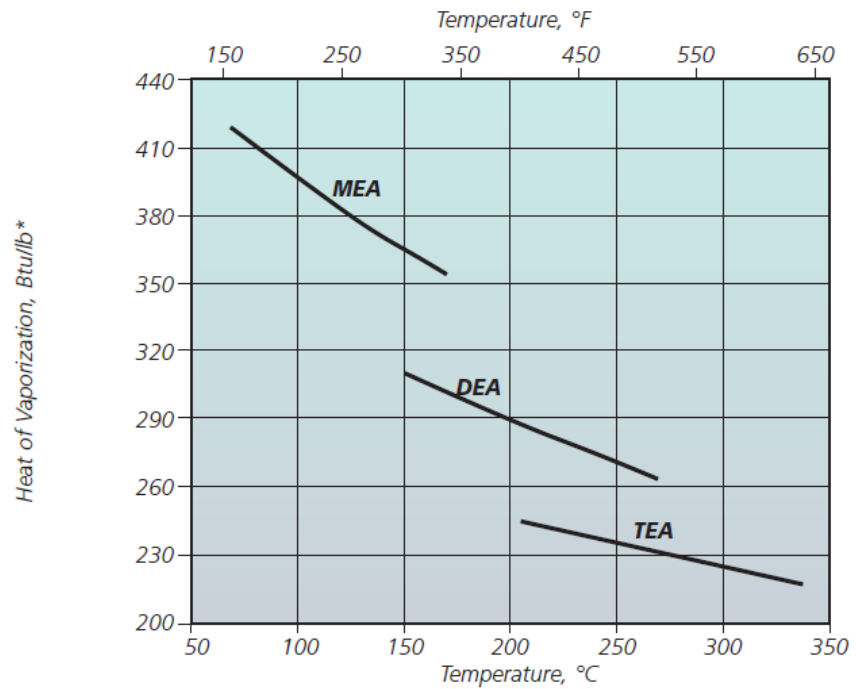
Figure 3.35: heat of evaporation for different alkanolamine
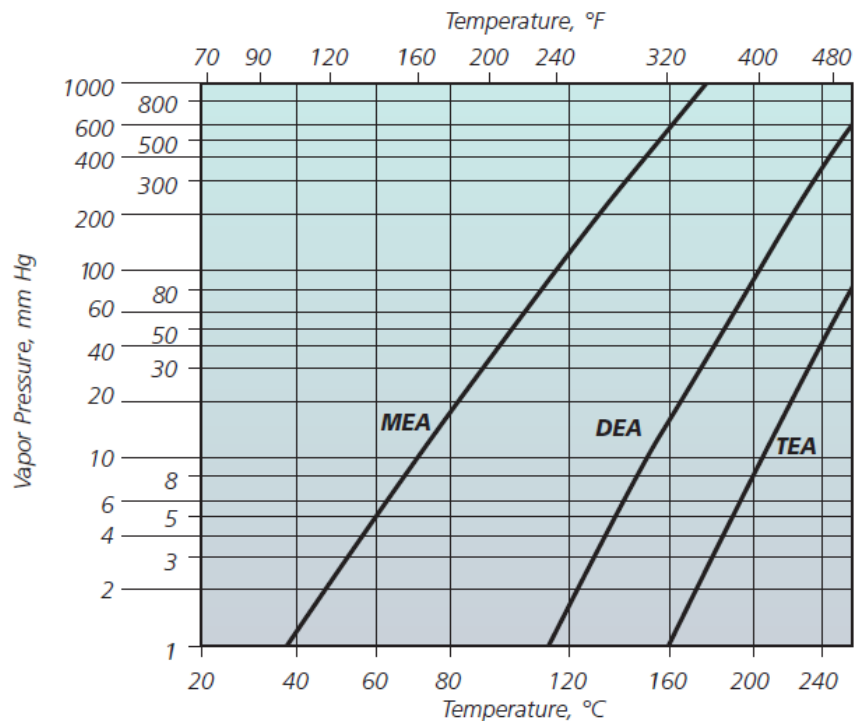

Figure 3.36: alkanolamine vapor pressure

In order to reduce this kind of environmental and economic drawbacks, both biomethane and vented CO_2 fluxes could be properly treated by a water scrubber to reduce MEA concentration and recover it. In order to design this kind of treatment we have to define:

- Henry's law constant for monoethanolamine in water: U.S. EPA suggests the value H = 4 x 10^{-8} atm·m^3/mol, that is to say 2.2 x 10^{-3} atm/mol frac; as a matter of fact, MEA is totally soluble in water, and so the Henry's law constant is extraordinarily favourable to its absorption;
- MEA diffusivity in water: the definition of Wilke and Chang (1955) leads to a value around 1.6 x 10^{-5} cm^2/s;
- Mass transfer coefficients: based on the already described Sherwood and Holloway (1940) approach, in the case the scrubber has a diameter of 1 m and water flow rate is 1 m^3/h, the overall mass transfer coefficient K_ga is larger than 150 777 mol/m^3/atm/h (4270 mol/ft^3/atm/h).

The exposure limit TLV-TWA for MEA is 3 ppm, that is MEA odour threshold as well: therefore, the scrubbing target is to reduce MEA concentration of gaseous fluxes from saturation conditions (400 mg/Nm^3, that is 148 ppm) to less than 3 ppm. This result can be easily achieved by a 0.5 m (diameter) x 2 m (height) scrubber operating at atmospheric pressure and temperature, employing around 1 m^3/h of fresh water as a solvent, for both the analysed gaseous flow rates (biomethane, 12031 mol/h, and carbon dioxide, 9988 mol/h). The described abatement device would involve negligible energy consumption because of the very low operative pressures.

On the other hand, MEA losses could be reduced by lowering MEA solution concentration (with consequently higher liquid flow rate L_a) or using less volatile reactants to upgrade biogas.

As far as pressure drops are concerned, the case of MEA solution is particularly favourable as there is no need for strong compression of the involved flow rates, both the chemo-absorption and the stripping work at atmospheric pressure or very close to that. Moreover liquid flow rates that are needed to treat biogas are very low if compared to other technical solutions (also because flash tank recirculation doesn't occur). As a consequence, the pressure requirements deal with the hydraulic head of the towers (very low if compared to pressurized water absorption), as reported by Table 3.33, the hydraulic circuit and the gas phases piping.

Table 3.33: energy consumption for MEA aqueous solution compression (absorbing tower hydraulic head)

tower diam (m)	0.5	0.5	0.5	0.5	0.5	0.5
P (atm)	1	1	1	1	1	1
T (K)	313	313	313	313	313	313
La (m3/h)	20	15	15	10	14	8.5
La (mol/h)	970189	657181	727642	438120	679132	372402
X MEA top (kmol/m3)	3	5	3	5	3	5
Liquid maximum density (g/l)	1002.17	1003.617	1002.17	1003.617	1002.17	1003.617
absorbing tower height Z_a (m)	3.25	3.07	4.05	3.87	4.32	4.22
regeneration tower height Z_r (m)	~3.76	~3.76	~3.76	~3.76	~3.76	~3.76
$\Delta P = f (Z_a+Z_r)$ atm	0.7	0.7	0.8	0.7	0.8	0.8
Power required (kW$_e$, η=0.65)	**0.6**	**0.4**	**0.5**	**0.3**	**0.5**	**0.3**
specific consumption (kWh$_e$/m^3 raw biogas)	**0.00119**	**0.00087**	**0.00100**	**0.00065**	**0.00096**	**0.00058**

The pressure drops of MEA aqueous solution through pipes have been calculated for the worst conditions as follows:
L = 20 m^3/h;
Pipe diameter D = 50 mm;
Mean water velocity V = 2.83 m/s;
Maximum MEA solution dynamic viscosity = 0.00225 Pa·s;
Roughness of commercial steel pipes: 0.046 mm;
Reynolds number = 63 014;
Relative roughness = 0.00092;
Friction factor ξ = 0.022 (from the Moody Diagram reported in Figure 3.14 of chapter 3.1);

Circuit length l = 100 m (hypothesis);

$$\Delta P\,[Pa] = \zeta \cdot \frac{l}{D} \cdot \frac{V^2}{2} \cdot \rho \cong 184,610\ \ Pa$$

Therefore the pressure drops for a 100 m circuit of circulating MEA solution could be as large as 1.8 atm, that is pretty small, more or less 1.5 kW_e for tha largest liquid flow rate (moreover, some concentrated pressure drops could take place at the heat exchanger between lean and rich MEA solution). On the other hand, pipelines pressure drops regarding the gaseous phase are surely not influent in our analysis.

Finally, since produced biomethane must be injected into natural gas grid, assuming that the reference maximum pressure for local grid is 5 atm, a compression of biomethane is required up to P_{grid}; the energy requirement calculated by Table 3.34 for the so called grid compression is lower than 0.05 kWh_e/m^3 raw biogas, moreover up to 15 thermal kW could be recovered from compression heat in order to reduce energy requirements of MEA regeneration, that could be as large as 200 kW_{th}.

Table 3.34: energy consumption for biomethane compression to natural gas grid pressure

Va (mol/h)	12031.4
y	0.03
Va (lb/h)	446.7
γ	1.311
MW (Va) (lb/lb-mol)	16.8
T1 (°C)	40
T1 (°F)	104
T2 (°F)	366.2
T2 (°C)	185.6
P1 (atm)	1
Pgrid (atm)	5
P1 (psia)	14.7
P2 (psia)	73.5

w (Btu/lb) isentrop	130.3
power required (kW$_e$, η=0.75)	**22.7**
specific consumptions (kWh$_e$/m^3 raw biogas)	**0.046**
thermal recovery (kW)	**15.3**

Nevertheless, the overall electric energy consumptions seems to be well below 0.1 kWh_e/m^3 raw biogas, as claimed by many literature reports.

In conclusion, chemical absorption as an upgrading solution seems to have many positive aspects, the very low electricity consumptions, the pretty small equipments, a high purity biomethane and negligible methane losses. On the other hand, due to the high volatility of some reactants, the environmental impact of the waste gas emissions could be considerable, apart from enforcing to frequent and conspicuous refills. Possible solutions could be studied in relation to waste gas and biomethane water scrubbing and reactant recovery to the process; also in this case, high removal/recovery efficiencies can be reached at very low energy consumptions.

3.4   Pressure Swing Adsorption (PSA)

The last upgrading technique that is analysed in the present study is PSA (pressure swing adsorption) and VSA (vacuum swing adsorption) that uses a column filled with a molecular sieve, typically activated carbon, silicagel, alumina or zeolite, for differential adsorption of the gas CO_2, letting CH_4 pass through. The molecules are adsorbed in the porosities of the adsorbent material and not irreversible bound. PSA is the second most applied techniques for biogas upgrading, after pressurized water scrubbing. It is a cyclic batch process where biogas is generally compressed to a pressure between 4 and 10 atm; desorption (regeneration) is performed at lower pressure. H_2S, that would be adsorbed irreversibly, must be removed before the PSA or VSA unit to prevent poisoning of the molecular sieve. Moreover, the PSA process requires dry gas so the crude biogas is dried before it enters the treatment process. PSA and VSA are similar systems, but VSA has a supplementary vacuum pump: the differential pressure is situated at lower absolute pressure.

Multi-column arrays are usually employed to produce a continuous process, as reported by Figure 3.37 where the 4 phases, adsorption, depressurization, desorption and pressurization are pointed out.
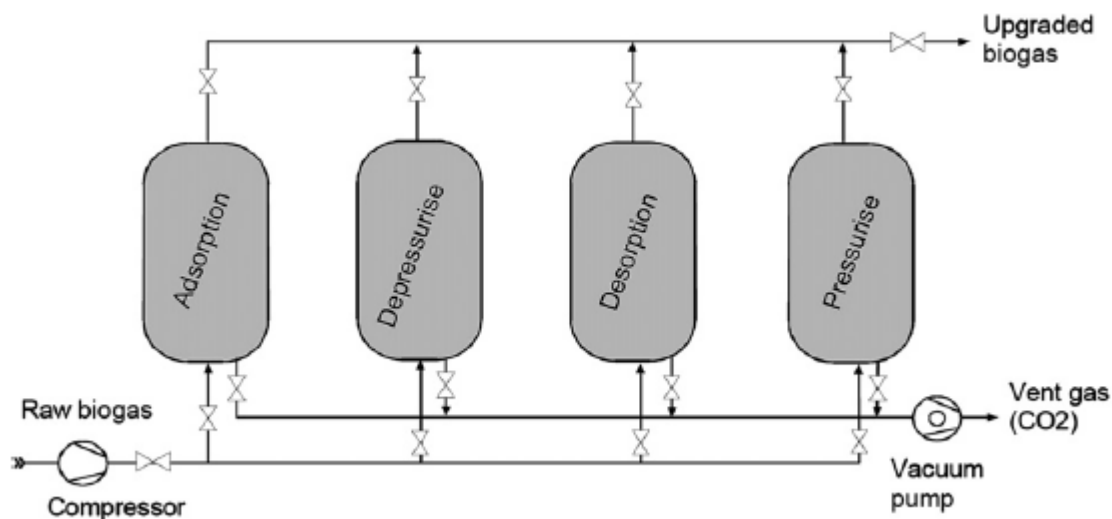
Figure 3.37: layout of vacuum pressure swing adsorption (Ryckebosch et al., 2011)

Adsorption is an exothermic spontaneous process and the loading of CO_2 in the adsorbent depends specifically on the properties of the material employed (surface area and composition, pore size, etc). It should be remembered that since the material is continuously used and regenerated, there comes a point where the process achieves a "cyclic steady state" (CSS). The most important aspect of PSA design relies in choosing a regeneration protocol for the adsorbent able to spend small amount of energy (reduce energetic penalty) and do it in the fastest way possible (increase productivity).

Figure 3.38, taken from Grande (2010), reports the operational principle of PSA process for 2 different adsorbing materials, where the absorbent may contain CO_2 up to the loading concentration (q_{feed}, mol CO_2/kg adsorbent) established by CO_2 partial pressure (P_{feed}); the report curves are examples of the adsorption equilibrium lines, the so called isotherms. Then, after saturation, the material is regenerated at a lower pressure and CO_2 is released according to the quantity $q_{feed} - q_{reg}$ (Δq, also called cyclic capacity). It is easy to observe that what does really matter for adsorbing efficiencies is not the absolute adsorbing capacity; on the contrary cyclic capacity (that is higher for material 1 than for material 2, $\Delta q_1 > \Delta q_2$) determines the process performances. Based on the reported reasoning, it is easy to observe that for PSA

application, linear isotherms are better than steep ones. Moreover, the choice of the regenerating pressure is crucial in order to assure a good adsorbing efficiency.

Several materials can be used to adsorb CO_2 but 2 are the main categories: PSA can be operated either on the basis of equilibrium or kinetic selectivity.

For separation based on equilibrium selectivity, the more strongly adsorbed components of a gas mixture are retained within the column, while the effluent contains the less strongly adsorbed species. In the case of separation based on kinetic selectivity, the faster diffusing species are retained by the adsorbent and the high pressure product is concentrated in slower diffusing components.

In the first case, termed as equilibrium-based adsorbent, CO_2 can create stronger bonds with surface groups than CH_4. For the second case, termed as kinetic materials, the pores of the adsorbent can be adjusted in such a way that CO_2 (kinetic diameter of 3.4 Å) can easily penetrate into their structure while larger CH_4 molecules (kinetic diameter of 3.8 Å) have size limitations to diffuse through them.
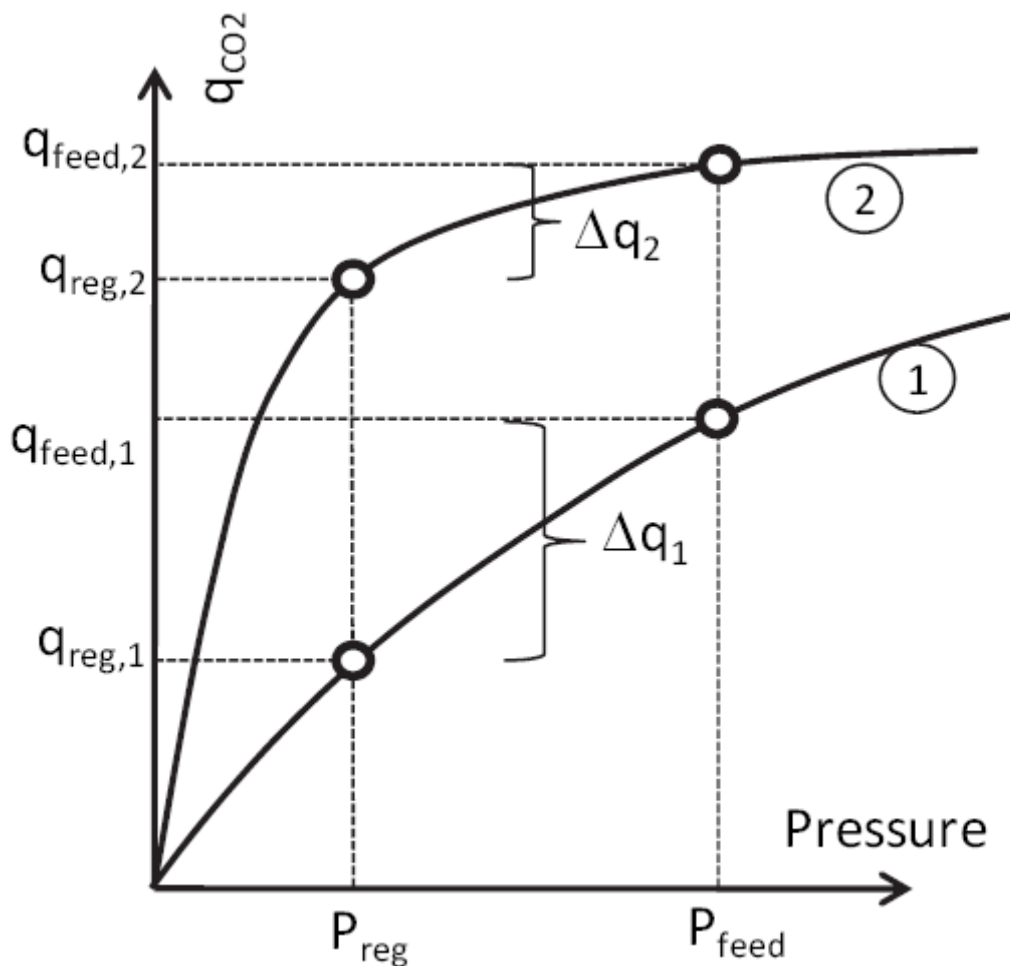
Figure 3.38: example of generic isotherms for 2 CO_2 adsorbing materials

Carbon molecular sieves are one of the most employed materials for biogas upgrading. Figure 3.39 reports equilibrium isotherms of CO_2 and CH_4 in CMS-3K (Takeda Corp., Japan). The material has both an equilibrium selectivity and kinetic selectivity, but the latter makes the difference. As a matter of fact, CO_2 is adsorbed much faster than CH_4 because the pore dimension is lower than kinetic diameter of CH_4.
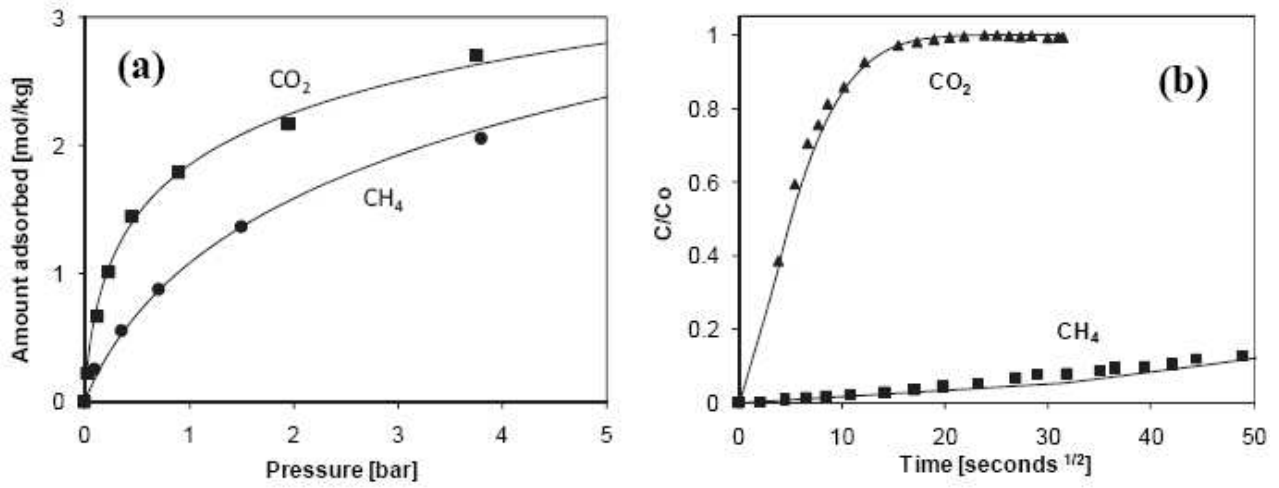
Figure 3.39: adsorption in carbon molecular sieve 3K (data from Cavenati et al, 2005)

Besides carbon molecular sieves, zeolites and activated carbon are generally used for PSA. These materials are considered equilibrium adsorbent since diffusion of both CO_2 and CH_4 is very fast and loading difference are exploited to adsorb more CO_2 than CH_4. Cavenati et al. (2004) reports the experimental data for methane and carbon dioxide adsorption equilibrium for Zeolite 13X (CECA, France): Figure 3.40-3.43 report the interpolation attempts made on the experimental data to obtain the analytical expression of the isotherm for specific partial pressure ranges; Figure 3.44 summarizes the results for both the adsorbates.

$$y = 0,8145 \, Ln(x) + 4,6683$$
$$R^2 = 0,9994$$
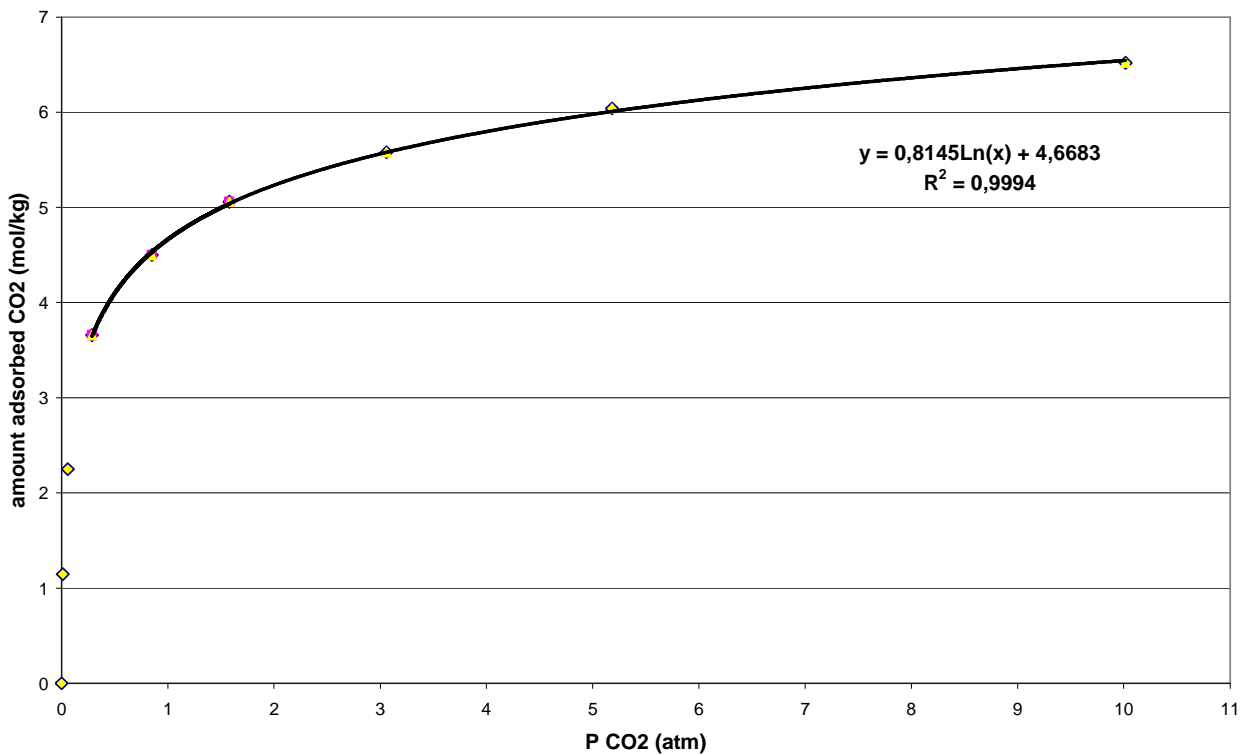
Figure 3.40: adsorption isotherm for CO_2 at 298 K (Zeolite 13X)
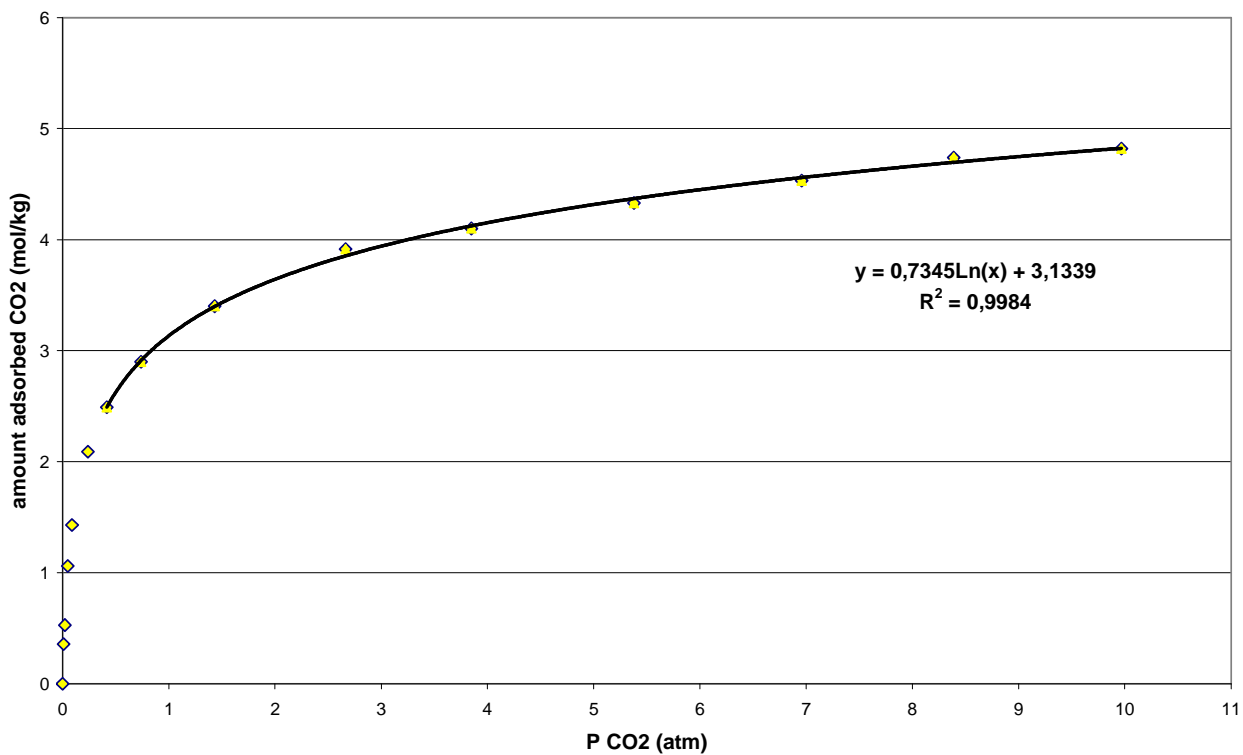
Figure 3.41: adsorption isotherm for CO_2 at 323 K (Zeolite 13X)

$$y = 0{,}7345 Ln(x) + 3{,}1339$$
$$R^2 = 0{,}9984$$
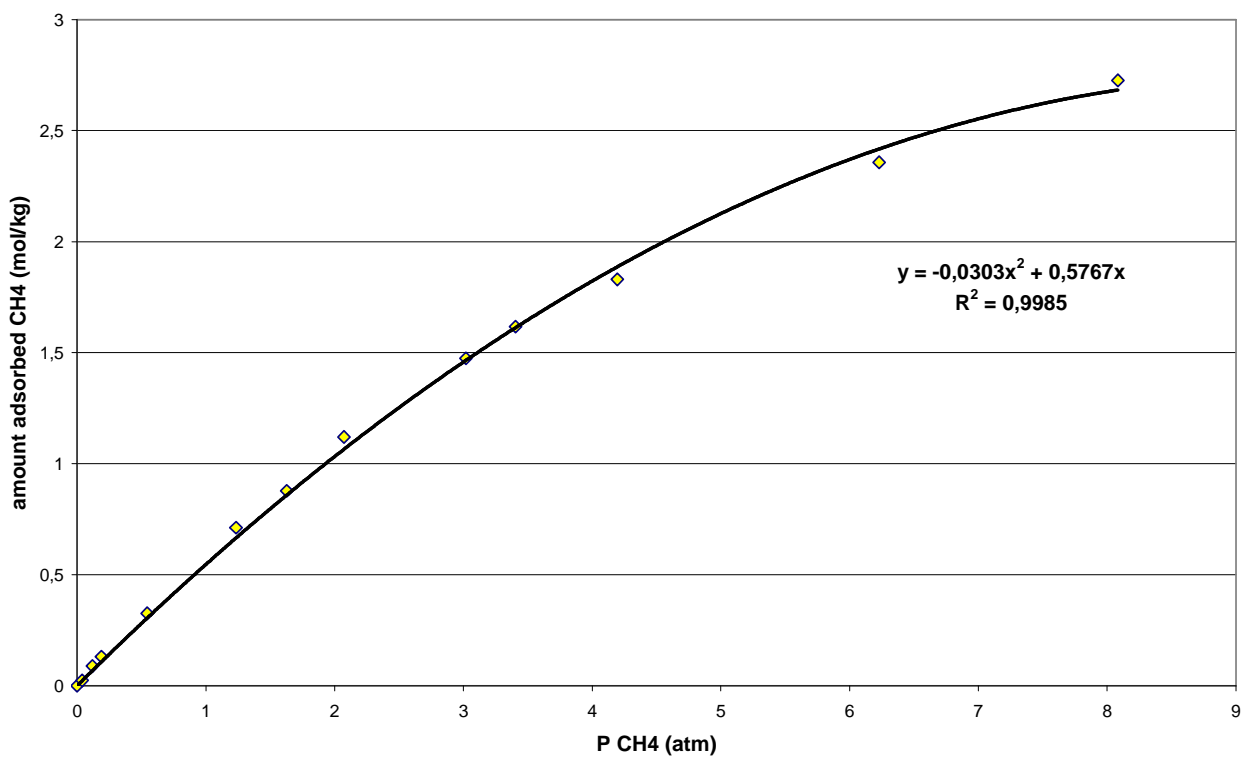
Figure 3.42: adsorption isotherm for CH_4 at 298 K (Zeolite 13X)

$$y = -0{,}0303x^2 + 0{,}5767x$$
$$R^2 = 0{,}9985$$
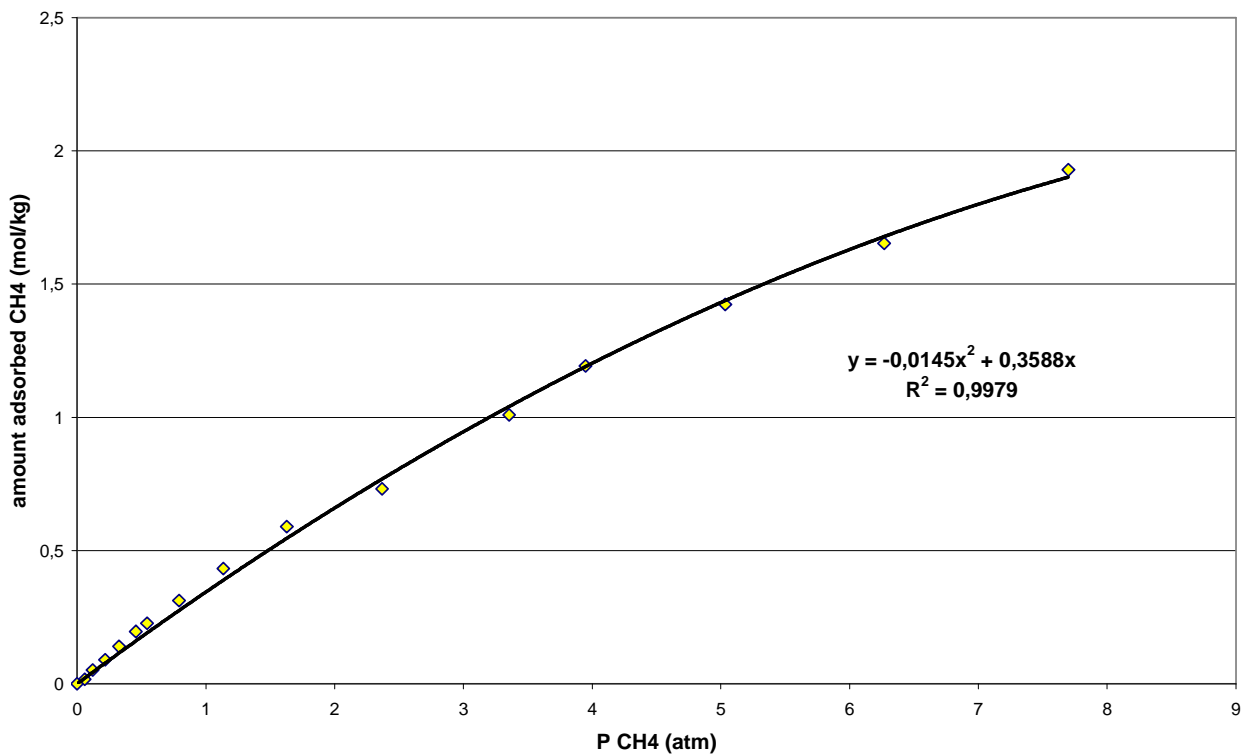
Figure 3.43: adsorption isotherm for CH_4 at 323 K (Zeolite 13X)
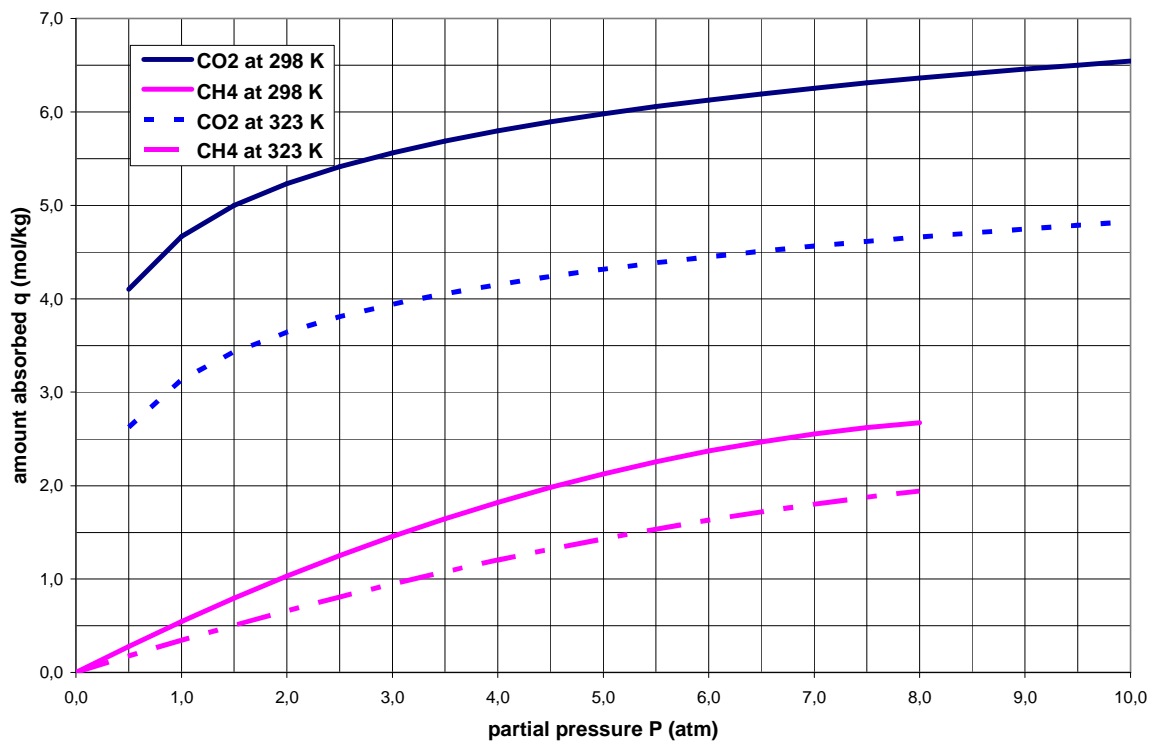
Figure 3.44: adsorption isotherms for CO_2 and CH_4 at 298 and 323 K for Zeolite 13X

The reported interpolation expressions are valid within the partial pressure range 0÷8 atm for methane and 0.43÷10 atm for CO_2 (however, between 0.05 and 0.43 atm the same equation for CO_2 involves very small errors, always below 13%).

Based on Figure 3.44, it should be observed that CO_2 cyclic capacity at lower temperature (the one generally chosen for adsorption since the absolute loading capacity q is higher than at higher temperature, where adsorbate tends to desorb) is smaller than at higher temperatures, that is Zeolite 13X could be more efficiently used at 323 K than at 298 K.

As already commented, a separation process is based not only on thermodynamics, that is equilibrium curves; dispersion and diffusion phenomena, that is mass transport properties, plays a crucial role in determining the process design.
Equations for mass transfer in fixed bed adsorption are obtained by making an adsorbate material balance for a section dL of the bed:

$$\varepsilon \frac{\delta c}{\delta t} + (1 - \varepsilon) \cdot \rho_p \frac{\delta q}{\delta t} = -u_0 \frac{\delta c}{\delta L}$$

where c is adsorbate concentration in the gas phase, q is adsorbate loading (mol/kg or g/kg), ε is the external void fraction of the bed (column porosity or bulk porosity), ρ_p is density of particle (kg/m^3), u_0 is superficial velocity of fluid (m/s). For adsorption from a gas, the first term, the accumulation in the fluid, is usually negligible compared to the accumulation on the solid.
The transfer to the solid includes diffusion through the fluid film around the particle and diffusion in the pores to internal adsorption sites. The actual adsorption is practically instantaneous and equilibrium is assume to exist between solid and gas at each point inside the particles. Mass transfer is approximated using an overall volumetric coefficient K_c and an overall driving force:

$$(1 - \varepsilon) \cdot \rho_p \frac{\delta q}{\delta t} = K_c a \cdot (c - c^*)$$

Where a is the mass transfer area (taken as the external surface of particles), c^* is gaseous concentration that would be in equilibrium with the average concentration q in the solid.
The overall coefficient K_c depends both on the external coefficient and on an effective internal coefficient that is directly depending on diffusion phenomena inside particles (influenced by particle porosity, pore diameter, tortuosity and nature of diffusing gaseous molecules). Generally, the limiting condition for mass transfer is due to internal coefficient $k_{c,int}$, that could be approximated (McCabe et al, 2005) as $10 \cdot D_e / d_p$, where D_e is effective diffusivity (cm^2/s) and d_p is particle diameter (m). As a consequence:

$$\frac{1}{K_c} = \frac{1}{k_{c,ext}} + \frac{d_p}{10 \cdot D_e}$$

In fixed bed adsorption, the concentrations in the gas phase and the solid phase change with time as well as with the position in the bed. At first, most of the mass transfer takes place near the inlet of the bed, the concentration in the fluid phase c drops exponentially essentially to zero before the end of the bed, as reported by Figure 3.45. After a few minutes, the solid near the inlet is saturated and the mass transfer occurs further from the inlet. Similar profiles could be drawn for the adsorbate concentration on the solid q; the plot of concentration *vs* time is called breakthrough curve.
The concentration change area is called mass-transfer zone and its width depends on mass transfer coefficients.
In the case mass transfer phenomena are quite fast, the mass transfer zone is narrow relative to the bed length L_T, that is the breakthrough curve will be rather steep. This is a desirable configuration as most of the adsorption capacity of the solid will be utilized at the breakpoint.

The reported mass-transfer equations could be analytically solved only under particular conditions, for example linear isotherms or irreversible adsorption. All solutions involve a dimensionless time τ and a parameter N proportional to mass transfer coefficient:

$$\tau = \frac{u_0 \cdot c_0 \cdot t}{\rho_p \cdot (1 - \varepsilon) \cdot L_T \cdot q_{sat}}$$

$$N = \frac{K_c \cdot a \cdot L_T}{u_0}$$

where the numerator of τ represents the total adsorbate fed to a unit cross section of bed up to time t, and the denominator is the adsorbing capacity of the bed. If there were no resistances to mass transfer (very large N, ~100), the adsorber would operate up to $\tau = 1$ and the concentration curve would jump from 0.0 to 1.0. On the contrary, with a finite rate of mass transfer, breakthrough curve occurs at $\tau < 1.0$, and the steepness of the curve depends mainly on N (the larger N, the steeper the breakthrough curve).
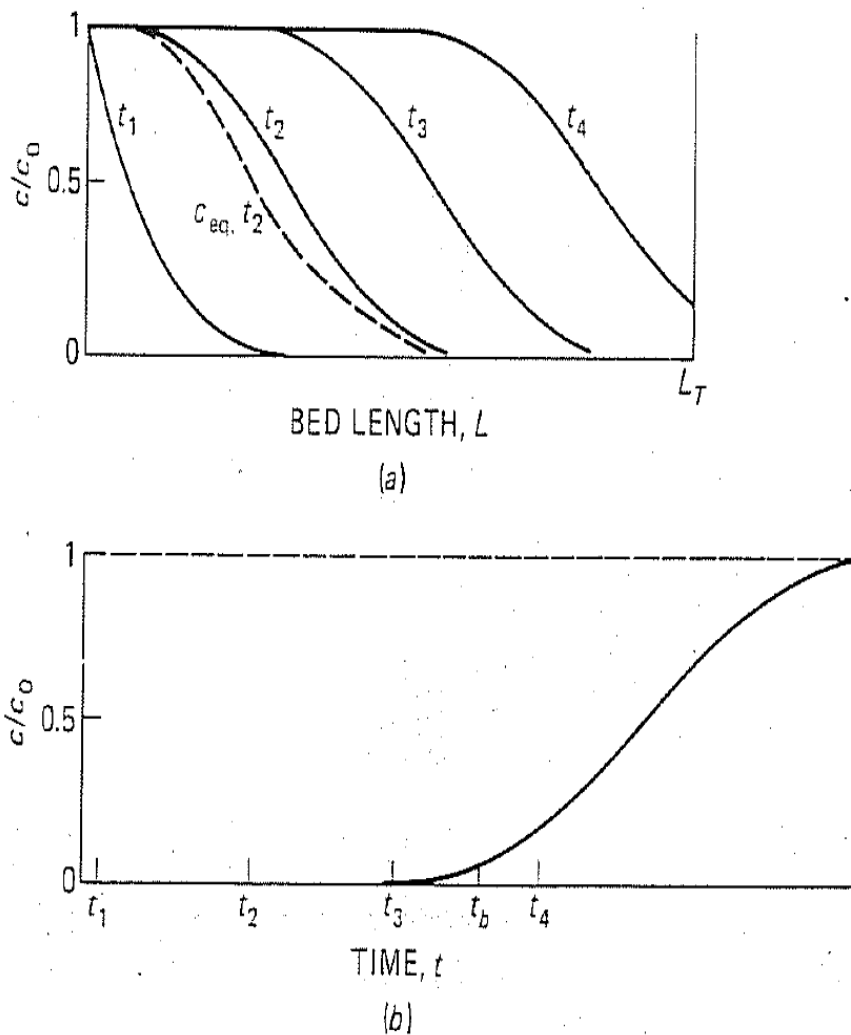

Figure 3.45: concentration profiles (a) and breakthrough curve (b) for adsorption (from McCabe et al., 2005).

Since adsorption phenomena are one of the most complex process as far as unit operation of chemical engineering is concerned and that design is usually carried out by means of numerical simulation (partial differential equations linked by non-linear isotherm) and experimental scale-ups, considering that mass transfer influences just a portion of the bed, being the upstream part of the bed in equilibrium with the adsorbate concentration, in the present work an ideal adsorption is considered, where no mass transfer resistance occurs (the concentration curves are vertical, and $\tau = 1.0$). The described assumption is reasonable for the process conditions considered in our simulation, carried out for Zeolite X13 as the adsorber, in particular when the bed length is quite long (the predicted contact time could be tenth of seconds). The main physical features of Zeolite X13 are showed by Figure 3.46 from Cavenati et al. (2004); this material have been chosen because isotherms at different temperatures were at disposal for methane and CO_2 and the kinetic behaviour (mass transfer coefficients) is claimed to be fast for both the molecules.

parameters	value
pellet particle density ($kg \cdot m^{-3}$)	1130
pellet diameter (m)	1.6×10^{-3}
crystal size (m)	7.0×10^{-7}
pellet porosity	0.54
macropore radius (m)	1.61×10^{-7}

Figure 3.46: Zeolite X13 physical properties.

One of the crucial point for PSA efficiency is the reduction of methane loss that usually take place in the regeneration phase (blowdown and purge): immediately before CO_2 breaks through, the feed is stopped and the column is depressurized, letting both CO_2 and CH_4 adsorbed desorb (blowdown); after depressurization, a purge step could be performed to displace CO_2 and CH_4 molecules that remains in the gas phase within the column by means of some biomethane injected counter-current to feed step. Petterson and Wellinger (2011) report methane slip in PSA processes in the range 3÷12%, other studies (Persson, 2003) inform that methane losses up to 10% have been measured due to leakages in valves between columns, many suppliers say that methane losses for PSA are somewhat higher than 2%, probably 3-4%.

In order to minimize methane slip, many could be the regeneration strategies to put in practice.
Literature reports that after saturation, the bed is depressurized, releasing a CH_4/CO_2 mixture with a high CH_4 content, which will be recycled to the inlet of the PSA-unit. The next step is to regenerate the adsorbent bed by further depressurization (PSA) or by putting it under vacuum (VSA), releasing a gas flow of CO_2 with little CH_4 (Ryckebosch et al., 2011). This kind of approach could be termed as "*depressurization step recycle*".
Another possibility is to apply multiple pressure equalization steps between different columns, as reported by Cavenati et al. (2005).
Finally, the most efficient choice in terms of methane losses reduction could be the recirculation of a part of all the desorbed gas phase (depressurization+desorption), that is probably the most expensive configuration as far as energy costs are concerned. This strategy could be called "*desorption recirculation*".
The present study will deepen the first and the third technical options in order to assess the possible optimization of PSA process carried out by Zeolite X13. As obvious, the best choice and the consequent energy and environmental performances deal mainly with thermodynamics conditions given by solid-gas equilibrium; then, the present analysis in the case of PSA can be defined as a methodological approach to the problem that cannot give a complete overview of all possibilities, materials, process conditions and so on.
As far as "depressurization step recycle" is concerned, Figure 3.47 reports the simplified process layout, assuming that depressurization step (from P_{ads} to P_{dep}) and desorption step (from P_{dep} to P_{des}) are forced to occur in the same time interval called $t_{sat,CO2}$ (that is saturation time as far as CO_2 is concerned). This is a consistent hypothesis as adsorption phase usually lasts much more than depressurization + desorption.

The overall mass balance for the "depressurization step recycle" technique can be written as the following equation system (5 equations in 5 unknown quantities):

$$V_b \cdot t_{sat,CO_2} = V_a \cdot t_{sat,CO_2} + V_{des} \cdot t_{sat,CO_2}$$

$$V_{dep} \cdot t_{sat,CO_2} = Q_z \cdot \left(\Delta q_{dep} + \Delta q'_{dep} \right)$$

$$y = \frac{v_b \cdot y_b \cdot t_{sat,CO_2} + Q_z \cdot \Delta q_{dep}}{V_b \cdot t_{sat,CO_2} + V_{dep} \cdot t_{sat,CO_2}}$$

$$t_{sat,CO_2} = \frac{Q_z \cdot \left(\Delta q_{dep} + \Delta q_{des} \right)}{\left(V_b + V_{dep} \right) \cdot y}$$

$$V_{des} \cdot t_{sat,CO_2} = Q_z \cdot \left(\Delta q_{des} + \Delta q'_{des} \right)$$
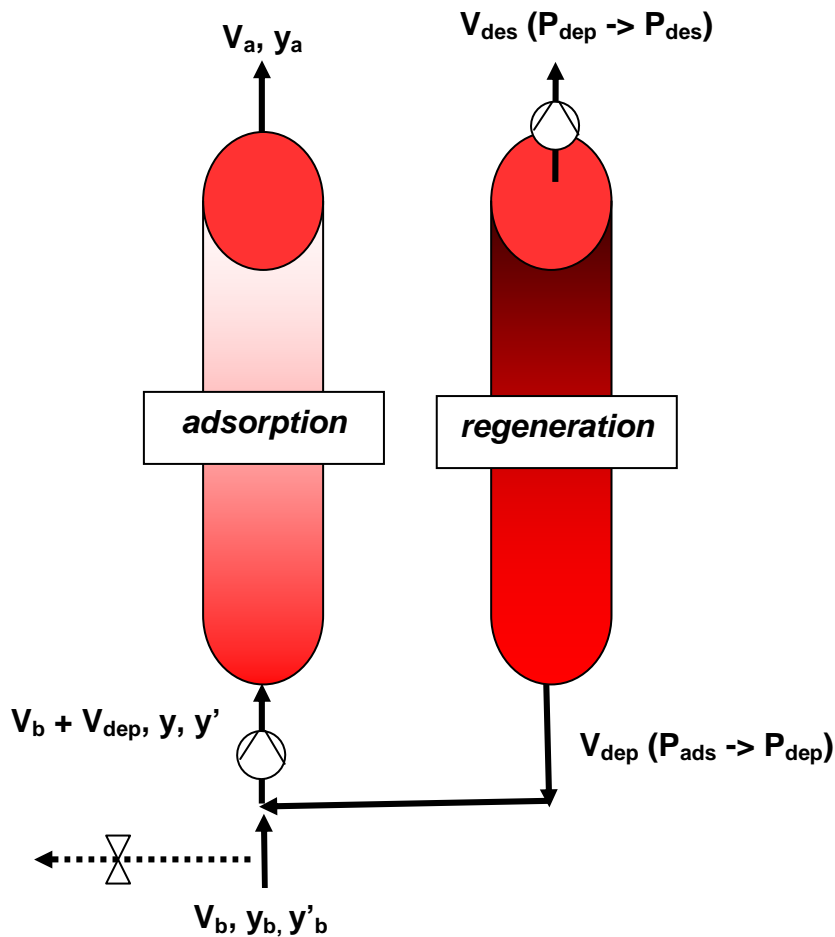

Figure 3.47: general layout for the "depressurization step recycle" regeneration technique

where V_b is the raw biogas flow rate (~22 020 mol/h), y_b is 0.47 as always, Q_z is adsorbent weight for each column (kg), Δq_{des} and $\Delta q'_{des}$ are adsorption capacities, respectively for CO_2 and CH_4, between adsorption

and depressurization pressures, Δq_{dep} and $\Delta q'_{dep}$ are adsorption capacities, respectively for CO_2 and CH_4, between depressurization and desorption pressures, $t_{sat,CO2}$ is saturation time for CO_2, that is breakthrough time, V_a is biomethane flow rate, y_a is assumed equal to 1; saturation time for CH_4 is obviously smaller than that for CO_2, that is methane go through the column during a time interval before breakpoint.

The sum of Δq_{des} and Δq_{dep} represents Δq, that is the cyclic adsorption capacity for CO_2. The same reasoning is valid for methane adsorption capacity ($\Delta q'$), calculated between adsorption and desorption pressures.

Based on literature suggestions, the following boundary conditions have been assumed:
- Q_z = 5000 kg for each column;
- T = 323 K (at this temperature the cyclic adsorption capacities are more favourable than at lower T);
- Adsorption pressure P_{ads} 2÷6 atm;
- depressurization pressure P_{dep} 0.5÷1.5 atm;
- desorption pressure P_{des} 0.1÷0.5 atm.

Table 3.35 reports the simulation results, where CH_4 slip ranges from 4.2 to 17.4% of the inlet biogas methane; the results are absolutely consistent with literature indications.

As expected, the lower the depressurization pressure P_{dep} the lower methane losses, since the recycled quantity to adsorption tower is higher; at the same time, the lower desorption pressure P_{des}, the lower CH_4 losses, since cyclic adsorption capacity is more favourable for CO_2. On the other hand, adsorption pressure seems to be not much influent on methane losses.

As far as the second studied regeneration technique is concerned, Figure 3.48 points out the general layout, where r is recirculation rate, Q_z is adsorbent weight for each column (kg), Δq and $\Delta q'$ are cyclic adsorption capacity, respectively for CO_2 and CH_4, between adsorption and desorption pressures, V_a is biomethane flow rate, y_a is assumed equal to 1.

Assuming that the depressurization + desorption phases take (or are forced to take) the same time as the adsorption step, the overall mass balance can be expressed as:

$$V_b \cdot t_{sat,CO_2} = V_a \cdot t_{sat,CO_2} + (1-r) \cdot V_{reg} \cdot t_{sat,CO_2}$$

$$V_{reg} \cdot t_{sat,CO_2} = Q_z \cdot (\Delta q + \Delta q')$$

$$y = \frac{v_b \cdot y_b \cdot t_{sat,CO_2} + r \cdot Q_z \cdot \Delta q}{V_b \cdot t_{sat,CO_2} + r \cdot V_{reg} \cdot t_{sat,CO_2}}$$

$$t_{sat,CO_2} = \frac{Q_z \cdot \Delta q}{(V_b + r \cdot V_{reg}) \cdot y}$$

$$V_a \cdot t_{sat,CO_2} = V_b \cdot y'_b \cdot t_{sat,CO_2} - (1-r) \cdot Q_z \cdot \Delta q'$$

Table 3.36 points out the simulation results, where CH_4 slip ranges from 1.4 to 37% of the inlet biogas methane.

As one can easily observe, the higher the recirculation rate and the lower the final desorption pressure P_{des}, the lower the methane loss. At the same time, due to the specific shapes of the isotherms, conditions are more favourable when adsorption pressure is not so high, giving the best performance within the range 1.5÷2 atm; for this configuration, CO_2 adsorption cyclic capacity is much higher than that for methane.

The direct comparison between the 2 regeneration strategies highlights that the strong difference is the flow rate of the recirculating gas, much larger in the case of "desorption recirculation" (V_{reg}·r could be up to 209000 mol/h when r is 0.95), then higher energy consumptions are expected. On the other hand, however, "desorption recirculation" technique, under very large recirculation rate and very low P_{des} conditions, could achieve lower methane losses, below 2%, performances that are not expected for the "depressurization step recycle" configuration, at least when Zeolite X13 is used.
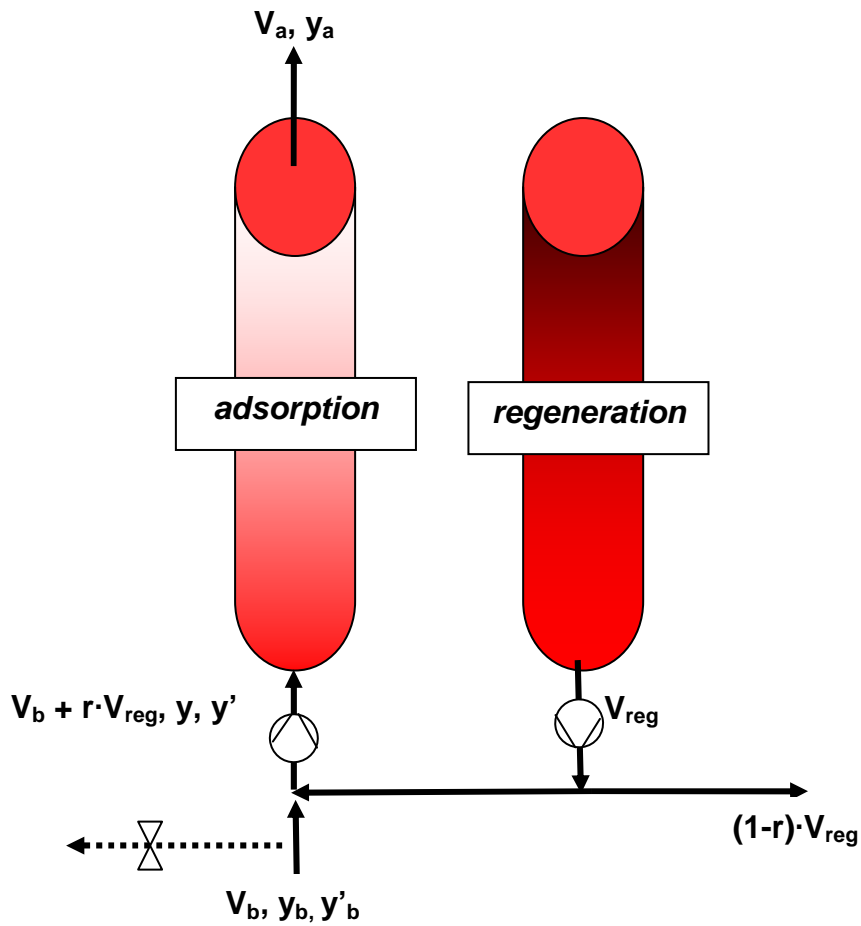
Figure 3.48: general layout for the "desorption recirculation" regeneration technique

Nevertheless, it should be remembered that the larger the recirculating flow rate, the higher the superficial velocity u_0, the smaller the parameter N (described in the previous chapter as a tool to measure the steepness of the breakthrough curve). Then, when the superficial velocity is particularly large, the assumption of neglecting the width of the mass transfer zone could be less precise.

Table 3.35: simulation results for the "depressurization step recycle" regeneration technique

T (K)	323	323	323	323	323	323	323	323	323	323	323	323	323	323	323	323	323
P_{des} (atm)	0.5	0.5	0.3	0.1	0.1	0.5	0.5	0.3	0.1	0.1	0.5	0.5	0.3	0.1	0.1	0.1	0.1
P_{dep} (atm)	1.5	1	1	1	1.5	1.5	1	1	1	2	1.5	1	1	1	0.5	0.5	0.5
P_{ads} (atm)	6	6	6	6	6	4	4	4	4	6	3	3	3	2	6	4	2
V_b (moli/h)	22019.7	22019.7	22019.7	22019.7	22019.7	22019.7	22019.7	22019.7	22019.7	22019.7	22019.7	22019.7	22019.7	22019.7	22019.7	22019.7	22019.7
y_b	0.47	0.47	0.47	0.47	0.47	0.47	0.47	0.47	0.47	0.47	0.47	0.47	0.47	0.47	0.47	0.47	0.47
y'_b	0.53	0.53	0.53	0.53	0.53	0.53	0.53	0.53	0.53	0.53	0.53	0.53	0.53	0.53	0.53	0.53	0.53
CO_2 in (mol/h)	10349.3	10349.3	10349.3	10349.3	10349.3	10349.3	10349.3	10349.3	10349.3	10349.3	10349.3	10349.3	10349.3	10349.3	10349.3	10349.3	10349.3
CH_4 in (mol/h)	11670.5	11670.5	11670.5	11670.5	11670.5	11670.5	11670.5	11670.5	11670.5	11670.5	11670.5	11670.5	11670.5	11670.5	11670.5	11670.5	11670.5
Q_z (kg)	5000	5000	5000	5000	5000	5000	5000	5000	5000	5000	5000	5000	5000	5000	5000	5000	5000
y	0.54	0.60	0.57	0.53	0.51	0.54	0.62	0.57	0.53	0.49	0.54	0.61	0.57	0.52	0.59	0.60	0.59
y'	0.46	0.40	0.43	0.47	0.49	0.46	0.39	0.43	0.47	0.51	0.46	0.39	0.43	0.48	0.41	0.40	0.41
Δq_{dep} (mol CO2/kg)	1.02	1.32	1.32	1.32	1.02	0.72	1.02	1.02	1.02	0.81	0.51	0.81	0.81	0.51	1.83	1.53	1.02
$\Delta q'_{dep}$ (mol CH4/kg)	0.64	0.63	0.68	0.73	0.68	0.37	0.38	0.42	0.45	0.61	0.23	0.26	0.29	0.16	0.71	0.46	0.21
Δq_{des} (mol CO2/kg)	0.81	0.51	0.88	1.69	1.99	0.81	0.51	0.88	1.69	2.20	0.81	0.51	0.88	1.69	1.18	1.18	1.18
$\Delta q'_{des}$ (mol CH4/kg)	0.16	0.07	0.11	0.15	0.24	0.16	0.07	0.10	0.15	0.33	0.16	0.07	0.11	0.15	0.06	0.06	0.06
Δq (mol CO2/kg)	1.83	1.83	2.20	3.01	3.01	1.53	1.53	1.90	2.71	3.01	1.32	1.32	1.69	2.20	3.01	2.71	2.20
$\Delta q'$ (mol CH4/kg)	0.80	0.70	0.79	0.87	0.92	0.52	0.45	0.52	0.60	0.94	0.39	0.33	0.39	0.32	0.77	0.52	0.27
V_{dep} (moli/h) x $t_{sat,CO2}$ (h)	8280.6	9750.4	9986.8	10215.5	8474.2	5437.9	7002.0	7190.6	7361.6	7075.3	3688.4	5340.3	5476.0	3364.3	12697.2	9959.5	6155.3
V_{des} (moli/h) x $t_{sat,CO2}$ (h)	4827.4	2894.2	4952.7	9194.5	11143.1	4821.6	2882.9	4945.7	9192.6	12654.9	4835.5	2885.6	4951.6	9222.2	6198.5	6194.1	6203.8
$t_{sat,CO2}$ (h)	0.390	0.246	0.427	0.817	0.961	0.390	0.246	0.427	0.817	1.064	0.390	0.246	0.427	0.817	0.571	0.571	0.571
V_{dep} (mol/h)	21233.7	39635.7	23366.9	12497.2	8818.7	13935.2	28482.9	16824.6	9007.8	6649.4	9468.1	21711.0	12815.4	4116.7	22228.5	17435.5	10776.0
V_{des} (mol/h)	12378.7	11765.1	11588.2	11248.2	11596.1	12355.8	11726.9	11572.0	11248.2	11893.1	12412.8	11731.7	11588.3	11284.8	10851.4	10843.7	10860.8
V_a (mol/h)	9641.0	10254.6	10431.6	10771.6	10423.6	9663.9	10292.8	10447.8	10771.5	10126.6	9606.9	10288.0	10431.5	10734.9	11168.3	11176.0	11158.9
CH_4 loss (mol/h)	2029.5	1415.9	1238.9	898.9	1246.8	2006.6	1377.7	1222.7	898.9	1543.8	2063.5	1382.4	1239.0	935.5	502.2	494.4	511.6
CH_4 loss (%)	17.4%	12.1%	10.6%	7.7%	10.7%	17.2%	11.8%	10.5%	7.7%	13.2%	17.7%	11.8%	10.6%	8.0%	4.3%	4.2%	4.4%

Table 3.36: simulation results for the "desorption recirculation" regeneration technique

T (K)	323	323	323	323	323	323	323	323	323	323	323	323	323	323	323	323
P_{des} (atm)	0.5	0.5	0.5	0.5	0.5	0.5	0.3	0.3	0.3	0.3	0.1	0.1	0.1	0.1	0.1	0.1
P_{ads} (atm)	6	6	2	6	4	3	3	4	10	3	3	5	2	1.5	1.5	1.5
V_b (moli/h)	22019.7	22019.7	22019.7	22019.7	22019.7	22019.7	22019.7	22019.7	22019.7	22019.7	22019.7	22019.7	22019.7	22019.7	22019.7	22019.7
y_b	0.47	0.47	0.47	0.47	0.47	0.47	0.47	0.47	0.47	0.47	0.47	0.47	0.47	0.47	0.47	0.47
y'_b	0.53	0.53	0.53	0.53	0.53	0.53	0.53	0.53	0.53	0.53	0.53	0.53	0.53	0.53	0.53	0.53
CO_2 in (mol/h)	10349.3	10349.3	10349.3	10349.3	10349.3	10349.3	10349.3	10349.3	10349.3	10349.3	10349.3	10349.3	10349.3	10349.3	10349.3	10349.3
CH_4 in (mol/h)	11670.5	11670.5	11670.5	11670.5	11670.5	11670.5	11670.5	11670.5	11670.5	11670.5	11670.5	11670.5	11670.5	11670.5	11670.5	11670.5
Q_z (kg)	5000	5000	5000	5000	5000	5000	5000	5000	5000	5000	5000	5000	5000	5000	5000	5000
recirculation rate (r)	0.5	0.8	0.8	0.9	0.9	0.9	0.9	0.9	0.9	0.95	0.95	0.95	0.95	0.95	0.8	0.9
y	0.56	0.67	0.75	0.74	0.79	0.82	0.84	0.82	0.70	0.90	0.92	0.90	0.93	0.93	0.79	0.88
y'	0.44	0.33	0.25	0.26	0.21	0.18	0.16	0.18	0.30	0.10	0.08	0.10	0.07	0.07	0.21	0.12
Δq (mol CO_2/kg)	1.83	1.83	1.02	1.83	1.53	1.32	1.69	1.90	2.58	1.69	2.50	2.87	2.20	1.99	1.99	1.99
$\Delta q'$ (mol CH_4/kg)	0.76	0.59	0.13	0.47	0.25	0.16	0.15	0.24	0.92	0.09	0.08	0.18	0.05	0.03	0.11	0.06
V_{reg} (moli/h) x $t_{sat,CO2}$ (h)	12933.6	12067.0	5738.0	11494.7	8881.8	7370.8	9229.6	10688.8	17485.6	8927.1	12908.0	15255.2	11245.7	10114.6	10470.5	10252.3
$t_{sat,CO2}$ (h)	0.441	0.177	0.098	0.089	0.074	0.064	0.082	0.092	0.124	0.041	0.060	0.069	0.053	0.048	0.194	0.096
V_{reg} (mol/h)	29335.1	68423.8	58320.5	130357.5	120365.1	115926.7	112957.4	116287.8	140522.7	218510.4	213897.7	219783.4	211574.4	210508.7	54478.8	106687.0
V_{reg} x r (mol/h)	14667.5	54739.1	46656.4	117321.8	108328.6	104334.1	101661.7	104659.0	126470.4	207584.9	203202.8	208794.2	200995.7	199983.3	43583.0	96018.3
V_a (mol/h)	7351.8	8345.9	10354.5	9015.6	9979.3	10423.3	10721.3	10387.1	7962.5	11091.0	11330.7	11033.5	11468.1	11506.3	11175.3	11348.0
CH_4 loss (mol/h)	4318.7	3324.6	1316.0	2654.8	1691.1	1247.1	949.1	1283.3	3708.0	579.4	339.7	636.9	202.4	164.2	495.1	322.5
CH_4 loss (%)	37.0%	28.5%	11.3%	22.7%	14.5%	10.7%	8.1%	11.0%	31.8%	5.0%	2.9%	5.5%	1.7%	1.4%	4.2%	2.8%

As far as energy consumptions are concerned, power requirements can be divided into 3 main categories:
1. biogas compression energy,
2. vacuum producing energy,
3. pressure drops within the columns,
4. biomethane compression to natural gas grid pressure.

The first group consumptions could be calculated according to an adiabatic compression process, as already widely described for other upgrading techniques.

The second aspect, involving the use of vacuum pump to reduce pressure below atmospheric, should take into account the gas quantities to be removed from the column during regeneration, in particular when passing from atmospheric pressure to final desorption pressure P_{des} (0.1÷0.5 atm). The gas flow rate to be taken away by the vacuum pump (the most used are rotary vane pump, showed by Figure 3.49) is the sum of the desorbed quantity ($\Delta q + \Delta q'$) and the gas quantities that can be contained within void volumes of the column, being the first value much larger than the latter. For example, if we assume that the adsorption column contains 5000 kg of adsorbent, the pellet density is 1130 kg/m^3 as reported by Figure 3.46 and the column porosity is around 40% (a typical value), then the column will be 7.37 m^3 and, at 1 atm, it will contain 111 mol of gas within voids (from perfect gas law) and 11 mol at 0.1 atm. On the contrary, the desorbed gas quantity between 1 and 0.1 atm will be in the order of thousands moles, that is the desorbed flow rates rules the energy consumption of vacuum generator.
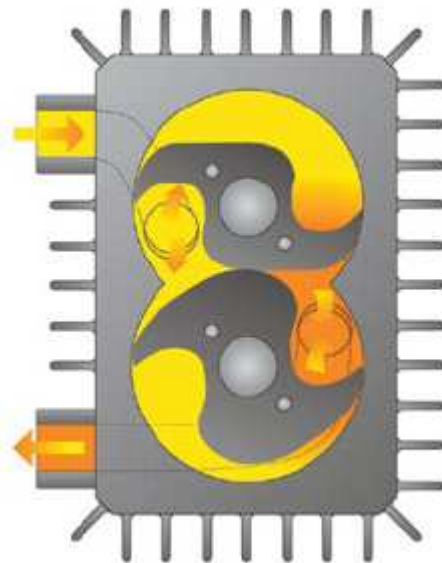

Figure 3.49: example of rotary vane vacuum pump

As far as specific energy consumptions for vacuum pump, they strongly depends on the final pressure to be reached; however, a frequent values range that can be found in literature for vacuum down to 0.1 atm (abs) is around 12 cfm/hp (cubic feet per minute / horse power), that can be translated as 27 m^3/h/kW, a quite conservative value that will be used in the following assessment. Since desorption tends to compensate pressure decreasing and its flow rate is dominant if compared to void volume gas, in order to have a rough knowledge of vacuum energy consumptions one could consider that most of removed gas is sucked at pressures close to atmospheric one, so that taken away volumes could be considered at normal conditions.

Finally, pressure drops (Pa/m) within the column can be calculated by Ergun expression for packed column:

$$\frac{\Delta P}{L} = 150 \frac{\mu_g \cdot (1-\varepsilon)^2 \cdot u_0}{\varepsilon^3 \cdot dp^2} + 1.75 \frac{1-\varepsilon}{\varepsilon^3} \cdot \frac{\rho_g \cdot u_0^2}{dp} :$$

where ε is column porosity (assumed equal to 0.4), dp is adsorbing particle diameter (in the simulated case $1.6 \cdot 10^{-3}$ m), u_0 is superficial velocity, μ_g and ρ_g are gas viscosity and density (for raw biogas respectively $1.19 \cdot 10^{-5}$ kg/m/s and 1.3 kg/m^3).

Finally, since produced biomethane must be injected into natural gas grid, assuming that the reference maximum pressure for local grid is 5 atm, a further compression of biomethane is required because not always P_{ads} is larger than P_{grid}.

Table 3.37 and 3.38 report the final results as far as energy consumptions (and recoverable thermal energy from compression) are concerned. It is worth mentioning that thermal energy due to compression is primarily used to heat gas flows up to adsorption temperature that is 323 K (the calculated final thermal recovery value is net). Secondly, as adsorption is exothermic process, columns should be cooled to be maintained isothermal: this amount of recoverable thermal energy has been neglected in our calculations.

Moreover, column dimension has been decided in order to minimize pressure drops calculated by Ergun expression: since pressure drops are inversely proportional to diameter to the power of 4, column diameter has been fixed equal to 2 m. The column could be divided into multiple slimmer columns operating in parallel.

Finally, in order to be strictly conservative, the reported simulations don't consider the possibilities of using the releasing gas pressure in one vessel for pressurization of another in order to reduce energy consumptions.

As far as the "depressurization step recycle" technique is concerned, the total energy consumption is quite small ($0.10 \div 0.20$ kWh$_e$/m^3 of raw biogas), also for the configurations aiming at minimizing methane losses under 5% (highlighted in green). At the same time, net thermal energy recovery could be larger than 30 kW$_{th}$. The "desorption recirculation" technique is characterized by methane losses potentially lower than 2%; however, as widely expected, these performances are obtained by spending more energy, since energy consumptions could be in the order of $0.5 \div 0.6$ kWh$_e$/m^3 of raw biogas. The same technical configurations could produce from 20 to 60 thermal kW.

On the basis of the described simulated operations for PSA and the data reported by literature, it could be observed that the minimization of methane losses is particularly difficult for adsorption and the best achievable performances could be not satisfying if compared to other upgrading techniques. Apart from the economical value of wasted methane, it is of extreme importance to minimize the methane slip since methane is a strong greenhouse gas. The release of methane to the atmosphere should be minimized by treating the off-gas even though the methane cannot be utilized.

The off-gas from an upgrading plant seldom contains a high enough methane concentration to maintain a flame without addition of natural gas or biogas. One way of limiting the methane slip is to mix the off-gas with air that is used for possible combustion processes.

Alternatively the methane can be oxidized by thermal or catalytic oxidation, that could be auto-thermal when the VOC oxidiser is very performing in terms of energy recovery (regenerative oxidizer for example) and methane concentration is at least 1 g/Nm^3. In the case of simulated PSA processes, when methane slip passes from 1% to 5%, methane concentration results to be 8 to 40 g/Nm^3 of waste gas, that is methane could be eliminated by VOC oxidizers without the addition of support fuels, on the contrary, some thermal energy could be recovered from it. If methane losses are larger than 8%, the off-gases could be used as a fuel in a boiler since calorific value is pretty high.

Table 3.37: total energy consumption for the "depressurization step recycle" regeneration technique

T (K)	323	323	323	323	323	323	323	323	323	323	323	323	323	323	323	323	323
Pdes (atm)	0,5	0,5	0,3	0,1	0,1	0,5	0,5	0,3	0,1	0,1	0,5	0,5	0,3	0,1	0,1	0,1	0,1
Pdep (atm)	1,5	1	1	1	1,5	1,5	1	1	1	2	1,5	1	1	1	0,5	0,5	0,5
Pads (atm)	6	6	6	6	6	4	4	4	4	6	3	3	3	2	6	4	2
Qz (kg)	5000	5000	5000	5000	5000	5000	5000	5000	5000	5000	5000	5000	5000	5000	5000	5000	5000
y	0,54	0,60	0,57	0,53	0,51	0,54	0,62	0,57	0,53	0,49	0,54	0,61	0,57	0,52	0,59	0,60	0,59
tsat,CO2 (h)	0,390	0,246	0,427	0,817	0,961	0,390	0,246	0,427	0,817	1,064	0,390	0,246	0,427	0,817	0,571	0,571	0,571
Vdep (mol/h)	21233,7	39635,7	23366,9	12497,2	8818,7	13935,2	28482,9	16824,6	9007,8	6649,4	9468,1	21711,0	12815,4	4116,7	22228,5	17435,5	10776,0
Vdes (mol/h)	12378,7	11765,1	11588,2	11248,2	11596,1	12355,8	11726,9	11572,0	11248,2	11893,1	12412,8	11731,7	11588,3	11284,8	10851,4	10843,7	10860,8
Vb+Vdep (mol/h)	43253,4	61655,5	45386,6	34516,9	30838,4	35954,9	50502,6	38844,3	31027,5	28669,2	31487,8	43730,8	34835,2	26136,4	44248,2	39455,3	32795,7
Va (mol/h)	9641,0	10254,6	10431,6	10771,6	10423,6	9663,9	10292,8	10447,8	10771,5	10126,6	9606,9	10288,0	10431,5	10734,9	11168,3	11176,0	11158,9
CH4 loss (mol/h)	2029,5	1415,9	1238,9	898,9	1246,8	2006,6	1377,7	1222,7	898,9	1543,8	2063,5	1382,4	1239,0	935,5	502,2	494,4	511,6
CH4 loss (%)	17,4%	12,1%	10,6%	7,7%	10,7%	17,2%	11,8%	10,5%	7,7%	13,2%	17,7%	11,8%	10,6%	8,0%	4,3%	4,2%	4,4%
column pressure drop (ERGUN)																	
column porosity	0,4	0,4	0,4	0,4	0,4	0,4	0,4	0,4	0,4	0,4	0,4	0,4	0,4	0,4	0,4	0,4	0,4
tower diam (m)	2	2	2	2	2	2	2	2	2	2	2	2	2	2	2	2	2
column lenght LT (m)	2,35	2,35	2,35	2,35	2,35	2,35	2,35	2,35	2,35	2,35	2,35	2,35	2,35	2,35	2,35	2,35	2,35
dp (m)	0,0016	0,0016	0,0016	0,0016	0,0016	0,0016	0,0016	0,0016	0,0016	0,0016	0,0016	0,0016	0,0016	0,0016	0,0016	0,0016	0,0016
µg (kg/m/s)	0,0000121	0,0000123	0,0000121	0,0000121	0,0000120	0,0000121	0,0000124	0,0000122	0,0000121	0,0000120	0,0000121	0,0000124	0,0000122	0,0000120	0,0000123	0,0000123	0,0000123
ρg (kg/m3)	1,3898	1,4655	1,4225	1,3797	1,3477	1,3941	1,4821	1,4298	1,3813	1,3300	1,3837	1,4780	1,4236	1,3574	1,4571	1,4648	1,4476
u0 (m/s)	0,09	0,12	0,09	0,07	0,06	0,07	0,10	0,08	0,06	0,06	0,06	0,09	0,07	0,05	0,09	0,08	0,07
ΔP (atm)	0,01	0,02	0,01	0,01	0,01	0,01	0,01	0,01	0,01	0,01	0,01	0,01	0,01	0,01	0,01	0,01	0,01
compression to Pads																	
Vb+Vdep (lb/h)	2970,5	4464,9	3190,2	2353,3	2053,7	2476,9	3698,7	2744,4	2117,9	1884,2	2152,9	3194,0	2450,5	1753,1	3185,9	2855,9	2345,9
γ	1,312	1,312	1,312	1,312	1,311	1,312	1,312	1,312	1,312	1,311	1,312	1,312	1,312	1,311	1,312	1,312	1,312
MW (Vb) (lb/lb-mol)	29,2	57,2	85,2	113,2	141,2	169,2	197,2	225,2	253,2	281,2	309,2	337,2	365,2	393,2	421,2	449,2	477,2
MW (Vreg) (lb/lb-mol)	33,2	19,3	-18,3	-114,0	-246,8	-186,7	-93,5	-220,7	-512,2	-802,5	-615,9	-275,2	-540,7	-1909,8	-352,2	-493,0	-876,3
MW (Vb+Vreg x r) (lb/lb-mol)	31,2	32,8	31,9	30,9	30,2	31,2	33,2	32,0	31,0	29,8	31,0	33,1	31,9	30,4	32,7	32,8	32,4
T1 (°C)	20	21	22	23	24	25	26	27	28	29	30	31	32	33	34	35	36
T2 (°C)	171,4	172,9	174,4	175,9	177,4	137,4	138,8	140,2	141,6	185,0	116,7	118,0	119,3	84,4	192,6	151,2	88,0
w (Btu/lb) isentrop	73,1	69,6	71,9	74,4	76,4	54,1	51,1	53,2	55,2	78,8	42,1	39,5	41,2	25,4	73,1	53,3	24,1
power required (kWe, η=0.75)	84,8	121,3	89,6	68,4	61,3	52,4	73,8	56,9	45,6	57,9	35,4	49,3	39,4	17,4	90,9	59,4	22,1
thermal recovery (kW)	57,0	81,5	60,2	45,9	41,2	35,2	49,6	38,3	30,7	38,9	23,8	33,1	26,5	11,7	61,1	39,9	14,8
compression to win pressure drops																	
T1 (°C)	20	21	22	23	24	25	26	27	28	29	30	31	32	33	34	35	36
T2 (°C)	20,7	22,2	22,8	23,6	24,5	25,6	26,9	27,7	28,5	29,4	30,5	31,8	32,6	33,4	34,8	35,7	36,6
w (Btu/lb) isentrop	0,3	0,5	0,4	0,3	0,2	0,3	0,4	0,3	0,2	0,2	0,2	0,4	0,3	0,2	0,4	0,3	0,3
power required (kWe, η=0.75)	0,4	0,9	0,5	0,2	0,2	0,3	0,6	0,3	0,2	0,2	0,2	0,4	0,3	0,1	0,5	0,4	0,2
thermal recovery (kW)	0,3	0,6	0,3	0,2	0,1	0,2	0,4	0,2	0,1	0,1	0,1	0,3	0,2	0,1	0,3	0,2	0,2
vacuum pumping																	
Vacuum desorption (mol/h) 1 atm -> Pdes	7553,7	11765,1	11588,2	11248,2	9609,6	7541,3	11726,9	11572,0	11248,2	8698,9	7572,4	11731,7	11588,3	11284,8	15928,3	15911,3	15949,1
Vdes (m3/h) 1 atm -> Pdes	169,3	263,7	259,7	252,1	215,4	169,0	262,8	259,4	252,1	195,0	169,7	263,0	259,7	252,9	357,0	356,6	357,5
power required (kWe)	6,3	9,8	9,6	9,3	8,0	6,3	9,7	9,6	9,3	7,2	6,3	9,7	9,6	9,4	13,2	13,2	13,2
grid compression																	
Va (mol/h)	9641,0	10254,6	10431,6	10771,6	10423,6	9663,9	10292,8	10447,8	10771,5	10126,6	9606,9	10288,0	10431,5	10734,9	11168,3	11176,0	11158,9
Va (lb/h)	340,1	994,7	1655,8	2374,7	2941,5	3323,6	4175,3	4883,1	5699,3	5983,2	6269,2	7348,8	8095,1	8993,3	10045,8	10742,6	11415,0
γ	1,311	1,313	1,308	1,310	1,310	1,310	1,310	1,310	1,310	1,310	1,310	1,310	1,310	1,310	1,310	1,310	1,310
MW (Va) (lb/lb-mol)	16,0	44,0	72,0	100,0	128,0	156,0	184,0	212,0	240,0	268,0	296,0	324,0	352,0	380,0	408,0	436,0	464,0
T1 (°C)	50	51	52	53	54	55	56	57	58	59	60	61	62	63	64	65	66
T2 (°C)	36,3	37,2	38,3	39,2	40,2	72,8	73,9	74,9	76,0	45,0	102,8	104,0	105,1	144,4	49,8	83,3	148,2
w (Btu/lb) isentrop	0,0	0,0	0,0	0,0	0,0	1,7	1,5	1,3	1,1	0,0	2,2	2,0	1,8	3,2	0,0	0,6	2,7
power required (kWe, η=0.75)	0,0	0,0	0,0	0,0	0,0	2,2	2,4	2,4	2,5	0,0	5,3	5,7	5,8	11,4	0,0	2,7	11,9
thermal recovery (kW)	0,0	0,0	0,0	0,0	0,0	1,5	1,6	1,6	1,7	0,0	3,6	3,8	3,9	7,6	0,0	1,8	8,0
specific consumptions (kWhe/m3 raw biogas)	0,19	0,27	0,20	0,16	0,14	0,12	0,18	0,14	0,12	0,13	0,10	0,13	0,11	0,08	0,21	0,15	0,10
net thermal recovery (kW)	45,96	66,05	48,67	37,09	33,26	27,48	38,42	29,98	24,39	31,55	19,27	25,86	21,47	12,58	49,84	31,64	14,41

Table 3.38: total energy consumption for the "desorption recirculation" regeneration technique

T (K)	323	323	323	323	323	323	323	323	323	323	323	323	323	323	323	323
Pdes (atm)	0,5	0,5	0,5	0,5	0,5	0,5	0,3	0,3	0,3	0,3	0,1	0,1	0,1	0,1	0,1	0,1
Pads (atm)	6	6	2	6	4	3	4	10	3	3	5	2	1,5	1,5	1,5	1,5
Qz (kg)	5000	5000	5000	5000	5000	5000	5000	5000	5000	5000	5000	5000	5000	5000	5000	5000
recirculation rate (r)	0,5	0,8	0,8	0,9	0,9	0,9	0,9	0,9	0,9	0,95	0,95	0,95	0,95	0,95	0,8	0,9
y	0,56	0,67	0,75	0,74	0,79	0,82	0,84	0,82	0,70	0,90	0,92	0,90	0,93	0,93	0,79	0,88
tsat,CO2 (h)	0,441	0,176	0,098	0,088	0,074	0,064	0,082	0,092	0,124	0,041	0,060	0,069	0,053	0,048	0,192	0,096
Vreg (mol/h)	29335,1	68423,8	58320,5	130357,5	120365,1	115926,7	112957,4	116287,8	140522,7	218510,4	213897,7	219783,4	211574,0	210508,7	54478,8	106687,0
Vreg x r (mol/h)	14667,5	54739,1	46656,4	117321,8	108328,6	104334,1	101661,7	104659,0	126470,4	207584,9	203202,8	208794,2	200995,7	199983,3	43583,0	96018,3
Vb+Vreg x r (mol/h)	36687,3	76758,8	68676,1	139341,5	130348,3	126353,8	123681,4	126678,7	148490,1	229604,6	225222,5	230814,0	223015,4	222003,0	65602,8	118038,0
Va (mol/h)	7351,8	8345,9	10354,5	9015,6	9979,3	10423,3	10721,3	10387,1	7962,5	11091,0	11330,7	11033,5	11468,1	11506,3	11175,3	11348,0
CH4 loss (mol/h)	4318,7	3324,6	1316,0	2654,8	1691,1	1247,1	949,1	1283,3	3708,0	579,4	339,7	636,9	202,4	164,2	495,1	322,5
CH4 loss (%)	37,0%	28,5%	11,3%	22,7%	14,5%	10,7%	8,1%	11,0%	31,8%	5,0%	2,9%	5,5%	1,7%	1,4%	4,2%	2,8%
column pressure drop (ERGUN)																
column porosity	0,4	0,4	0,4	0,4	0,4	0,4	0,4	0,4	0,4	0,4	0,4	0,4	0,4	0,4	0,4	0,4
tower diam (m)	2	2	2	2	2	2	2	2	2	2	2	2	2	2	2	2
column lenght LT (m)	2,35	2,35	2,35	2,35	2,35	2,35	2,35	2,35	2,35	2,35	2,35	2,35	2,35	2,35	2,35	2,35
dp (m)	1,6E-03	1,6E-03	1,6E-03	1,6E-03	1,6E-03	1,6E-03	1,6E-03	1,6E-03	1,6E-03	1,6E-03	1,6E-03	1,6E-03	1,6E-03	1,6E-03	1,6E-03	1,6E-03
µg (kg/m/s)	1,22E-05	1,26E-05	1,29E-05	1,28E-05	1,30E-05	1,31E-05	1,32E-05	1,31E-05	1,27E-05	1,34E-05	1,34E-05	1,34E-05	1,35E-05	1,35E-05	1,30E-05	1,33E-05
ρg (kg/m3)	1,4	1,6	1,7	1,6	1,7	1,7	1,8	1,7	1,6	1,8	1,9	1,8	1,9	1,9	1,7	1,8
u0 (m/s)	0,07	0,15	0,14	0,28	0,26	0,25	0,25	0,25	0,29	0,46	0,45	0,46	0,44	0,44	0,13	0,23
ΔP (atm)	0,01	0,02	0,02	0,06	0,05	0,05	0,05	0,05	0,06	0,14	0,13	0,14	0,13	0,13	0,02	0,05
compression to Pads																
Vb+Vreg x r (lb/h)	2571,9	5901,2	5616,9	11301,8	10986,7	10845,8	10751,5	10857,3	11626,7	20876,5	20721,3	20918,7	20642,2	20607,4	5505,2	10552,5
γ	1,312	1,312	1,312	1,312	1,312	1,312	1,312	1,312	1,312	1,312	1,312	1,312	1,312	1,312	1,312	1,312
MW (Vb) (lb/lb-mol)	29,2	29,2	29,2	29,2	29,2	29,2	29,2	29,2	29,2	29,2	29,2	29,2	29,2	29,2	29,2	29,2
MW (Vreg) (lb/lb-mol)	35,8	37,2	40,8	38,2	40,1	41,0	41,7	40,9	36,6	42,5	43,1	42,4	43,4	43,5	42,6	43,2
MW (Vb+Vreg x r) (lb/lb-mol)	31,8	34,9	37,1	36,8	38,2	38,9	39,4	38,9	35,5	41,2	41,7	41,1	42,0	42,1	38,1	40,6
T1 (°C)	20	20	20	20	20	20	20	20	20	20	20	20	20	20	20	20
T2 (°C)	171,4	171,4	69,3	171,5	130,7	104,0	104,0	130,7	228,8	104,0	104,0	152,8	69,4	46,7	46,7	46,7
w (Btu/lb) isentrop	71,6	65,3	20,0	61,9	43,5	32,4	32,0	42,8	88,4	30,6	30,3	48,5	17,7	9,5	10,5	9,9
power required (kWe, η=0.75)	71,9	150,5	43,8	273,2	186,7	137,3	134,4	181,4	401,5	249,5	244,7	396,3	142,3	76,6	22,6	40,7
thermal recovery (kW)	48,3	101,2	29,5	183,7	125,6	92,4	90,4	122,1	269,9	167,9	164,8	266,7	95,8	51,6	15,2	27,4
compression to win pressure drops																
T1 (°C)	20	20	20	20	20	20	20	20	20	20	20	20	20	20	20	20
T2 (°C)	20,6	21,6	21,4	23,9	23,6	23,5	23,4	23,5	24,2	29,1	28,9	29,2	28,8	28,8	21,4	23,2
w (Btu/lb) isentrop	0,3	0,7	0,6	1,6	1,4	1,3	1,3	1,4	1,8	3,3	3,2	3,3	3,2	3,1	0,5	1,2
power required (kWe, η=0.75)	0,3	1,6	1,3	7,0	6,1	5,7	5,5	5,7	8,0	27,0	25,9	27,3	25,4	25,2	1,2	4,9
thermal recovery (kW)	0,2	1,1	0,9	4,7	4,1	3,8	3,7	3,9	5,4	18,2	17,5	18,4	17,1	16,9	0,8	3,3
vacuum pumping																
Vacuum desorption (mol/h) 1 atm -> Pdes	6638,3	16020,7	28092,0	31282,2	36990,5	42581,1	56619,7	50605,6	38581,6	111277,5	142202,1	124181,6	160841,8	178053,0	45429,5	90086,6
Vdes (m3/h) 1 atm -> Pdes	148,8	359,1	629,7	701,2	829,1	954,4	1269,1	1134,3	864,8	2494,2	3187,3	2783,4	3605,1	3990,9	1018,3	2019,2
power required (kWe)	5,5	13,3	23,3	26,0	30,7	35,3	47,0	42,0	32,0	92,4	118,0	103,1	133,5	147,8	37,7	74,8
grid compression																
Va (mol/h)	7351,8	8345,9	10354,5	9015,6	9979,3	10423,3	10721,3	10387,1	7962,5	11091,0	11330,7	11033,5	11468,1	11506,3	11175,3	11348,0
Va (lb/h)	259,3	294,4	365,2	318,0	352,0	367,7	378,2	366,4	280,9	391,2	399,7	389,2	404,5	405,9	394,2	400,3
γ	1,311	1,311	1,311	1,311	1,311	1,311	1,311	1,311	1,311	1,311	1,311	1,311	1,311	1,311	1,311	1,311
MW (Va) (lb/lb-mol)	16,0	16,0	16,0	16,0	16,0	16,0	16,0	16,0	16,0	16,0	16,0	16,0	16,0	16,0	16,0	16,0
T1 (°C)	50	50	50	50	50	50	50	50	50	50	50	50	50	50	50	50
T2 (°C)	50,0	50,0	128,5	50,0	67,6	91,6	91,6	67,6	50,0	91,6	91,6	50,0	128,5	156,9	156,9	156,9
w (Btu/lb) isentrop	0,0	0,0	73,9	0,0	16,5	39,2	39,2	16,5	0,0	39,2	39,2	0,0	73,9	100,6	100,6	100,6
power required (kWe, η=0.75)	0,0	0,0	10,5	0,0	2,3	5,6	5,8	2,4	0,0	6,0	6,1	0,0	11,7	15,9	15,5	15,7
thermal recovery (kW)	0,0	0,0	7,1	0,0	1,5	3,8	3,9	1,6	0,0	4,0	4,1	0,0	7,8	10,7	10,4	10,6
specific consumptions (kWhe/m³ raw biogas)	0,16	0,34	0,16	0,62	0,46	0,37	0,39	0,47	0,89	0,76	0,80	1,07	0,63	0,54	0,16	0,28
net thermal recovery (kW)	38,95	82,21	19,47	152,06	97,15	66,99	65,68	94,41	236,55	130,20	127,53	224,87	62,52	21,26	9,27	10,48

4 New developments in upgrading technology

Chapter 3 reported a detailed analysis about the possible optimization of the upgrading techniques that have been considered the most used, proven, suitable and technically advantageous.
Nevertheless, it's worth mentioning that we are observing strong improvements regarding other technologies that have been excluded by the previous analyses because of the large methane losses and/or energy costs, namely membrane processes and cryogenic separation.

As far as membrane processes are concerned, dry membranes for biogas upgrading are made of materials that are permeable to carbon dioxide, water and ammonia. Hydrogen sulphide and oxygen permeate through the membrane to some extent while nitrogen and methane only pass to a very low extent (see Figure 4.1). The process is often performed in two stages. Before the gas enters the hollow fibres it passes through a filter that retains water and oil droplets and aerosols, which would otherwise negatively affect the membrane performance. Additionally, hydrogen sulphide is usually removed by cleaning with activated carbon before the membrane. Membrane separation is one of the classical methods for landfill gas upgrading. As already mentioned, the early designs operating at elevated pressures (up to 30 bars) suffered from considerable methane losses (up to 25%). Newer designs operate around 8 bars with far lower methane losses (Petersson and Wellinger, 2009).
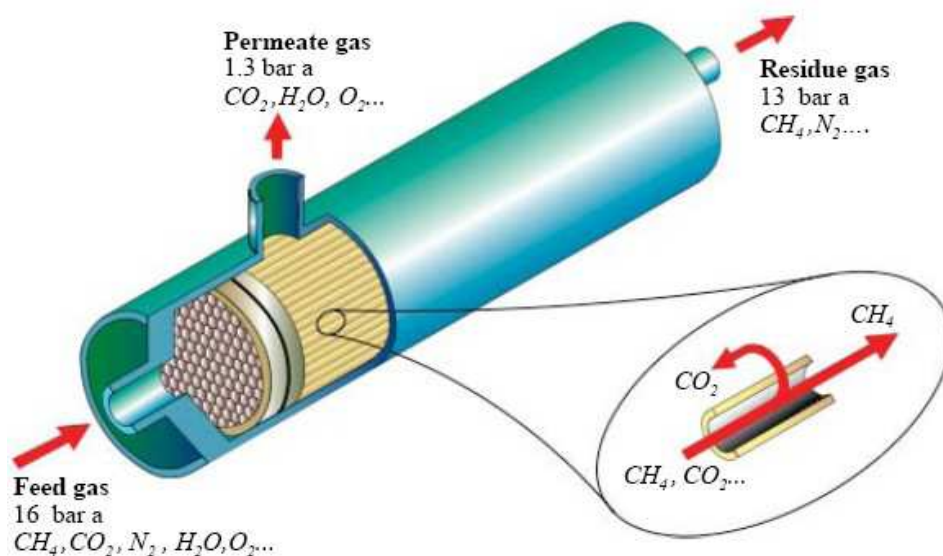
Figure 4.1: membrane technique (BioMil AB)

According to the experience done by the Institute of Chemical Engineering of the Technical University of Vienna in Bruck/Leitha (AT), the use of dense polyimide membranes to separate methane and carbon dioxide brings about many advantages, such as continuity, compactness, simultaneous drying and removal of traces of hydrogen sulphide and ammonia (Miltner et al., 2008).
Figure 4.2 reports the details of the different gas separation between permeate and retentate phase; as one can easily observe, besides the simultaneous removal of water, ammonia and hydrogen sulphide, this specific membrane techniques allow the separation of oxygen from biomethane in order to comply with the legislation restrictions for natural gas: as a matter of fact, the upgrading system is preceded by a desulphurisation plant that introduces pure oxygen to treat H_2S biologically, the reported upgrading technique can reduce final oxygen concentration to less than 0.2%.
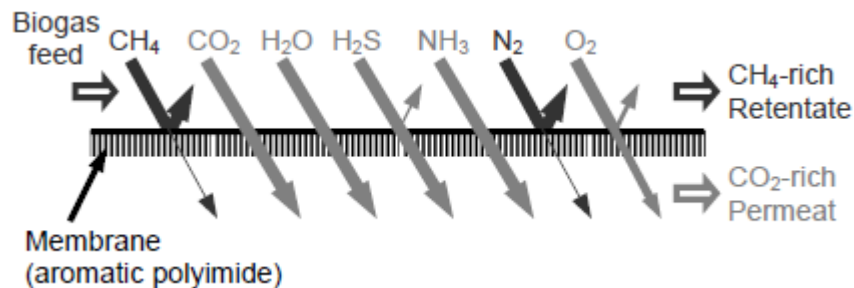
Figure 4.2: principle of gas separation using the membrane technique (Miltner et al., 2008)

In order to minimize methane losses, the studied plant has been equipped with two stages of membrane modules: the permeate stream from the second stage, which contains significantly higher amounts of methane compared to the permeate of the first stage, is brought back for recompression, similarly to the recirculations calculated in the previous chapter for the same reasons. This way, methane losses are claimed to be usually from 2 to 3 % of the produced biomethane, whereas BioMil AB reports for the same plant that methane losses are lower than 5%. In order to reduce environmental impacts dealing with CH_4 slip, the CO_2-rich offgas is delivered back to an existing biogas engine to be completely oxidized.

The energy consumptions reported for the described membrane separation techniques come out to be around 0.19 kWh_e/m^3 of raw biogas that is a pretty good result if compared to competing technologies.

On the other hand, Deng and Hägg (2010) report that the biogas upgrading by membrane separation process using a polyvinylamine/polyvinylalcohol (PVAm/PVA) blend membrane could be a very effective technical choice: the methane recovery rate is higher than 95% (CH_4 losses lower than 5%) even when operative conditions are strongly different from design ones (see Figure 4.3).
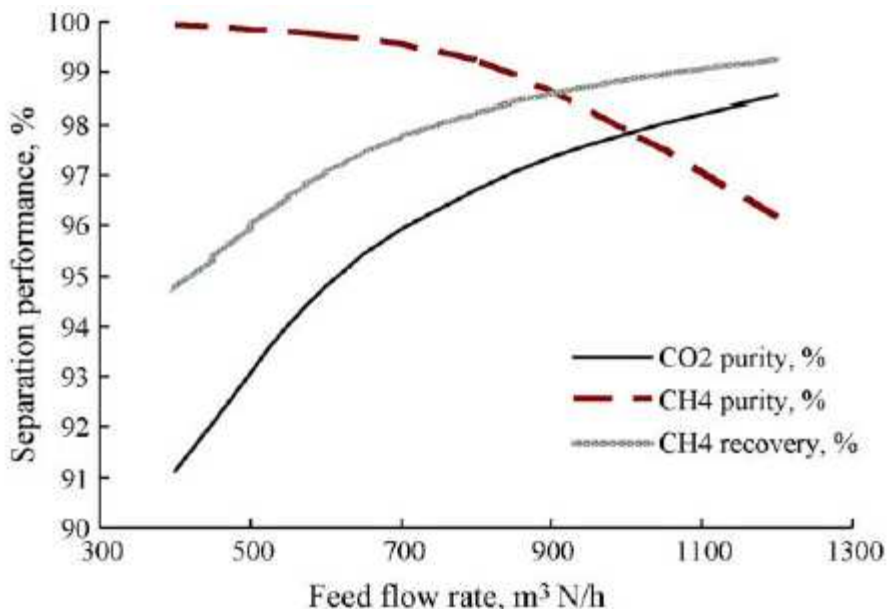
Figure 4.3: Influence of feed flow rate on separation performance for a PVAm/PVA membrane

On the basis of the reported data, it can be concluded that membrane separation can be considered a feasible and absolutely interesting option to upgrade biogas; as already widely described, the challenge is to

understand how much does it cost to further reduce methane losses in order to reach technological performances comparable to those relating to chemical and physical absorption.

As far as cryogenic separation is concerned, the principle makes use of the distinct boiling/sublimation points of the different gases particularly for the separation of carbon dioxide and methane. The raw biogas is cooled down to the temperatures where the carbon dioxide in the gas condenses or desublimates and can be separated as a liquid or a solid fraction, while methane accumulates in the gas phase. Water and siloxanes are also removed during cooling of the gas. The desublimation point of pure carbon dioxide is 194.65 K (-78.5 °C) at atmospheric pressure (see Figure 4.4), while methane condenses at -161 °C .
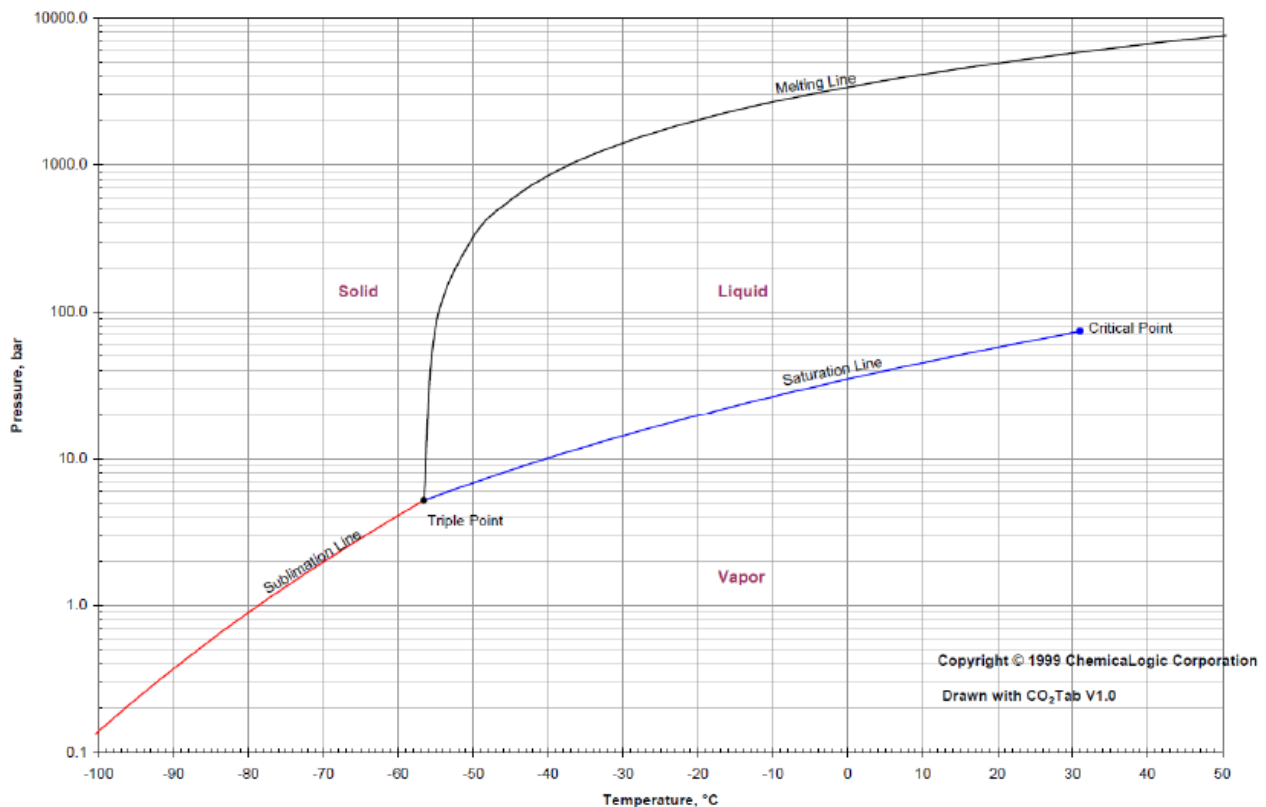
Figure 4.4: phase diagram for CO_2 (Jonsson and Westman, 2011)

However, the content of methane in the biogas affects the characteristics of the gas, i.e. higher pressures and/or lower temperatures are needed to condense or desublimate carbon dioxide when it is in a mixture with methane. Figure 4.5 shows the vapour pressure of CO_2 at lower pressures. When the CO_2 in the biogas is desublimated, it follows that the partial pressure of CO_2 is reduced, then a lower temperature is required in order to further desublimate the CO_2.

Cryogenic separation produces CH_4 at much lower temperatures than other upgrading technologies. The separation can be run at high pressures in order to increase efficiency and to increase the pressure of the output CH_4. Since final CH_4 is cold and at an elevated pressure, the additional energy required for liquefaction is lower than for other technologies. This is one of the main advantages of cryogenic separation, particularly interesting when a capillary natural gas distribution network is not at disposal, such as in Scandinavian countries.

As far as technical performances are concerned, Benjaminsson (2006) reports that, according to the process proposed by Gastreatment Power Package (Gastreatment Services GPP® technique), condensation occurs in two steps where the first condensation takes place at -56°C and 10.2 bar, then, the remaining carbon condenses and desublimates at -85 °C and 10 bar with a drop in temperature caused by cooling. The biogas

is purified to a quality equivalent to Swedish standard and the outgoing gas can be supplied with a pressure of 8 bar.

Gastreatment Services has indicated energy costs around 0.42 kWh_e/Nm^3 of upgraded biomethane; an electricity demand 0.63 kWh_e/Nm^3 of upgraded biomethane was also calculated using a one stage propane heat pump cycle operating between -100 °C and 40 °C (Jonsson and Westman, 2011).

Finally, Gastreatment Services assures that methane losses are below 2% and they are due to a certain percentage of methane triggered in liquefied carbon dioxide: as a matter of fact methane is soluble in liquefied CO_2 and the first upgrading step for the GPP® technique is condensation and than solidification, and not directly desublimation.
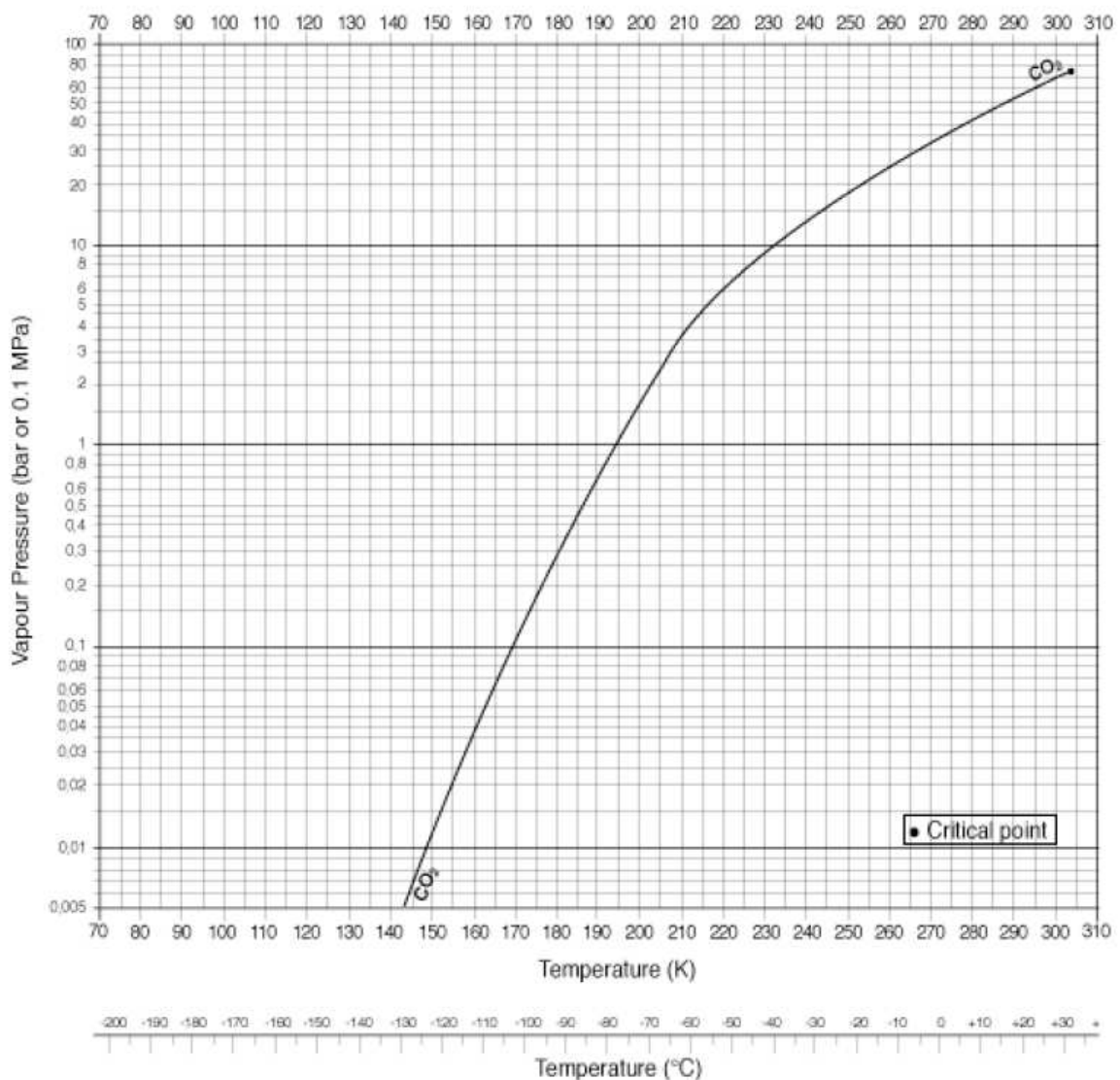
Figure 4.5: vapor pressure diagram for CO_2 (Jonsson and Westman, 2011)

Another source (Johansson, 2008) reports that cryogenic technologies suppliers claim that methane losses are virtually zero, since all vented CH_4 is collected and treated. However, no methane losses is not realistic, a more convenient expression could be "very low". The same source reports some very interesting data, both for energy consumption and methane losses, resumed by Figure 4.6, where the electricity consumed to

upgrade biogas lies in the range 0.80÷1.54 kWh$_e$/Nm^3 of upgraded biomethane (corresponding to 0.42÷0.82 kWh$_e$/Nm^3 of raw biogas when biogas contains 53% of methane), a considerable energy input if compared to traditional technologies.

Table 7 Information regarding different CH_4 and CO_2 parameters for the three cryogenic upgrading technologies (for original data, see Appendix 3, Table A3 4).

Company:	CH$_4$ content in LBG (%):	CH$_4$ recovery (%):	CH$_4$ loss (%):	CO$_2$ recovery (%):	LCO$_2$ purity (%):
Scandinavian GtS	99	>99	0.5	~100	"food grade"
Acrion	99.2[*]	>99	"None"	30 – 50[**]	99.99
Prometheus-Energy	>97	Not available	"None"	-	-

[*] CH$_4$ content in the gas produced during the pilot project at Burlington County Landfill
[**] Depends on economics; if the product can be sold or not.

Table 8 Electricity demand for production of LBG from raw gas. The specified scales for the technology from Acrion and Prometheus-Energy are the scales on actual available designs (for original and conversion data, see Appendix 3, Table A3 2 and Table A3 5).

Company:	Electricity: (kWh/Nm^3 clean gas)	Drive:	Scales: (Nm^3 raw gas /h)
Scandinavian GtS	0.8	Electricity	50 – 2400
Acrion	1.42[*]	Electricity	230, 465, 930
Prometheus-Energy[**]	1.54	LFG fired gas engine	90 – 930

[*] Mean value from two different sources.
[**] Based on actual numbers for the LBG production plant at Bowerman landfill (for calculations, see Appendix 3).

Figure 4.6: information about technical performances for three different cryogenic technologies (Johansson, 2008)

On the basis of the reported data, it could be concluded that emerging upgrading technologies are very interesting and promising. However, membrane separation could be characterized by low energy requirements but the further minimization of methane losses should be properly analysed whereas cryogenic technologies seems to involve very low methane losses but electricity consumptions are still much higher than traditional upgrading processes, even for their "low CH$_4$ slip" configurations.

5 Post-methanation recovery and ammonia removal

Besides the strong environmental impact that a massive introduction of biogas engines could bring about in very delicate areas as far as air quality is concerned, it should be remembered that intensive farming activities such those of Northern Italy involve evident damages to the atmospheric and groundwater compartment, mainly due to nitrogen management.

As a matter of fact, the use of animal manure as a fertilizer isn't much effective due to the chemical form of nitrogen compounds and the operative aspects of land spreading; it can be calculated that in large part of the Po valley, just around half of land spread nitrogen become vegetal protein, the remaining part being lost towards atmosphere (as ammonia) and aquifers (nitrate contamination of surface and ground-water resources). Figure 5.1 reports an example of nitrogen balance for the Province of Cuneo, N-W Italy, referred to the year 2007 (Brizio, 2011), where one can easily observe that more than 50% of nitrogen at disposal is wasted and causes a significant environmental damage.

volatilized N
13,857 t/y

excreted N
37,360 t/y

N to the field
34,965 t/y

useful N
19,000 t/y

fertilizer N
7,988 t/y

leached N
12,491 t/y
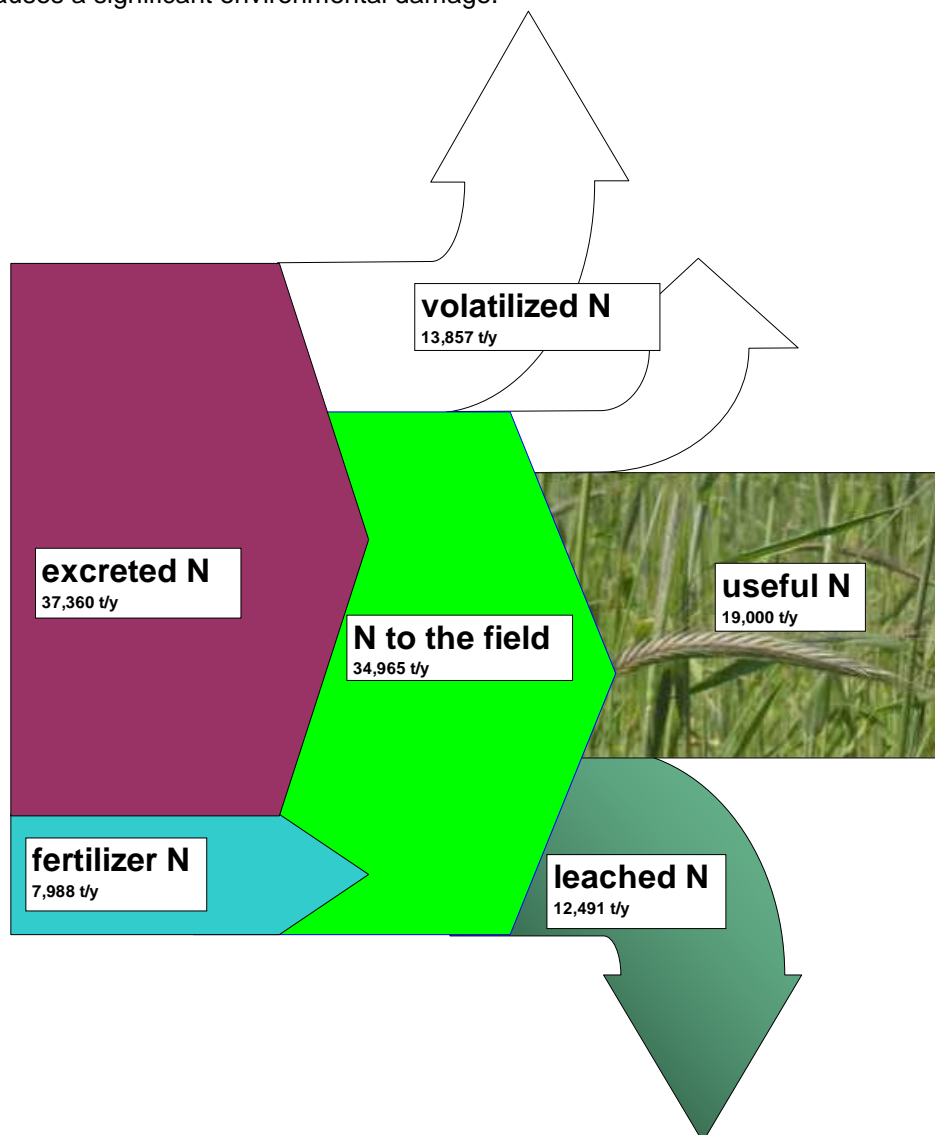
Figure 5.1: example of nitrogen balance for the Province of Cuneo

The atmospheric impact due to intensive farming is well pointed out by the satellite image showed by Figure 5.2 regarding ammonia air concentration, considerably higher in Northern Italy if compared to the rest of Europe.
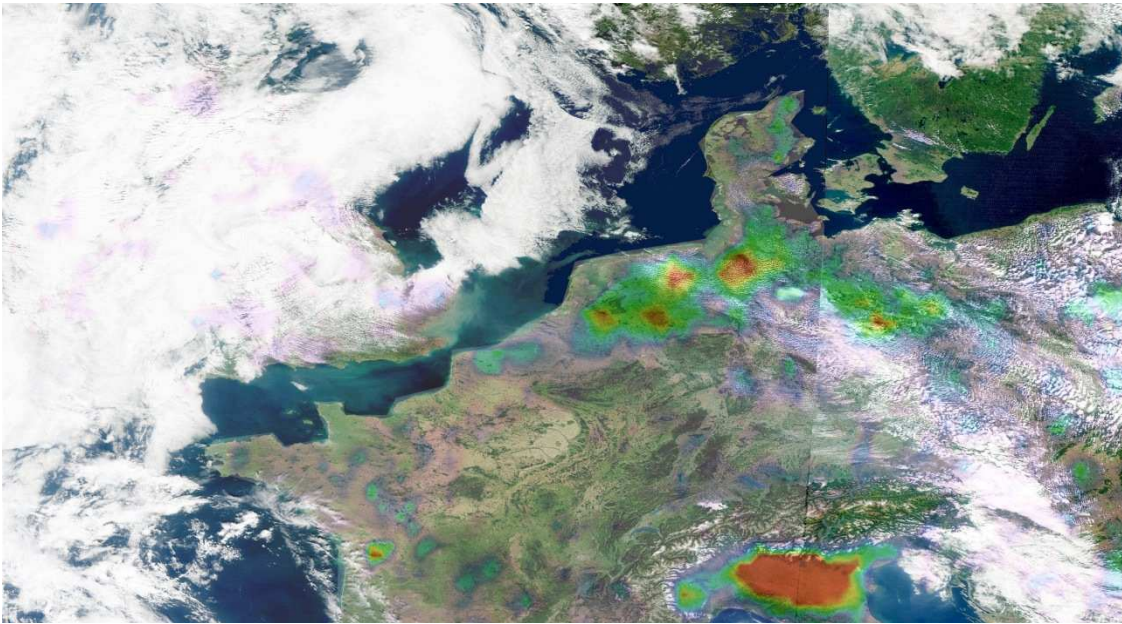
Figure 5.2: ammonia atmospheric concentration from the satellite (ESA MetOP, Infrared Atmospheric Sounding Interferometer, 2008)

As already described, anaerobic digestion of manure and energy crops could even worsen the described environmental contamination conditions as ammonia volatilization potential from digested materials is larger than that from fresh manure and nitrogen to be managed after digestion can be much higher than traditional manure management due to the strong use of energy crops to enhance methane production. Moreover, interesting amount of residual biogas could be produced during the storage of digested materials, making the overall GHG balance of anaerobic digestion at least uncertain.

Since the possible drawbacks of anaerobic digestion could be many, the following chapter analyses a possible treatment of digested materials based on the use of produced biogas to strip ammonia from the storage (see Figure 5.3) and produce a fertilizer (ammonium sulphate).
The study analyses the technical feasibility of the stripping-absorbing treatment, reports the removal efficiency according to different pH and T conditions, works out the energy balance (electric and thermal) of the described treatment; the study has been already presented at the 7th European Congress of Chemical Engineers ECCE-7 held in Prague (28 august- 1 September 2010).

5.1   Biogas production during digested materials storage

In the present paper we took into account a mesophilic (42 °C) digestion plant fed by 41 t/d of cattle slurry and 40 t/d of maize (109 m^3/d of fresh matter), with a hydraulic retention time around 60 days, producing 11845 Nm^3/d of biogas (53% formed by methane). The reported data are the same than those considered for biogas upgrading assessment. The energy recoverable by a Otto engine would be around 1 MW_e and more or less the same amount as far as the thermal energy is concerned. The digested materials (around 95

m^3/d), are addressed to a storage tank with a diameter of 26 m and a depth of 5 m (hydraulic retention time around 27 days). If we assume that digestate still contains around 50% of the initial volatile solid content, by this retention time and without any heating of the tank, the post-methanation production is expected at least around 30 l CH$_4$/kg VS (300 Nm^3 of methane per day) that would be dispersed in the case of open storage. These assumptions have been confirmed by some measurements carried out on plants that actually recover residual biogas from the storage tank in the south of Piedmont.

The described methane release represents a loss of profitability of the plant (at least 5% more energy could be produced from the same materials) and a strong environmental impact as methane has a global warming potential of 25 with respect to CO$_2$.

A gas-tight storage tank offers the possibility to recover the post-production of biogas and deliver it to the engine or to the biogas upgrading treatment to produce biomethane; nevertheless, in this case, ammonia contained in biogas could damage the engine and increase NOx emissions or result unacceptable for the upgrading and then it should be washed before any further treatment. At the same time, biogas produced during the post-methanation could be recirculated at the bottom of the storage tank and used as a stripper for ammonia contained in digested materials. The present analysis aims at investigating the feasibility of ammonia desorption according to different pH, temperature and biogas recirculated flows conditions.
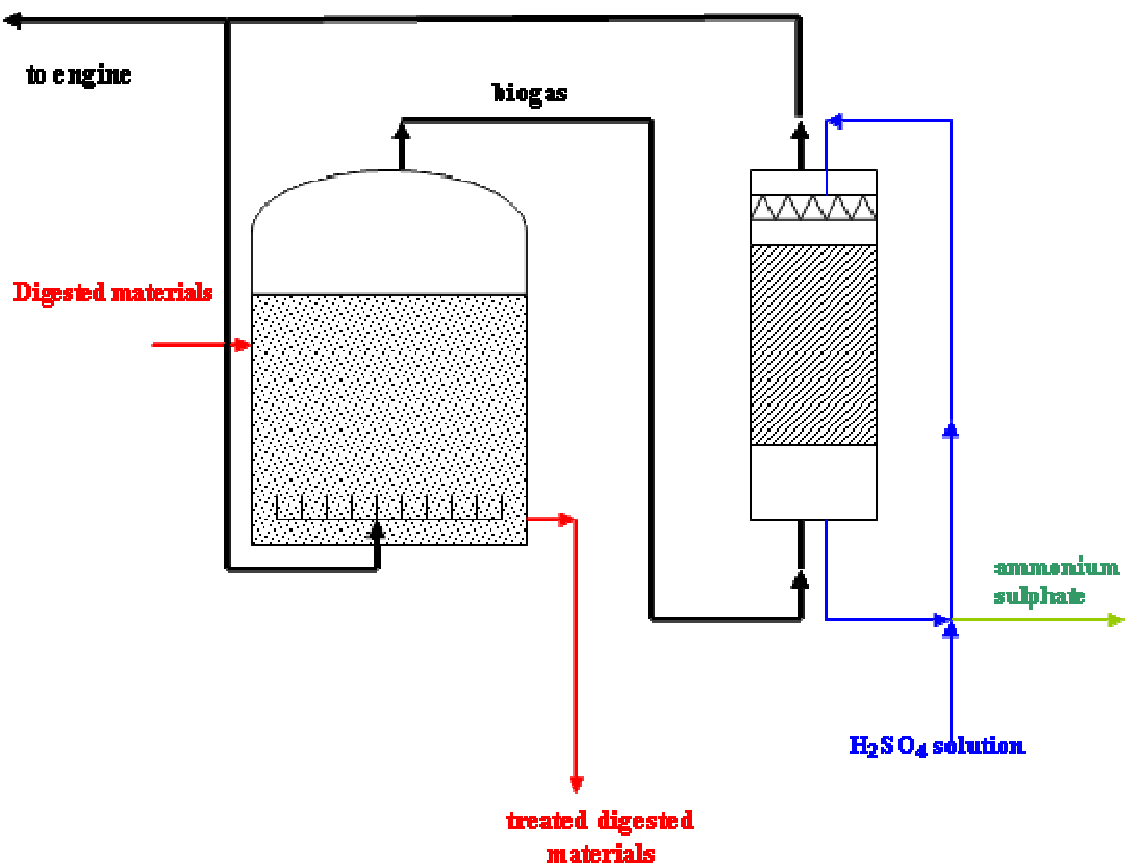
Figure 5.3: physico-chemical treatment of digested materials

5.2 Ammonia removal

Ammonia removal efficiency from manure or digested materials strongly depends on physical conditions of the liquid matter, which is ammonium concentration and the acidic dissociation NH_4^+/NH_3. Within fresh manure, ammonium N (NH_3-N + NH_4^+-N) usually represents 40-60% of total nitrogen, whereas in digested materials the ammonia nitrogen fraction is much higher, around 80% of total N. In the present study we considered a starting concentration of 3000 mg/l of ammonia nitrogen as suggested by several reports. The dissociation constant can be calculated as follows (Olesen et al., 1993):

$$NH_4^+ \leftrightarrow NH_3 + H^+$$

$$K_d = \frac{[NH_3][H^+]}{[NH_4^+]}$$

$$K_d = \exp(-177.95292 - \frac{1843.22}{T} + 31.4335 \cdot \ln T - 0.0544943 \cdot T)$$

Provided that digested materials pH can range from 8 to 8.5, Table 5.1 show the expected NH_3 concentration in the raw materials to be desorbed.

Table 5.1: Dissociation equilibrium for digested materials

N-NH$_4^+$ (mg/l)	3000

T (K)	pH	K$_d$	[NH$_4^+$]/[NH$_3$]	NH$_3$ (mg/l)
293	8	3.91E-10	25.6	137.3
303	8	8.01E-10	12.5	271.2
313	8	1.57E-09	6.4	496.8
323	8	2.93E-09	3.4	835.3
293	8.5	3.91E-10	8.1	403.1
303	8.5	8.01E-10	3.9	744.5
313	8.5	1.57E-09	2.0	1228.7
323	8.5	2.93E-09	1.1	1799.1

The ammonia removal from digested materials could be carried out in a stripping tower which could maximise the mass transfer parameters but this solution is generally not applied in order to reduce investment costs. A possible different option is the dispersion of biogas from the bottom of the storage tank as very small bubbles (2-5 mm), to realize a so called bubble column. In this case, using the two-resistance theory, the mass transfer flux N (kg/m^2/s) across the interface is given by:

$$N = K \cdot \left(C_L^\infty - \frac{C_G}{H} \right)$$

in which H is the Henry's law constant for the system ammonia-digestate, K is the overall mass transfer coefficient (m/s), C_L^∞ and C_G refers to ammonia concentration in the bulk liquid phase and in the gas phase (kg/m^3). As far as the mass transfer coefficient is concerned we can write another time the general equation:

$$\frac{1}{K} = \frac{1}{k_L} + \frac{1}{H \cdot k_G}$$

Mass transfer within the bubbles is rapid because molecular diffusivities in gases are large and the resistance to mass transfer on the liquid side is predominant, that is $K=k_L$.

Akita and Yoshida (1974) suggest the following equation based on several data for different gas-liquid systems:

$$k_L = 0.25 \cdot \frac{D_L}{R_b} \cdot \left(\frac{v_L}{D_L}\right)^{1/2} \cdot \left(\frac{8gR_b^3}{v_L^2}\right)^{1/4} \cdot \left(\frac{4gR_b^2 \rho_L}{\sigma}\right)^{3/8}$$

where D_L is ammonia diffusivity in manure/digested materials (2×10^{-9} m/s^2 for 298 K), v_L is kinematic viscosity (dynamic viscosity of digested materials is around 0.60 kg/s/m), σ is surface tension (around 7.2×10^{-2} N/m for 298 K), R_b is the bubble radius. The order of magnitude for k_L is around 1×10^{-4} m/s, as reported in literature for this kind of desorption plants.

As far as Henry's law constant for ammonia is concerned, we assumed Van der Molen's (1990) suggested relation:

$$H\left[\frac{atm}{mg/l}\right] = 1.1561 \cdot e^{-4151/T}$$

Several studies showed that H doesn't depend from pressure up to 5 bar.
The material balance of ammonia transfer is then based on the following relation:

$$\frac{d}{dt}(C_G \cdot V_b) - K \cdot A_b \cdot \left(C_L^\infty - \frac{C_G}{H}\right) = 0$$

where V_b and A_b are, respectively, the bubble volume and superficial area and t (s) is time for ascending bubbles.

In the analysed case, ammonia is the only molecule to be transported from a phase to another; CO_2, that represent 30-40% of biogas and that is soluble in manure or digested materials, remains in the bubbles because the liquid phase is saturated.

The bubble volume variation during the ascension could be an important variable for mass transfer as the expansion involves a drop in the partial pressure of solute inside the bubbles, being the stripping process enhanced. In the present paper, provided that the hydrostatic pressure head is relatively small, bubble volume variation may be neglected. As a consequence, the previous differential equation can be easily solved as follows:

$$\frac{C_G(t) - H \cdot C_L^\infty}{C_G(t=0) - H \cdot C_L^\infty} = e^{-\frac{3 \cdot K}{H \cdot R_b} \cdot t}$$

The bubble ascension velocity through the liquid phase can be calculated by the Stoke's relation (taken from Pinheiro, 2001):

$$u = \frac{\rho \cdot g}{18 \cdot \mu} \cdot d^2$$

where μ is the liquid viscosity and d is the bubble diameter. As one can easily understand, ascension velocity tends to increase as the bubble approach the liquid surface. The bubble volume can be calculated as follows:

$$V = n_i \frac{RT}{(P_{in} - p)}$$

where n_i is the number of moles of "inert" gas in the bubble (CO_2 and CH_4), R is the universal gas constant, T is temperature, P_{in} is the pressure inside the bubble and p is the partial pressure of solute in the bubble (always negligible in our analysis). Pressure inside the bubble is:

$$P_{in} = P_{out} + \frac{4\sigma}{d} \cong P_{out} = P^s + \rho g h$$

The contribution of surface tension (σ) is negligible, P^s is pressure above the liquid free surface (around 1 atm), h is the depth of immersion.
If we assume that the initial diameter of bubbles at the bottom of the pool is 5 mm, and the maximum depth of the tank is 5 m, the diameter would change from 5 to 5.7 mm when approaching the surface and the ascension velocity would be 2.3-3 cm/s. In the present study we considered the average values for bubble volume and diameter during the rise.

Based on the described approach and formulas, it is important to observe that, within temperature and bubble dimension ranges assumed in the present study, the gas contained in the bubble is almost instantaneously saturated with ammonia. As a consequence, bubble dimensions and the tank depth don't influence the mass transfer of ammonia and they can be managed in order to minimize the investments and operational costs of the treatment plant. Ammonia removal efficiency is then governed by thermodynamics, in particular by pH, temperature and biogas flow injected at the spargers.
The storage tank can now be considered as an ideal reactor and the biogas injected at the bottom provide the tank with a strong mixing that aims at homogenizing ammonia concentrations. Hence, the tank can be seen as a CSTR (continuously stirred tank reactor) and the ammonia concentration inside the reactor is the same as the output one. Figure 5.4 shows the mass balance of the reactor that can be written as:

$$Q \cdot \left(C_L{}^{IN} - C_L{}^{OUT} \right) = F \cdot \left(C_G{}^{OUT} - C_G{}^{IN} \right) = F \cdot \left(H \cdot C_L{}^{OUT} - C_G{}^{IN} \right)$$

where $C_L{}^{IN}$ is the ammonia concentration of the input materials (deriving from the equilibrium with ammonium), $C_L{}^{OUT}$ is the same as $C_L{}^{\infty}$ of the previous formulas (it represents the unknown of the expression), $C_G{}^{IN}$ is the ammonia concentration in the injected biogas (always very low, around 10 ppm) and $C_G{}^{OUT}$ is the ammonia concentration in the bubble at the free surface of the liquid phase (that is $C_G(t)$ with t= h/u), Q is digested material flow and F is biogas flow injected at the bottom. $C_G{}^{OUT}$ corresponds to the equilibrium concentration given by the Henry's law.
The mass balance has also to comply with the dissociation equilibrium as the desorbed ammonia tends to be replaced by ammonium according to $NH_4^+ \leftrightarrow NH_3 + H^+$. For the described equilibrium, also the pH should change along the dissociation reaction but we assumed that it could be considered constant due to the action of carbonates (buffer solution) or, at worst, some basic agent added in order to assure a low acidity and support the ammonia stripping. The solution of both the conditions (mass balance and dissociation equilibrium) requires an iterative process as far as convergence is reached.
As far as biogas flow is concerned, both ammonia removal efficiency and operating costs are strongly dependent by this parameter that should be chosen carefully. In our paper F ranges from 50 000 to 120 000 m^3/d of injected biogas, corresponding to a gas holdup of 4 and 10%, respectively.
In relation to the power input in the reactor, in the case of static spargers, the energy transferred is the kinetic energy of the gas flow and the compression energy to overcome the pressure drop. Hence, the power input (kW_e) by the gas flow is given by Deckwer (1985):

$$P_G = F \cdot \rho_G \cdot \left[RT \cdot \ln(1+\alpha) + u_{G0}^2 / 2 \right]$$

$$\alpha = \frac{\rho_L \cdot (1-\varepsilon_G) \cdot g \cdot h}{P^s}$$

where F is the gas flow, ρ_G the gas density (1.3 kg/m^3), α is the ratio of maximum hydrostatic head to the pressure above the liquid free surface, ε_G is the gas holdup, u_{G0} is the gas velocity at the sparger holes (3÷300 m/s). The energy to overcome the hydrostatic head (h=5 m) is much more intensive than the sparger pressure drop that can be therefore neglected.

Table 5.2 shows expected ammonia removal efficiencies and many operative parameters (diffusivity, Henry's constant, dissociation constant) depending on T, pH and biogas flows. As one can easily notice, when temperature is above 40 °C or pH is maintained around 8.5, ammonia is removed for at least 15%. The efficiency can reach 30-50% when T is 50°C and the gas flow around 120 000 m^3/d.
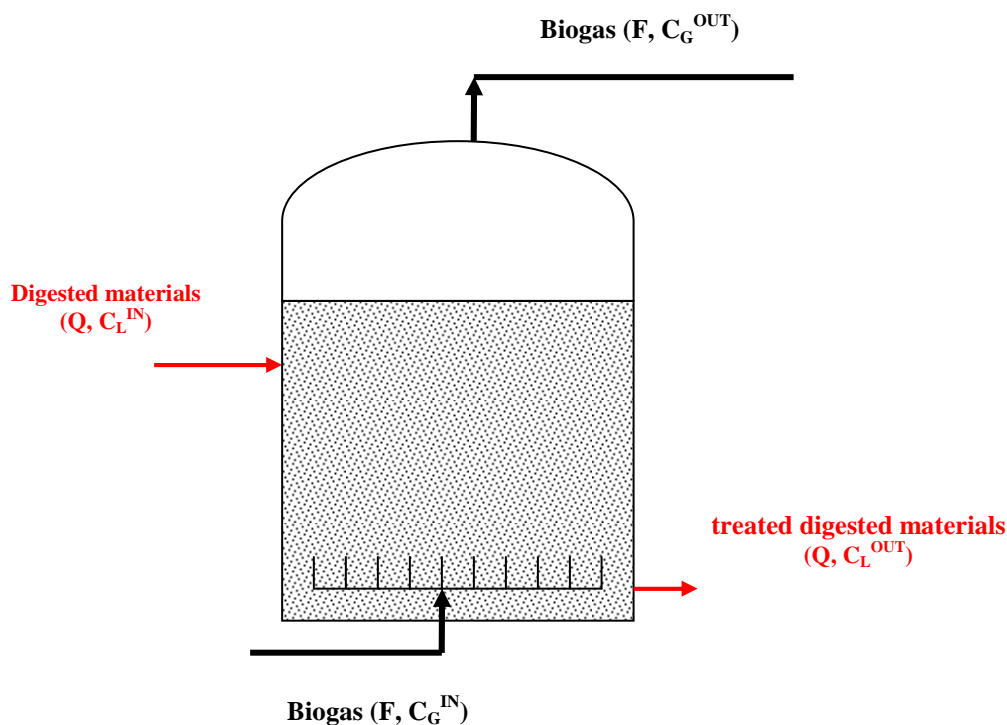
Figure 5.4: mass balance for ammonia stripping within the digestate storage tank

The described treatment could be very effective in order to minimize greenhouse gases emissions (the recovery of post-methane assumed by the present analysis could correspond to 235 g CO_{2eq}/kWh$_e$, around 50 g CO_{2eq}/kWh$_e$ per each percent of methane released into atmosphere) and reduce the environmental burden of ammonia on ground waters and air quality.

Nonetheless, ammonia stripping and post-methanation recovery can be economically sustainable as well: as already commented, biogas produced during the storage of digested materials under ambient temperature of temperate climates could be around 5 % of that produced by anaerobic digesters, more or less 300 m^3/d of methane for the analysed case. The residual biogas production therefore corresponds to 48 kW$_e$ and around 50 kW of thermal power in the case biogas is burned by internal combustion engines on site; in the case

biogas is delivered to a cleaning/upgrading device, biomethane flow rate could be increased by almost 5% (methane losses should be taken into account for the residual biogas fraction too) that is a very important amount, in many cases larger than CH_4 losses during upgrading process.

Table 5.2: Ammonia removal efficiency according to different conditions of T, pH and injected gas flows

T (K)	303	313	323	303	313	323	303	313	323
pH	8	8	8	8	8	8	8	8	8
F (m^3/d)	50 000	50 000	50 000	100 000	100 000	100 000	120 000	120 000	120 000
K_d	8.01E-10	1.57E-09	2.93E-09	8.01E-10	1.57E-09	2.93E-09	8.01E-10	1.57E-09	2.93E-09
D_L (m^2/s)	2.4E-09	3.20E-09	4.3E-09	2.4E-09	3.20E-09	4.3E-09	2.4E-09	3.20E-09	4.3E-09
k_L (m/s)	2.65E-04	3.08E-04	3.57E-04	2.65E-04	3.08E-04	3.57E-04	2.65E-04	3.08E-04	3.57E-04
H ((kg/m^3)gas/(kg/m^3)liq)	8.76E-04	1.31E-03	1.92E-03	8.76E-04	1.31E-03	1.92E-03	8.76E-04	1.31E-03	1.92E-03
N-ammon (mg/l) IN	3000	3000	3000	3000	3000	3000	3000	3000	3000
C_L^{IN} NH_3 (mg/l)	270.1	493.0	824.8	270.1	493.0	824.8	270.1	493.0	824.8
C_L^{IN} NH_4^+ (mg/l)	3571.1	3335.1	2983.8	3571.1	3335.1	2983.8	3571.1	3335.1	2983.8
C_L^{OUT} NH_3 (mg/l)	262.0	453.0	676.0	254.0	418.0	573.0	251.0	406.0	540.0
C_L^{OUT} NH_4^+ (mg/l)	3463.8	3064.4	2445.4	3358.1	2827.6	2072.8	3318.4	2746.5	1953.5
C_G^{IN} NH_3 (ppm)	10.0	10.0	10.0	10.0	10.0	10.0	10.0	10.0	10.0
C_G^{OUT} NH_3 (mg/m^3)	229.5	595.1	1297.4	222.5	549.1	1099.7	219.9	533.3	1036.4
desorbed NH_3 (kg/d)	11.0	29.3	64.4	21.2	53.9	109.0	25.2	62.8	123.2
removal (% N)	3.07%	8.20%	18.04%	5.95%	15.11%	30.54%	7.05%	17.60%	34.52%
P_G (kW_e)	27.12	27.12	27.12	49.07	49.07	49.07	61.77	61.77	61.77

T (K)	303	313	323	303	313	323	303	313	323
pH	8.5	8.5	8.5	8.5	8.5	8.5	8.5	8.5	8.5
F (m^3/d)	50 000	50 000	50 000	100 000	100 000	100 000	120 000	120 000	120 000
K_d	8.01E-10	1.57E-09	2.93E-09	8.01E-10	1.57E-09	2.93E-09	8.01E-10	1.57E-09	2.93E-09
D_L (m^2/s)	2.4E-09	3.20E-09	4.3E-09	2.4E-09	3.20E-09	4.3E-09	2.4E-09	3.20E-09	4.3E-09
k_L (m/s)	2.65E-04	3.08E-04	3.57E-04	2.65E-04	3.08E-04	3.57E-04	2.65E-04	3.08E-04	3.57E-04
H ((m^3)gas/(kg/m^3)liq)	8.76E-04	1.31E-03	1.92E-03	8.76E-04	1.31E-03	1.92E-03	8.76E-04	1.31E-03	1.92E-03
N-ammon (mg/l) IN	3000	3000	3000	3000	3000	3000	3000	3000	3000
C_L^{IN} NH_3 (mg/l)	736.2	1206.1	1751.0	736.2	1206.1	1751.0	736.2	1206.1	1751.0
C_L^{IN} NH_4^+ (mg/l)	3077.7	2580.1	2003.1	3077.7	2580.1	2003.1	3077.7	2580.1	2003.1
C_L^{OUT} NH_3 (mg/l)	676.0	988.0	1192.0	625.0	837.5	904.0	607.0	789.5	825.0
C_L^{OUT} NH_4^+ (mg/l)	2826.2	2113.5	1363.6	2613.0	1791.6	1034.1	2537.7	1688.9	943.8
C_G^{IN} NH_3 (ppm)	10.0	10.0	10.0	10.0	10.0	10.0	10.0	10.0	10.0
C_G^{OUT} NH_3 (mg/m^3)	592.1	1297.8	2287.7	547.5	1100.1	1734.9	531.7	1037.1	1583.3
desorbed NH_3 (kg/d)	29.1	64.4	113.9	53.7	109.0	172.6	62.6	123.3	188.9
removal (% N)	8.15%	18.04%	31.91%	15.05%	30.54%	48.33%	17.53%	34.53%	52.90%
P_G (kW_e)	27.12	27.12	27.12	49.07	49.07	49.07	61.77	61.77	61.77

The surplus deliverable energy from a biogas engine could provide the treatment device with almost all thermal energy requirements up to a stripping process occurring at 50°C (the maximum thermal need to warm the digested materials up to 50°C and maintain that temperature is 53 kW during the coldest month) and the power to push biogas at the bottom of the reactor up to 100 000 m^3/d.

To this end, it should be remembered that:
1. hydrostatic head and then power requirements could be reduced by designing a larger storage tank;
2. at high temperature (40-50°C), an higher biogas production could be expected from the reaction tank: the CROPGEN project reports methane yields of 73-120 l CH_4/kg VS at 20°C and 133-197 l CH_4/kg VS at 35°C, for hydraulic retention time larger than 100 days. As a consequence, the storage tank could be designed in order to maximise post-methanation phenomena up to 6-7 times larger than the predicted one in the present analysis;
3. the strong public subsidies granted to renewable energy production in Italy and western Europe can justify a further investment finalised to a more complete environmental compatibility of anaerobic digestion.

Figure 5.5 reports the same information regarding ammonia removal efficiency in a graphical structure.
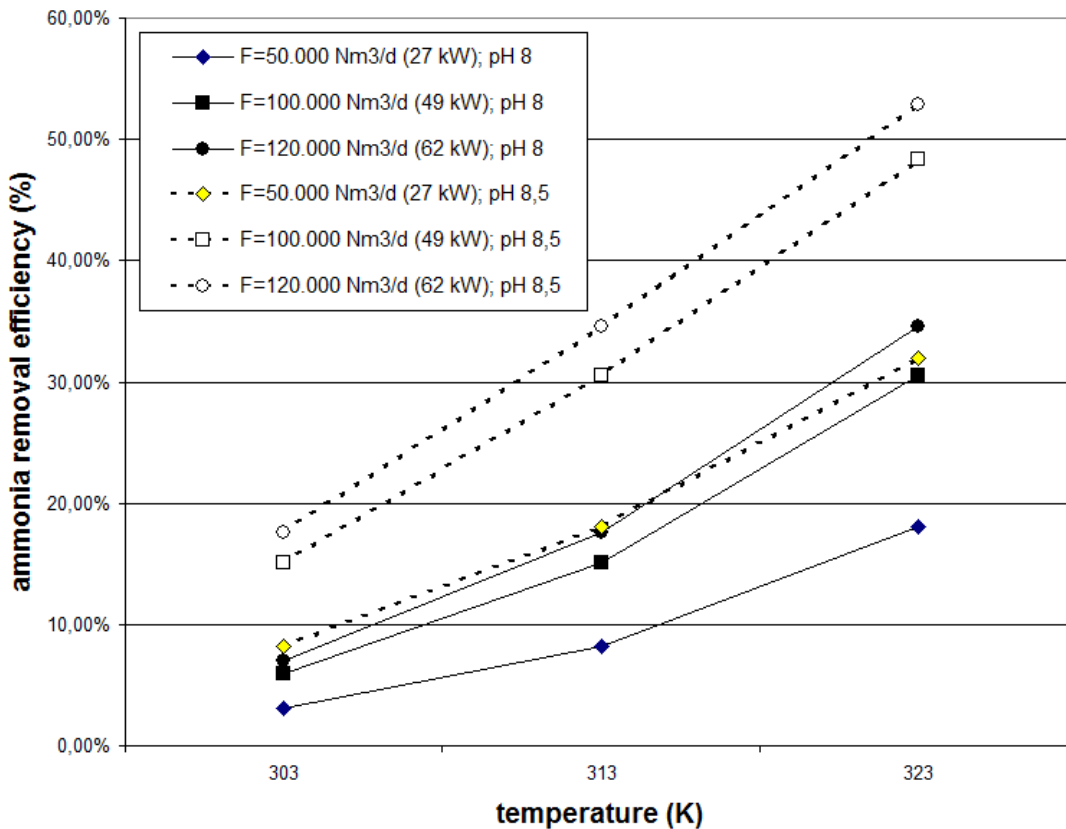
Figure 5.5: ammonia removal through digestate storage stripping

Finally, it should be remembered that residual biogas could be also burned in a boiler in order to produce thermal energy required by anaerobic digesters (around 300 kW) or upgrading devices, for example MEA solution regeneration. In this case, more than 110 kW_{th} could be recovered.

6 Conclusions

Since the process simulations carried out in the previous chapters give back several data regarding technical performances, energy consumptions, undesired releases (methane and solvent losses) for the mostly applied biogas upgrading techniques, it is necessary to summarize all results in a comprehensible way. This is the target of Table 6.1.

As far as the collection methodology is concerned, the author chose to report only the results deriving from configurations where technologies are applied to maximize biomethane production and minimize methane losses: for example, when water or organic solvent absorption is applied, biogas recirculation from flash tank must be surely applied, at a pressure that should be decided on the basis of the best match between operative costs (producibility and energy) and environmental costs (methane slip). The same example could be done for PSA, when regeneration strategy and desorption pressure have to be decided.

Moreover, the reported ranges of sorbent flows, tower dimensions, power required and recoverable heat refers closely to methane slip performances: for example, the highest values for power requirement, recoverable heat, sorbent flow and specific tower dimensions generally coincide to the lowest methane loss for the considered technique and vice versa.

Table 6.1 highlights that there are strong differences among the analysed upgrading techniques under many aspects, in particular:

- specific sorbent flow L/V, when pertinent (PSA doesn't use solvents): the calculated values lie in a very large range, from 2 to 35 m^3 of solvent for every 100 Nm^3 of raw biogas;
- absorbing tower dimensions, when pertinent (adsorbing column dimensions for PSA, above a certain threshold, don't influence separation performances): for example absorbing tower using pressurized water could be 40 times larger than chemo-absorbing columns using MEA;
- methane losses: all the analysed upgrading techniques could be designed in order to achieve very low methane slip, below 0.1%, except PSA that would not be able to decrease methane losses below 1.4%, for the materials and operative conditions considered here. The actual range of methane slip for all the considered upgrading techniques is 0.1÷5%;
- power required, mainly due to biogas compression: the calculated range covers one order of magnitude, from 25 to 266 kW_e, justified by the strong differences in pressure requirements and recirculation flow rates;
- recoverable heat from compressors: from 15 to more than 100 kW_{th};
- environmental impacts involving gaseous releases towards atmosphere.

Based on the reported data, it is quite easy to observe that upgrading techniques based on chemical absorption could bring about strong advantages as far as methane slip, electric power requirements and plant dimensions are concerned, since these technical parameters are by far the lowest among the analysed options; moreover, the upgrading plant would work close to atmospheric pressures, making operations surely safer. On the other hand, it should be underlined that these advantages are counterbalanced by other less positive aspects. First of all, thermal energy required by regeneration of amine solution in the case of MEA is little lower than 0.5 kWh/m^3 of raw biogas, roughly 200 kW_{th} (net of the possible heat recovery from biomethane compression) are needed, whereas the other techniques generally don't need thermal energy (physical absorption work better with low temperatures, heat for adsorption on Zeolite X13 at 50°C is provided by compression and exothermicity of the reaction). Moreover, MEA is a poisonous, aggressive, volatile and odorous liquid, that means much attention is needed for management: for example, extra costs are required to reduce corrosion and foaming within structure and to replace reactant that could be released toward atmosphere up to more than 60% in a year. The latter aspect brings about a heavy environmental impact as MEA, as VOC, is precursor of secondary PM_{10} and its emissions could involve strong odour nuisances. Then an abatement/recovery device for released reactant should be applied, for example a system scrubber/biofilter could be appropriate.

Table 6.1: upgrading techniques' calculated performances

	absorption with water	absorption with DEPG	chemical absorption with MEA	PSA/VSA with Zeolite X13
biogas production (Nm^3/h)	493.55	493.55	493.55	493.55
biogas CO_2 molar fraction	0.47	0.47	0.47	0.47
biomethane CH_4 purity	0.97	0.97	0.97	0.97
simulated process temperature (K)	303	298	313	323
process pressure (atm abs)	6÷12	6÷12	1	0.1÷6
sorbent flow L/V (m^3 for every 100 Nm^3 of raw biogas)	16÷35	8÷11	2÷4	-
absorbing tower dimensions (m^3·h/kg removed CO_2)	0.013÷0.043	0.011÷0.036	0.001÷0.002	-
methane losses low CH_4 slip	0.05 %	0.09 %	0.04 %	1.40 %
methane losses high CH_4 slip	3.85 %	1.07 %	0.08 %	4.40 %
power required (kW_e) low CH_4 slip	215	181	25	266
power required (kW_e) high CH_4 slip	81	66	23	47
heat required (kW_{th})	-	-	~210	-
recoverable heat (kW_{th}) low CH_4 slip	84	101	~15	21
recoverable heat (kW_{th}) high CH_4 slip	29	33	~15	14
specific consumption (kWh_e/m^3 of raw biogas)	0.16÷0.43	0.13÷0.37	~0.05	0.10÷0.54
specific consumption (kWh_e/m^3 of biomethane)	0.32÷0.82	0.26÷0.69	~0.10	0.19÷1.03
specific recoverable heat (kWh_{th}/m^3 of raw biogas)	0.06÷0.17	0.07÷0.20	~0.03	0.03÷0.04
environmental advices	water should be regenerated	-	MEA losses should be avoided	CH4 losses should be burned
remarks	flash tank pressure @ 2÷5 atm	flash tank pressure @ 2 atm	MEA concentration 3÷5 kmol/m3	partial recirculation of all desorbed gas gives higher reduction of CH_4 slip

The second observation that it's worth mentioning is that physical absorption with glycol ethers mixtures such as DEPG (Dimethyl Ether of Polyethylene Glycol, or Selexol as a trade name) can achieve good methane slip performances (around 1%) with low energy costs (0.13 kWh_e/m^3 of raw biogas) and a relevant amount of recoverable thermal energy (33 kW); the performances are valid when the flash tank operates at pressure ≤ 2 atm.

Finally, upgrading techniques based on adsorption generally show pretty high methane losses, from 3% to more than 10%; the reported calculations points out that is very difficult to minimize methane slip below 2%, even at very high energy consumptions (larger than 0.50 kWh_e/m^3 of raw biogas). In general, based on our analysis and literature reports, PSA seems to have quite low energy requirements when the minimization of methane losses is not a crucial point for designers. On the other hand, it should be remembered that large amounts of methane slip coming from PSA need to be burned in a post-combustor that would bring about extra investment costs and environmental impact due to CO and NO_x emissions.

Given that the technology assessments of upgrading processes are just one aspect of the global design of a technical choice, the present study should be properly deepened as far as economy is concerned as the choice of biomethane recovery performance (allowable methane slip) is a matter of equilibrium between costs and benefits, both industrial and environmental.

To this end, it is important to remember that power costs to run an upgrading facility represent just a part of total operative costs (comprehensive of amortization of investment costs), and not the main one. The feasibility study proposed by Regione Piemonte (2009), reports some costs simulation for a plant upgrading 500 Nm^3/h of biogas where upgrading electric energy costs are lower than 4% of yearly operative costs. On the other hand, apart from the energy crops producing costs, the second largest operative cost refers to digesters' heating (provided by the combustion of not upgraded biogas in a boiler). As a consequence, being heat requirements for anaerobic digestion something like 250÷300 kW_{th} on the yearly average, given that in the case of chemical absorption amine regeneration needs around 200 kW_{th}, thermal energy costs could be more important than power requirements according to different upgrading technique and methane slip performances: indeed, the lowest methane slip achievable generally correspond to the highest values for heat recoverable from compression, thus balancing the extra costs due to highest power requirements. Moreover it should be taken into account heat recovery possibilities offered by the post-methanation recovery from the digestate storage tank (corresponding to more than 100 kW_{th}).

In order to have a rough idea of energy costs, Regione Piemonte (2009) considered a cost of 13.6 $c€/kWh_e$ for the cost assessment. This value is confirmed by some recent reports (Camera di Commercio di Cuneo, 2011) for consumption above 1200 MWh per year. As far as natural gas cost from the national grid, the Italian National Energy Authority provides a total cost around 35.432 $c€/m^3$ (http://www.autorita.energia.it/it/dati/gp35.htm and http://www.autorita.energia.it/allegati/dati/gas/gp30.xls) for consumptions larger than 200,000 m^3/y.

Finally, the already mentioned biomethane feasibility study by Regione Piemonte (2009) suggests a feed-in-tariff for biomethane of 10.8 c€/kWh of biomethane (that corresponds to the existing tariff of 28 $c€/kWh_e$ and a transformation electric efficiency of 39%). The described tariff represents the economic income of the investment; provided that 10.8 c€//kWh of biomethane will be the actual ruled public subsidy for upgrading, any thermal energy requirements should be satisfied, if possible, by natural gas taken from the grid and not directly by raw biogas, for obvious economic reasons (natural gas cost is around one third of biomethane value).

Based on the reported data, Table 6.2 reports a general assessment of the energy total costs (electricity and heat) for the 4 upgrading techniques according to 2 opposite technical set-up:
- *high CH₄ slip*, that is the configuration with the lowest power requirements and the highest methane losses,
- *low CH₄ slip*, that is the configuration with the largest power requirements and the lowest methane losses.
The main assumptions are:
- yearly operating hours: 8400;
- boiler thermal efficiency: 90%;
- anaerobic digestion heat requirement: 300 kW_{th}.
The calculations include costs for digester heating and solvent regeneration (in the case of MEA solution) and thermal energy that could be recovered from compressors in order to reduce heat requirements.

Moreover, the energy cost doesn't include power consumptions for anaerobic digestion operation as they can be considered constant for all the analysed conditions.

The results are quite surprising as they point out that PSA is the least expensive as far as the *high CH$_4$ slip* configuration is concerned, followed by physical absorption; the most expensive technology turns out to be chemical absorption with MEA in spite of the very low power requirements, due to thermal energy consumed by reactant regeneration. Opposite results can be found for the low CH$_4$ slip configuration, where chemical absorption has the lowest energy costs; indeed, for physical absorption and adsorption upgrading techniques, the minimization of methane losses to the chemo-absorption level is very difficult and demanding, maybe impossible for PSA in spite of very high energy employment.

Table 6.2: yearly energy costs for analysed upgrading techniques

	absorption with water	*absorption with DEPG*	*chemical absorption with MEA*	*PSA/VSA with Zeolite X13*
digester + upgrading heat requirements (MWh/y)	2520	2520	4284	2520
digester + upgrading thermal energy costs with NG (EURO/y)	106 371	106 371	180 830	106 371
upgrading electricity costs *high CH$_4$ slip* (EURO/y)	92 534	75 398	26 275	53 693
upgrading electricity costs *low CH$_4$ slip* (EURO/y)	245 616	206 774	28 560	303 878
thermal energy saved *high CH$_4$ slip* (EURO/y)	10 283	11 701	5 319	4 964
thermal energy saved *low CH$_4$ slip* (EURO/y)	29 784	35 812	5 319	7 446
total energy costs high CH$_4$ slip (EURO/y)*	188 623	170 068	201 787	155 100
total energy costs low CH$_4$ slip (EURO/y)*	322 203	277 334	204 072	402 803

* power requirements for anaerobic digester is not included as they are the same for both the upgrading configurations high/low methane slip

However, the reported figures are not completely rigorous as up to now the item regarding the lost income is totally missing, that is biomethane released to atmosphere represents a loss of profitability that could be not neglectable, as highlighted by Table 6.3. The new perspective substantially changes the previous results, as chemical absorption with MEA and physical absorption with DEPG become the most interesting options for both the configurations, low and high methane slip, as far as industrial costs, as actual costs or lost profits, are concerned.

Finally, it should be remembered that methane slip represents a clear external cost: externalities deriving from any production cycle represent the costs imposed on society as well as on the environment that are not accounted for by the producers and consumers of goods, that is which are not included in the market price. External costs constitute an heavy market failure which justifies strong intervention policies.

The present paper is not focused on this kind of economic assessment but it's worth mentioning that any ton of emitted methane bring about a global damage that can be estimated. The ExternE project (European Commission, 1999) is the first and, at the moment, the most advanced and reliable attempt to use a consistent methodology to assess the external costs deriving from different fuel cycles and for different polluting molecules. The most recent ExternE documents (Externalities of Energy: Extension of accounting framework and Policy Applications, 2005; Externalities of Energy: methodology update) report an external

cost of 19 €/t CO_2 as a low estimate within EU15 (high estimate can be up to 80 €/t CO_2, but this value won't be taken into account in the present study). Methane externality would be obviously 25 times larger than CO_2 ones (as indicated at http://ecoweb.ier.uni-stuttgart.de/ecosense_web/ecosensele_web/frame.php).

Therefore, the second part of Table 6.3 tries to internalise the external costs due to methane slips within industrial costs, aiming at finding the most favourable overall configuration, with respect to private and public interests as a whole. According to the described approach the best balances seems to be assured by absorption with DEPG (releasing 1.07% of biomethane) and chemical absorption with MEA (with methane losses < 0.1%).

The reported data relating to costs (private and public) should be accurately compared to the yearly income assured by the assumed feed-in-tariff (10.8 c€//kWh of biomethane), that would lie in the range 2,175,638 €/y (in the case of a methane slip of 4.4%) and 2,274,634 €/y (in the case of a methane slip of 0.05%).

Table 6.3: yearly energy and external costs for analysed upgrading techniques

	absorption with water	*absorption with DEPG*	*chemical absorption with MEA*	*PSA/VSA with Zeolite X13*
total energy costs *high CH$_4$ slip* (EURO/y)	188 623	170 068	201 787	155 100
total energy costs *low CH$_4$ slip* (EURO/y)	322 203	277 334	204 072	392 521
lost income *high CH$_4$ slip* (EURO/y)	87 617	24 351	1 821	100 134
lost income *low CH$_4$ slip* (EURO/y)	1 138	2 048	910	31 861
total energy costs + lost income *high CH$_4$ slip* (EURO/y)	276 240	194 419	203 608	255 234
total energy costs + lost income *low CH$_4$ slip* (EURO/y)	323 341	279 382	204 982	434 664
CH$_4$ externalities *high CH$_4$ slip* (EURO/y)	28 684	7 972	596	32 782
CH$_4$ externalities *low CH$_4$ slip* (EURO/y)	373	671	298	10 431
total energy costs + lost income + CH$_4$ externalities *high CH$_4$ slip* (EURO/y)	304 924	202 391	204 204	288 015
total energy costs + lost income + CH$_4$ externalities *low CH$_4$ slip* (EURO/y)	323 713	280 052	205 280	445 095

The same approach, dealing with technical, economic and environmental aspects, could be applied to residual biogas recovery and ammonia stripping treatment described in chapter 4. In this case, the energy costs regard power requirements (27÷62 kW$_e$ according to the stripping gas flow) and thermal energy recoverable from the direct combustion of residual biogas (in the case upgrading plant follows anaerobic digestion and there is no biogas engine on site). The external costs, on the contrary, concern the potential release of post-methanation into atmosphere (that could be avoided through the recovery treatment, then involving a positive externality) and ammonia releases from the storage of digested materials (that could be avoided because the storage tank is totally closed). Finally the ammonia removed through the stripping and

transformed into a fertilizer would be absent from the traditional and generally inefficient land spreading of digested materials, allowing a proportional saving of ammonia releases towards atmosphere from this phase (that could be up to 15% of nitrogen content).

The assumed technical set-ups are:

- cattle slurry contains 4.4 kg N/t of fresh matter, whereas maize contains 4 kg N/t fresh matter: digested materials contain 113 t/y of nitrogen to be managed after anaerobic digestion;
- under meteorological conditions of Northern Italy, 19% of nitrogen contained in the storage tank is emitted as NH_3-N from the storage and 15% from traditional land spreading;
- *low NH_3 removal* represents the configuration with the lowest power requirements (27 kW_e) and ammonia removal efficiency assumed around 15%,
- *high NH_3 removal* represents the configuration with the largest power requirements and ammonia removal efficiency assumed around 30%.

Moreover, as far as ammonia external cost is concerned, the ExternE methodology has been applied for airborne pollutants in many countries of European Union. The Clean Air For Europe (CAFE) Programme (2005) provides, for Italy, the following external costs, referring to the year 2010:

NH_3: 17 000 €/t;

NO_x: 8 600 €/t;

$PM_{2.5}$: 52 000 €/t;

SO_2: 9 300 €/t;

VOC: 1 600 €/t.

The reported costs take into account both the impact at the local scale, within 20 km from the source, and those on a regional scale, referring to the secondary pollutants generated from the reported primary molecules (this is in particular the case of fine particulates, mainly composed by ammonium nitrates, sulphates and nucleated/condensed VOC).

The results of the rough industrial and environmental costs are reported by Table 6.4. It is easy to observe that the heat recovery of residual biogas could cover, alone, the power costs required by ammonia stripping for the low efficiency configuration. Indeed, it is very important to notice that environmental benefits arising from the recovery of residual biogas from the storage of digested materials and, most of all, the reduction of ammonia emissions towards atmosphere are strongly overwhelming the industrial costs.

Table6 4: yearly energy and external costs analysis for biogas recovery/ammonia stripping treatment

electricity costs *low NH_3 removal* (EURO/y)	30 845
electricity costs *high NH_3 removal* (EURO/y)	70 829
thermal energy saved (EURO/y)	39 003

CH_4 avoided externalities (EURO/y)	35 603

ammonia avoided externalities *low NH_3 removal* (EURO/y)	408 213
ammonia avoided externalities *high NH_3 removal* (EURO/y)	451 435

In conclusion, anaerobic codigestion of manure and energy crops is strongly encouraged by European legislation but its effect on environmental quality could be negative due to ammonia releases from digested materials, criteria pollutants from biogas combustion and GHG indirect emissions.

Anyway, technical solutions that can ensure the compatibility of anaerobic codigestion do exist and their effectiveness can be very satisfying. In particular, biogas produced during the post-fermentation in the storage tank should be recovered and burned in order to obtain sustainable greenhouse gas emission balance. Moreover, recovered biogas could be opportunely used to desorb ammonia from digested materials. This way, the energy production could increase at least by 5 % (potentially up to 30%) and ammonia removal efficiency could range from 15 to 50%, according to pH, temperature and gas injected flow

conditions. Finally, biogas could be upgraded to biomethane to be injected into natural gas grid or used as a vehicle fuel, avoiding strong atmospheric emissions at the local scale from small biogas engines and making it possible to achieve satisfying energy efficiency.

In this sense, the present study confirms that technology is absolutely ready and suitable to reach very high levels of productivity, efficiency and environmental performances at sustainable costs and the right technological approach could solve many environmental problems regarding nitrate contamination, ammonia emissions and global warming issues.

Unfortunately, so far, the Italian economic subsidies strategy, mainly based on electricity production, and the technical legislation (that is not suitable to manage the possible environmental impacts), didn't help to minimize the negative effects of a massive introduction of renewable energy plants and maximize the advantages, both environmental and socio-economics. The future decisions regarding green subsidies and in particular biomethane production are surely the right chance to improve environmental sustainability of biogas plant and make it a crucial real energy source for our territory.

References

Akita K., Yoshida F., Bubble size, interfacial area and liquid phase mass transfer coefficients in bubble column reactors, Ind. Eng. Chem. Process Des. Dev. 13, 84-91, 1974.

Amon B., Kryvoruchko V. Amon T., Influence of different methods of covering slurry stores on greenhouse gas and ammonia emissions, International Congress Series 1293 (2006) 315– 318.

Astarita G., Mass Transfer with Chemical Reaction, Elsevier, 1967.

Balsari P., Biogas dal comparto agro biogas dal comparto agro-zootecnico: zootecnico: l'esperienza europea esperienza europea, Workshop internazionale digestione anaerobica: la situazione italiana, 2009.

Balsari P., Incontro di lavoro sui risultati conclusivi del progetto PROBIO-BIOGAS, 13 dicembre 2010.

Benjaminsson J., Nya renings-och uppgraderingstekniker för biogas. Malmö, Sweden : Swedish Gas Center, SGC Report No. 163, 2006.

BioMil AB, New biogas upgrading techniques, 2nd Nordic Biogas Conference, Johan Benjaminsson.

Blengini G.A., Brizio E., Cibrario M., Genon G., LCA of bioenergy chains in Piedmont (Italy): A case study to support public decision makers towards sustainability. Resources, Conservation and Recycling 57, 36– 47, 2011.

Brizio E., Genon G., Environmental compatibility of renewable energy plants, AIR POLLUTION 2009. Wessex Institute of Technology, Tallinn, 20-22 luglio 2009, proceedings.

Brizio E., Genon G., Environmental compatibility of renewable energy plants, AIR POLLUTION XVIII, Wessex Institute of Technology Press, 149-159, 2010.

Brizio E., Bilancio energetico/ambientale nella produzione di biogas: criticità del settore agro-energetico, Convegno EnergETICA, 28 aprile 2011. www.agroenergia.eu

Brizio E., Genon G., Panepinto D., Criteria for Environmental compatibility of energy plants, ICAE 2011, international conference of applied energy, Perugia, May 16-18 2011.

Bryan Research & Engineering Inc., A COMPARISON OF PHYSICAL SOLVENTS FOR ACID GAS REMOVAL.
www.bre.com/portals/0/technicalarticles/A%20Comparison%20of%20Physical%20Solvents%20for%20Acid%20Gas%20Removal%20REVISED.pdf

Camera di Commercio di Cuneo, Sistema di Monitoraggio delle tariffe e dei prezzi, 2011, http://www.cn.camcom.gov.it/Page/t04/view_html?idp=1670.

Cavenati S., Grande C.A., Rodrigues A.E, Upgrade of Methane from Landfill Gas by Pressure Swing Adsorption, Energy & Fuels, Vol. 19, No. 6, pp 2545-2555, ISSN 0887-0624, August 2005.

Clean Air For Europe (CAFE) Programme, Damages per tonne emission of PM2.5, NH3, SO2, NOx and VOCs from each EU25 Member State (excluding Cyprus) and surrounding seas, 2005.

Clemens J., Trimborn M., Weiland P., Amon B., Mitigation of greenhouse gas emissions by anaerobic digestion of cattle slurry, Agriculture, Ecosystems and Environment 112 (2006) 171–177.

Coelho Pinheiro M.N., Stripping in a bubbling pool under vacuum-contribution of the interfacial tension to the pressure inside the bubbles, Int. Comm. Heat Mass Transfer, vol. 28, No. 8 pp. 1053-1063, 2001.

Commissione Nazionale Emergenza Inquinamento Atmosferico (CNEIA), Relazione conclusiva, 20 February 2006.

CROPGEN Project, Renewable energy from crops and agrowastes, Project D17: Database on the methane production potential from mixed digestion.

De Leeuw F, A set of emission indicators for longrange transboundary air pollution, Environmental Science & Policy, n. 5, pp. 135-145, 2002.

Deckwer W.D., Bubble Column Reactors. Wiley and sons. 1985.

Deng L., Hägg M., Techno-economic evaluation of biogas upgrading process using CO_2 facilitated transport membrane. s.l., International Journal of Greenhouse Gas Control 4 pp. 638–646, 2010.

Dey A., Aroonwilas A., CO_2 absorption into MEA-AMP blend: mass transfer and absorber height index, Energy Procedia 1 (2009) 211-215.

DOW Chemical Company Midland, January 2003. http://msdssearch.dow.com/PublishedLiteratureDOWCOM/dh_017d/0901b8038017d302.pdf?filepath=amines/pdfs/noreg/111-01375.pdf&fromPage=GetDoc

ENEL, Rapporto Ambientale 2009.

European Commission – DG XII, Externalities of Energy, volume 7: Methodology 1998 update, (EUR 19083 EN), Bruxelles, 1999.

Fisher, Integrating MEA regeneration with CO_2 compression and peaking to reduce CO_2 capture costs, The University of Texas at Austin, 2005. http://www.trimeric.com/Report%20060905.pdf.

Genon G., Brizio E., Panepinto D., Russolillo D., Becchis F., Production of green energy from co-digestion: perspectives for the province of Cuneo, energetic balance and environmental sustainability. Bionature 2011, Venice, May 2011.

Giugliano M., Lonati G., Polveri fini in atmosfera: la componente secondaria, ENERGIA 3/2005, July 2005.
Grande C. A., Biogas Upgrading by Pressure Swing Adsorption, SINTEF Materials and Chemistry, Oslo Norway, from the web, 2010.

Gronauer, A., Comparison of different technologies: the road to success, Conference Anaerobic Digestion: opportunities for agriculture and environment, Regione Lombardia, from the web.

Henni A., Tontiwachwuthikul P., Chakma A., Solubilities of Carbon Dioxide in Polyethylene Glycol Ethers, THE CANADIAN JOURNAL OF CHEMICAL ENGINEERING VOLUME 83, april 2005.

Henni A., Tontiwachwuthikul P., Chakma A., Solubility Study of Methane and Ethane in Promising Physical Solvents for Natural Gas Sweetening Operations, J. Chem. Eng. Data, 51, 64-67, 2006.

Immovilli A., Fabbri C., Valli L., Odour and ammonia emissions from cattle slurry treated with anaerobic digestion, Centro Ricerche Produzioni Animali, 2007
http://www.crpa.it/nqcontent.cfm?a_id=4076&tt=crpa_www&aa=seqcurera&sp=seq-cure.

Johansson N., Production of liquid biogas, LBG, with cryogenic and conventional upgrading technology, Master's thesis, LUNDS University, Department of Technology and society, 2008.

Jonsson S., Westman J., Cryogenic biogas upgrading using plate heat exchangers, Master's Thesis within the Sustainable Energy Systems Master's programme, CHALMERS UNIVERSITY OF TECHNOLOGY, Göteborg, Sweden 2011.

Kaparaju P.L.N., Rintala J.A., Effects of temperature on postmethanation of digested dairy cow manure in a farm-scale biogas production system, Env. Technol. 24,1315–1321, 2003.

Kidnay A. J., Parrish W., Parrish W. R., Fundamentals of natural gas processing, Taylor and Francis Group, 2006.

Kirk, Othmer, Encyclopaedia of chemical technology, 4th edition, 1998.

Kohl A., Nielsen R. B., Gas Purification, 5th ed., Gulf Publishing Company,Houston, Texas, 1997.

Lide D. R., Frederikse H. P. R., CRC Handbook of Chemistry and Physics, 76th Edition, CRC Press, Inc., Boca Raton, FL, 1995.

Liu G.B., Yu K.T., Yuan G., Liu C.J., Guo Q.C., Simulations of chemical absorption in pilot-scale and industrial-scale packed columns by computational mass transfer, Chemical Engineering Science 61, 6511 – 6529, 2006.

McCabe W.L., Smith J.C., Harriott P., Unit Operations of Chemical Engineering, 7th edition, 2005.

Miltner M., Makaruk A., Harasek M., Application of Gas Permeation for Biogas Upgrad - Operational Experiences of Feeding Biomethane into the Austrian Gas Grid, 16th European Biomass Conference, 978-88-89407-58-1; S. 1905-1911, 2008.

Olesen J. E., Sommer S. G., Modelling effects of wind speed and surface cover on ammonia volatilization from stored pig slurry, Atmospheric Environment, Part A, General Topics, 1993, 27(16), 2567–2574.

Onda K., Takeuchi H., Okumoto Y., Mass transfer coefficients between gas and liquid phases in packed columns, Journal of Chemical Engineering of Japan 1, 56–62, 1968.

Persson M., Report SGC 142, Evaluation of upgrading techniques for biogas, Lund institute of technology, 2003.

Petersson A., Wellinger A., Biogas upgrading technologies – developments and innovations. IEA BioEnergy, TASK 37.

Pettersson A., Wellinger A., Biogas Upgrading Technologies – Developments and Innovation, 02.04.2011.
http://www.iea-biogas.net/

Raney D. R., Remove Carbon Dioxide with Selexol, Hydrocarbon Processing, p. 73, April, 1976.

Regione Piemonte, D.D. 717 del 24/11/2008, Studio di fattibilità della filiera del biometano da effluenti zootecnici e/o da discarica per autotrazione/immissione in rete, a cura di CRPA, Novembre 2009.

Ryckebosch E., Drouillon M., Vervaeren H., Techniques for transformation of biogas to biomethane, Biomass and Bioenergy 35 (2011), 1633-1645.

SGC Report 118, Adding gas from biomass to the gas grid, Swedish Gas Center, July 2001.

Sherwood T. K., Holloway F. A. L., Trans. Inst. Am. Chem. Eng. 36, 39 (1940).

Van der Molen J., Beljaars A.C.M., Chardon W.J., Jury W.A., Vanfaassen H.G., Ammonia volatilization from arable land after application of cattle slurry. Derivation of a transfer model, Netherlands Journal of Agricultural Science, 38(3), 239-254,1990.

Weiland P., Production and energetic use of biogas from energy crops and wastes in Germany, Appl. Biochem. Biotechnol. 109: 263–274, 2003.

Weiland R.H., Dingman J.C., Cronin D.B., Browning G.J., Density and viscosity of some partially carbonated aqueous alkanolamine solutions and their blends, Journal of Chemical and Engineering Data 43, 378–382, 1998.

Wellek R.M., Brunson R.J., Law F.H., Enhancement factors for gas absorption with 2nd-order irreversible chemical-reaction, Canadian Journal of Chemical Engineering 56, 181–186, 1978.

Wilke C.R., Chang P., Correlations of diffusion coefficients in dilute solutions, A.I.Ch.E. Journal, June 1955.